An automated platform for multistep synthesis based on a new paradigm for combining flow modules

A Dissertation

Submitted in Partial Fulfilment of the Requirements for the Degree of

Doctor rerum naturalium (Dr. rer. nat.)

to the Department of Biology, Chemistry, Pharmacy

of Freie Universität Berlin

by

Mara Guidi

Berlin, 2020

Supervisor: Prof. Dr. Peter H. Seeberger
Second examiner: Prof. Dr. Matthew Hopkinson

Date of defense: 03.03.2021

My doctoral degree thesis entitled “An automated platform for multistep synthesis based on a new paradigm for combining flow modules” has been prepared by myself and is based on my own work; the work from others has been specifically acknowledged in the text. This thesis is submitted to the Department of Biology, Chemistry, Pharmacy of Freie Universität Berlin to obtain the academic degree Doctor rerum naturalium (Dr. rer. nat.) and has not been submitted for any other degree.

Acknowledgements

First and foremost, I would like to thank Prof. Dr. Peter H. Seeberger and Prof. Dr. Kerry Gilmore for giving me the opportunity to perform research at the Max Planck Institute of Colloids and Interfaces, and for their trust and confidence in my work and my abilities. I thank Prof. Dr. Hopkinson for kindly agreeing to review my thesis.

I´m deeply grateful to all my colleagues of the Biomolecular Systems department for providing an excellent working environment, especially to Sourav, Sooyeon, Dario and Lucia for fruitful work collaborations which contributed to this thesis. To Dario and Matt for carefully correcting my thesis and to Bart for his guidance and for revising the translation of my summary.

A special thanks goes to Bart, Jiawei and Matt who welcomed me in the lab and took care of me at the beginning of my PhD. To all the people who passed by the flow lab during my staying and left a mark on my heart: Karen, Anita, Nabyl (so glad you are coming back), Dario (so glad you are my boss now), Lucia and Friederike, To all the great friends that I found here: Martina, Ankita, Alonso, Mauro, Bart, Matt, Dario, José, Eric, Monica, CD, Jiawei, Jamal, Renée, Majd, Vittorio, Antonella, Mike, Debbie, Max… you are so many and you are all responsible for my happiness and mental health!

A heartfelt thanks goes also to my old friends back home, who are always there and always will be (and will never read this thesis, so I can avoid mentioning them name by name). I can´t wait to be able to hug you again! To all my teachers, professors and supervisors who shared their knowledge with me and shaped my mind throughout my life of studies, especially Dr. Mauro Amelio, who was my first supervisor in a chemistry lab and still follows my research and cares about my success.

Finally, the warmest thanks go to my family. To my parents, for setting the bar high for me and always giving the best example, but still being proud of me no matter whether I succeed or fail. To Sere for being my lifetime best friend. And to Pietro, for having my back and being my home in these past three years.

List of Publications

Chatterjee, S;* **Guidi, M.**;* Seeberger, P. H.; Gilmore, K. Automated radial synthesis of organic molecules. *Nature* **2020**, 579**,** 379–384. DOI: 10.1038/s41586-020-2083-5.

Guidi, M.; Seeberger, P. H.; Gilmore, K. How to approach flow chemistry. *Chem. Soc. Rev.* **2020**, 49, 8910–8932. DOI: 10.1039/c9cs00832b.

* Equal authorship

Table of Contents

Acknowledgements ..... **v**

List of Publications ..... **vii**

Table of Contents **1**

Abbreviation list **3**

Summary **5**

Zusammenfassung **6**

1 Introduction **9**

1.1 Chemistry in the era of automation 9

1.2 Flow microreactors enabling new chemistries and multistep synthesis 10

1.3 Automated synthesizers - linear *vs*. iterative processes 15

1.3.1 Automated platforms based on a linear approach 15

1.3.2 Automated platforms based on an iterative approach 18

1.4 The radial synthesis paradigm 20

1.5 Aim of this thesis 21

2 The radial synthesizer **23**

2.1 Design and hardware 23

2.1.1 System compatibilities 29

2.1.2 Reagent delivery system (RDS) 30

2.1.3 Central switching station (CSS) 34

2.1.4 Standby module (SM) 38

2.2 Precipitation handling and prevention of system fouling 40

2.3 Pathways 41

2.4 Calibrations 50

2.4.1 Calibration of solvent and reagent selectors 50

2.4.2 Calibration of flow rate: 51

2.5 Software 59

3 Proof of concept 61

3.1 Convergent vs linear syntheses 61

3.1.1 Radial *convergent* synthesis of rufinamide 64

3.1.2 Radial *linear* synthesis of rufinamide 76

3.2 Library Generation 87

3.2.1 Arenes scope 88

3.2.2 Amines scope 91

3.2.3 Mixed derivatives 94

3.3 Modular expansion 100

3.3.1 General procedure for flow metallophotoredox process 101

3.4 Comparison of radial and continuous flow 110

3.4.1 Synthesis of paracetamol (39) 111

3.4.2 Synthesis of lidocaine (40) 116

3.4.3 Synthesis of nifedipine (41) 121

4 Experimental section 127

4.1 General chemical information 127

4.2 Compound characterization 128

5 Conclusions and perspective 139

6 References 143

7 Appendix: NMR spectra 147

Abbreviation list

API	Active Pharmaceutical Ingredient
BPR	Back Pressure Regulator
C1	1st step of convergent synthesis of rufinamide
C2	2nd step of convergent synthesis of rufinamide
C3	3rd step of convergent synthesis of rufinamide
CSS	Central Switching Station
CSTR	Continuous Stirred Tank Reactor
CV	Collection Vessel
DABCO	1,4-diazabicyclo[2.2.2]octane
DMA	Dimethyl Acetamide
DMSO	Dimethyl Sulfoxide
FEP	Fluorinated Ethylene Propylene
HPLC	High Performance Liquid Chromatography
ID	Inner Diameter
IR	Infrared
Ir cat	$(Ir[dF(CF_3)ppy]_2(dtbpy))PF_6$
L1	1st step of linear synthesis of rufinamide
L2	2nd step of linear synthesis of rufinamide
L3	3rd step of linear synthesis of rufinamide
LED	Light Emitting Diode
Li-1	1st step of synthesis of lidocaine
Li-2	2nd step of synthesis of lidocaine
MFC	Mass Flow Controllers
MIDA	N-methyliminodiacetic acid
n-BuLi	Normal butyllithium
NMP	N-methyl-2-pyrrolidone
NMR	Nuclear Magnetic Resonance
OD	Outer Diameter
P1	1st step of photochemical process
P2	2nd step of photochemical process
PEEK	Polyether Ether Ketone
PFA	Perfluoroalkoxy Alkanes
POM	Polyoxymethylene

PTFE	Polytetrafluoroethylene
RDS	Reagent Delivery System
R-C	Reagent delivery system – Collection
R-R	Reagent delivery system - Reagent delivery system
R-S	Reagent delivery system – Standby module
S-C	Standby module - Collection
S-R	Standby module - Reagent delivery system
S-S	Standby module - Standby module
SM	Standby Module
SMBR	Serial Micro-Batch Reactors
THF	Tetrahydrofuran

Summary

Automation of organic synthesis has seen rapid progress in the past decade with the development of many platforms for execution, investigation and optimization of chemical reactions and multistep processes. Each of these platforms relies on a different approach to chemical synthesis; including traditional batch chemistry, solid-phase synthesis and flow chemistry, and uses a different dedicated hardware to translate and operate processes. The aim of this thesis was to identify both strengths and limitations of the existing synthesizers and to develop a new platform based on a hybrid approach that takes the best elements from each of them.

First, the radial paradigm was established; a new arrangement of reaction modules that allows for their reuse within the same process, uses discrete volumes of solutions and decouples reaction steps so that each reaction in a multistep synthesis can be performed at optimal conditions, minimizing the waste of materials and equipment required (chapter 1, section 1.4). The hardware of the instrument is described thoroughly in chapter 2 with details of each module (broken down into its basic components), explanation of the possible flow pathways, troubleshooting and calibration data.

Once the hardware was assembled, the radial synthesizer was validated by performing a series of showcase processes (chapter 3). First, convergent and linear syntheses of the active ingredient rufinamide were chosen to demonstrate the capability of switching between different synthetic routes without the need for physical rearrangement of the instrument (section 3.1). Second, a library of twelve derivatives was generated within a short amount of time and minimum waste of starting materials to show the potential of the radial synthesizer for a possible application in medicinal chemistry (section 3.2). Next, the synthetic and analytical capabilities of the instrument were expanded by integrating a module for photochemistry and flow-NMR spectroscopy via standard flow connectors (section 3.3). Finally, radial synthesis and continuous flow synthesis were compared by preparing three pharmaceutical ingredients (paracetamol, lidocaine, and nifedipine), developing and optimizing each step in the radial synthesizer and performing a scale-up in gram scale in a commercial continuous flow apparatus (section 3.4).

Zusammenfassung

Die Automatisierung der organischen Synthese hat in den letzten zehn Jahren mit der Entwicklung vieler Plattformen zur Ausführung, Untersuchung und Optimierung chemischer Reaktionen und mehrstufiger Prozesse rasante Fortschritte erzielt. Diese Plattformen basieren auf verschiedenen Ansätzen um chemische Synthesen mittels Batch-Verfahren, Festphasensynthese, oder der Druchflusschemie vollautomatisch durchzuführen. Die unterschiedlichen Strategien benötigen jeweils spezielle Hardware. Das Ziel dieser Doktorarbeit war es, die Stärken und Schwächen der vorhandenen Automatisierungsmethoden zu identifizieren und eine neue Plattform zu entwickeln, die die Vorteile der jeweiligen Strategien kombiniert.

Aufgrund dieser Analyse wurde ein radialer Syntheseautomat konzipiert. Eine neue Anordnung von Reaktionsmodulen ermöglicht diese, innerhalb desselben Prozesses, mehrmals zu verwenden. Durch diskrete Lösungsvolumina und entkoppelte Reaktionsschritte kann jede Reaktion in einer mehrstufigen Synthese unter optimalen Bedingungen durchgeführt werden, wodurch die Verschwendung von Chemikalien und Ausrüstung minimiert wird (Kapitel 1, Abschnitt 1.4). Die Hardware des entwickelten Syntheseautomaten wird in Kapitel 2 ausführlich beschrieben. Dies umfasst die Grundkomponenten jedes Moduls, Erläuterungen zu möglichen Durchflusswegen, Fehlerbehebung und Kalibrierungsdaten.

Der radiale Syntheseautomat wurde anhand mehrerer mehrstufiger Synthesen validiert (Kapitel 3). Zunächst wurden konvergente und lineare Synthesen des Wirkstoffs Rufinamid durchgeführt, um zu veranschaulichen, dass der Syntheseautomat im Stande ist zwischen verschiedenen Synthesewegen zu wechseln eine der Hardware vorzunehmen (Abschnitt 3.1). Zudem wurde eine Bibliothek mit zwölf Derivaten von Rufinamid erstellt, um das Potenzial des Syntheseautomaten für die Anwendung Anwendung in der medizinischen Chemie aufzuzeigen (Abschnitt 3.2). Anschließend wurden die synthetischen und analytischen Möglichkeiten des Instruments durch die Integration eines Moduls für Photochemie und eines Moduls für Durchfluss-NMR-Spektroskopie erweitert (Abschnitt 3.3). Schließlich wurde die „radiale Synthese“ mit der kontinuierlichen Druchflusssynthese für die Herstellung von drei pharmazeutischen Wirkstoffen (Paracetamol, Lidocain und Nifedipin) verglichen. Jeder Reaktionsschritt wurde im radialen Syntheseautomat entwickelt und optimiert. Anschließend wurde eine Skalierung der entwickelten Syntheseroute im Gramm-Maßstab in einem kontinuierlichen Flussgerät durchgeführt (Abschnitt 3.4).

1 Introduction

This chapter has been partly modified from: Chatterjee, S.; * Guidi, M.; * Seeberger, P. H.; Gilmore, K. Automated Radial Synthesis of Organic Molecules. *Nature* **2020**, 579, 379–384. DOI: 10.1038/s41586-020-2083-5 and Guidi, M.; Seeberger, P. H.; Gilmore, K. How to approach flow chemistry. *Chem. Soc. Rev.* **2020**, 49, 8910–8932. DOI: 10.1039/C9CS00832B.

Further permissions related to the material excerpted should be directed to Springer Nature and Royal Society of Chemistry.

* equal authorship

1.1 Chemistry in the era of automation

Our world relies on automation for applications ranging from the simplest task, like a traffic light controlling vehicle movement at an intersection, to extremely complex control systems managing industrial plants, telecommunications, and spacecrafts. In principle, every situation in which a machine could replace a human being´s action can be improved or facilitated by automation. Repetitive tasks, in particular, benefit the most from being automated, because a machine can be faster, more efficient, and more reproducible accomplishing them, than a human operator, thus resulting in labor and time savings. Since the advent of assembly lines, work is repetitively performed from workstation to workstation, for instance, in manufacturing plants, where processes are now automated as robotic assembly lines in which human intervention is required only for the definition and supervision of the protocols, and the “manual” work is left to the machines.

The technological transformation of the world has affected the field of chemistry too. At the laboratory level, thermostatic baths, centrifuges, and autosamplers are so deeply rooted in our routine that we barely notice them at all. Not only routine operations, but also more complex matters such as organic synthesis have been turning towards automation. Replacing the operator, when it comes to synthetic chemistry, is not trivial, because synthetic processes are composed of a huge number of diverse chemical transformations, achievable through an even bigger number of manual operations, which can be linked together in a countless number of combinations. Therefore, it is difficult to treat it like an assembly line and break it down in workstations which can be run by machines.

Aside from the operational complexity, chemistry itself poses some intrinsic hurdles, such as manipulation of toxic/corrosive species, rational tuning of many different variables, and integration of precise yet robust analytical methods. Thus, every process

results in a set of different complications that must be addressed as a unique challenge. As a direct consequence of this uniqueness, it is extremely difficult to conceive of a universal machine for chemical synthesis. Although robots (defined in the collective imagination as machines capable of moving independently and performing complex actions) might seem the most obvious choice to meet this goal, as they are the closest we can get to the artificial version of a fully operative human being, their complexity is often excessive for what is the actual task.

Automation cannot simply mean letting a robot performing processes the exact same way a human operator would. The process of automating a task inevitably alters the task, simplifying it at its core[1]. The ultimate goal of automation, aside from disburdening people from mere and tedious jobs, is to outperform humans in productivity, reproducibility, and reliability.

Robots intended as humanoid machines (or machines which mimic parts of a human body e. g. robotic arms) have some of the same limitations of humans, while being less flexible and more complex. For this reason, aside from a few examples of batch approaches relying on robotic systems[2,3], when it comes to the automation of chemical synthesis, the attention is generally turned to flow chemistry[4,5] or solid-phase chemistry[6-8], which are powerful techniques capable of streamlining synthetic operations and which require much simpler hardware and software than robots.

1.2 Flow microreactors enabling new chemistries and multistep synthesis

Currently, flow chemistry is a widely studied field, with many researchers looking to it for a convenient way to automate processes providing reproducible access to a range of chemistries that are otherwise inefficient or problematic[9].

At its core, a flow process is composed of a continuous stream of a solution containing reagents, delivered by pumps and combined at a mixing junction, passing into a reactor unit to which specific conditions are applied. After a defined amount of time, the reaction mixture leaves the reactor unit and can have several different fates such as collection, utilization in a following step by flowing in another unit, such as a purification module or an analytical checkpoint (Figure 1.1).

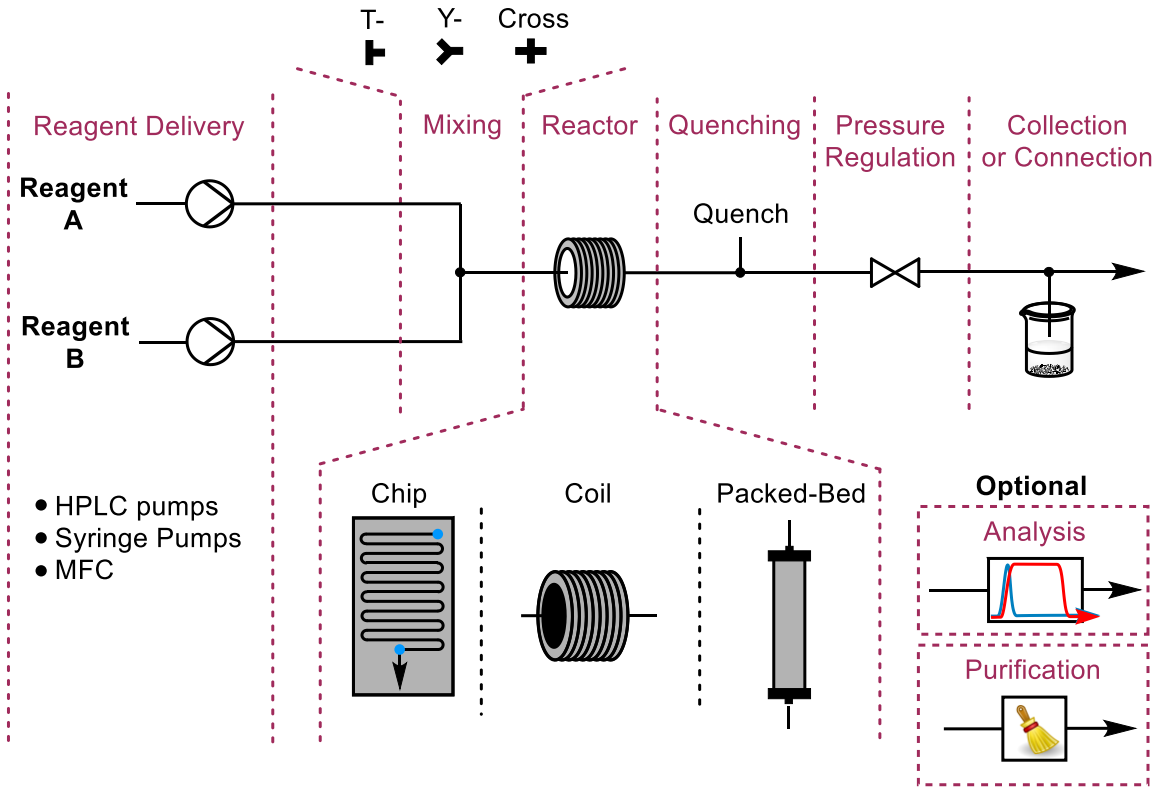

Figure 1.1. Breakdown of the basic components of a continuous flow system.

Organic synthesis has considerably benefited from the advent of flow chemistry. The integration of flow technology has contributed to paving the way for the development and application of photochemistry in synthesis[10] and for accessing unstable, reactive species, which can be generated *in-situ* in flow[11], in a safe and reproducible manner, resulting in cleaner and more efficient processes.

Thanks to the small reactor volumes, good control over temperature and residence time and resistance to high pressure, flow processes have proven to be safer, more selective, and greener than traditional batch chemistry. Running reactions in sealed, pressurized systems allows for working with solvents above their boiling points, while the extensive surface-to-volume ratio of microreactors ensures good heat transfer, thus providing the opportunity of applying rapid temperature ramps with certainty that the same temperature is applied simultaneously to the entire flowing solution with negligible gradient. For endothermic reactions, this means that it is possible to shorten the reaction time from several hours to minutes, and for highly exothermic reactions, that it is possible to circumvent the use of cryogenics by exploiting the good heat dissipation offered by the narrow tubes. The extremely fast mixing offered by microreactors also plays an important role, especially when it comes to harnessing very fast reactions which traditionally suffer

from product selectivity. Micromixing shortens the diffusion path improving the control on kinetics[12].

One often underestimated but very important feature of flow chemistry is the direct correlation between reaction time and physical position in flow reactors. In a given reactor, the reaction time (a concept that translates into residence time when switching from batch to flow) is a function of flow rate and volume, which is itself the result of two factors: tube diameter and length. Once the system has reached its steady state, the reaction progress in every part of the reactor is constant, with the new species forming along the length of the fluid path. The implications of this space-time analogy are significant, particularly for fast reactions or those proceeding through reactive intermediates, for which it is possible to define a spatial position in the reactor. When one writes out a reaction, reagents are drawn coming together, creating an intermediate such as an organolithium species that then reacts e.g. with an electrophile to give the desired product. Traditionally, all these species are present together presenting multiple potential reaction pathways, including the formation of side products. In an attempt to control the reaction selectivity cryogenic conditions are often required. However, flow modules can be designed to create a system that reflects the elementary steps of a reaction, including the physical position of its intermediates, similar to the way it is drawn (Figure 1.2). Thereby, short living and highly reactive species can be reproducibly formed and harnessed in flow more efficiently and safely than in batch[13].

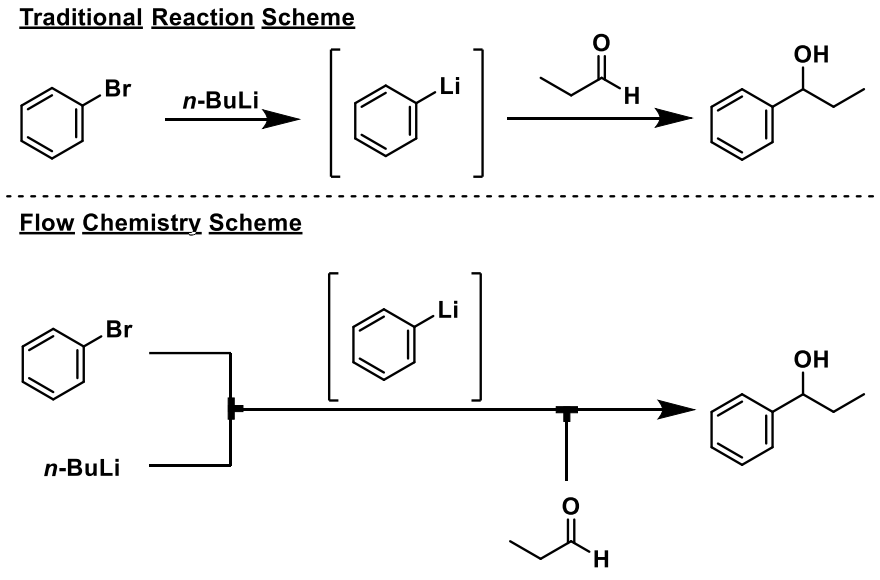

Figure 1.2. (top) A typical example of how chemists write out a reaction. (bottom) flow generation of an organolithium. The reactive species is generated cleanly and delivered directly to the electrophile – creating a flow system identical to the “ideal” written process.

Developing a process in a flow system offers easier scalability, because scale-up can be achieved by using the same equipment adopted for the development phase, and

simply letting the system running for a longer time, or by *numbering-up* multiple systems of the same kind operating in parallel[14,15].

The mentioned advantages have attracted to flow chemistry not only academics, but also researchers from pharmaceutical agrochemical industries, as processes which are safe, efficient, green, cost-effective and have a low footprint are of great appeal[16,17].

Having reproducible access to intermediates and chemical transformations offers the possibility of using such single-step processes as units for chemical assembly lines[18]. Single-step modules can be connected together to create a multi-step process, whether that is combining synthesis and work-up/purification or stitching together multiple synthetic operations in the pursuit of a target molecule. In flow chemistry, when multiple units are linked together in a continuous linear setup, it is called a telescoped process[9].

The advantages of such processes are significant, with considerable reduction of purification steps, time of synthesis, waste, and manual operations and of course the prospect of automating the whole sequence of operations[1,4]. However, there are several limitations that must be considered as well. Due to the continuous addition of reagent mixtures via the feed lines, there is a constraint between flow rate, reactor volume and residence time: slow reactions require large reactors/low flow rate, whereas fast reactions need small reactors/high flow rate (Figure 1.3).

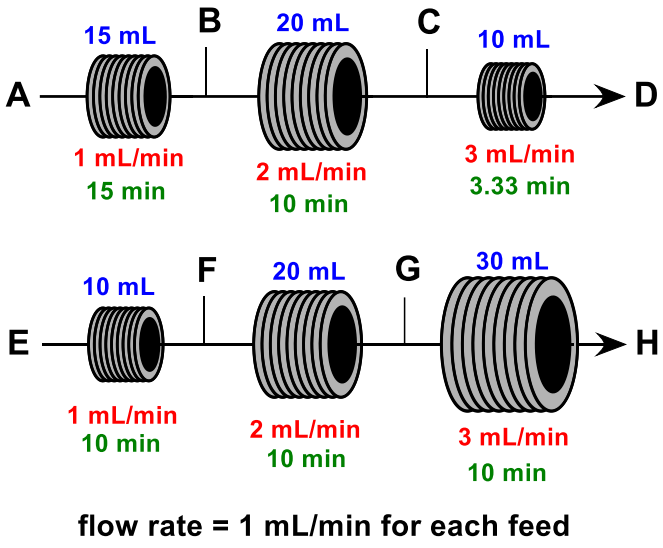

Figure 1.3. Relationship between flow rate, reactor volume and residence time: flow rate is dependent on the set values for new feeds and previous steps, and the residence time depends on flow rate. Different reactors with different volumes are needed in each step. For every new process reactors must be replaced with others of the proper size.

This constraint entails that a particular multistep process requires a specific sequence of reactors with customized volumes determined by the residence times necessary for each step. This means that such systems must be reconfigured for every new target molecule and physical intervention is required to resize and recombine

modules, increasing the arduousness of automating the related processes[19]. For this reason, each telescoped process is typically designed to make one specific molecule, meaning that once completed, the entire process must be broken down, redesigned, and rebuilt for the next target. Thus, even though the equipment itself is reusable, the telescoped linear setups are single purpose, because they are dedicated to the synthesis of only one target.

Byproducts and unused reagents from previous steps are carried through the subsequent modules. These can sometimes be removed via inline workups (creating more complex processes), otherwise they can have a significant impact on the yield, selectivity, or even compromise the achievement of the desired product. The same goes for solvents. While prototypes[20] and reagent-specific workarounds[21] exist, the most common approach to telescoped flow reactions is to find a solvent that is compatible with all the different transformations to be performed. However, this compromise often means that the chosen solvent is not optimal for each transformation, and can negatively impact reaction yield, selectivity, and productivity. The general rule of thumb for solvents and reagents in a continuous flow synthesis is that once something is added for one step, it is there throughout the rest of the process, for better, or more commonly, for worse.

The more units are linked together, the more complex the system becomes. This is true from a hardware perspective (having enough equipment available), an operations perspective (more potential points of failure, longer time to reach steady-state[22]), and a chemical perspective (impact of byproducts on the downstream processes, potential solubility issues).

Furthermore, running a multistep process in continuous flow means that every step is happening simultaneously, therefore if the same conditions are needed at more than one stage of the process the related modules must be repeated (Figure 1.4). Linear systems often require multiple heated reactor units, a considerable number of identical work-up modules, and a copious number of pumps that increases with the number of steps. This redundancy causes the costs of such processes to skyrocket and equipment availability becomes a limiting factor for the implementation of long multistep flow syntheses.

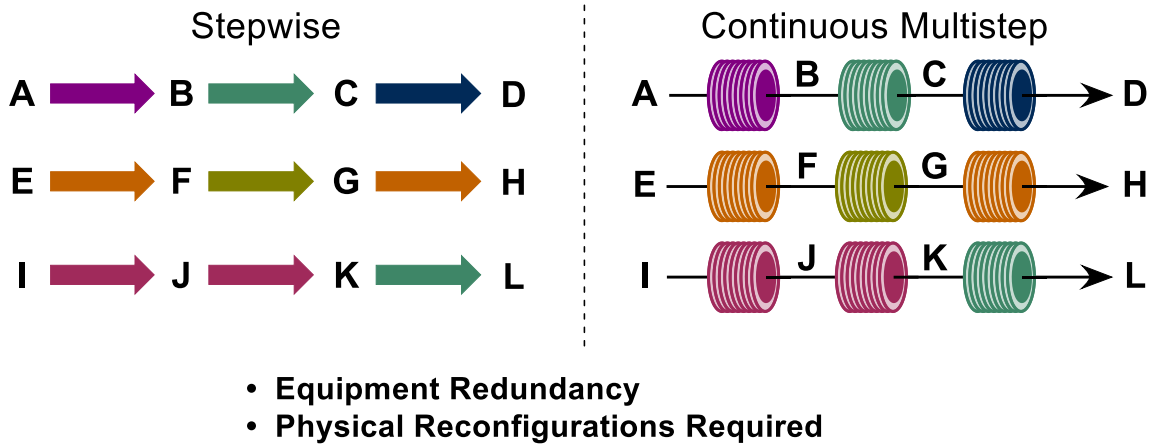

Figure 1.4. Multistep continuous flow processes. Every linear combination is dedicated to one target and if the same conditions are required twice in the same process, two identical modules need to be repeated.

1.3 Automated synthesizers - linear *vs*. iterative processes

Several efforts have been made to build an automated platform to serve as a universal synthesizer which allows for the synthesis of as many targets as traditional organic synthesis, with minimum need of manual intervention. Such systems can be distributed in two main classes: linear synthesizers, which rely in general on continuous flow chemistry, and iterative synthesizers, which are based on solid-phase synthesis. In the following sections a brief overview on both approaches will follow, with a focus on their application to the automated synthesis of small molecules and the identification of their main advantages and disadvantages.

1.3.1 Automated platforms based on a linear approach

Flow systems are immediately suitable for automation as their basic components are electronic devices such as pumps, flowmeters, and valves. Another strength of flow technology in this respect is its modularity. As described before, flow modules provide standardizable access to chemical transformations and can therefore be used as interchangeable pieces in a multistep process. Such reconfigurable setups can target many different compounds through an indefinite number of combinations of chemical reactions, ensuring versatility and enabling the exploration of a wide chemical space.

On the other hand, reconfiguration of these linear systems based on continuous flow is a physical operation that includes disassembly and re-assembly of the relevant modules and the automation of such processes is rather challenging.

Few examples of automated synthesizers exist, based on this linear continuous-flow approach linking flow chemistry modules in a telescoped manner[23,24,25]. The effort required to automate these machines has generally been justified by the need of platforms

for *on-demand* production of pharmaceuticals as an alternative to the current non-continuous or “batch” manufacturing. Therefore such systems have focused on the end-to-end continuous flow synthesis and formulation of active pharmaceutical ingredients (API) programmable through software interfaces[23]. One of the first significant synthesizers of this class was developed by researchers from the Massachusetts Institute of Technology (MIT) and showed a sequence of modules, which could be used or skipped in the synthesis process as needed[24]. Thus the system is reconfigurable, though the possible combinations are limited by the position of the modules and therefore equipment redundancy cannot be avoided (Figure 1.5). The capabilities of this on–demand reconfigurable synthesizer were showcased by synthesizing four different APIs: diphenhydramine hydrochloride, lidocaine hydrochloride, diazepam, and fluoxetine hydrochloride.

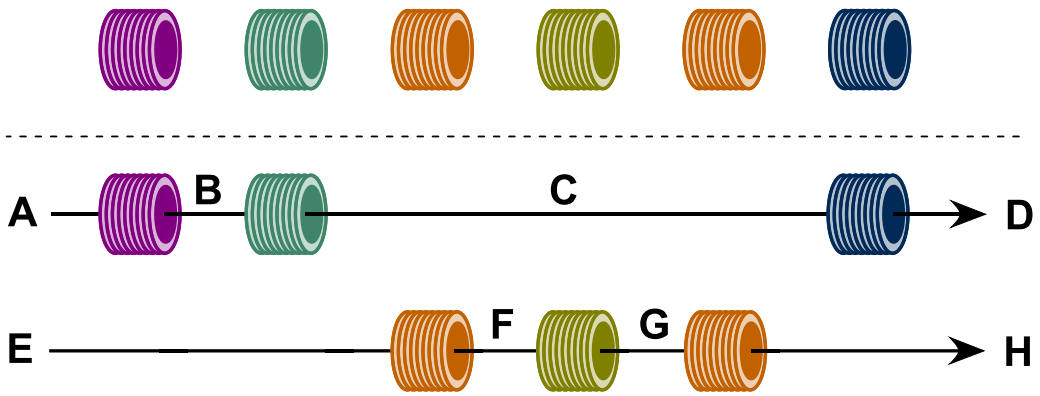

Figure 1.5. Reconfigurable automated system based on the linear continuous flow approach[24].

Automated synthesizers based on a linear approach have evolved over the past decade. The latest version of the MIT system is able to provide access to every module at any point of the synthesis through automatic reconfiguration performed by a robotic arm[25] (Figure 1.6). This system has a set of reactors held in a storage location that can be selected and inserted into the flow stream using a six-axis robotic manipulator. The same robotic arm is also capable of connecting the requisite tubing between the different units.

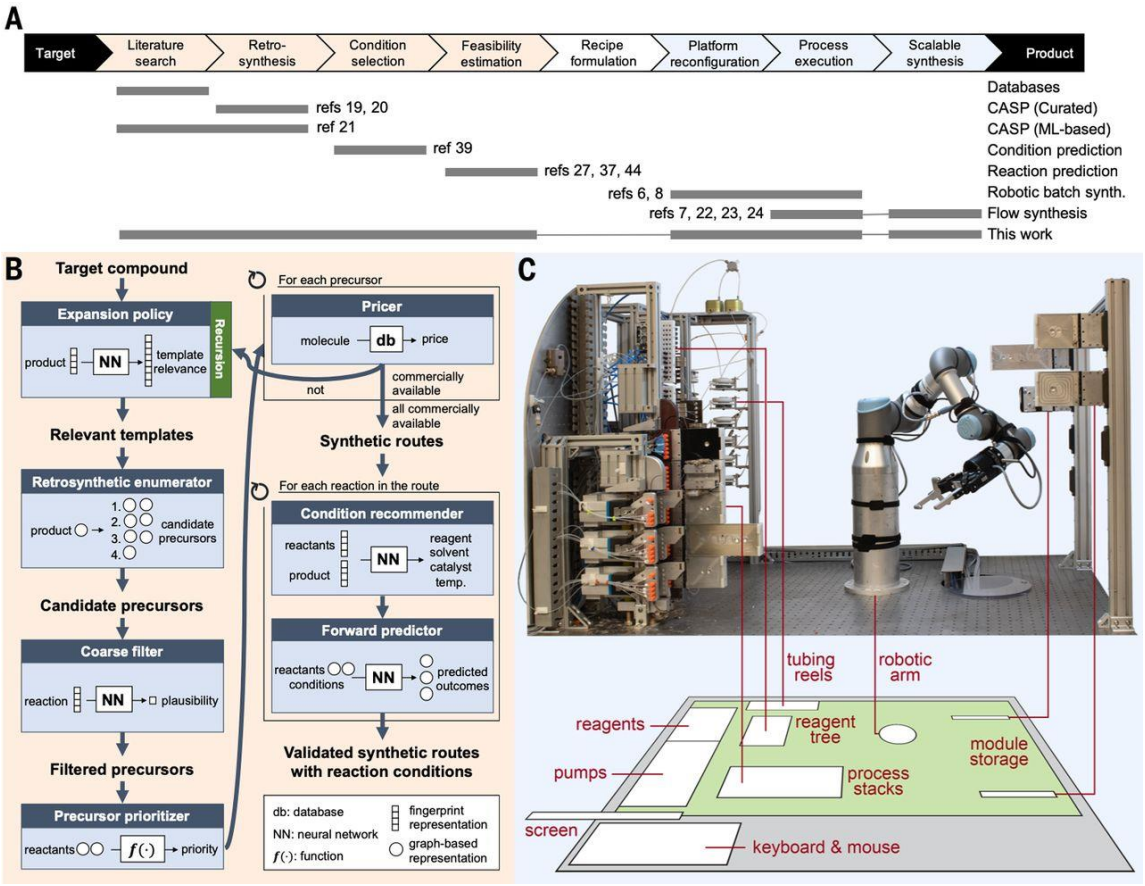

Figure 1.6. linear syntheses: an automated, robotic platform for the flow synthesis of organic compounds informed by AI planning. Reprinted with permission from reference 25.

The reagents are connected to the process stack through a dedicated switchboard that connects the fluid pumps, outlets, and waste streams to each module as required by the chosen chemical process. Two pumps are equipped with selection valves, connected with up to twenty-four feedstocks each, thus potentially allowing a wide variety of syntheses to be performed. The reaction modules include flow reactors of different volumes (100 mL to 3 mL), packed bed reactors (1 to 2 mL) capable of operating at temperatures from ambient to 200 °C with pressures up to 17 bar, and a membrane separator for liquid–liquid extraction. Fluid connections between adjacent units are achieved by vertically stacking them in the required order and a continuous stream of reagents is then passed through the sequence.

The concept was demonstrated by synthesizing six different active pharmaceutical ingredients (aspirin, secnidazole, lidocaine, diazepam, (S)-warfarin, and safinamide) and two libraries of quinapril and celecoxib derivatives.

Although way more flexible than the previous one, this upgraded version of the modular linear synthesizer still suffers from some of the limitations of continuous flow systems. The issue related with the reconfiguration of modules is solved by the introduction of the robotic arm, but processes are still happening under continuous flow

conditions. This implies that equipment redundancy cannot be circumvented when the same conditions are needed more than one time within the same synthesis and that parameters like flow rate and concentration are still affected by the values chosen for every feed along the process.

1.3.2 Automated platforms based on an iterative approach

Conscious of the limitations of the customized linear approach for small-molecule synthesis, particularly when it comes to automation, researchers started considering whether generalized processes could be developed for the production of many different products using the same manufacturing strategy. For example, solid-phase synthesis constitutes an automatable alternative to continuous flow that is particularly well-suited for the synthesis of biopolymers such as peptides[6], oligonucleotides[7], and oligosaccharides[8]. Assembly is accomplished by executing iterative cycles of activation, coupling and deprotection steps. Using this strategy monomers are linked together through the same type of chemical bond; therefore, the task of the machine is limited to the repetitive execution of one type of chemical transformation. The diversity in the final product is given by the choice of building blocks and the order of the assembly of the building blocks, which are synthesized and functionalized in advance (Figure 1.7).

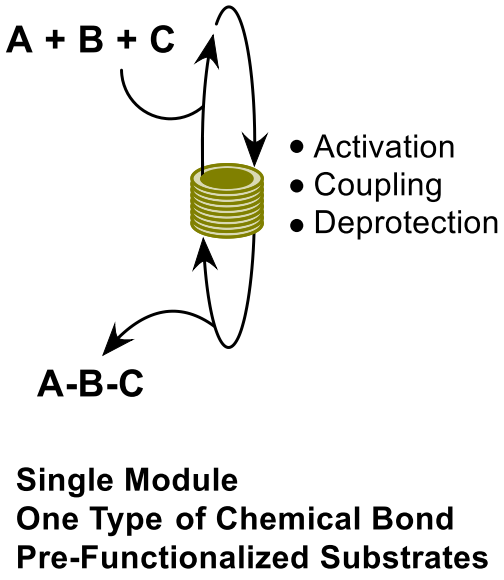

Figure 1.7. Iterative approach: based on the repetition of iterative cycles of activation, coupling, and deprotection steps to attach pre-functionalized monomers to a growing chain.

Access to synthetic oligomers has been expedited with the introduction of automated instruments based on solid-phase synthesis. Given the impact that these platforms have made in the related fields, chemists have started investigating whether small molecules might be accessed through a similar building-block-based approach. Despite their structural diversity, when considering only particular disconnection patterns

(e.g. C-C cross-coupling), many types of small molecules can be considered “modular”. Additionally, a study of 2014 on the database of U.S. FDA (Food and Drug Administration) approved pharmaceuticals highlighted how many small-molecule drugs present some degree of redundancy at the fragment level (e.g. 59% of unique small-molecule drugs contain a nitrogen heterocycle)[26]. Such findings suggested that many small molecules can be achieved by assembling together common subunits (building blocks) through the repetition of one chemical transformation, thus utilizing an iterative synthesis method similar to that of the biopolymer synthesizers.

This concept was demonstrated by Burke et al. synthesizing a broad library of small molecules from different classes, using Suzuki-Miyaura couplings to fuse together pre-functionalized building blocks[27]. An automated synthesis platform based on this technology was developed, employing N-methyliminodiacetic acid (MIDA)-boronate building blocks. This synthesizer exploits the features of the trivalent MIDA-ligand which is able to tune the reactivity of a boronic acid. The stabilization of boronic acids in the MIDA-boronate form is reversible, the MIDA-ligand can be removed under aqueous or mild basic conditions, releasing the reactive boronic acid. Bifunctional halo MIDA-boronate building blocks can be assembled through iterative cycles of cross-coupling and deprotection (Figure 1.8).

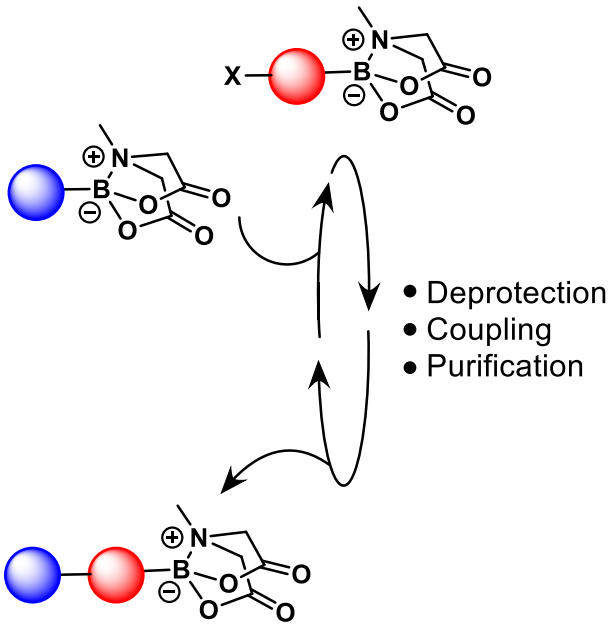

Figure 1.8. Automated cycle involving deprotection, coupling, and purification steps. Each cycle couples a boron-protected haloboronic acid (red sphere) to a growing synthetic intermediate or an initial building block (blue sphere).

This process works in solution-phase; therefore, a purification module must be implemented to separate the growing product from the rest of the reaction mixture after each cycle. A purification step could be added at the sequence exploiting one unique

feature of MIDA-boronates, which have no mobility on silica gel with eluents such as diethyl ether and methanol but are instantly released with tetrahydrofuran (THF). This allowed the development of a catch-and-release[28] purification process for the MIDA-boronate-containing intermediates that was coupled to their automated iterative assembly.

This iterative approach is more easily automated than the linear one, but it requires multiple off-line operations prior to the automated assembly of the molecules (like the synthesis of the properly functionalized building blocks) and the concept itself lacks the versatility required to access the structural diversity of organic molecules because each synthesizer based on this approach would only be capable of creating one type of chemical bond (e.g. $C(sp^2)$ - $C(sp^2)$ bond).

1.4 The radial synthesis paradigm

Once the advantages and disadvantages of both linear and iterative approach to automated multistep synthesis are identified, it results evident that the two approaches complement each other. Aiming at a universal synthesizer, it is desirable to combine some features from both. On one hand, the versatility of modular flow systems is needed to give access to chemical diversity. This diversity is unattainable with simple iterative approaches, which are only capable of forming a single class of bonds. On the other hand, the iterative reutilization of modules in different steps of the same synthesis is crucial to escape the limitations of telescoped synthesis previously described; it enables the user to select conditions, such as flow rate and residence time, independently from the values set for previous steps while avoiding redundancy of equipment.

The radial synthesis concept is thought to combine the advantages and overcome the limitations of linear and iterative approach to multistep synthesis. It is based on a series of individually accessible reactors arranged around a central switching station[29] (Figure 1.9). In the radial paradigm, single transformations and multistep sequences are performed as sequential, but not simultaneous, series of operations. By decoupling the subsequent steps, reactors can be reused under different conditions and residence times are independent of any previous step(s). Thus, the amount of equipment required can be considerably reduced and reconfigurations of the physical system between synthetic processes are avoided. In this way, instead of a multiple-module, single-purpose setup (like continuous flow setups) or a single-module, multiple-purpose one (like the iterative synthesizers), it is possible to conceive a multiple-module, multiple-purpose instrument that expands the chemical diversity achievable.

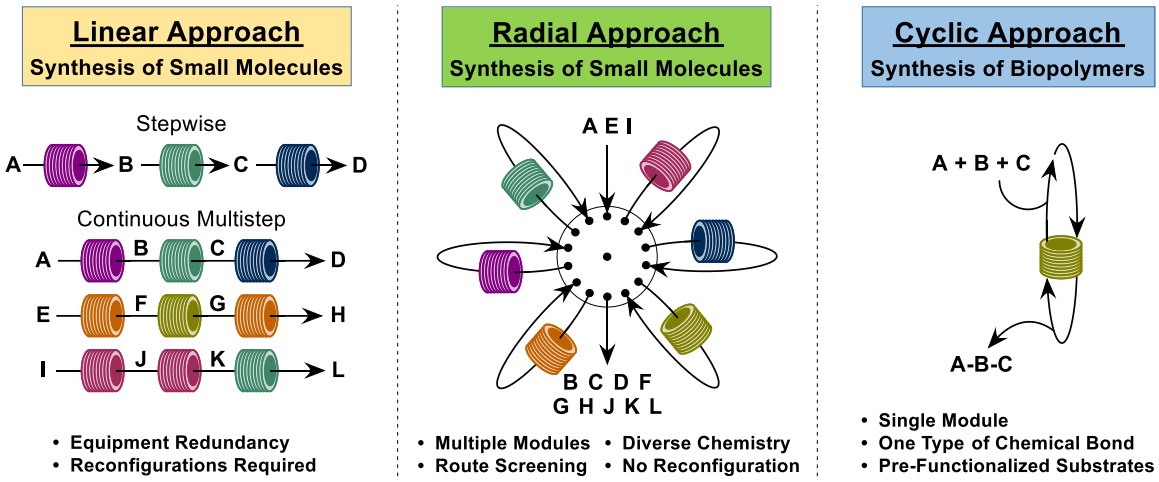

Figure 1.9. Radial synthesis combines the advantages of the cyclic and the linear approach. Flow modules surrounding a central core require minimal equipment while retaining maximum synthetic versatility. Reprinted with permission from ref 29

Several technical challenges need to be addressed to put this concept into practice. Solutions must be moved in a radial fashion in a closed system, stable intermediates need to be stored, and various flow paths necessary for a wide breadth of synthetic routes have to be programmed and controlled.

Breaking the linearity of continuous flow processes means that reagents cannot be pumped continuously, therefore an instrument based on the radial approach must work with discrete amounts of solutions. Such liquid segments containing the reaction mixture must be pushed by a carrier (a fluid or gas that is inert and not miscible with the reaction mixture). This difference from continuous flow systems allows for minimum waste of material during process development, though concerns about transferability of such processes in continuous flow will have to be addressed.

1.5 Aim of this thesis

The aim of this thesis was to develop and validate an automated platform for multistep synthesis based on the radial paradigm. Such a prototype was built from commercially available parts and was designed in order to require no physical reconfiguration between different synthetic processes.

Thanks to the sequential but non-continuous nature of the steps the same reactor can be used at different temperatures within one multistep process. By not performing all steps simultaneously, the flow rates for each reaction, that define the reaction times, are independent of each other. In this way, long and short residence times can be combined in any order without changing the equipment.

Storing stable intermediates makes both convergent and linear syntheses possible and enables the comparison of different synthetic approaches on the same instrument. In

addition, concentrations can be screened to accelerate optimizations via inline dilution of reagents. A total of twelve different reagents can be stored in the reagent delivery system and recombined at will, allowing for the quick generation of compound libraries. In-line analysis is possible thanks to the incorporation of different analytical devices (IR and NMR spectrometers) which provide feedback on each individual synthetic operation. Thanks to its modularity and compatibility with standard flow chemistry setups, the integration of new modules within the instrument is straightforward and its capabilities can be rapidly and easily implemented.

This platform is capable of complete flexibility over accessible reaction conditions for single or multistep synthesis and is driven by a software that was developed in-house upon construction of the hardware and controls all components as an ensemble

2 The radial synthesizer

This chapter has been partially modified from: Chatterjee, S.;* Guidi, M.;* Seeberger, P. H.; Gilmore, K. Automated Radial Synthesis of Organic Molecules. *Nature* **2020**, 579, 379–384. DOI: 10.1038/s41586-020-2083-5

Further permissions related to the material excerpted should be directed to Springer Nature.

* equal authorship

2.1 Design and hardware

The radial synthesizer (Figure 2.1 and Figure 2.2) is composed of ten valves (seven multiposition and three injection valves), connected by perfluoroalkoxy alkanes (PFA) tubes and polyether ether ketone (PEEK) fittings and junctions. The system is filled with nitrogen gas (used to push and regulate the liquid flow) and pressurized. The stream of N_2 is regulated by three mass flow controllers (MFC, Bronkhorst EL-FLOW Prestige) and the pressure is maintained by a digital back pressure regulator (BPR, Bronkhorst EL-PRESS P-702CV). All the fluidic connections are made with PFA tubing (Bola) with an internal diameter (ID) 1/32” (0.79 mm) and an outer diameter (OD) 1/16” (1.58 mm).

PFA was chosen for the wetted parts because of its higher temperature resistance, in comparison to fluorinated ethylene propylene (FEP) and its higher transparency when compared to polytetrafluoroethylene (PTFE). A gas carrier (N_2) was preferred to fluorinated oils as inert carrier fluid, due to the latter’s propensity to become miscible with organic solvents at elevated temperatures[30].

Figure 2.1. Picture of the radial synthesizer

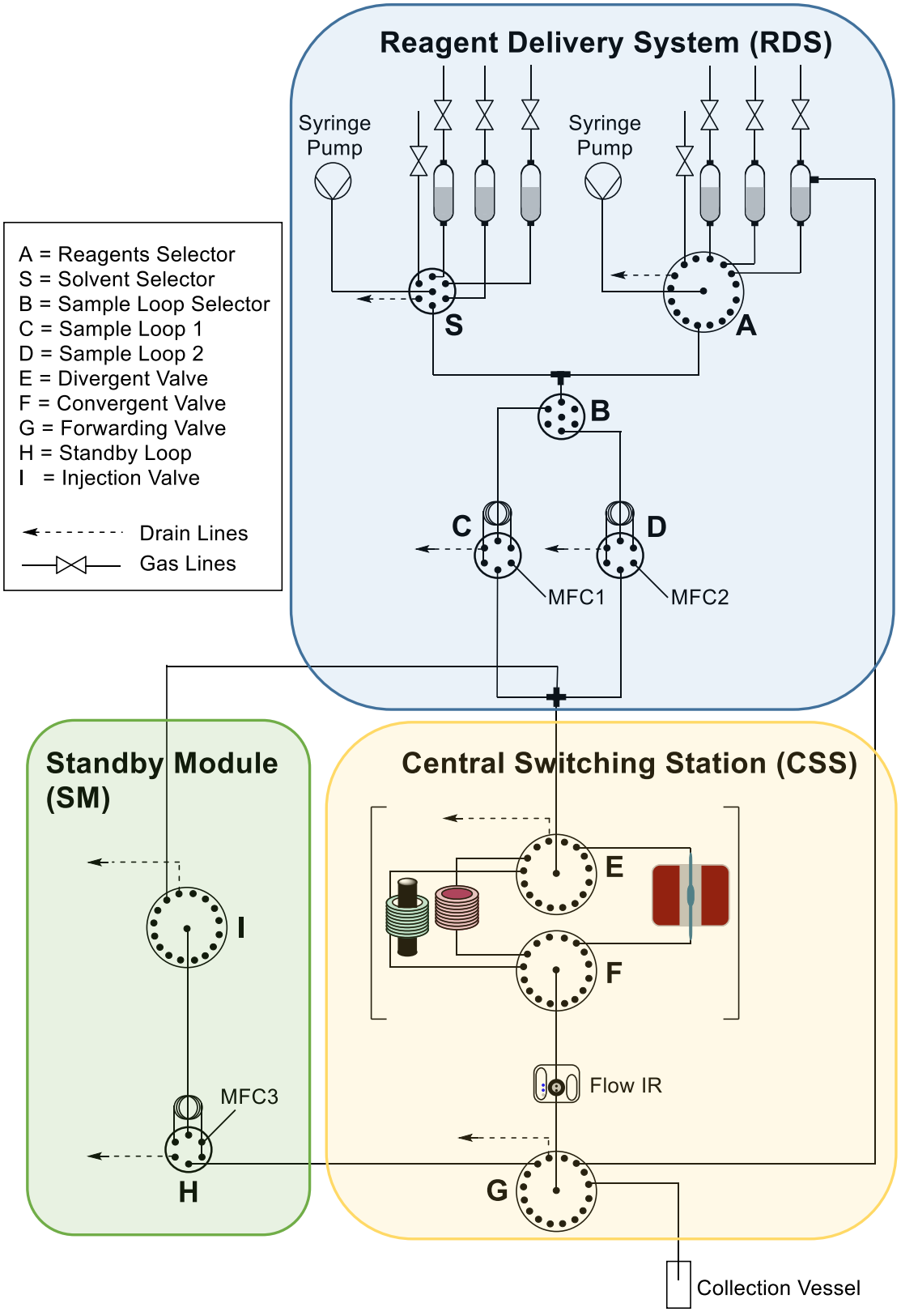

Figure 2.2. The radial synthesizer is composed of three main blocks: the reagent delivery system (RDS), the central switching station (CSS) and the standby module (SM).

In order to avoid ambiguity, all the lines of the system potentially utilized by gas or liquid are represented as solid lines. The synthesis pathway lines connect the valves to

each other, and each pathway finally leads to a pressurized vessel or the waste container. The pressurized gas lines are directly connected to the BPR. Drain lines are connected to the waste container that is itself pressurized by a connection to the BPR. All drain lines (leading to the waste) are dashed lines, and all lines crossed only by gas are distinguished by solid lines featuring the backpressure symbol (Figure 2.3).

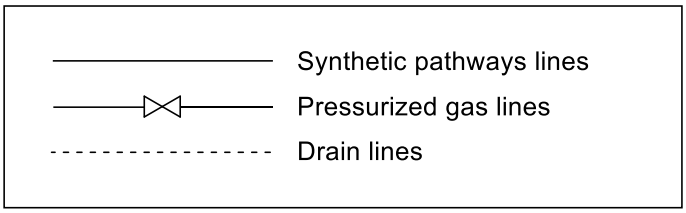

Figure 2.3. Legend for the three different types of lines in the synthesizer. All lines are PFA tubes ID 1/32", OD 1/16".

All tubing is joined together and connected to valves, reactors, and syringes using standard HPLC fittings. Tee junctions and cross junctions are PEEK, PTFE and ETFE (ethylene tetrafluoroethylene) (IDEX H&S) (Figure 2.4). A cross junction is used between the reagent delivery system and the central station and it is the site where reagents and intermediates are mixed. Tee and cross junctions are used to combine all the gas lines together converting them to the BPR, and to combine all the drain lines together conveying them to the waste container.

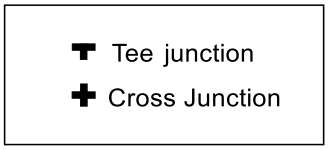

Figure 2.4. Tee and cross junctions are used for the connection between lines.

Three types of valves are utilized in the system: 16 ports and 6 ports multiposition valves as well as 6 ports injection (two-position) valves (Figure 2.5). All the valves are KNAUER valves of the series AZURA. Multiposition valves have the capability to connect one peripheral port at a time to the central one. Two-position valves have the capability to connect their ports through two different pathways; one for loading and one for injection.

Figure 2.5. The three types of valves utilized in the synthesizer.

Solvents and reagents are stored in homemade pressurized vessels of 5 mL and 10 mL volumes (Figure 2.6). The vessels are built using PTFE tubes (Bola, OD 12 mm, ID 10 mm) and they are provided with two outlets (necks) made with reducing unions 1/4 to 1/16” (from Swagelok) at the top and at the bottom of the vessel.

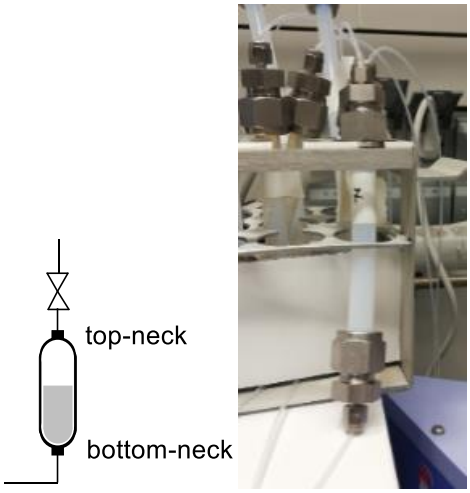

Figure 2.6. Two-neck pressurized vessel for storage of reagents and solvents. The bottom-neck is connected to the Reagents Selector **A** (section 2.1.2.1) while the top-neck is connected to one of the pressurized gas lines.

Similar vessels were built for the storage of the intermediates generated during multistep processes. Those vessels have an additional neck made with a Tee union (1/4”) and another reducing union 1/4" to 1/16” (from Swagelok) connected via a PFA tube (OD 1/16”) to an outlet of the forwarding valve **G** for the collection of the intermediate (Figure 2.7).

A three-neck vessel identical to the one used for the storage of intermediates but with a larger volume (30 mL) is used as a pressurized waste container. There are eight drain lines in the system (dashed lines in Figure 2.2) that are joined together with tee and cross junctions, merging into a common line that leads to the side-neck of the waste container.

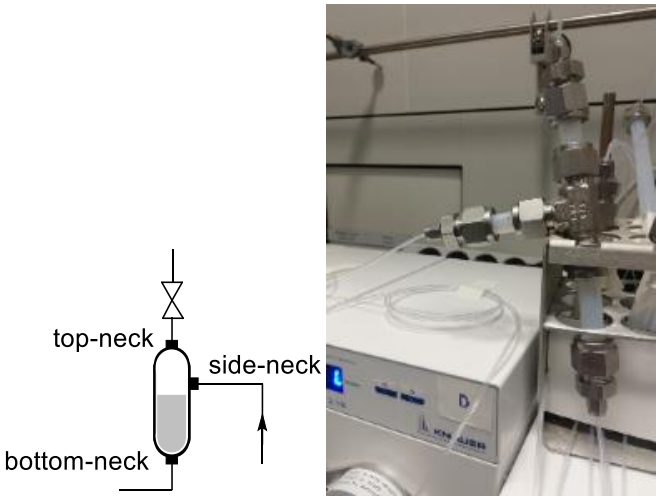

Figure 2.7. Three-neck pressurized vessel for storage of intermediates**.** The bottom-neck is connected to the Reagents Selector **A**, the top-neck is connected to one of the pressurized gas lines and the side-neck is connected to a line coming from the forwarding valve **G**.

Reagent and solvent delivery is accomplished by a syringe pump (Harvard Apparatus ELITE infusion/withdrawal) (Figure 2.8) equipped with a gas-tight glass syringe (Hamilton, volume 5 mL).

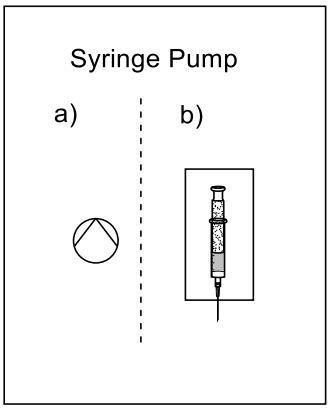

Figure 2.8. Syringe pump infusion/withdrawal are depicted in two variations in the schemes of this document, either as a) schematic representation or b) detailed representation.

The loops are PFA coils of 0.5 mL, the heated reactor is a 20 mL coil connected to a heated reactor module (Vapourtec R4) and the photoreactor is a custom-built 10 mL FEP coil irradiated by a LED lamp (420 nm, 72 W) (Figure 2.9).

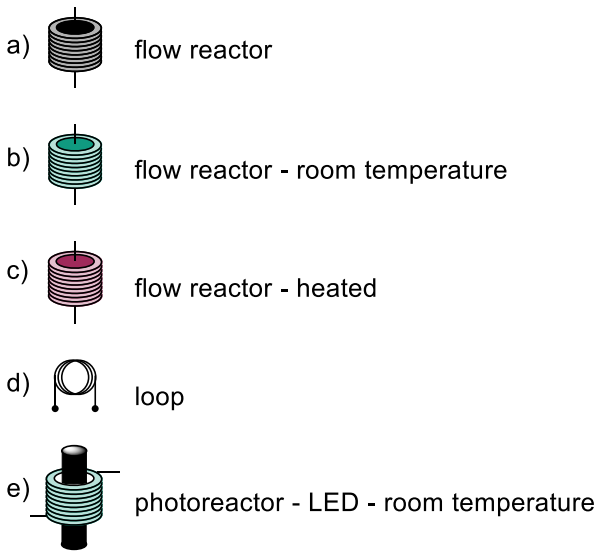

Figure 2.9. The variable temperature reactor connected to the system is represented in three different manners within this document a-c). a) General representation of the flow reactor. b) representation of the flow reactor when at room temperature. c) Representation of the flow reactor when heated. d) The 0.5 mL loop used in both the reagent delivery system and the storage module. e) Representation of the flow photoreactor

The analytics are an in-line IR spectrometer (Mettler Toledo Flow-IR) (Figure 2.10 a and b) and a benchtop NMR spectrometer (Magritek Spinsolve 40 MHz NMR) (Figure 2.10 c and d).

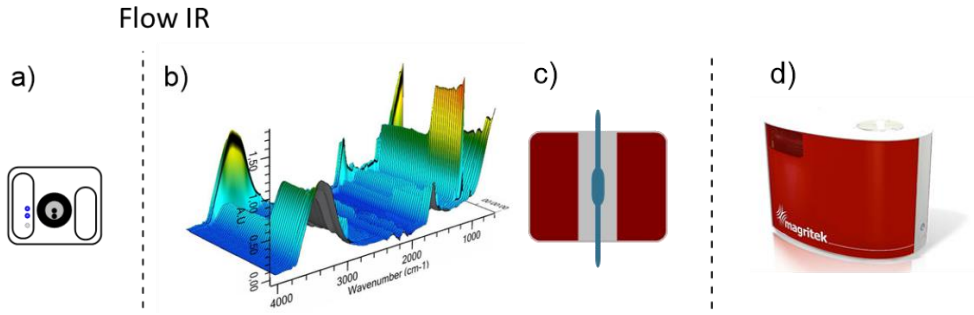

Figure 2.10. a) Schematic representation of the flow-IR. b) Three-dimensional profile of a multistep synthesis passing through the flow-IR (axes: x = wavelength; y = intensity; z = time). c) Schematic representation of the flow-NMR. d) Picture of Magritek Spinsolve benchtop NMR.

The three sections of the radial synthesizer (RDS, CSS, SM) will be described separately in detail, with a focus on the function of every component.

2.1.1 System compatibilities

The system proved to be compatible with all common organic solvents and all reagents utilized in the current work. The only incompatibility found to date is to triflic anhydride, which caused the corrosion of the rotor seal of one valve. After consulting the manufacturer (KNAUER) we learned that their rotor seals are made of polyoxymethylene

(POM), and can be replaced with components made of different materials when specifically needed. All the other parts did not show any weakness neither in the presence of strong acids nor bases, showing good performances at high pressure (the system was tested up to 8 bar) and temperature (up to 150 °C).

2.1.2 Reagent delivery system (RDS)

Reagent and solvent delivery is accomplished using a set of five valves, two syringe pumps and 15 pressurized vessels in which initial reagents and solvents – as well as the intermediates formed during the syntheses – can be stored (Figure 2.11).

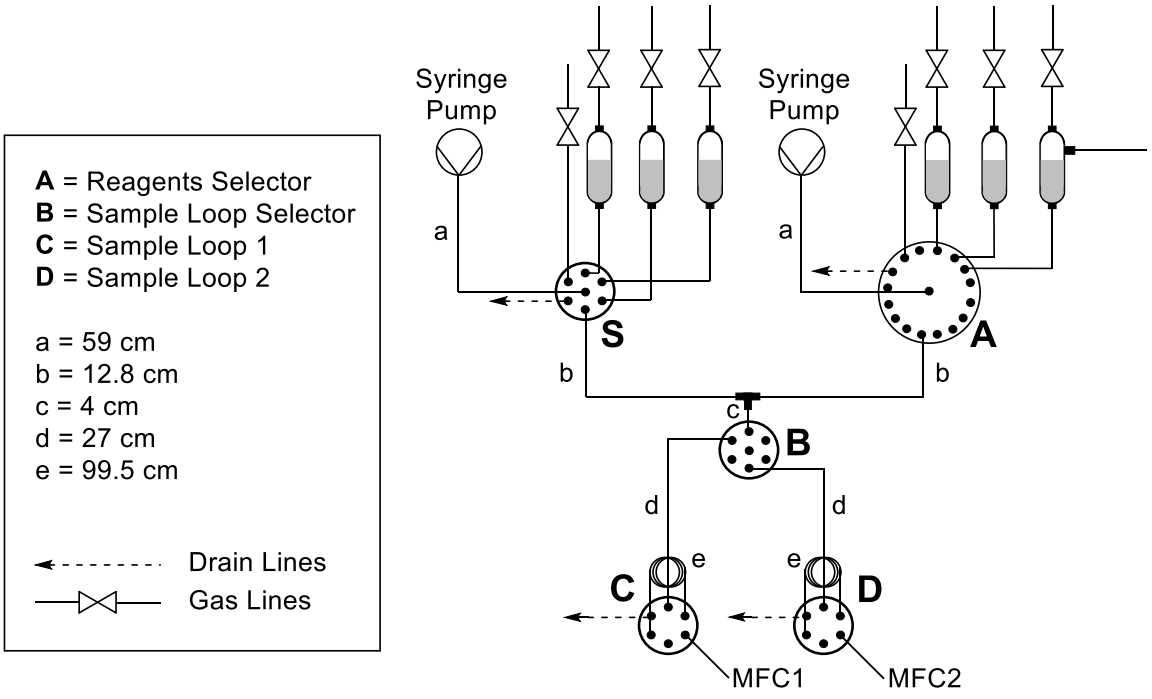

Figure 2.11. Detail of the reagent delivery system with its components, as well as the length of each significant line. The lines that connect the pressurized vessels to the reagent selector **A** and/or solvent selector **S** are not significant, they are all 50 cm PFA tubes, but their volume is not relevant since they are always full of solution once primed.

2.1.2.1 Reagent and solvent selectors (A and S)

The reagent selector works in withdrawal and infusion mode: a line connects the syringe pump to its central port that can be connected in turn to a single peripheral port at a time. Four out of sixteen peripheral ports are dedicated to specific purposes (see below), the rest are connected to the homebuilt vessels which contain reagents and solvents.

Special peripheral ports in the reagent selector (A):

Port 12: Used to load the reagents in the vessels at the beginning of the process (before pressurizing the system). Using the syringe pump, the reagents are withdrawn

from port 12 and then injected into the desired vessels. Port 12 is then properly sealed before the pressurization of the system (Figure 2.12).

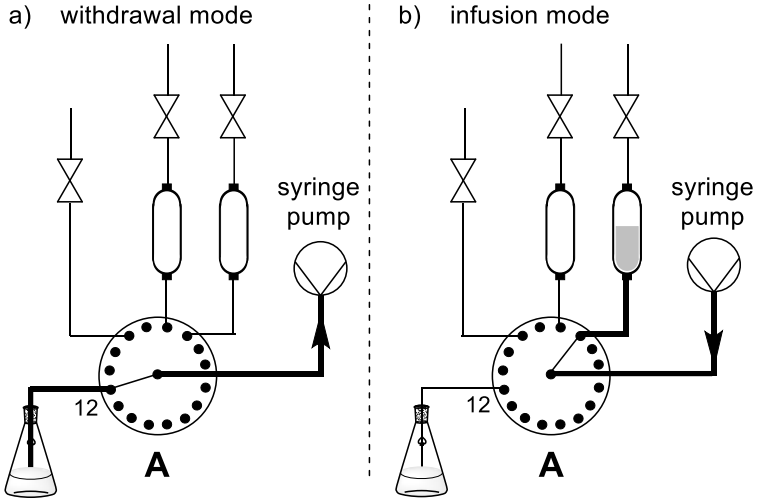

Figure 2.12. a) Withdrawal of reagent solution through port 12 in the syringe pump. b) Infusion of reagent solution from the syringe pump to the intended vessel.

Port 16: Drain line to vent out the excess of reagents and solvents during the syringe wash and priming cycles. This port is always used when the RDS is in infusion mode.

Port 4: Outlet towards the sample loop selector (**B**) to fill the loops with the reagent solution previously withdrew. This port is always used when the RDS is in infusion mode (Figure 2.13).

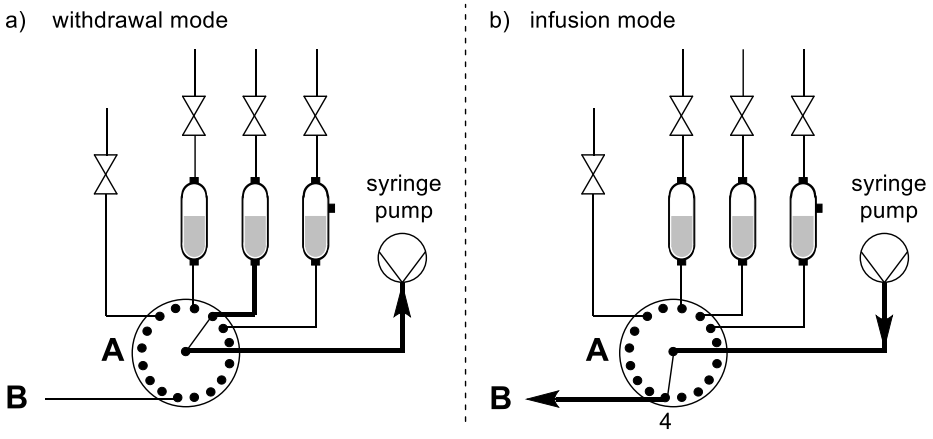

Figure 2.13. a) Withdrawal of reagent solution from the vessel in the syringe pump. b) Infusion of reagent solution from the syringe pump through port 4 towards sample loop selector **B**.

Port 15: Connected to a pressurized gas line. This port is necessary because every reagent injection towards the sample loops needs to be followed by a certain volume of gas (0.4 mL) to clear the common lines (lines a and b in Figure 2.11) before the withdrawal of a new reagent. The syringe positioned in the syringe pump is facing down so that the gas withdrawn stays above the liquid and cleans the syringe tip and the tubes during the

infusion. Thus, every withdrawal of reagents is followed by a 0.4 mL withdrawal of gas from port 15 (Figure 2.14 b) and the total volume will be infused through port 4 towards the sample loops (Figure 2.14 c).

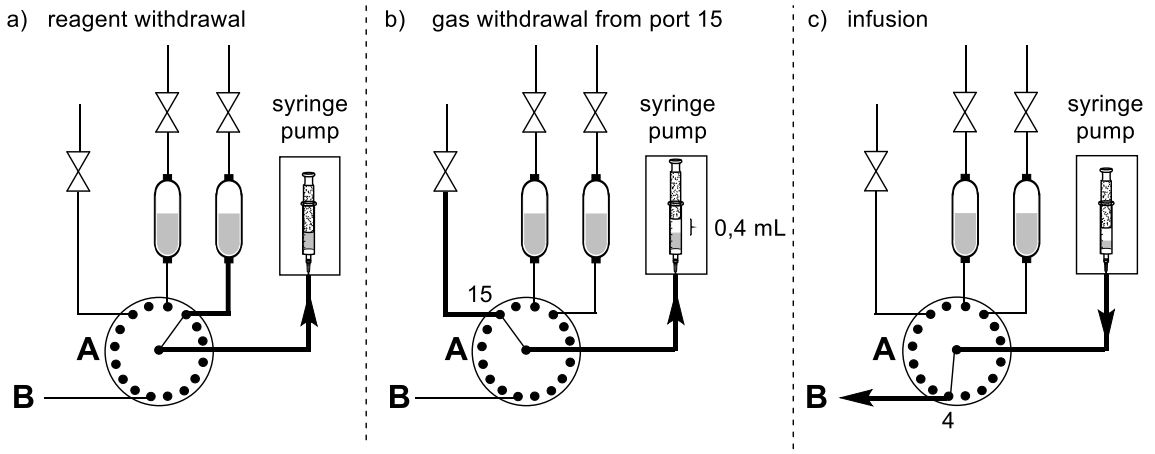

Figure 2.14. a) Withdrawal of reagent solution from the vessel in the syringe pump. b) Withdrawal of 0.4 mL of gas from port 15. c) Infusion of reagent solution and gas from the syringe pump through port 4 towards sample loop selector **B**.

The remaining 12 ports are all connected to pressurized vessels containing reagents solutions and solvents (two-neck vessels as in Figure 2.6) or dedicated to the storage of intermediates (three-neck vessels as in Figure 2.7).

Special peripheral ports in the solvent selector (S):

The solvent selector works in the same way as the reagent selector. Four out of six peripheral ports are dedicated to some specific purposes (see below), the remaining two are connected to the homebuilt vessels containing solvents.

Port 3: Used to load the reagents in the vessels at the beginning of the process (before pressurizing the system). Using the syringe pump, the solvents are withdrawn from port 3 and then injected into the desired vessels. Port 3 is then properly sealed before the pressurization of the system (equal to port 12 in reagent selector: Figure 2.12).

Port 6: Drain line to vent out the excess of reagents and solvents during the syringe wash and priming cycles. This port is always used when the RDS is in infusion mode.

Port 4: Outlet towards the sample loop selector (**B**) to fill the loops with the reagent solution previously withdrawn. This port is always used when the RDS is in infusion mode (equal to port 4 in reagent selector: Figure 2.13).

Port 5: Connected to a pressurized gas line. This port is used to clear the common lines (equal to port 15 of the reagents selector: Figure 2.14 b). Thus every withdrawal of reagents is followed by a 0.4 mL withdrawal of gas from port 5 and the total volume will be infused through port 4 towards the sample loops (equal to port 4 in reagent selector: Figure

2.14 c). The reagent and solvent selector work simultaneously at different flow rates which are tuned in order to achieve the desired concentrations in the sample loops.

2.1.2.2 Sample loop selector (B)

The sample loop selector is a six-port multiposition valve that (like the other selectors described above) can connect its central port to one peripheral port at a time. It receives the combined streams delivered by the syringe pumps of the reagent and solvent selector and it diverts the mixture towards the selected sample loop (Figure 2.15).

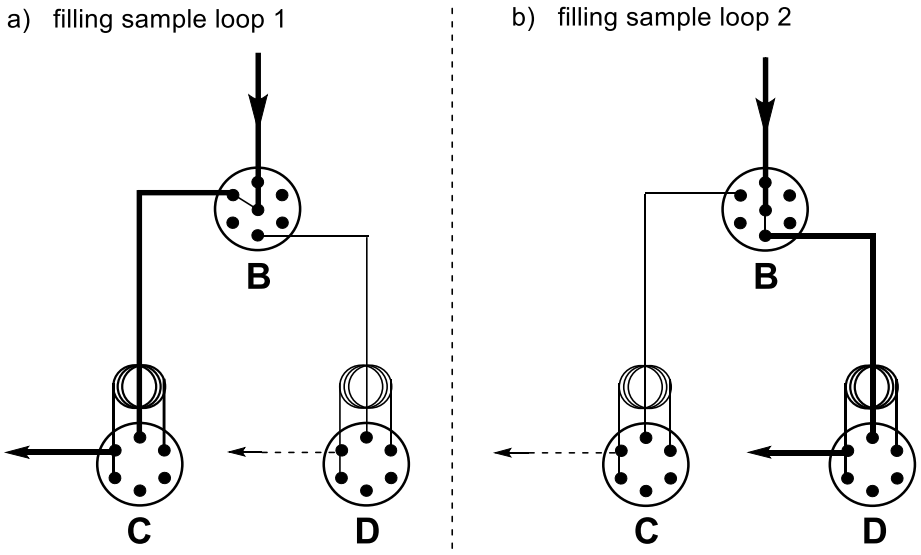

Figure 2.15. Sample loop selector **B**. In both cases, the reagent solution comes from port 4 of reagents selector **A**. The sample loop selector diverts it to a) port 6 loading sample loop 1 (**C**); b) port 4 loading sample loop 2 (**D**).

2.1.2.3 Sample loops (C and D)

The two sample loops are six-port, injection valves that allow two different flow pathways, respectively for loading or injection mode (Figure 2.16). When the sample loop is in loading mode, its loop is connected to the inlet line (coming from the sample loop selector and containing the reagent solution) and to the drain, allowing the excess solution to vent. When the sample loop is in injection mode instead, its loop is connected to the MFC (which pushes nitrogen through the loop) and to the outlet line that leads to the CSS. The two sample loops are sequentially loaded, and they then switch to injection mode simultaneously. The MFCs push both the solutions at the same flow rate.

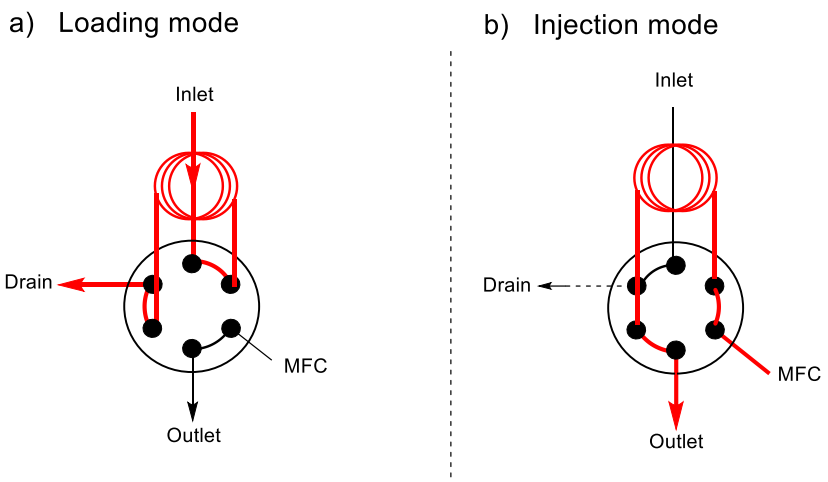

Figure 2.16. Two-position injection valve with sample loop. a) Loading mode: inlet port connected to the loop, connected to the drain port; MFC connected to the outlet port. b) Injection mode: MFC connected to the loop, connected to the outlet port; inlet port connected to the drain port.

2.1.3 Central switching station (CSS)

The two liquid segments coming from the sample loops **C** and **D**, pushed by MFC1 and MFC2, meet each other at a cross junction where they mix and form a liquid segment (reaction mixture) whose volume is the combination of the two reagent segments. This segment enters the central switching station (Figure 2.17). The components of the central switching station are described in detail below.

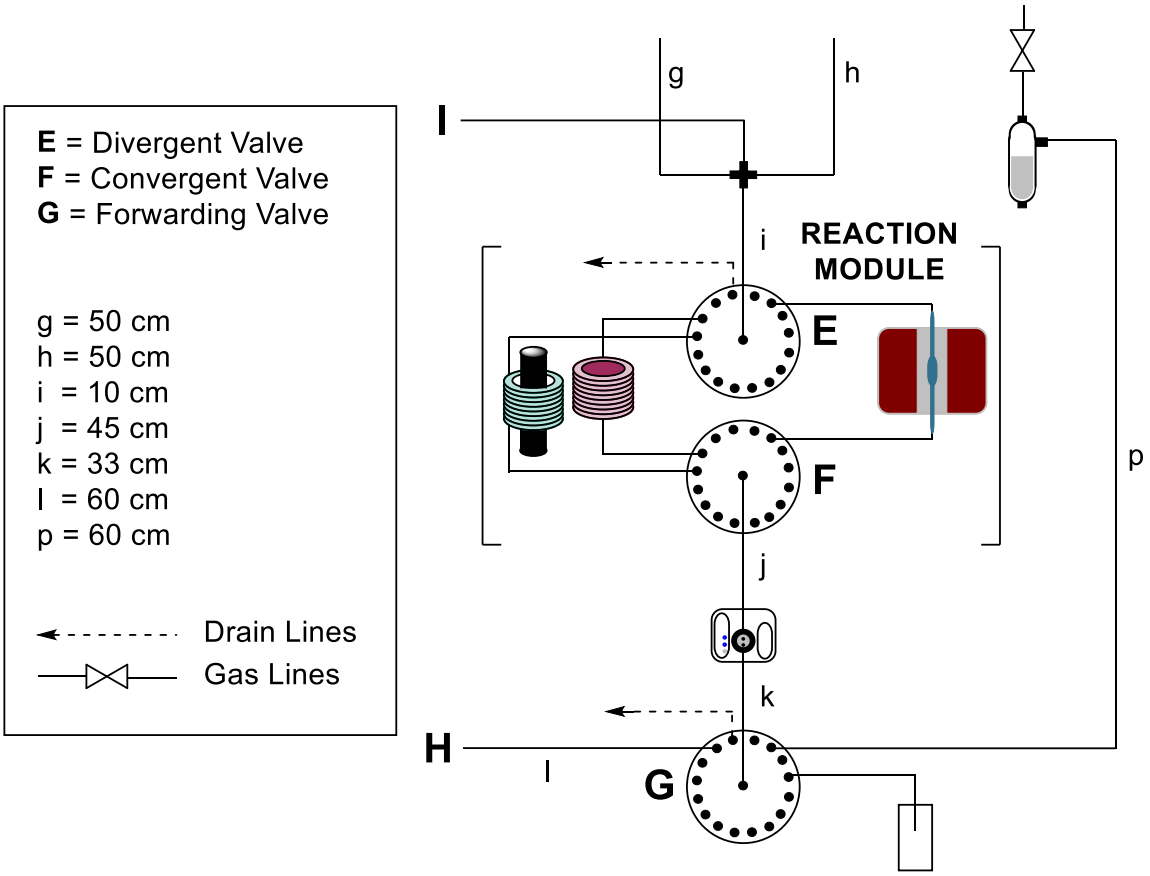

Figure 2.17. The central switching station is composed of three 16-port multiposition valves: divergent valve **E**, convergent valve **F**, and forwarding valve **G**.

2.1.3.1 Reaction module

The reaction mixture slug formed by the meeting of the reagents at the cross junction first reaches the divergent valve (**E**), a 16-port multiposition valve that can connect the central port with a single peripheral port at a time. Selection of peripheral ports gives access to the different reactors. The divergent valve can host up to 15 different reactors (port 16 is connected to a drain line leading to the waste container). The reactors connected to the CSS are so far a 20 mL coil reactor connected to a Vapourtec R4 heating module that can be used at room temperature (Figure 2.9 b) or heated (Figure 2.9 c) and a photoreactor (Figure 2.9 e) that is a 10 mL FEP coil reactor irradiated by a LED lamp (420 nm, 72 W) kept at room temperature by immersion in a water bath.

The reaction mixture flows into the selected reactor for the desired residence time and the stream then enters the convergent valve (**F**), a 16 port multiposition valve that collects all the outlet of the different reactors and channels them into a common line that passes through a Flow-IR (Figure 2.18) before reaching the forwarding valve (**G**).To avoid confusion, inlet and outlet of the same reactor are connected to ports with the same number on the divergent and convergent valves (e.g. the inlet of the heated reactor is

connected to port 14 of the divergent valve and its outlet is connected to port 14 of the convergent valve).

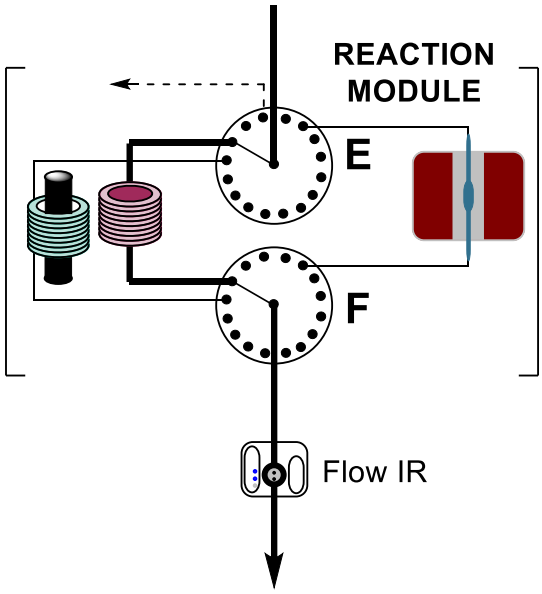

Figure 2.18. Divergent valve **E** and convergent valve **F** form the reaction module that can divert the reaction stream towards different routes dedicated in theory to different chemical transformations and then re-converge it into a common path that passes through the flow-IR.

In the reaction module, a flow-NMR spectrometer is also connected as an additional in-line analysis tool. This is not an obligatory stage of the flow path like the flow-IR (which is positioned across a common line), but must be selected like the reactors. After a step is accomplished the crude mixture can be sent to the reagent delivery system by the forwarding valve (Figure 2.20 a), mixed with a deuterated solvent (or a solution of internal standard if required) and sent to the flow-NMR. In order to allow for enough time for the NMR experiment this module can be used in stop-flow conditions (*vide infra*).

2.1.3.2 Stop-Flow conditions:

In order to allow longer residence times into the different modules a “stop-flow” capability was implemented that isolates the module in which the step is being performed, diverting the nitrogen stream to another one. The desired module is selected at the beginning of the step and the liquid segment is sent there, once the liquid segment reaches the desired position inside the module, divergent and convergent valves switch to different ports sealing the liquid segment. After the desired time for the operation has passed, the divergent and convergent valves switch back to the ports connected to the module which is holding the liquid segment allowing it to leave and follow the rest of the programmed pathway (Figure 2.19).

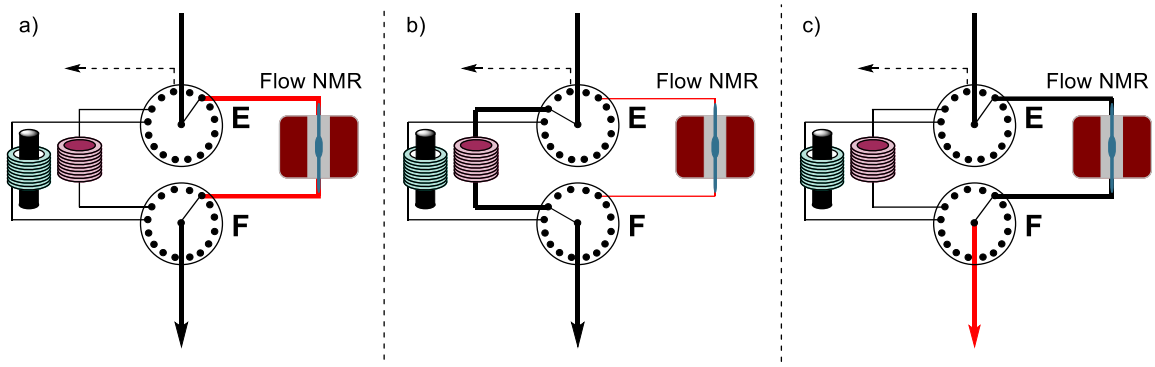

Figure 2.19. Stop-Flow mode: the stream is sent in one module (a) and once the entire liquid segment is contained inside that module, valves E and F switch to different ports isolating the module for the desired time (b). Once the set time has passed, valves E and F switch back to the original ports allowing the liquid segment to leave the module (c).

2.1.3.3 Forwarding Valve (G)

After passing through the Flow-IR, the reaction mixture meets the forwarding valve (**G**) (Figure 2.17), another 16-port multiposition valve that directs the reaction solution towards the next destination. There are four possible scenarios:

a) The intermediate formed is to be used later in a convergent multistep synthesis (not directly in the following step). The solution is then sent to the RDS and stored in a three-neck vessel (Figure 2.20 a) where it will wait to be used in the appropriate step.

b) The intermediate formed is to be used immediately in the following step (Figure 2.20 b). The solution is then sent to the standby module.

c) The final product of the synthesis was formed. The solution is then sent to a vessel for the final collection (Figure 2.20 c).

d) There is also a drain option, to send the reaction mixture to the waste container.

When the a) three-neck collection vessel in the RDS, b) loop of the standby module (**H**) or c) final collection vessel is full, the step is completed.

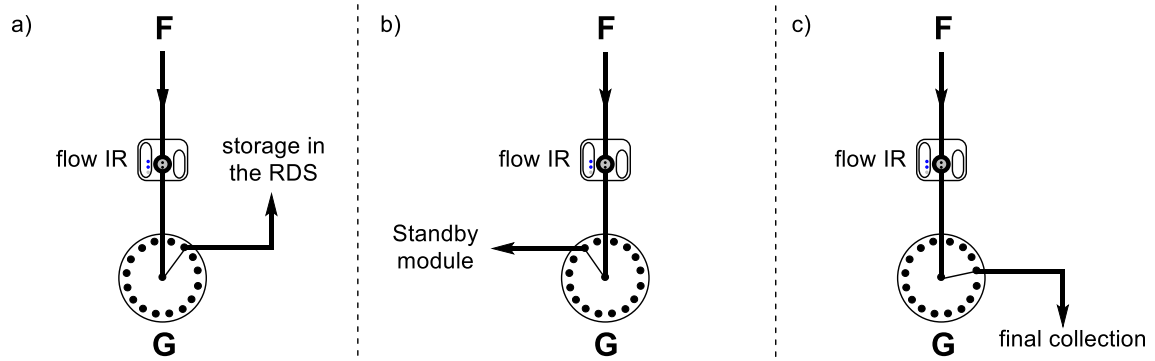

Figure 2.20. The forwarding valve **G** sends the reaction mixture towards the desired destination required by the step. a) Storage of the intermediate in the RDS (to be used in a later step). b) Storage of the intermediate in the standby module (to be used in the direct following step). c) Collection of the final product.

2.1.4 Standby module (SM)

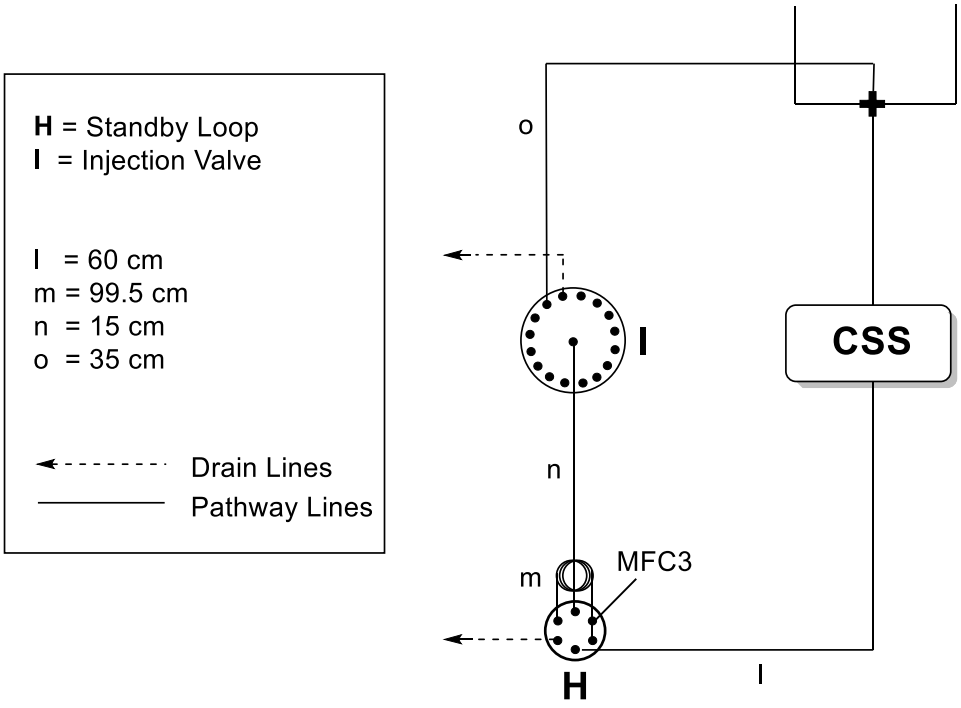

Figure 2.21. Standby module with its two components: the standby loop **H** and the injection valve **I**.

The standby module (Figure 2.21) has two components: the standby loop (**H**) and the injection valve (**I**). The standby loop (**H**) is a 6-port, injection valve that can allow two different flow pathways one for loading and one for injection (same as the sample loops of the RDS described in Figure 2.16). The injection valve (**I**) is a 16-port multiposition valve with the function of connecting or disconnecting the standby loop from the cross junction. When the connection of **H** with the cross junction is not needed, i.e. when the loop is being loaded (Figure 2.22 a) or when the loop is empty (Figure 2.22 c), the injection valve diverts the gas coming from MFC3 to a venting line (port 15). When the intermediate stored in **H** is to be mixed with the new reagents coming from the RDS for a subsequent step, valve **H** is set in injection mode and port 14 is opened on the injection valve **I**. This connects **H** with the cross junction and creates the scenario of Figure 2.22 b in which three liquid segments meet at the cross junction.

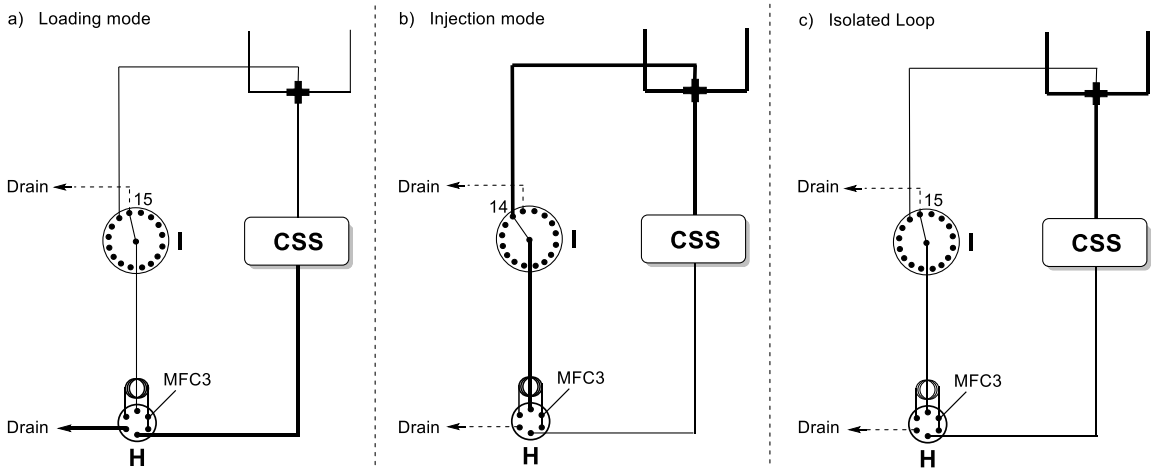

Figure 2.22. Standby module in three modes. a) Loop being loaded with the intermediate: **H** in loading mode; **I** set on venting port 15. b) Intermediate being injected from the loop and meeting new reagents coming from RDS for the next step: **H** in injection mode; **I** set on port 14 (connected to the cross junction). c) Standby module not in use: **H** can either be in loading or in injection mode; **I** set on venting port 15.

The injection valve **I** is also used to regulate the flow rate during the cycles. By opening the line that connects it with the CSS, it is possible to exploit the three mass flow controllers together, achieving higher flow rates. When the standby loop **H** is empty but the MFC3 is needed to increase the flow rate, the injection valve **I** can be switched to port 14 (Figure 2.23 b). It is important to take the precaution of opening the line only after the reagents have passed the cross junction (to avoid breaking the reaction mixture slug).

Similarly, when the standby loop **H** is being used to mix the intermediate with the reagents coming from RDS, but the upcoming cycle requires a low flow rate, it is possible to shut down the line right after the injection is complete. This isolates MFC3, diverting its stream to the venting port 15 of the injection valve **I** (Figure 2.23 a) and thus removing its contribution to the liquid flow rate in the system. In both scenarios, the position of the standby loop valve **H** (loading or injection) is not important. The time that the system has to wait before switching the destination of the injection valve **I**, in both scenarios described above, is referred to as *injection time*. When it is not necessary to change the destination of the injection valve **I** it is sufficient to set the injection time = 0 s.

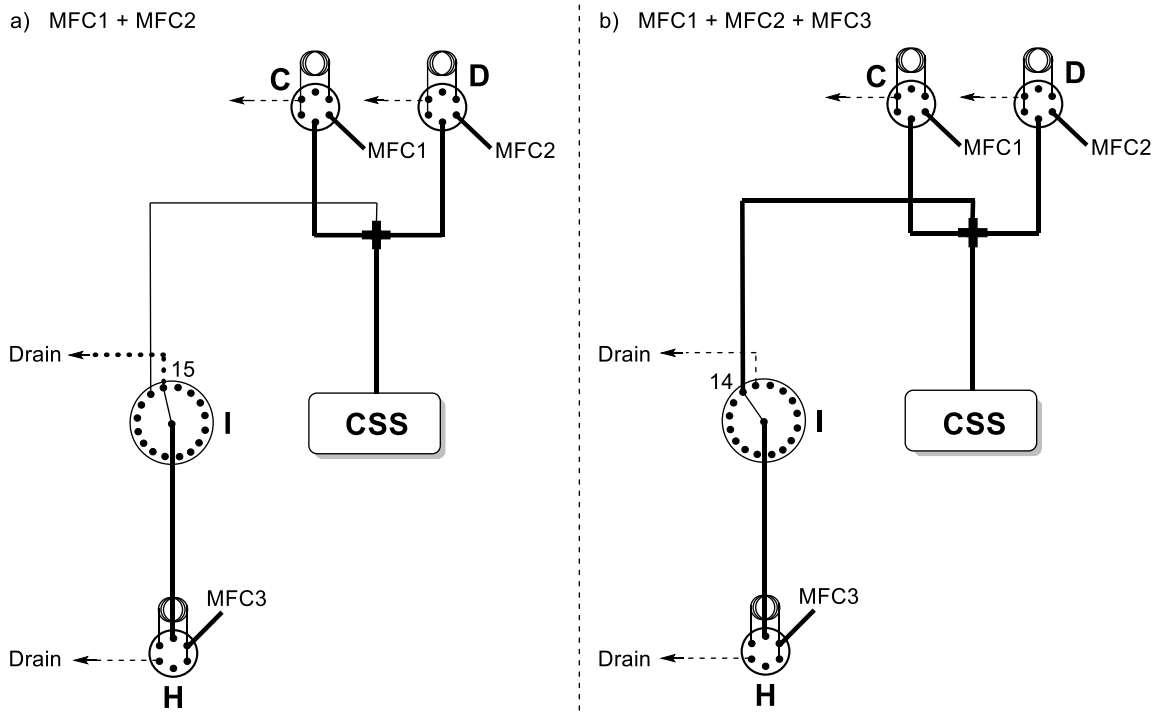

Figure 2.23. Injection valve of the standby module exploited to a) isolate MFC3 and run the steps at low flow rates; b) utilize all three mass flow controllers and work at high flow rates.

2.2 Precipitation handling and prevention of system fouling

Precipitation in a continuous flow reactor often leads to fouling of the system and failure of the process. To avoid system clogging, the radial synthesizer has three ports for rapid evacuation of the system in the event precipitation is observed: one at divergent valve **E** (in case precipitation is observed already at the mixing of the reagents), one at forwarding valve **G** (in case precipitation occurs in the reactor), and one at injection valve **I** (in case precipitation takes place in the standby loop **H**). These evacuation ports are connected to an unpressurized vessel. When the evacuation port is opened, a rapid depressurization occurs (from the set pressure inside the instrument to ambient pressure), causing the liquid slug to rapidly leave the system within one to ten seconds, depending on the position of the slug in the synthesizer. The system is then washed with solvents to ensure the removal of any remaining liquid/solid residue in the fluidic paths of the synthesizer.

2.3 Pathways

Combinations of the two ways the liquid segments can enter the CSS at the cross junction (Figure 2.23 a and b) and the three potential exits from the forwarding valve (Figure 2.20 a, b, and c), offer six possible “pathways” the solution can take in the radial synthesizer (not including options with regards to the choice of different reactor modules). The reagents can enter only from the reagent delivery system (single/1st steps) or from both reagent delivery system and standby module (cyclic steps) and the intermediate/product can be sent by the forwarding valve to the reagent delivery system (RDS), to the standby module (SM), or to a final collection vessel (CV). These combinations are reported in Figure 2.24 with the corresponding acronyms.

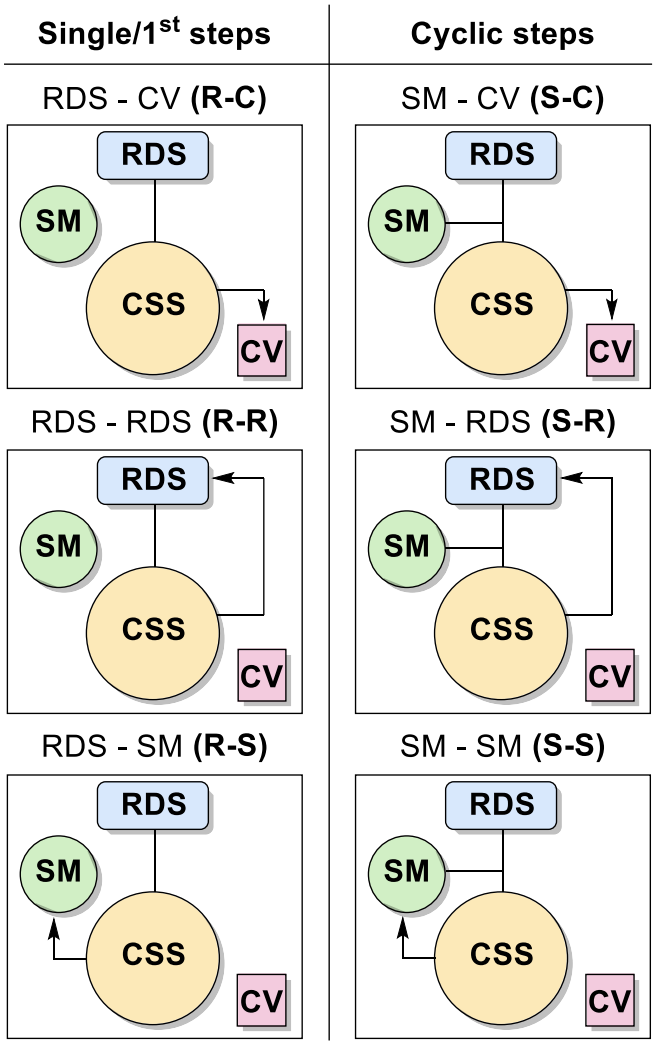

Figure 2.24. **R-R**: the reagents enter the CSS only from the RDS and the intermediate is stored in the RDS. **R-S**: the reagents enter the CSS only from the RDS and the intermediate is stored in the SM. **R-C**: the reagents enter the CSS only from the RDS and the intermediate is stored in the CV. **S-R**: the reagents enter the CSS from both RDS and SM and the intermediate is stored in the RDS. **S-S**: the reagents enter the CSS from both RDS and SM and the intermediate is stored in the SM. **S-C**: the reagents enter the CSS from both RDS and SM and the intermediate is stored in the CV.

Each pathway has fixed characteristic destinations at the forwarding valve **G**, standby loop **H** and injection valve **I**, while the port number of reagent and solvent selectors **A** and **S**, the port number of divergent and convergent valves (**E** and **F**), flow rate, temperature and the timings can be changed (Table 2.1 - Table 2.6). These six pathways are described in detail below (Figure 2.25 - Figure 2.30).

Table 2.1. Destination at Forwarding valve **G**, Standby Loop **H**, and Injection Valve **I** during a cycle following the **R-R** pathway.

	Divergent Valve (**E**) [a]	Convergent Valve (**F**) [a]	Forwarding Valve (**G**)	Standby Loop (**H**)	Injection Valve (**I**)	Time [a]
Initial position	…	…	DRAIN	LOAD	15	
Injection time	…	…	2	LOAD	15	…
Cycle time	…	…	2	LOAD	15	…
Final position	…	…	DRAIN	LOAD	15	

[a] variable parameters

Table 2.2. Destination at Forwarding valve **G**, Standby Loop **H**, and Injection Valve **I** during a cycle following the **R-S** pathway.

	Divergent Valve (**E**) [a]	Convergent Valve (**F**) [a]	Forwarding Valve (**G**)	Standby Loop (**H**)	Injection Valve (**I**)	Time [a]
Initial position	…	…	DRAIN	LOAD	15	
Injection time	…	…	15	LOAD	15	…
Cycle time	…	…	15	LOAD	15	…
Final position	…	…	DRAIN	LOAD	15	

[a] variable parameters

Table 2.3. Destination at Forwarding Valve **G**, Standby Loop **H**, and Injection Valve **I** during a cycle following the **R-C** pathway.

	Divergent Valve (**E**) [a]	Convergent Valve (**F**) [a]	Forwarding Valve (**G**)	Standby Loop (**H**)	Injection Valve (**I**)	Time [a]
Initial position	…	…	DRAIN	LOAD	15	
Injection time	…	…	DRAIN	LOAD	15	…
Cycle time	…	…	DRAIN	LOAD	15	…
Final position	…	…	4	LOAD	15	

[a] variable parameters

Table 2.4. Destination at Forwarding Valve **G**, Standby Loop **H**, and Injection Valve **I** during a cycle following the **S-R** pathway.

	Divergent Valve (**E**) [a]	Convergent Valve (**F**) [a]	Forwarding Valve (**G**)	Standby Loop (**H**)	Injection Valve (**I**)	Time [a]
Initial position	…	…	DRAIN	LOAD	15	
Injection time	…	…	2	INJECT	14	…
Cycle time	…	…	2	LOAD	15	…
Final position	…	…	DRAIN	LOAD	15	

[a] variable parameters

Table 2.5. Destination at Forwarding Valve **G**, Standby Loop **H**, and Injection Valve **I** during a cycle following the **S-S** pathway.

	Divergent Valve (**E**) [a]	Convergent Valve (**F**) [a]	Forwarding Valve (**G**)	Standby Loop (**H**)	Injection Valve (**I**)	Time [a]
Initial position	…	…	DRAIN	LOAD	15	
Injection time	…	…	15	INJECT	14	…
Cycle time	…	…	15	LOAD	15	…
Final position	…	…	DRAIN	LOAD	15	

[a] variable parameters

Table 2.6. Destination at Forwarding Valve **G**, Standby Loop **H**, and Injection Valve **I** during a cycle following the **S-C** pathway.

	Divergent Valve (**E**)[a]	Convergent Valve (**F**)[a]	Forwarding Valve (**G**)	Standby Loop (**H**)	Injection Valve (**I**)	Time [a]
Initial position	…	…	DRAIN	LOAD	15	
Injection time	…	…	DRAIN	INJECT	14	…
Cycle time	…	…	DRAIN	LOAD	15	…
Final position	…	…	4	LOAD	15	

[a] variable parameters

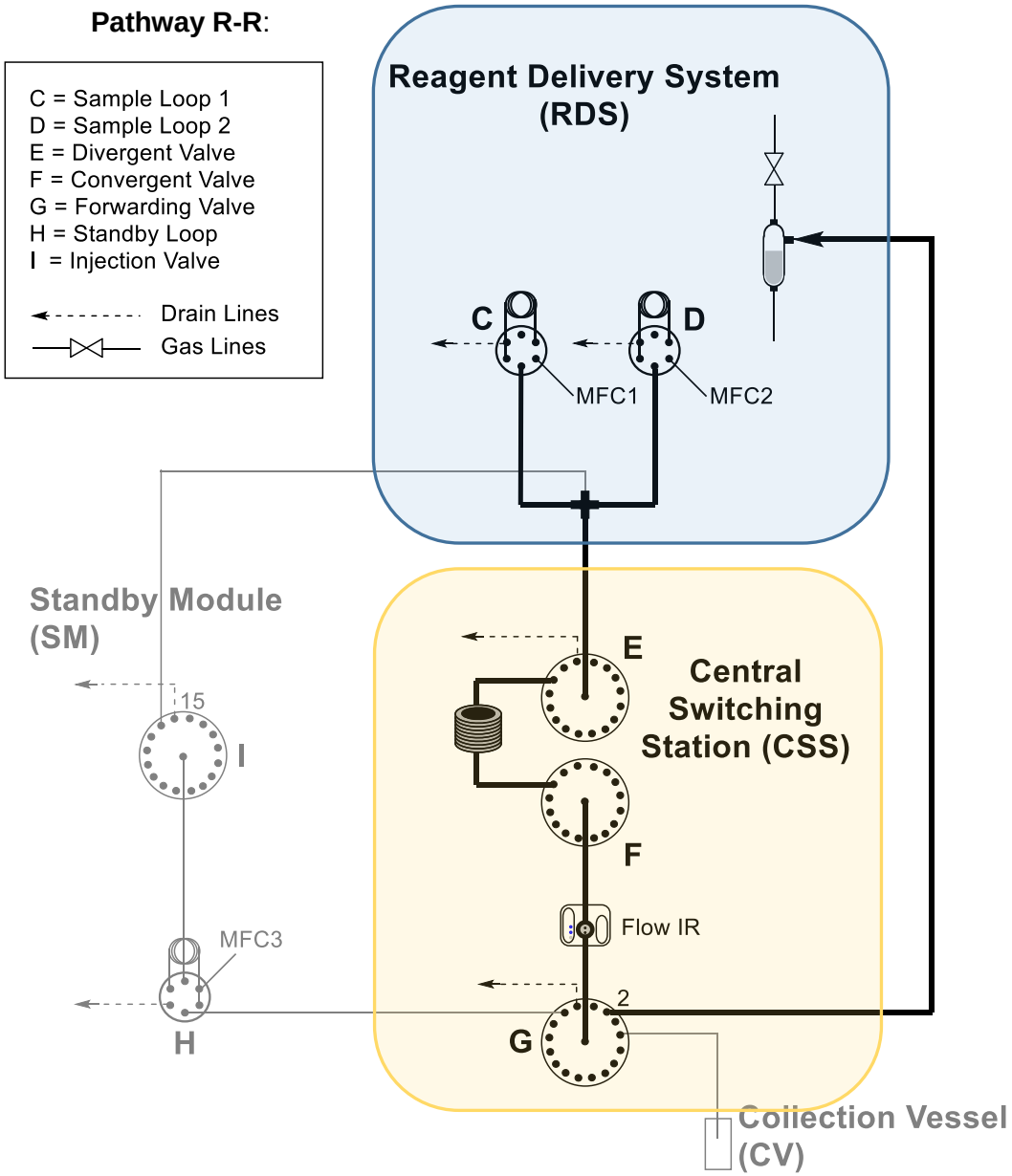

Figure 2.25. Pathway **R-R**: reagents coming only from the RDS and the generated intermediate is collected in RDS. Greyed-out sections are not utilized in this pathway.

Pathway R-S:

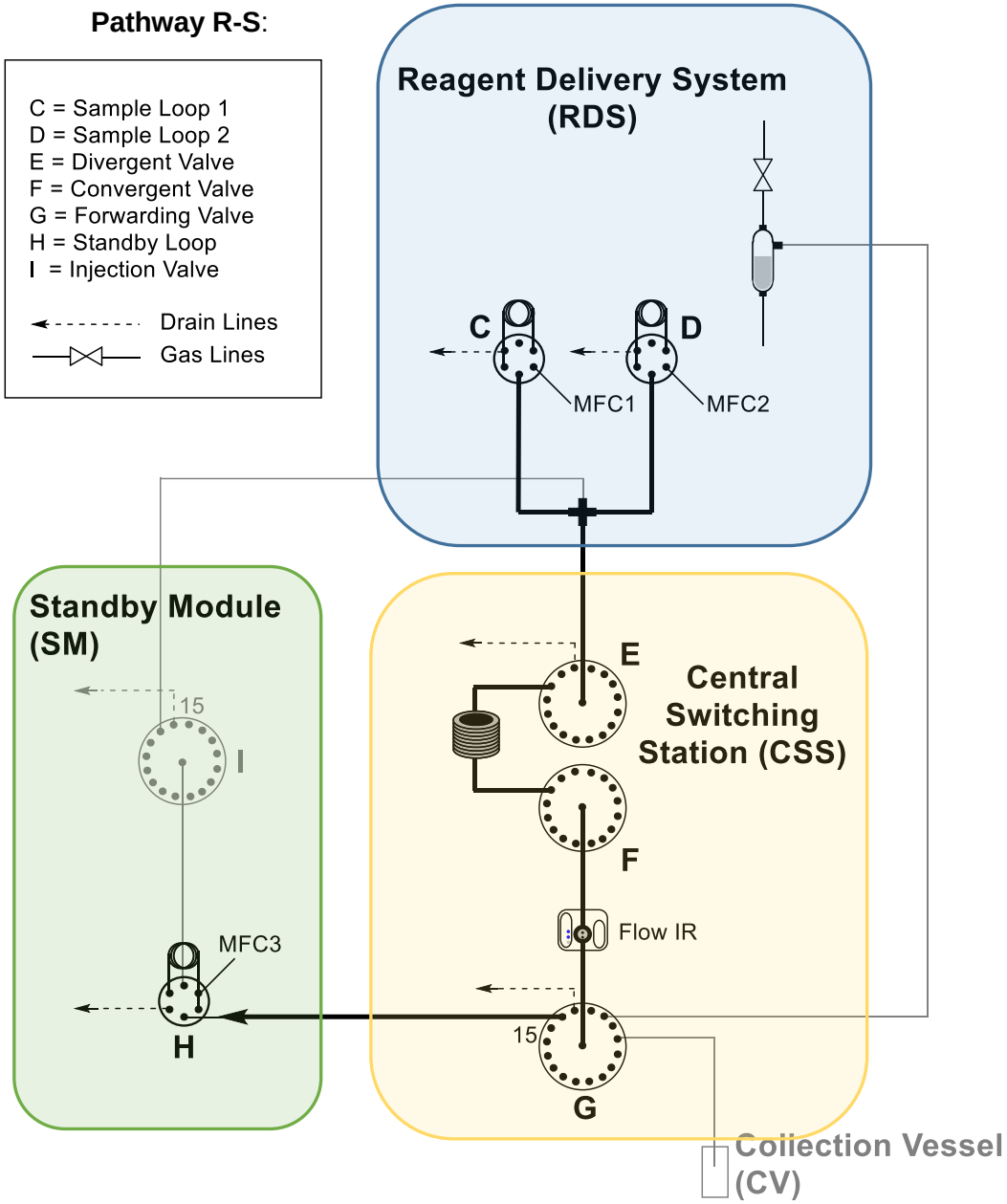

Figure 2.26. Pathway **R-S**: reagents coming only from the RDS and the generated intermediate is stored in the standby loop. Grayed-out sections are not utilized in this pathway.

Pathway R-C:

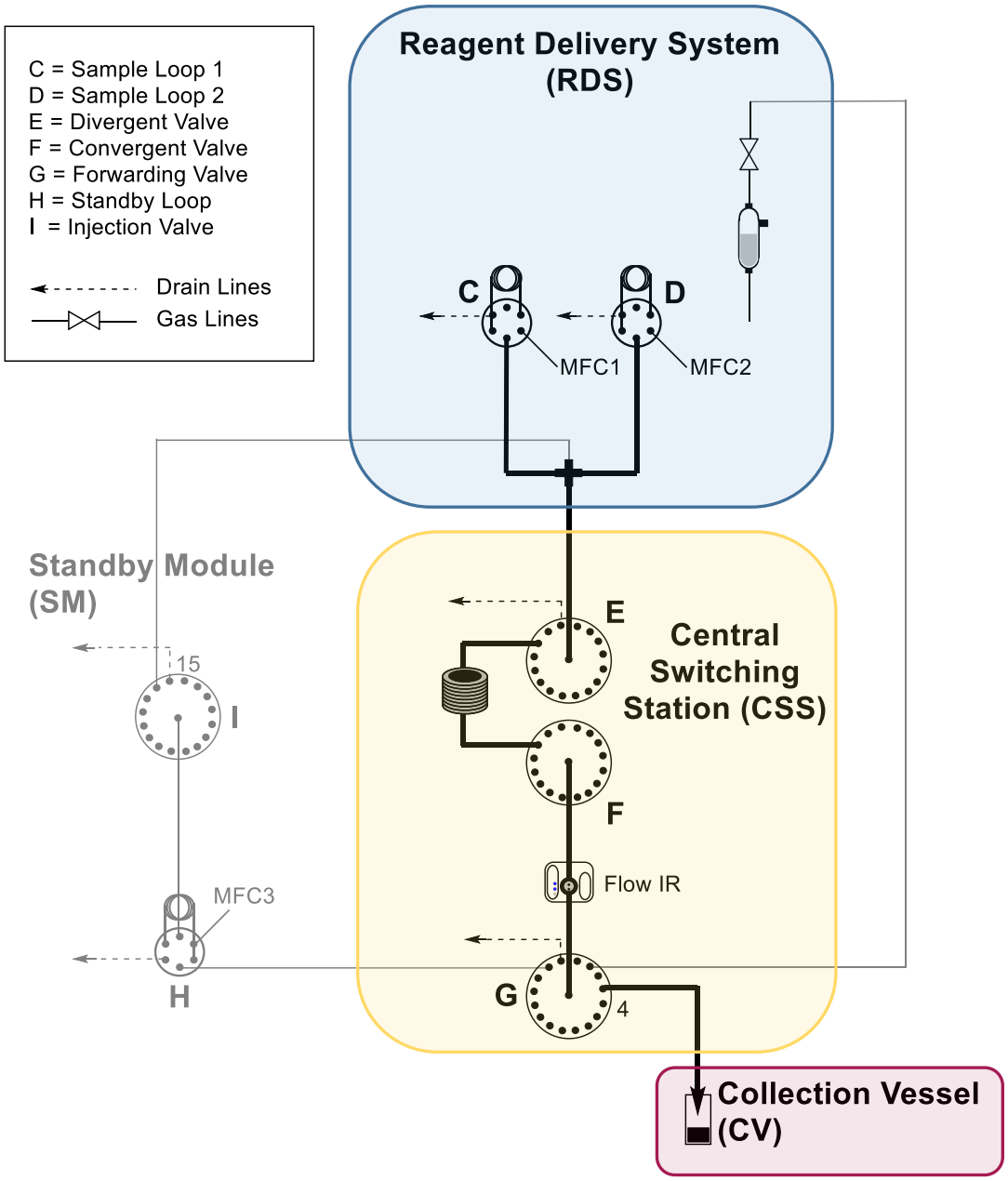

Figure 2.27. Pathway **R-C**: reagents coming only from the RDS and the generated product is collected in the final collection vessel. Grayed-out sections are not utilized in this pathway.

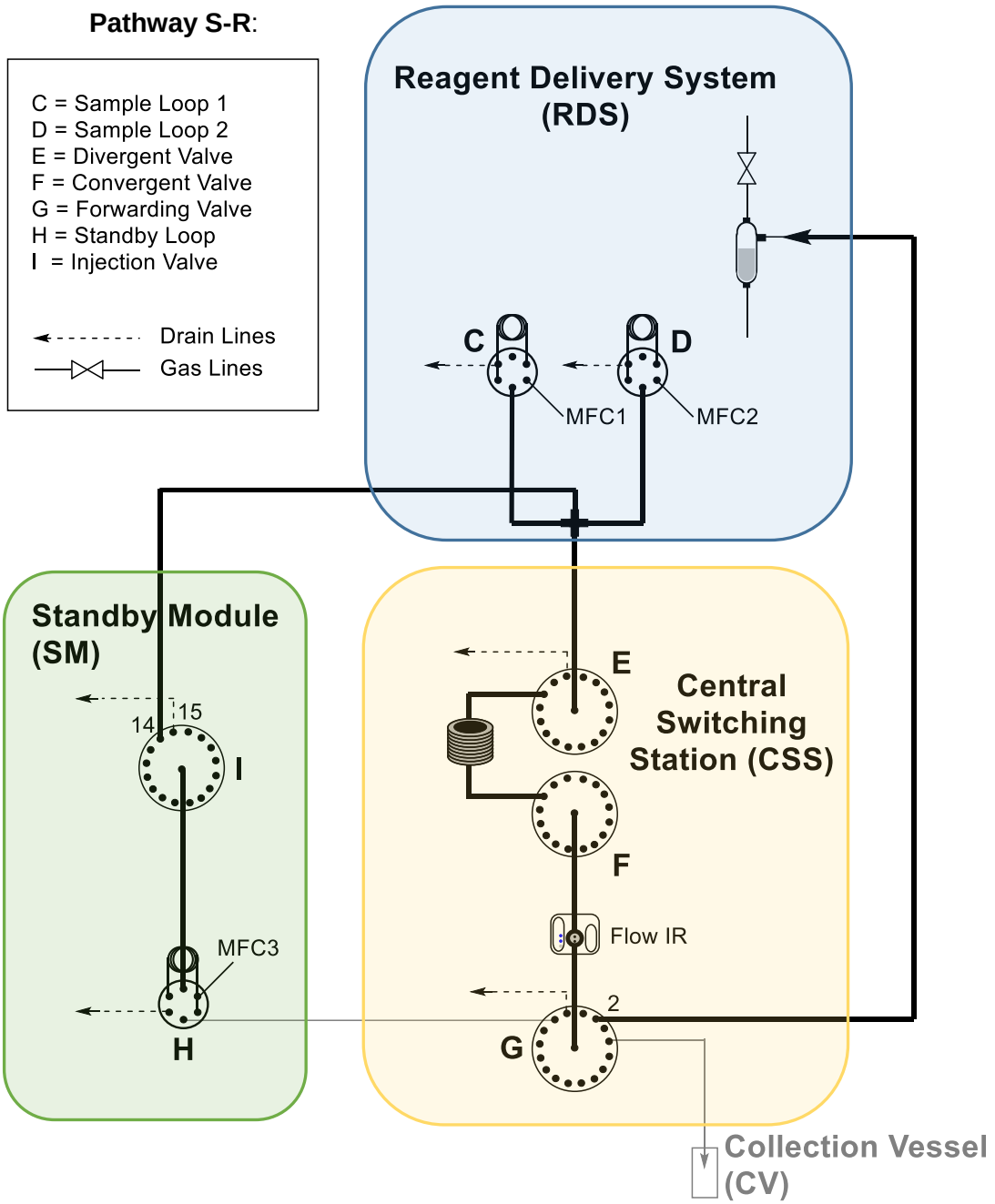

Figure 2.28. Pathway **S-R**: reagents coming from both RDS and SM and the generated intermediate is collected in the RDS. Grayed-out sections are not utilized in this pathway.

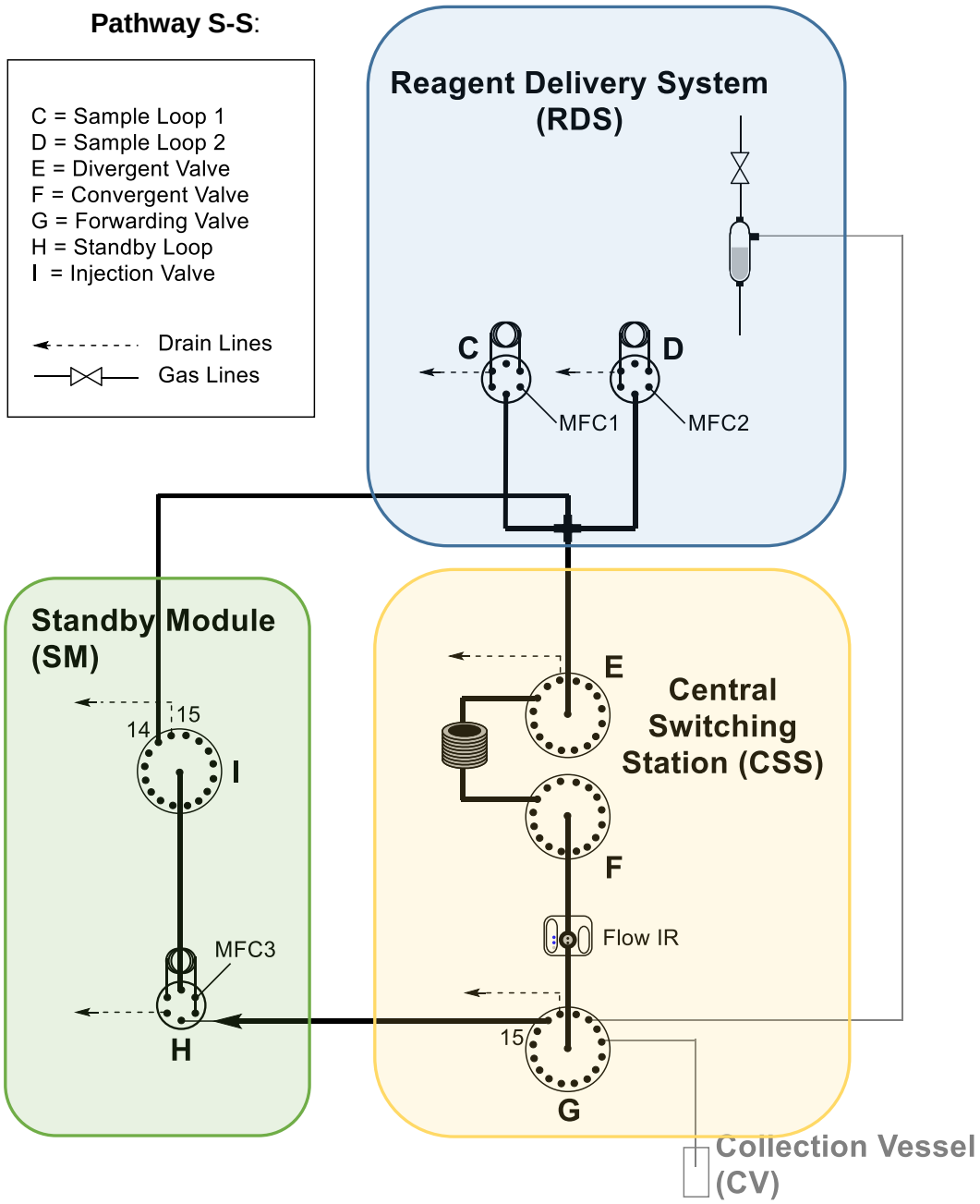

Figure 2.29. Pathway **S-S**: reagents coming from both RDS and SM and the generated intermediate is collected in the SM. Greyed-out sections are not utilized in this pathway.

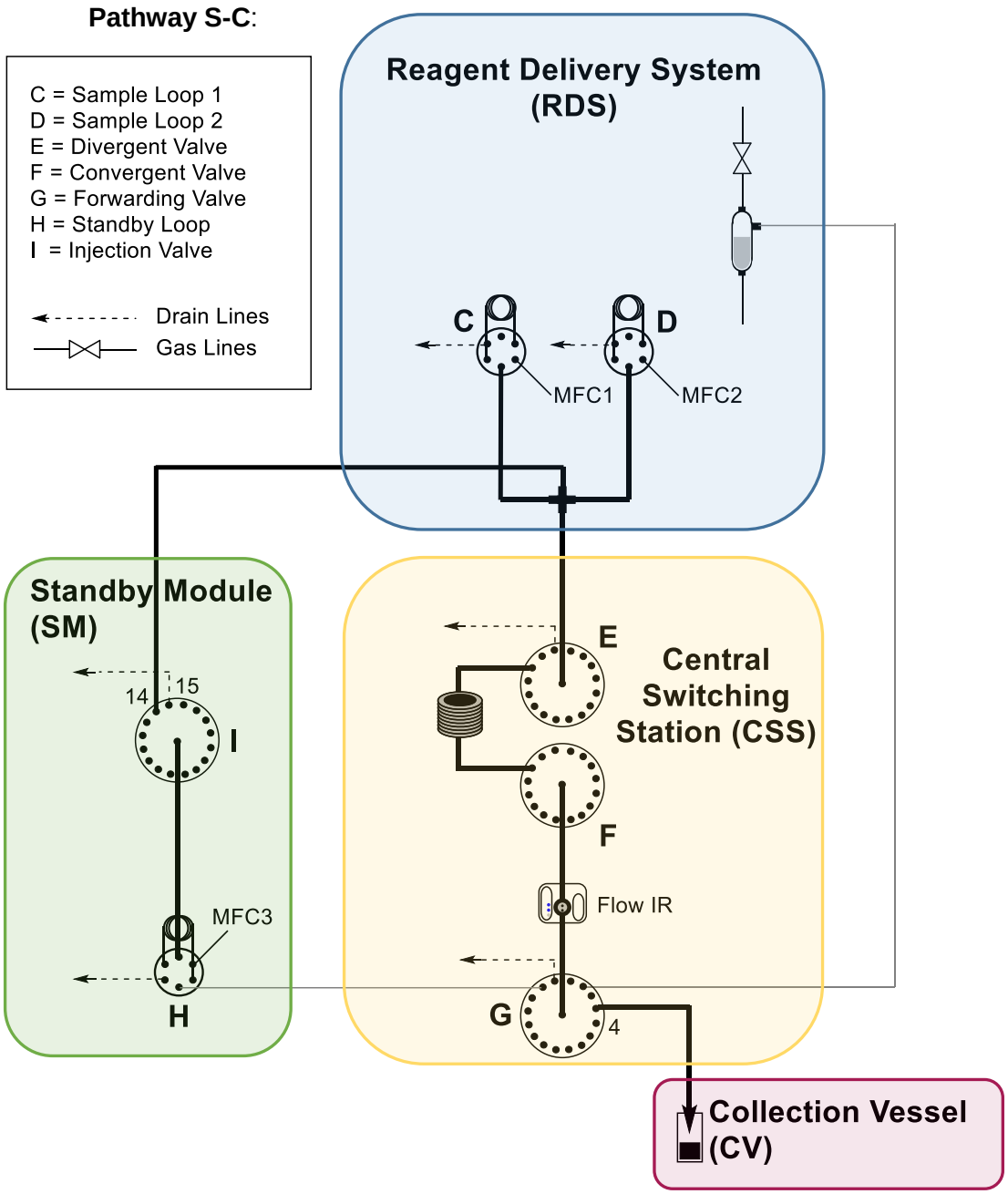

Figure 2.30. Pathway **S-C**: reagents coming from both RDS and SM and the generated product is collected in the CV.

2.4 Calibrations

2.4.1 Calibration of solvent and reagent selectors

Calibration tests were run to establish the reliability of the dilution capability of the reagent delivery system. In order to do that, a 1 M solution of 1,3,5-trimethoxy benzene in $CDCl_3$ was loaded in the solvent pool, a 1 M solution of 1,2,4,5-tetramethyl benzene in $CDCl_3$ was loaded into the reagent pool and a series of data was collected varying the infusion rate of both syringe pumps to achieve various concentrations in the sample loops.

The final concentrations were analyzed using the flow-NMR spectrometer in stop-flow mode: after the loops were loaded with the desired ratio of both solutions, port 15 of both divergent and convergent valves (connected to inlet and outlet of flow-NMR) were selected. Once the NMR flow cell was entirely filled with the freshly generated solution, port 2 of both divergent and convergent valves (connected to a 0.1 mL PFA tube) were selected diverting the stream towards an alternative line and leaving to the instrument enough time for the NMR experiment. After that time, both port 15s were reselected and the mixture was sent to collection.

Measurements of the same solutions with 400 MHz Bruker NMR spectrometer were consistent with the data of the flow-NMR. These tests were repeated 3 times and provided comparable results (Figure 2.31).

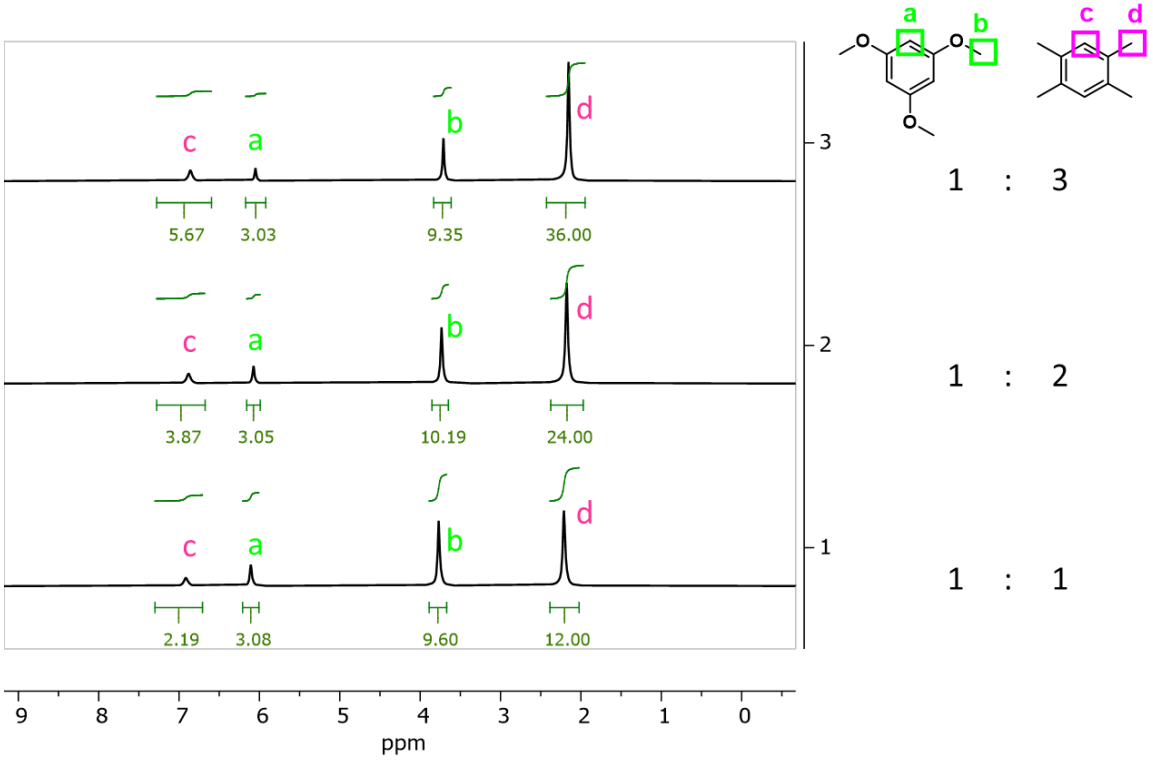

Figure 2.31. ^{1}H NMR spectra were recorded with the flow-NMR for different ratios of trimethoxy benzene and tetramethyl benzene generated by playing with different infuse rates of the syringe

pumps of reagent and solvent selectors. These tests were repeated three times giving comparable results.

2.4.2 Calibration of flow rate:

Since gas and liquid have different compressibility and every solvent has a different viscosity and a different expansion behavior when heated, calibration of the dependence of flow rate from the type of solvent and temperature was necessary to predict the residence time of our steps. The solvents I used for my studies were water, acetonitrile, and methanol. The observed liquid flow rate for these solvents reported in Table 2.7 and Figure 2.32 - Figure 2.39. I distinguished between two types of timings: a) residence time – the actual time that the reaction spends inside the reactor and b) cycle time – the overall time of each step (time that the reaction slug takes to go from the beginning to the end of its path). For the residence time, the time which the head of the reaction slug takes to go from the beginning to the end of the reactor was measured at different set flow rates and temperatures for the three different solvents. The flow rate was calculated as a function of the residence time and reactor volume (10 mL). Every test was performed in duplicate. While the residence time at the same conditions sometimes varied a couple of seconds, the resulting flow rates were reproducible.

Table 2.7. The observed liquid flow rate is dependent on temperature, solvent, and set gas flow rate during the residence time. Every test was made at 5 bar and was repeated twice.

Solvent	T °C	V (mL)	Set Gas Flow Rate (mL/min)	Time (s)	Resulting Liquid Flow Rate (mL/min)
Methanol	23	10	9	367.80 366.99	1.63 1.63
Methanol	40	10	9	349.59 347.99	1.72 1.72
Methanol	60	10	9	325.96 324.14	1.84 1.85
Water	23	10	9	375.66 374.22	1.60 1.60
Water	40	10	9	356.72 357.81	1.68 1.68
Water	60	10	9	338.64 338.45	1.77 1.77
Acetonitrile	23	10	9	370.55 370.23	1.62 1.62
Acetonitrile	40	10	9	355.22 354.02	1.69 1.69
Acetonitrile	60	10	9	336.85 337.19	1.78 1.78
Acetonitrile	23	10	4	846.38 844.12	0.71 0.71
Acetonitrile	23	10	3	1137.62 1131.99	0.53 0.53
Acetonitrile	60	10	3	1054.86 1061.10	0.57 0.57
Acetonitrile	60	10	5	690.61 693.59	0.87 0.87

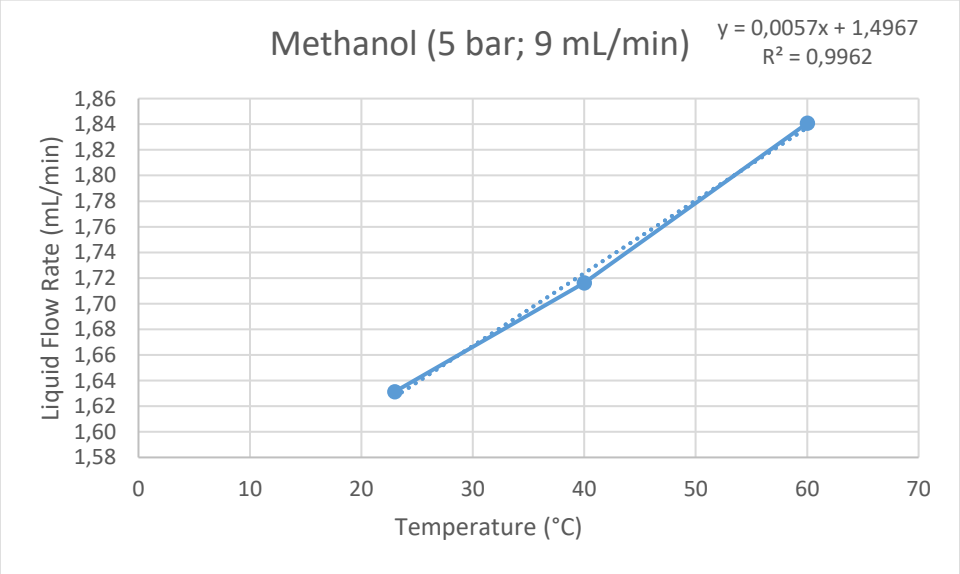

Figure 2.32. : Plot of the actual flow rate of a 1 mL methanol slug as a function of the temperature when pressure is 5 bar and the set gas flow rate is 9 mL/min.

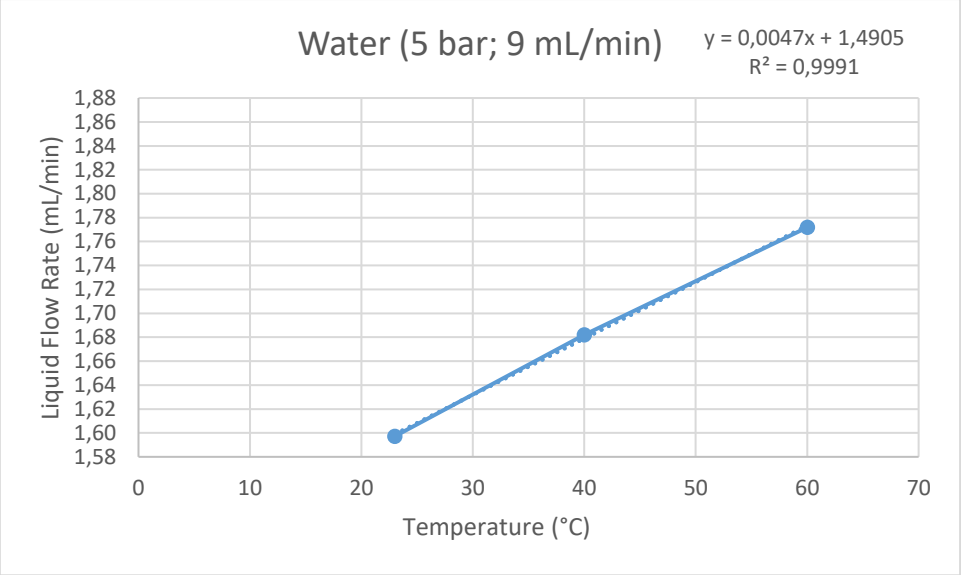

Figure 2.33. Plot of the actual flow rate of a 1 mL water slug as a function of the temperature when pressure is 5 bar and the set gas flow rate is 9 mL/min.

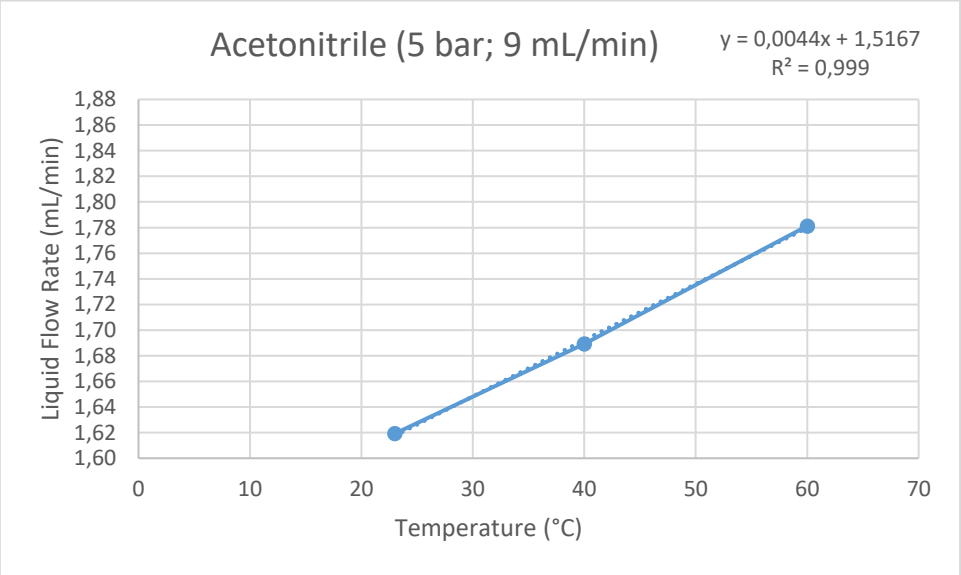

Figure 2.34. Plot of the actual flow rate of a 1 mL acetonitrile slug as a function of the temperature when pressure is 5 bar and the set gas flow rate is 9 mL/min.

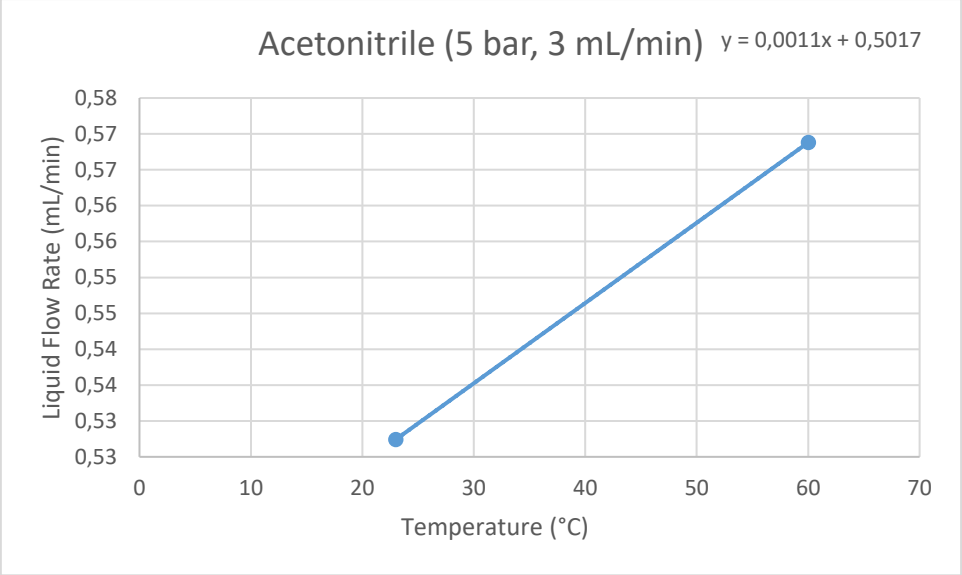

Figure 2.35. Plot of the actual flow rate of a 1 mL methanol slug as a function of the temperature when pressure is 5 bar and the set gas flow rate is 3 mL/min.

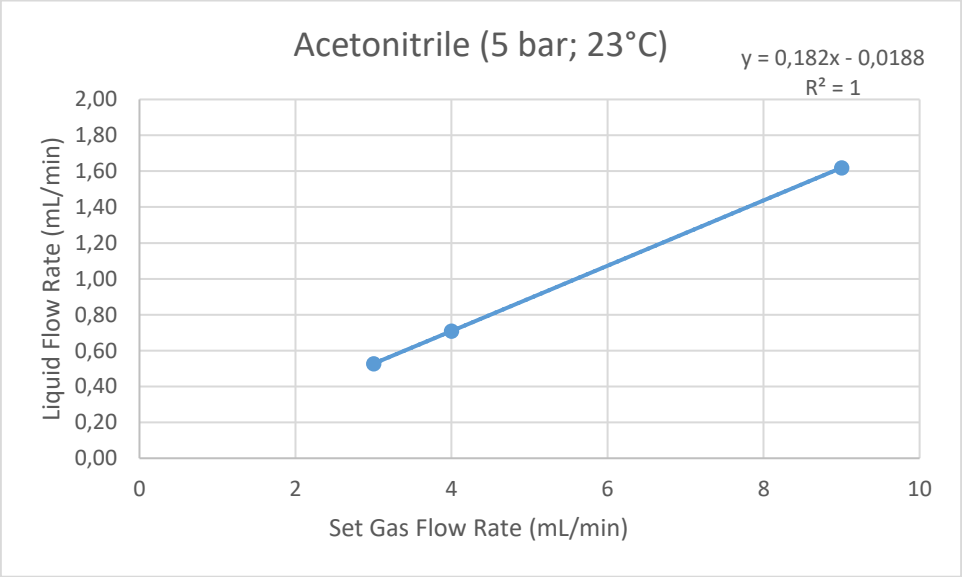

Figure 2.36. Plot of the actual flow rate of a 1 mL methanol slug as a function of the set gas flow rate when pressure is 5 bar and temperature is 23 °C.

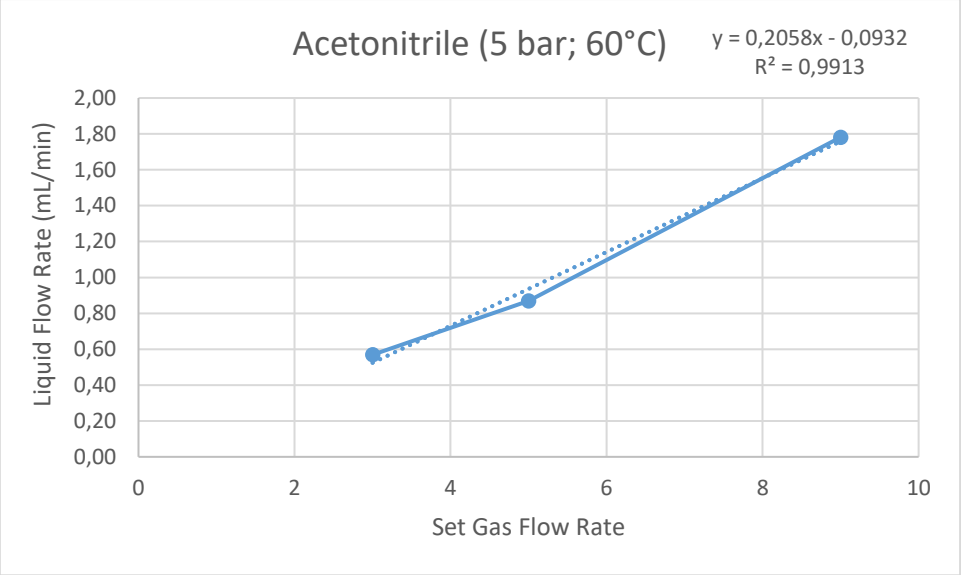

Figure 2.37. Plot of the actual flow rate of a 1 mL methanol slug as a function of the set gas flow rate when pressure is 5 bar and temperature is 60 °C.

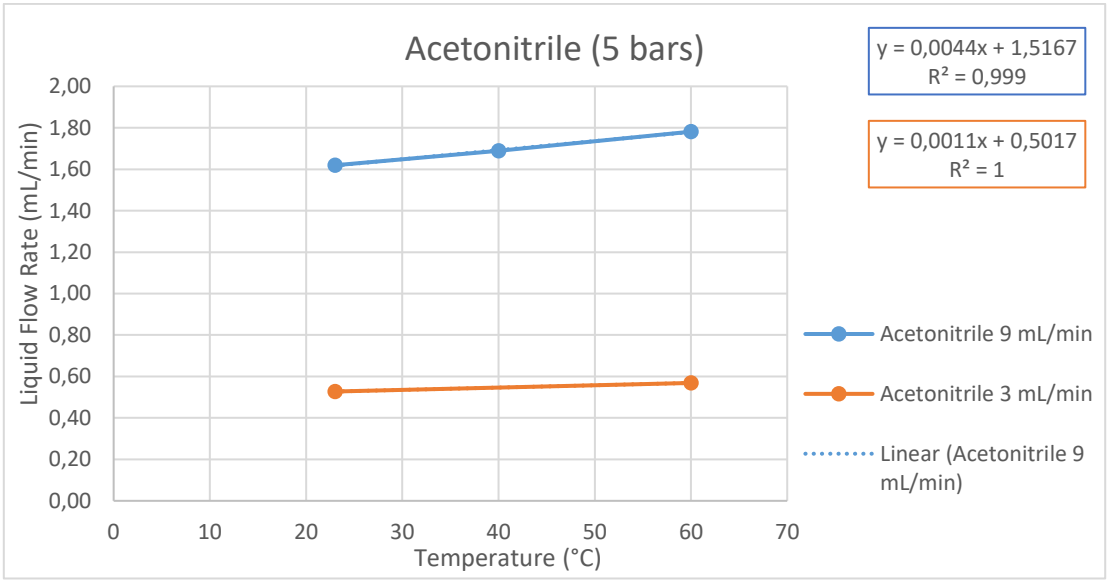

Figure 2.38. Plot of the actual flow rate of a 1 mL acetonitrile slug as a function of the temperature when pressure is 5 bar and the set gas flow rate is 9 mL/min (blue) and 3 mL/min (orange).

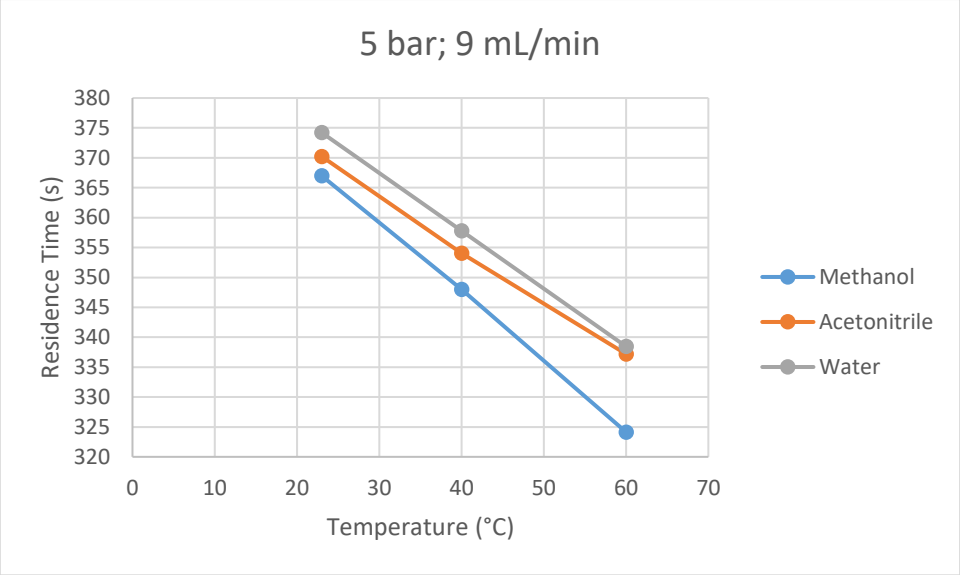

Figure 2.39. Plot of the residence time of a 1 mL slug of methanol, acetonitrile, and water as a function of the temperature when pressure is 5 bar and set gas flow rate is 9 mL/min.

During the cycle time, the liquid slug passes from an unheated area (from valves **C** and **D** to valve **E**), through the heated reactor (from valve **E** to valve **F**), to an unheated section again (valve **F** through flow-IR and valve **G** towards either **H** or RDS or final collection). The cycle times measured for the three solvents at different T are provided in Table 2.8 and Figure 2.40 - Figure 2.42 for the different solvents used.

Table 2.8. The observed liquid flow rate during the course of the entire cycle is dependent on the temperature, solvent and set gas flow rate. Every test was made at 5 bar and was repeated twice.

Solvent	T °C	V (mL)	Set Gas Flow Rate (mL/min)	Cycle Time (s)	Resulting Liquid Flow Rate (mL/min)
Methanol	23	12.43	9	458.47 459.31	1.63 1.62
Methanol	40	12.43	9	438.47 437.34	1.70 1.71
Methanol	60	12.43	9	415.82 414.56	1.80 1.80
Water	23	12.43	9	470.25 470.19	1.59 1.59
Water	40	12.43	9	451.27 453.52	1.65 1.64
Water	60	12.43	9	432.87 431.14	1.72 1.73
Acetonitrile	23	12.43	9	460.17 460.31	1.62 1.62
Acetonitrile	40	12.43	9	445.80 445.01	1.67 1.68
Acetonitrile	60	12.43	9	428.64 427.39	1.74 1.75

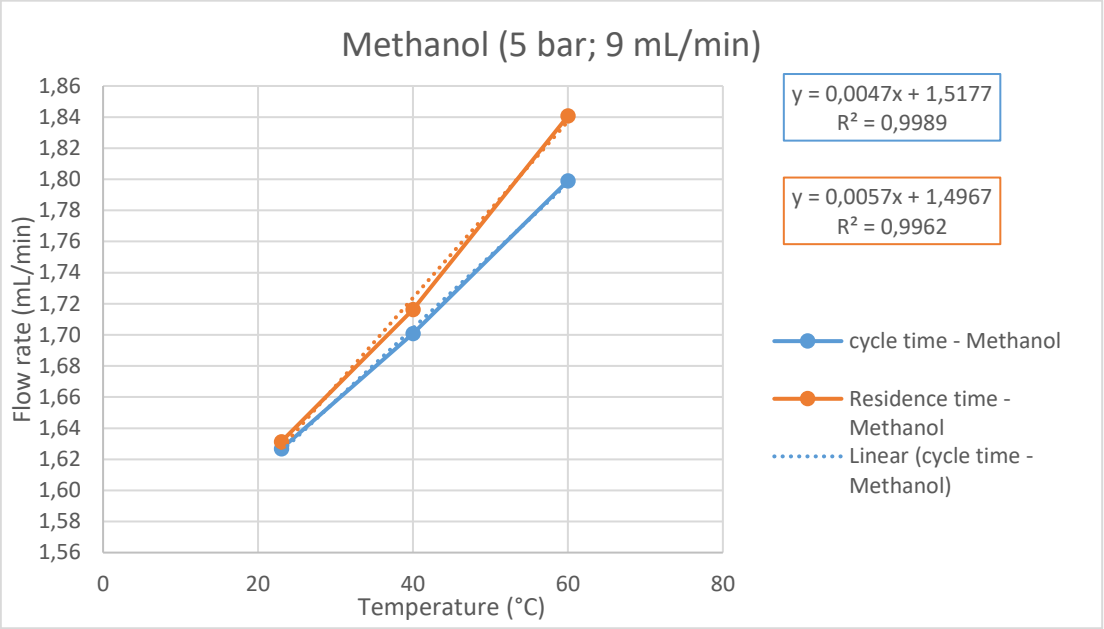

Figure 2.40. Plot of the actual flow rate of a 1 mL slug of methanol as a function of the temperature during the cycle time (blue) and during the residence time (orange). Pressure 5 bar, set gas flow rate 9 mL/min.

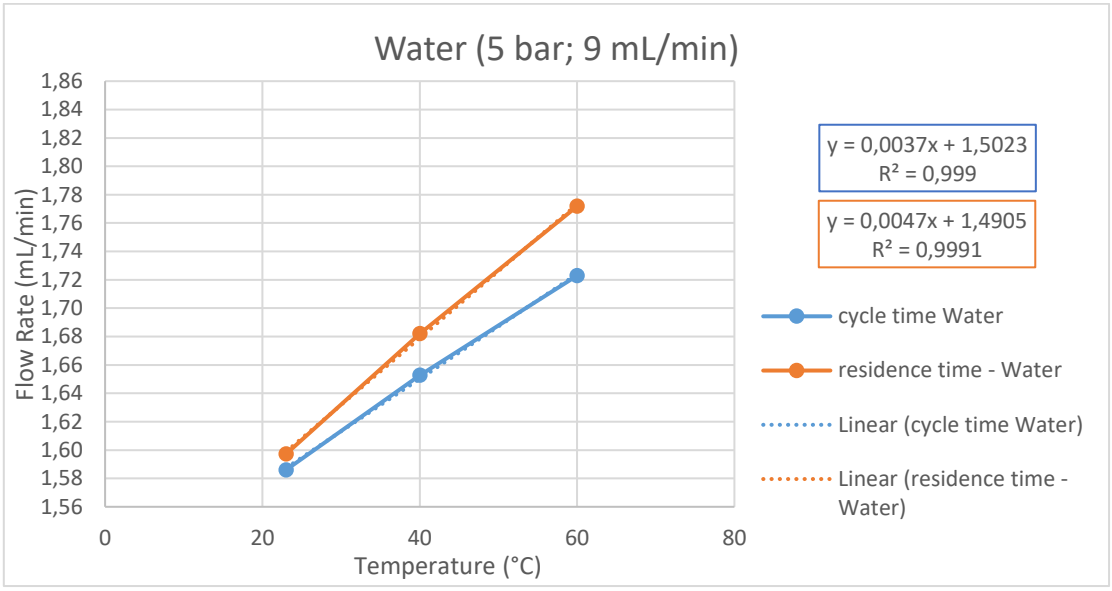

Figure 2.41. Plot of the actual flow rate of a 1 mL slug of water as a function of the temperature during the cycle time (blue) and during the residence time (orange). Pressure 5 bar, set gas flow rate 9 mL/min.

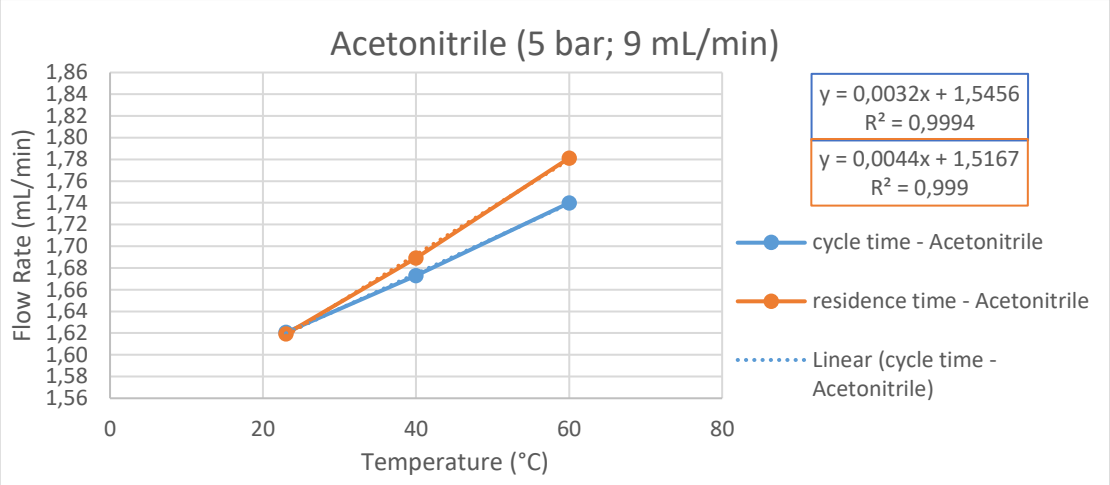

Figure 2.42. Plot of the actual flow rate of a 1 mL slug of acetonitrile as a function of the temperature during the cycle time (blue) and during the residence time (orange). Pressure 5 bar, set gas flow rate 9 mL/min.

The cycle time is different for the different pathways, and the degree of precision needed on each of them is also variable. The pathways ending in the RDS have as final destination from forwarding valve (**G**) the corresponding outlet port that delivers the solution to the three-neck vessel. When this is the case, the collection will continue until the beginning of the next step. As such, it is sufficient to give as a cycle time a value that is slightly longer than the predicted one (10 seconds to 1 minute depending on the chosen flow rate) to ensure that the entire solution will be collected.

There is also room for error with pathways ending in the collection vessel. For processes where the collection takes place in a pressurized vessel, the forwarding valve will be set to its final destination from the beginning of the step. Again, here it is sufficient to set a value for the cycle time that is slightly longer than the predicted one to ensure that the entire solution will be collected. Since the mass flow controllers do not stop the gas flow upon cycle end, the collection will continue until the operator manually stops the instrument.

In the instance where the collection takes place in an unpressurized vessel, the forwarding valve will switch to the unpressurized port right after the intended residence time is over and the collection will take place in the time in which the system depressurizes, and will continue until the operator manually switches off the mass flow controllers.

For pathways ending in the standby module, the accuracy of the cycle time is more important. The final destination of the forwarding valve is the drain port that diverts the gas stream from the line that feeds the standby loop, thus stopping the liquid slug there. In such cases, it is necessary that **G** feeds the loop for the time needed to fill it and switches to the drain port when the middle of the slug is held in the standby loop **H**. An error of few seconds is tolerated but by changing the solvent mixture and the temperature, the cycle

time may potentially vary by dozens of seconds (Figure 2.39). I considered it appropriate to time each step during the optimization phase (stopping it manually) in order to have empirical time values which will then be typed in the appropriate fields during the preparation of the automated sequence. As soon as the right timings are found, each step can be run autonomously, as under the same conditions, flow rate and the corresponding residence and cycle times, are fully reproducible.

Every synthetic step optimized in the following chapter (chapter 0), therefore, was first run “manually”, stopping the flow when the reaction mixture reached the desired point (by manually selecting the proper destination of each valve). The related timings were then integrated into automated sequences.

2.5 Software

The control software, written in LabVIEW, relies on a hierarchy of five layers of virtual instruments. At the graphical user interface[31], which is remotely accessible (the highest level), users enter information relating to the reagents delivery, pathway (section 2.3 of this document), reaction conditions, and destination to achieve a multistep process, a set of single-step reactions, or a combination thereof. Beneath the interface, a series of virtual instruments (VIs) control and interface the hard- and software. These VIs are timed to render the instrument fully autonomous.

Details about the software will not be included in this thesis because it was developed by my colleague: Dr. Sourav Chatterjee. Further information can be found in the supporting info of reference 29.

3 Proof of concept

This chapter has been partially modified from: Chatterjee, S.;* Guidi, M.;* Seeberger, P. H.; Gilmore, K. Automated Radial Synthesis of Organic Molecules. *Nature* **2020**, 579, 379–384. DOI: 10.1038/s41586-020-2083-5

Further permissions related to the material excerpted should be directed to Springer Nature.

* equal authorship

The last section of this chapter (3.4) has been adapted from: Guidi, M.; Moon, S.; Anghileri, L.; Cambié, D.; Seeberger, P. H.; Gilmore, K. Combining Radial and Continuous Flow Synthesis to Optimize and Scale-up the Production of Medicines. *Submitted*.

The processes for the validation of the radial synthesizer were chosen in order to demonstrate the capabilities of the instrument.

3.1 Convergent vs linear syntheses

The radial synthesizer can accommodate different synthetic strategies without instrument reconfiguration. In order to showcase this feature, I selected the synthesis of the anticonvulsant drug rufinamide that can be achieved through both linear and convergent approaches[32] (Scheme 3.1).

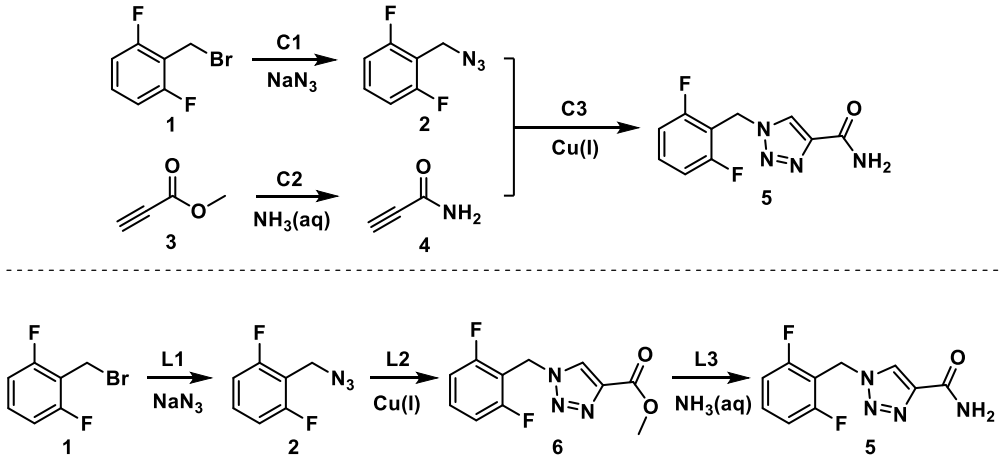

Scheme 3.1. Convergent (top) vs linear (bottom) synthesis of rufinamide.

These two processes would require two different setups if performed under continuous flow conditions and the repetition of similar, if not equivalent, pieces of equipment in different synthetic steps within the same process. Reutilization of the same modules, when switching from one synthesis to the other, is possible but a full disassembly

and reassembly of the setup is needed to reorganize the order of reactors and feeds (Figure 3.1).

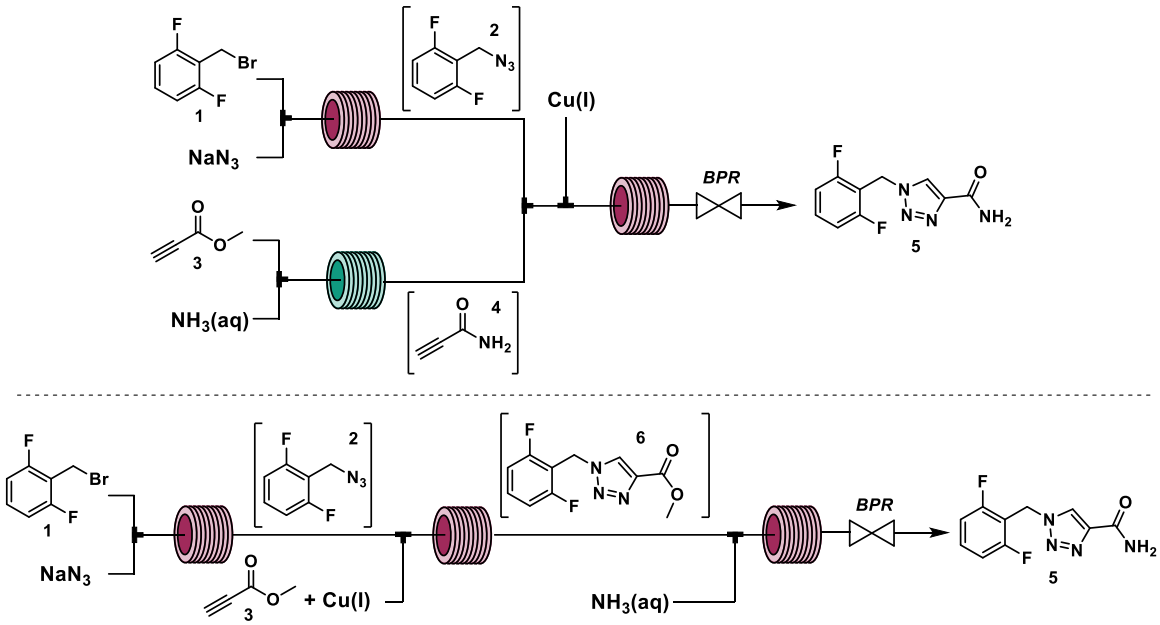

Figure 3.1. Convergent vs linear synthesis of rufinamide performed under continuous flow conditions. Recombination of equipment, as well as repetition of identical modules, are needed.

The radial synthesizer instead could switch between the two routes and perform the optimization of both via proper selection of the order of addition of reagents and destinations of the multiport valves. Reutilization of the same reactor within one radial process was possible to such an extent that all the synthetic steps shown in this section were performed using the same reactor at variable temperature (Figure 3.2).

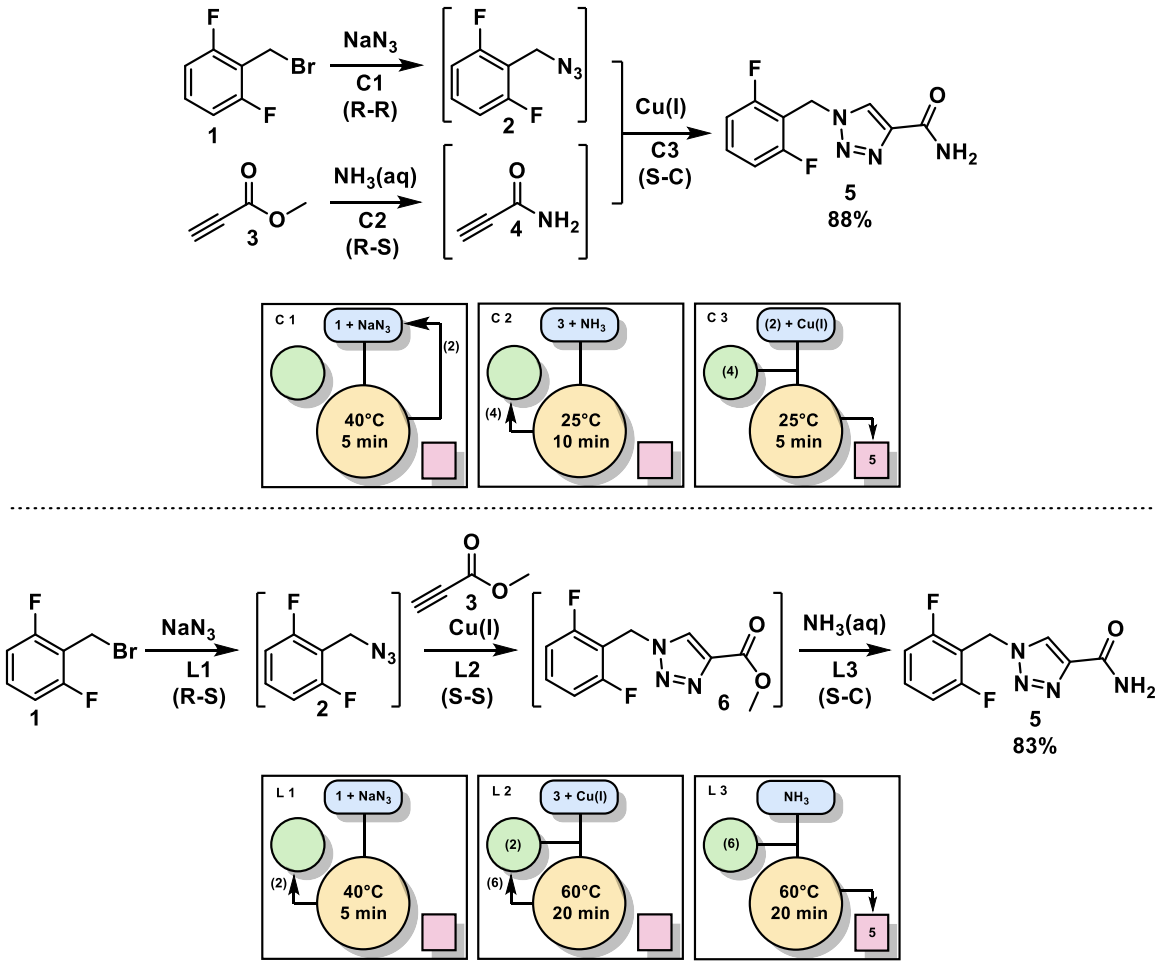

Figure 3.2. Rufinamide (**5**) was synthesized via convergent (top; **R–R**, **R–S**, **S–C**) and linear (bottom; **R–S**, **S–S**, **S–C**) processes using the same instrument without reconfiguration.

The two synthetic approaches to rufinamide could be performed starting from the same reagent solutions as inline dilution with different solvents are possible (section 2.1.2). The reagent delivery system was loaded with five solutions and two wash solvents in the reagent selector (Figure 3.3) and two solvents for dilution in the solvent selector (**Vessel 1:** MeOH and **Vessel 2:** CH_3CN).

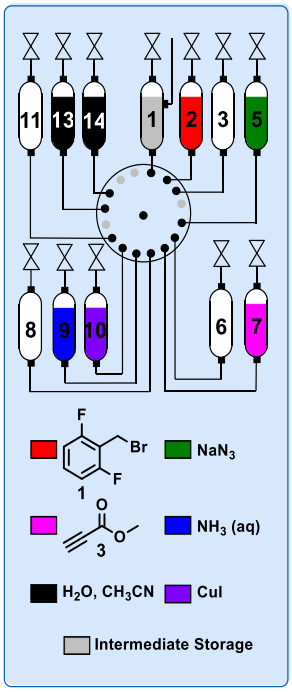

Vessel 1: empty (used for storage of intermediate **2** in the convergent synthesis)

Vessel 2: 2,6-difluorobenzyl bromide (**1**), 1.5 M in CH_3CN:MeOH = 1:4

Vessel 3: empty

Vessel 5: sodium azide, 1.6 M in H_2O:MeOH = 3.5:6.5

Vessel 6: empty

Vessel 7: methyl propiolate (**3**), 2 M in CH_3CN

Vessel 8: empty

Vessel 9: NH_3, 7.5 M in H_2O

Vessel 10: CuI, 0.0375 M in CH_3CN

Vessel 11: empty

Vessel 13: CH_3CN

Vessel 14: H_2O

Figure 3.3. Five reagents were used for both routes. White vessels were left empty and grey dots represent ports which are dedicated to other purposes other than connecting the reagent selector to the reagent vessels (see section 2.1.2.1).

Each reaction was initially optimized individually in the synthesizer by screening solvents, stoichiometry, concentration, temperature, and residence time. For individual optimization, the **R-C** pathway was employed, conversion was monitored inline by Flow-IR and yield was determined by offline analysis of collected samples. Then steps were coupled together in a convergent or a linear manner and the resulting multistep sequences were optimized in order to maximize overall yield and quality of the product.

3.1.1 Radial *convergent* synthesis of rufinamide

The following acronyms are used to refer to the individual reactions in the convergent process: Step 1 = **C1**, Step 2 = **C2**, Step 3 = **C3** (Scheme 3.2).

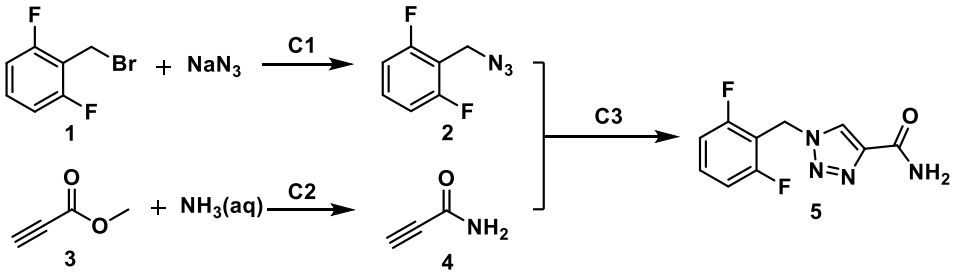

Scheme 3.2. Convergent synthesis of rufinamide **5** (**C1** + **C2** + **C3**), where either intermediate **2** or **4** is stored in the reagent delivery system for use in the final step (**C3**).

3.1.1.1 Individual optimization of C1

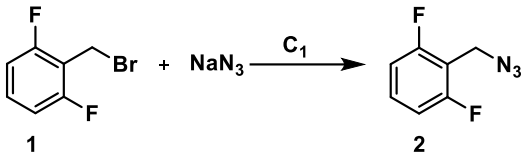

Scheme 3.3. Synthesis of 2,6-difluorobenzylazide **2** (**C1**) from 2,6-difluorobenzyl bromide and sodium azide.

A preliminary offline solvent screening was performed to identify solvents that fully solubilize the respective reagents. 2,6-Difluorobenzyl bromide (**1**) was found to have good solubility in CH_3CN and NaN_3 in H_2O. Two solutions of **1** (0.82 M and 1.64 M in CH_3CN) and two solutions of NaN_3 (0.98 M, 1.97 M in H_2O) were prepared and loaded into separate vessels in the reagent selector (Figure 3.3).

Initially, the effects of concentration, temperature, and residence time on the conversion of **1** were screened using the pathway **R-C** in the synthesizer (Figure 2.27). Upon collection, the solution was analyzed by ^{19}F NMR following the addition of 1 drop of deuterated DMSO to the NMR tube. Intermediate **2** was never isolated (except for characterization). The results of these experiments are reported in Table 3.1.

Table 3.1. Conditions screening for step C1.[a]

Entry	Conc. **1** (M)	NaN_3 equiv.	T (°C)	t (min)	Conv. %[b]
1	0.82	1.2	70	10[c]	79
2	0.82	1.2	70	20[d]	82
3	0.82	1.2	100	10[c]	85
4	0.82	1.2	100	20[d]	>95
5	1.64	1.2	100	20[d]	>95

[a] Conditions screened using the Pathway **R-C** pathway on the synthesizer; **1** solubilized in CH_3CN, **2** in H_2O; back pressure 5 bar. The reaction was monitored via Flow-IR following the formation of the peak at 2090 cm^{-1}. [b] Conversion determined by the ratio of the integrated area of **2** to the total area for peaks **1** + **2** in ^{19}F NMR. [c] Set gas flow rates: MFC1 = MFC2 = 4 ml/min. [d] Set gas flow rates: MFC1 = MFC2 = 2 mL/min.

Despite clean and full conversion to the desired 2,6-difluorobenzyl azide (**2**), the reaction mixture was biphasic. This was observed both within the synthesizer during the reaction and in the collection vessel. Aiming at storing intermediate **2** within the RDS I had to find a way to avoid phase separation that could compromise the correct delivery of **2** in future steps. Methanol prevented phase separation. Unfortunately, neither reagent **1** nor sodium azide were soluble in pure methanol, however, methanol was found to be an effective co-solvent for both reagents. Based on the findings in Table 3.1, different solvent

ratios, stoichiometries, concentrations, temperatures, and residence times were screened using the **R-C** pathway (Table 3.2). The final optimized conditions are those shown in entry 5.

Table 3.2. Conditions screening for step C1.[a]

Entry	Conc. **1** (M)	NaN_3 equiv.	Solvent (**1**)	Solvent (NaN_3)	T (°C)	t (min)	Conv. %[b]	Phases
1	1.64	1.2	MeOH (50) CH_3CN (50)	MeOH (50) H_2O (50)	100	25[c]	>95	2
2	1.64	1.2	MeOH (80) CH_3CN (20)	MeOH (50) H_2O (50)	100	25[c]	>95	2
3	1.5	1.05	MeOH (80) CH_3CN (20)	MeOH (65) H_2O (35)	100	25[c]	>95	1
4	1.5	1.05	MeOH (80) CH_3CN (20)	MeOH (65) H_2O (35)	40	25[c]	>95	1
5	1.5	1.05	MeOH (80) CH_3CN (20)	MeOH (65) H_2O (35)	40	5.5[d]	>95 (>95)	1

[a] Conditions screened using the **R-C** pathway on the synthesizer; back pressure 5 bar. The reaction was monitored via Flow-IR following the formation of the peak at 2090 cm^{-1}. [b] Conversion determined by the ratio of the integrated area of **2** to the total area for peaks **1** + **2** in ^{19}F NMR. NMR yield for entry **5** vs trifluorotoluene as internal standard is given in parenthesis. [c] Set gas flow rates: MFC1 = MFC2 = 2 mL/min. [d] Set gas flow rates: MFC1 = MFC2 = 9 ml/min.

3.1.1.2 Individual optimization of C2

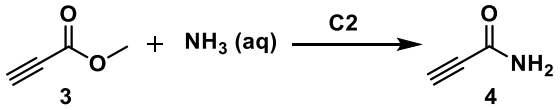

Scheme 3.4. Synthesis of propiolamide **4** (**C2**) via amidation of methyl propiolate (**3**) with aqueous ammonia.

A preliminary offline solvent screening was performed to identify solvents that solubilize the respective reagents. Methyl propiolate (**3**) is a liquid not miscible with water, but it is miscible with acetonitrile. Solutions of different concentration of **3** (1 M, 2 M, 2.36 M, 4 M) in acetonitrile were prepared and loaded in the reagent selector, along with a 7.5 M solution of aqueous ammonia. The amidation was then performed using the **R-C** path (Figure 2.27) on the synthesizer, varying stoichiometry, and residence times. Following collection, the crude mixture was collected, evaporated using a rotavap (to remove NH_3 and CH_3CN) and analyzed via ^1H NMR and ^{13}C NMR in deuterated methanol (CD_3OD).

Table 3.3. Condition screening for step C2.[a]

Entry	Conc. **3** (M)	t (min)	Conv. %[b]
1	2.4	5.5[c]	72
2	2.4	11[d]	>95
3	2	11[d]	>95
4	1	11[d]	>95

[a] Conditions screened using the **R-C** pathway on the synthesizer; all tests performed at room temperature, back pressure 5 bar. The reaction was monitored via Flow-IR following the formation of the peaks at 1670 and 1100 cm^{-1}. [b] Conversion determined by the ratio of the integrated area of **4** (proton bond to the sp carbon) to the total area for peaks of **3** + **4** in ^{1}H NMR and ^{13}C NMR. [c] Set gas flow rates: MFC1 = MFC2 = 9 ml/min. [d] Set gas flow rates: MFC1 = MFC2 = 4.5 ml/min.

3.1.1.3 Individual optimization of C3

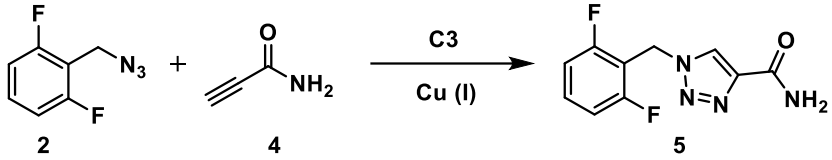

Scheme 3.5. Synthesis of rufinamide (**5**) via a copper-catalyzed Huisgen cycloaddition of 2,6-difluorobenzyl azide (**2**) and propiol amide (**4**).

The solubility of copper catalysts in different solvents and concentrations was first determined offline. The results are shown in Table 3.4. Entry 1, 2, 9, and 15 of Table 3.4 were then loaded into the RDS along with the previously made solution of intermediate **2** at two different concentrations (0.75 M and 0.375 M). The reactivity of the different catalysts for **C3** was then screened as part of a two-step sequence (**R-S**, **S-C**), with intermediate **4** freshly made and stored in the standby loop each time (reaction conditions Table 3.3, entry 4, conc. 1 M)**.**

Table 3.4. Solubility tests for copper catalyst.[a]

Entry	Catalyst System	Solvent	Concentration[b]	Solubility
1	$CuSO_4$:Sodium Ascorbate = 1:2	H_2O	5% (37.5 mM)	Soluble
2			10% (75 mM)	Soluble
3		CH_3CN	5% (37.5 mM)	Insoluble
4			10% (75 mM)	Insoluble
5		MeOH	5% (37.5 mM)	Insoluble
6			10% (75 mM)	Insoluble
7	CuAc	H_2O	5% (37.5 mM)	Insoluble
8			10% (75 mM)	Insoluble
9		CH_3CN	5% (37.5 mM)	Fine suspension[c]
10			10% (75 mM)	Insoluble
11		MeOH	5% (37.5 mM)	Insoluble
12			10% (75 mM)	Insoluble
13	CuI	H_2O	5% (37.5 mM)	Insoluble
14			10% (75 mM)	Insoluble
15		CH_3CN	5% (37.5 mM)	Soluble
16			10% (75 mM)	Insoluble
17		MeOH	5% (37.5 mM)	Insoluble
18			10% (75 mM)	Insoluble

[a] Solubility tests were performed in open test tubes. [b] Concentrations are of the copper species (if fully soluble); the percentage refers to the molar concentration with respect to **2** (0.75 M) in **C3**. [c] CuAc is not completely soluble in any of the tested solvents but in acetonitrile it forms a very fine suspension that could be used in flow without clogging.

Compatibility between these solutions was evaluated beside other reaction conditions in a series of tests carried out using the **S-C** pathway on the synthesizer. Screened parameters and results are shown in Table 3.5. The optimal conditions were determined to be entries 5 and 6.

Table 3.5: Conditions scouting for step C3.[a]

Entry	Conc. **2** (M)	Catalyst	t (min)[b]	Precipitation	Conv. %[e]
1	0.75	$CuSO_4$ 10% in H_2O	- [c]	at mixing station[c]	0
2	0.75	$CuSO_4$ 5% in H_2O	- [c]	at mixing station[c]	0
3	0.75	CuAc 5% in CH_3CN[e]	4[d]	in reactor[d]	>95
4	0.75	CuI 5% in CH_3CN	4[d]	in reactor[d]	>95
5	0.75	CuI 5% in CH_3CN	4	upon collection[d]	>95 (88)
6	0.375	CuI 5% in CH_3CN	4	not observed[d]	>95

[a] Conditions screened using the **S-C** pathway on the synthesizer; **4** was made according to the procedure described in entry 4 of Table 3.3 and stored in the standby module; all tests are performed at room temperature; back pressure 5 bar. The reaction was monitored via Flow-IR, following the formation of the peaks at 1640, 1500 and 1080 cm^{-1}. [b] Set gas flow rates: MFC1 = MFC2 = 4.5 ml/min; when precipitation was observed the reaction mixture was expelled as described in section 2.2. [c] Sodium ascorbate precipitates as soon as it comes into contact with the other solutions (at the mixing station) with consequent inactivation of the catalyst. The mixture was expelled using the unpressurized exit of the divergent valve E. These reactions were allowed to continue after collection, stirring for 10 minutes but they showed no conversion [d] Rufinamide

precipitation occurred in the reactor 4 minutes after mixing. The mixture was expelled using the unpressurized exit of the forwarding valve G. [d] CuAc solubility is as good as reported in Table 3.4 entry 9, the test was possible because the particles were small enough to avoid clogging at the beginning of the process and went into solution once diluted with the other solutions (at the mixing station). [e] Conversion determined after drying the crude for 30 minutes and analyzing it via ^{1}H, ^{13}C, ^{19}F NMR in DMSO-d6; NMR calculated yield *vs*. 1,3,5-trimethoxybenzene as internal standard is given in parenthesis for entry 5.

3.1.1.4 Final process optimization

Optimal conditions for the three steps were identified: **C1**: (Table 3.2, entry 5), **C2**: (Table 3.3, entries 2, 3, 4) **C3**: Table 3.5, entries 5 and 6. The optimal set of overall conditions were then selected from these options. The convergent synthesis uses the combination of pathways **R-R**, **R-S, S-C**. As such, the best process was:

C1: (**R-R**), Table 3.2 entry 5

C2: (**R-S**), Table 3.3 entry 3

C3: (**S-C**), Table 3.5 entry 5

The system was then pressurized to 5 bar and the following protocol was applied (Figure 3.4 and Figure 3.5 - Figure 3.7).

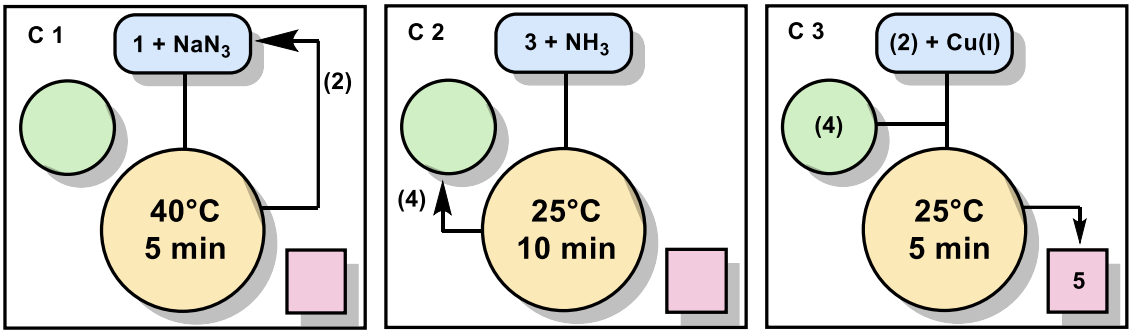

Figure 3.4. Pathways and conditions for the three steps (**C1**, **C2** and **C3**) of the convergent synthesis of rufinamide **5**.

C1 (Figure 3.5):

- Reagents withdrawn from vessel 2 (**1**) and vessel 5 (NaN_3).
- **R-R** pathway: product sent through port 2 of forwarding valve to vessel 1 (intermediate **2** stored in the RDS).
- Temperature of heated reactor: 40 °C.
- Back pressure: 5 bar.
- Gas flow rate set: MFC 1 = MFC 2 = 9 mL/min.
- Effective liquid flow rate: from each sample loop, 1.8 mL/min. Total liquid flow rate = 3.6 mL/min.
- Injection time: 0 s.
- Cycle time: 460 s (7 min 40 s).
- Residence time in the heated reactor: 5 min 30s.

Table 3.6: Destination at all valves for step **C1**

	Divergent Valve (**E**) [a]	Convergent Valve (**F**) [a]	Forwarding Valve (**G**)	Standby Loop (**H**)	Injection Valve (**I**)	Time (s)
Initial position	14	14	DRAIN	LOAD	15	
Injection time	14	14	2	LOAD	15	0
Cycle time	14	14	2	LOAD	15	460
Final position	14	14	DRAIN	LOAD	15	

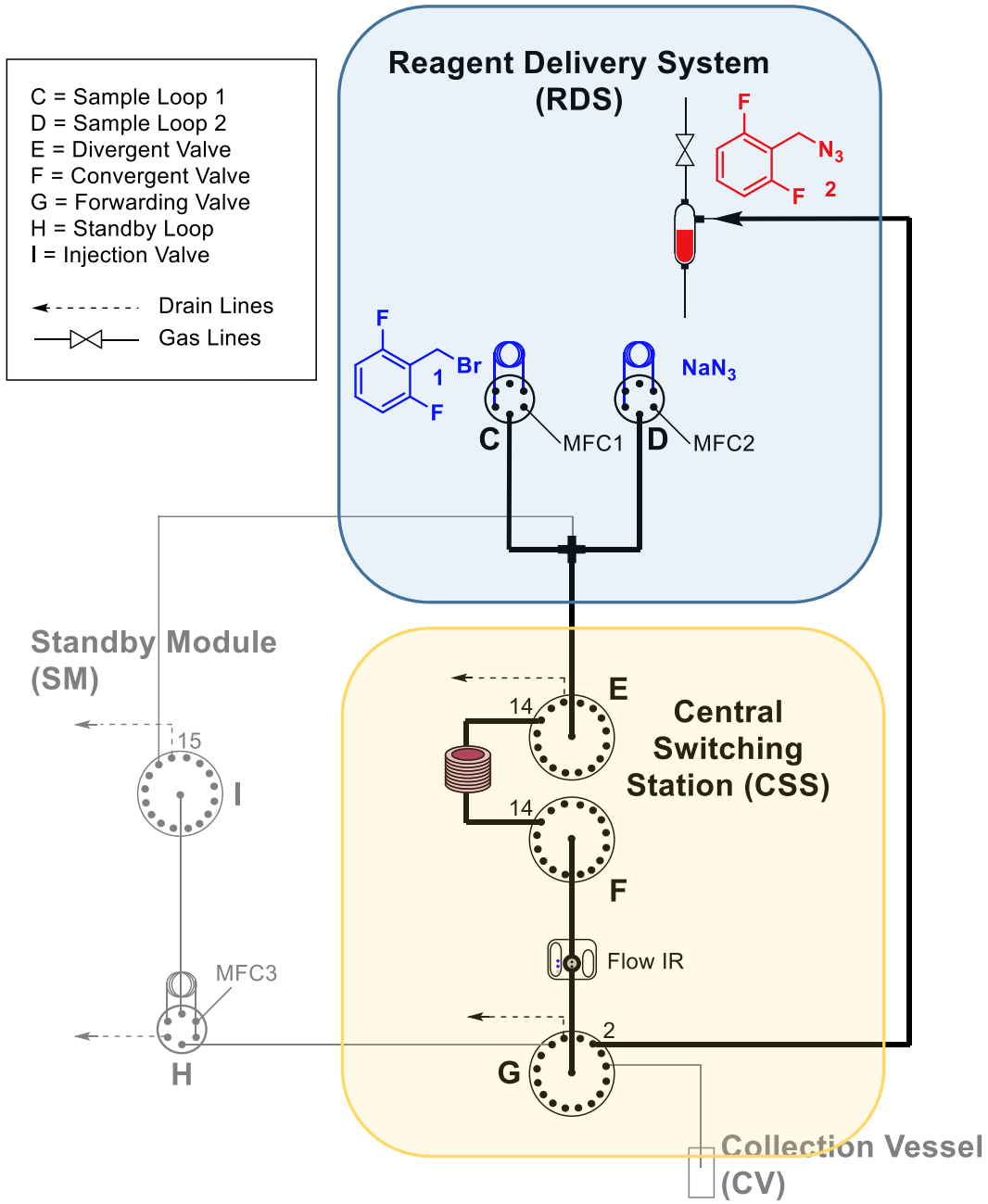

Figure 3.5. First step (**C1**) of the radial convergent synthesis of rufinamide (**R-R**), with storage of intermediate **2** in the RDS. Bold lines indicate the solution path. Starting materials are reported in blue and products in red.

C2 (Figure 3.6):

- Reagents withdrawn from vessel 7 (**3**) and vessel 9 (NH_3(aq)).
- **R-S** pathway: reagents coming from RDS, product sent through port 15 of forwarding valve towards the standby loop (intermediate 4 stored in the standby module).
- Temperature of reactor: room temperature.
- Back pressure: 5 bar.
- Gas flow rate set: MFC1 = MFC2 = 4.5 mL/min.
- Actual liquid flow rates: from each sample loop, 0.9 mL/min. Total liquid flow rate = 1.8 mL/min.
- Injection time: 0 s.
- Cycle time: 775 s (12 min 55 s).
- Residence time in the heated reactor: 11 min.

Table 3.7. Destination at all valves for step **C2**

	Divergent Valve (**E**) [a]	Convergent Valve (**F**) [a]	Forwarding Valve (**G**)	Standby Loop (**H**)	Injection Valve (**I**)	Time (s)
Initial position	14	14	DRAIN	LOAD	15	
Injection time	14	14	15	LOAD	15	0
Cycle time	14	14	15	LOAD	15	775
Final position	14	14	DRAIN	LOAD	15	

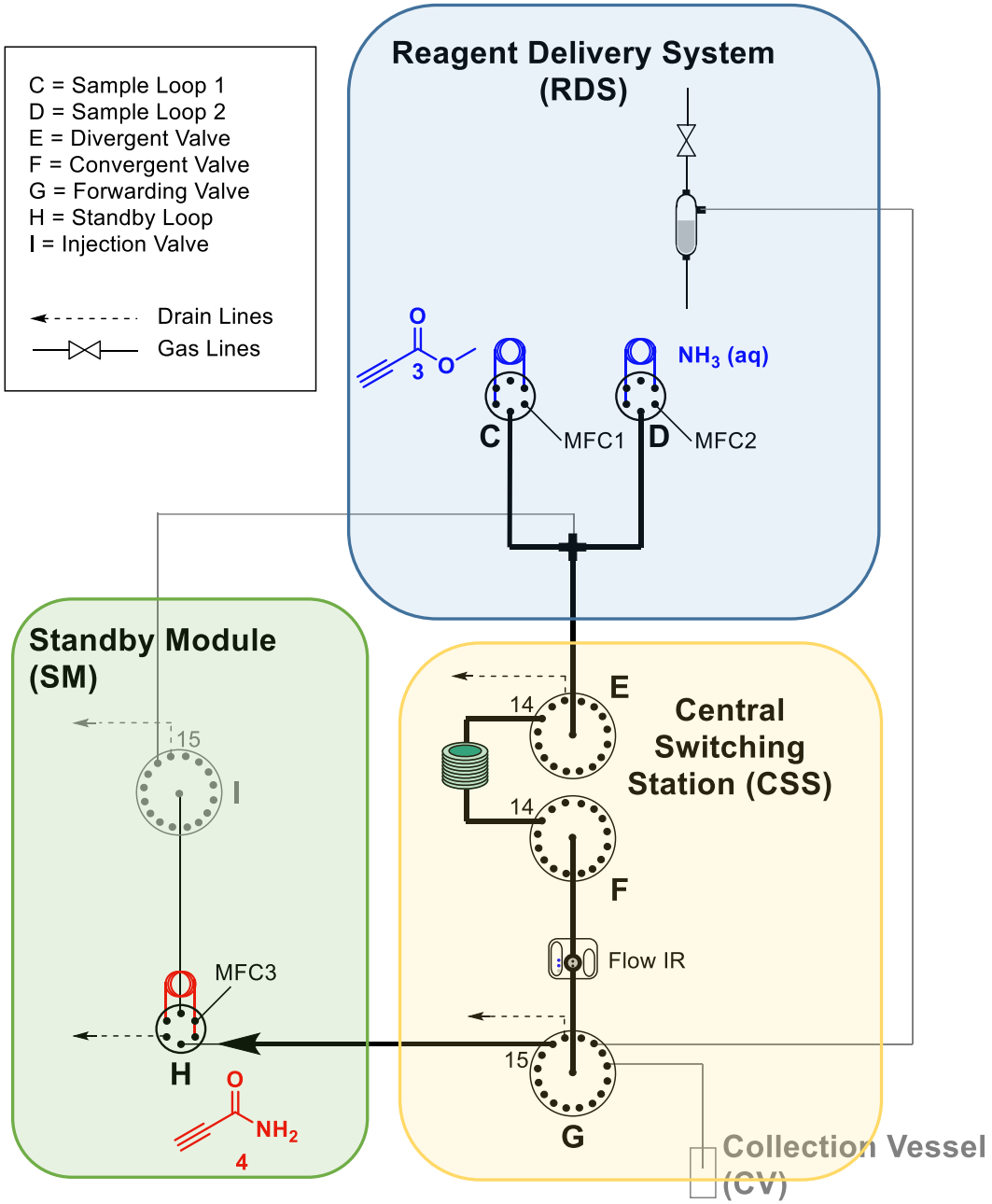

Figure 3.6. Second step (**C2**) of the radial convergent synthesis of rufinamide (**R-S**), with storage of the intermediate **4** in the standby module. Bold lines indicate the solution path. Starting materials are reported in blue and products in red.

C3 (Figure 3.7):

- Reagents withdrawn from vessel 1 (**2**) and vessel 10 (CuI).
- **S-C** pathway: reagents coming from both RDS and Standby module, product sent through port 14 of forwarding valve towards a pressurized collecting vial.
- Temperature of reactor: Room temperature.
- Back pressure: 5 bar.
- Gas flow rate set: MFC1 + MFC2 + MFC3 = 9 mL/min.
- Actual liquid flow rate: from each sample loop and standby loop, 1.8 mL/min. Total liquid flow rate = 5.4 mL/min.
- Injection time: 0 s.
- Cycle time: 180 s (3 min 50 s).
- Residence time: (3 min 42 s).

Table 3.8. Destination at all valves for step **C3**

	Divergent Valve (**E**)[a]	Convergent Valve (**F**)[a]	Forwarding Valve (**G**)	Standby Loop (**H**)	Injection Valve (**I**)	Time (s)
Initial position	14	14	DRAIN	LOAD	15	
Injection time	14	14	DRAIN	INJECT	14	0
Cycle time	14	14	DRAIN	INJECT	14	180
Final position	14	14	4	INJECT	14	

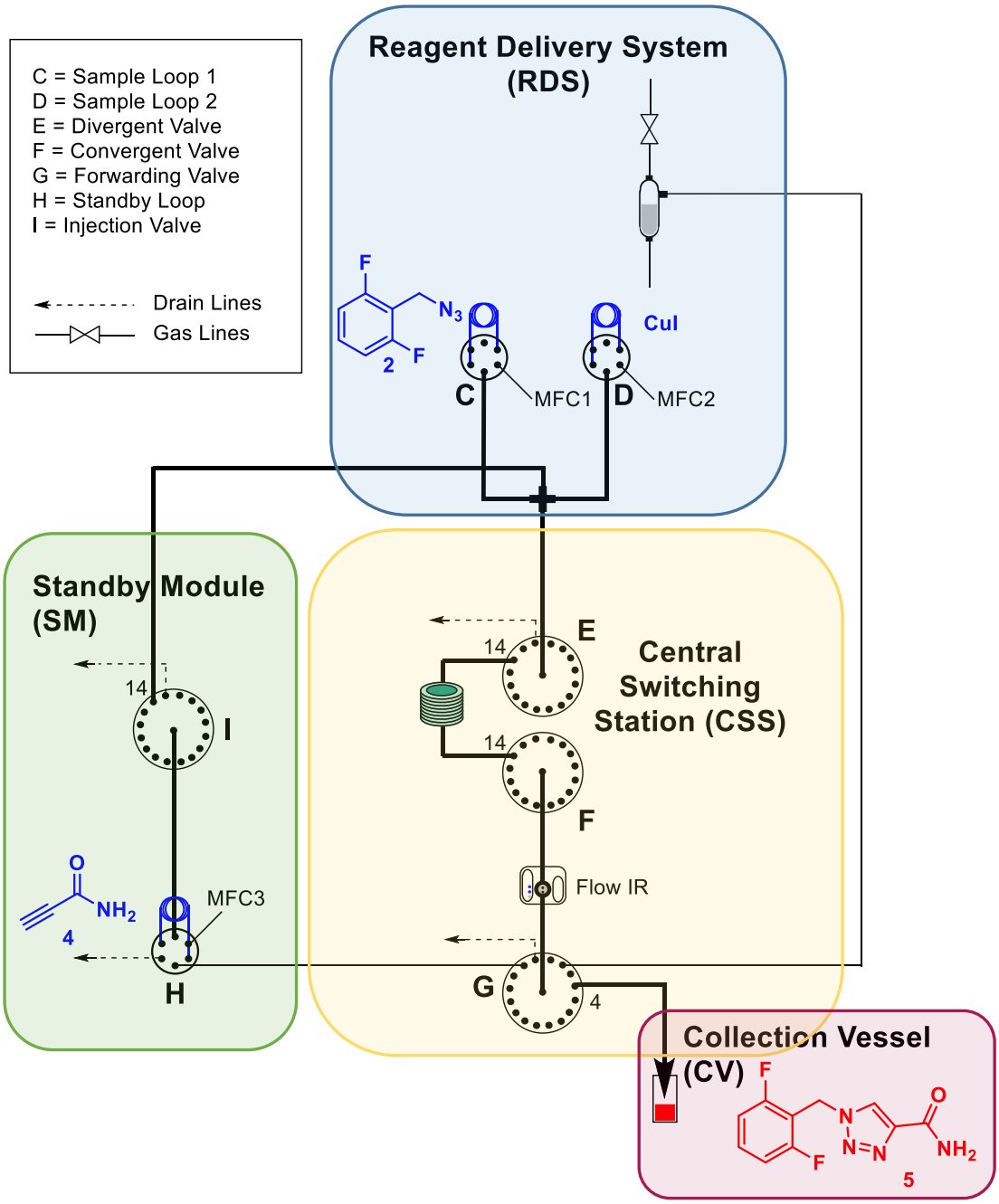

Figure 3.7. The third step (**C3**) of the radial convergent synthesis of rufinamide (**S-C**). Bold lines indicate the solution path. Starting materials are reported in blue and products in red.

The concentration of the final mixture is 0.25 M, at this concentration the precipitation of rufinamide starts after only 4 minutes from the meeting of reagents. It is therefore very important to expel the mixture from the system within 4 minutes in order to avoid clogging. The crude was stirred for 15 minutes at room temperature and the crystals of rufinamide were then filtered, washed two times with demineralized water, dried under vacuum, and analyzed via ^{1}H NMR. The ^{1}H NMR yield versus 1,3,5-trimethoxybenzene as an internal standard was 88%. Crystallization yielded 78.6 mg of material (70%).

3.1.2 Radial *linear* synthesis of rufinamide

Like for the convergent synthesis, also for the linear one each step of the linear sequence was individually optimized and then linked with the others for the optimization of the final process. The following acronyms are used to refer to the individual reactions in the linear process: Step 1 = **L1**, Step 2 = **L2**, Step 3 = **L3** (Scheme 3.6).

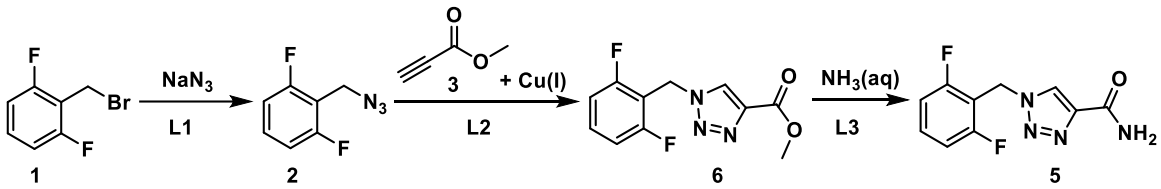

Scheme 3.6. Linear synthesis of rufinamide **5**: **L1** + **L2** + **L3**.

3.1.2.1 Individual optimization of L1

The first step of the linear synthesis is similar to the convergent synthesis **C1** (Scheme 3.3), with the only difference being that in this process intermediate **2** will be stored in the standby loop instead of the RDS. Due to the low solubility observed for rufinamide in the convergent process, lower concentrations of **1** were explored in order to prevent potential precipitation of the cycloadduct **6** in the subsequent step **L2**.

A concise screening was carried out varying concentration of the initial solution of **1** (Table 3.9) from the conditions previously optimized for **C1** (Table 3.2, entry 5). The reaction performs equally well in all conditions screened.

Table 3.9. New concentrations screened for step L1.[a]

Entry	Conc. **1** (M)	Conc. NaN_3 (M)	Conv. %[b]
1	1.5	1.57	>95%
2	1.0	1.05	>95%
3	0.75	0.79	>95%

[a] Conditions screened using **R-C** pathway (Figure 2.27) on the synthesizer; **1** solubilized in CH_3CN:MeOH = 1:4, **2** in H_2O:MeOH = 3.5:6.5 (1.2 equiv.); reactor temperature 40 °C; residence time 5 minutes; back pressure 5 bar; set gas flow rates: MFC1, MFC2 = 9 ml/min. The reaction was monitored via Flow-IR following the formation of the peak at 2090 cm^{-1}. [b] Conversion determined by the ratio of the integrated area of **2** to the total area for peaks **1** + **2** in ^{19}F NMR in $CDCl_3$.

3.1.2.2 Individual optimization of L2

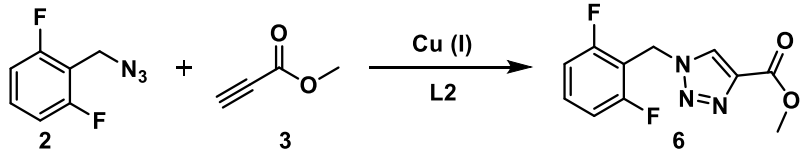

Scheme 3.7. Formation of cycloadduct **6** via a copper(I)-catalyzed Huisgen cycloaddition (**L2**).

The conditions for this step, also a Huisgen cycloaddition, are similar to what was already optimized for **C3** (Scheme 3.5). Differences in reactivity of **3** (step **L2**) and **4** (step **C3**) were taken into consideration, as well as the solubility of the formed intermediate (**6**), which must be temporarily stored in the standby loop prior to **L3**. The step was optimized as part of a two-step process (**L1** + **L2**), similar to how **C3** was optimized.

Starting from the conditions optimized in **C3**, a 1 M solution of methyl propiolate **3** and three solutions with different concentrations of CuI in CH_3CN (0.0375 M, 0.025 M, 0.0188 M) were loaded in the RDS. Their reactivity was tested with freshly made intermediate **2** (as in entries 1, 2 and 3 of Table 3.9) and stored in the standby loop each time. A series of tests were carried out using the **S-C** pathway (Figure 2.30), following the synthesis of **2** using the **R-S** pathway (Figure 2.26) on the synthesizer, to screen concentrations, stoichiometries, temperature, and reaction time (Table 3.10).

Table 3.10. Condition screening for step L2.[a]

Entry	Conc. **2** (M)	Conc. CuI (M)	T (°C)	Precipitation[c]	t [b]	Conv.%[f]
1	0.75	0.0375	25	-	15 min	33
2	0.75	0.0375	25	After 30 min	45 min[d]	77
3	0.75	0.0375	25	After 30 min	1 h[d]	91
4	0.75	0.0375	40	After 6 min	6 min[e]	51
5	0.5	0.025	40	After 30 min	20 min	49
6	0.5	0.025	60	After 30 min	20 min	>95
7	0.375	0.0188	60	-	20 min	>95

[a] Conditions screened using the **S-C** path on the synthesizer; **3** was 1 M in CH_3CN; CuI dissolved in CH_3CN; back pressure 5 bar. The reaction was monitored via Flow-IR following the disappearance of peak at 2090 cm^{-1} and the formation of peak at 1722 cm^{-1}. [b] MFC1 = MFC2 = MFC3 = 4 ml/min. Stop-flow conditions applied for residence times longer than 12 min 30 s. [c] When precipitation was observed, the reaction mixture was expelled (see general information) from the unpressurized port of the forwarding valve **G**. [d] Due to precipitation, I was forced to expel the reaction mixture from the synthesizer before the indicated reaction time, the reaction continued in a vial and was sampled and analyzed after the reported time. [e] Due to precipitation, I was forced to expel the reaction mixture from the synthesizer and it was analyzed immediately. [f] Conversion determined by the ratio of the integrated area of **6** to the total area for peaks **2** + **6** via ^{19}F NMR and ^{1}H NMR (following the disappearance of the benzylic peaks of **2** in favor of those of **6**) in DMSO-d6.

Intermediate **6** was also crystallized, adding few drops of demineralized water to the crude mixture coming from entry 6 of Table 3.10 and stirring for 4 hours. The crystals were filtered, washed with demineralized water, dried under vacuum, and characterized.

3.1.2.3 Individual optimization L3

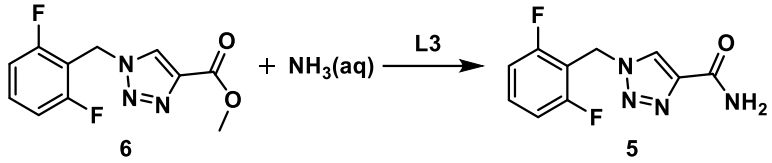

Scheme 3.8. Synthesis of rufinamide **5** via amidation of **6** using aqueous ammonia (L3).

Similar to **C2**, this step involves the formation of an amide bond from a methyl ester and aqueous ammonia. However, transfer of the identical conditions previously optimized (room temperature, 10 minutes, Table 3.3, entry 2, 3, 4) was not possible, with a ten minutes residence time at room temperature giving no conversion (Table 3.11, entry 1). As such, a screening of higher temperatures and longer residence times was performed. A 7.5 M ammonia solution in H_2O was reacted with intermediate **6** (0.25 M or 0.18 M), synthesized as reported in Table 3.10, entry 6 (for entries 1-4 of Table 3.11) and 7 (for entry 5 of Table 3.11). The **R-C** path (Figure 2.27) was used to screen different temperatures and residence times, following the synthesis of **6** using the **S-R** pathway. The optimal conditions are given in entries 3 and 5. Conditions of entry 5 were selected for the final process optimization in order to avoid precipitation of intermediate **6** that occurs after 30 minutes when using higher concentrations.

Table 3.11. Condition screening for step L3.[a]

Entry	Conc. **6** (M)	T (°C)	t (min)	Conv. %[e]
1	0.25	R.T.	10	0
2	0.25	R.T.	30 [b]	12
3	0.25	60	20 [c]	>95
4	0.25	60	10 [d]	55
5	0.18	60	20 [c]	>95 (83%)

[a] Conditions screened using the **R-C** path on the synthesizer; 7.5 M NH_3 in H_2O was used for every test; back pressure = 5 bar. The reaction was monitored via Flow-IR following the disappearance of peak at 1722 cm^{-1} and the formation of peaks at 1640, 1500 and 1080 cm^{-1}. [b] MFC1 = MFC2 = 4 ml/min; effective liquid flow rate: 1.6 mL/min; stop-flow applied for 20 minutes. [c] MFC1 = MFC2 = MFC3 = 2 ml/min. [d] MFC1 = MFC2 = MFC 3 = 4 ml/min. [e] The crude mixture was dried on the rotavap and conversion was determined by the ratio of the integrated area of **5** to the total area for peaks **6** + **5** via ^1H and ^{19}F NMR in deuterated DMSO. The NMR yield was determined via ^1H NMR vs 1,3,5-trimethoxybenzene as internal standard and is reported in parentheses.

3.1.2.4 Final process optimization

Optimal conditions for the three steps were found to be: **L1** (Table 3.9, entries 1, 2 and 3), **L2** (Table 3.10, entries 6 and 7), and **L3** (Table 3.11, entries 3 and 5). The linear synthesis uses the combination of pathways **R-S**, **S-S**, **S-C**. As such, I identified the best process as:

L1: (**R-S**), Table 3.9, entry 2
L2: (**S-S**), Table 3.10**,** entry 6
L3: (**S-C**), Table 3.11, entry 5

The system was then pressurized at 5 bar and the following protocol was applied (Figure 3.8 and Figure 3.9- Figure 3.11).

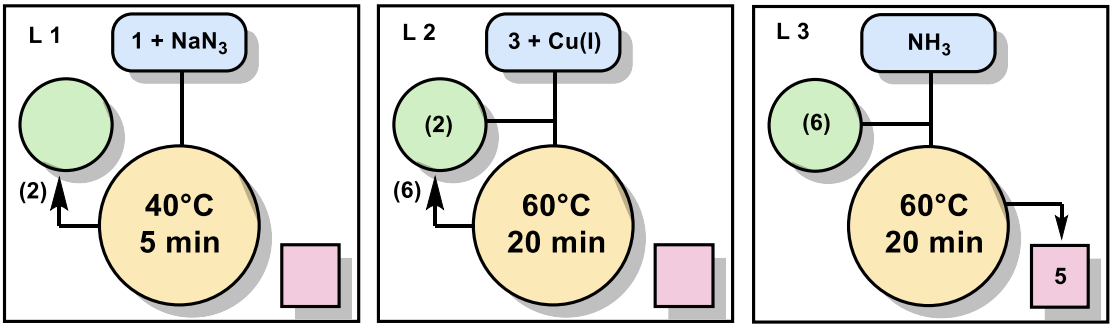

Figure 3.8. Pathways and conditions for the three steps (**L1**, **L2** and **L3**) of the linear synthesis of rufinamide **5**.

L1 (Figure 3.9):

- Reagents withdrawn from vessel 2 (**1**) and vessel 5 (NaN_3).
- **R-S** pathway: product sent through port 15 of forwarding valve to the standby loop (intermediate **2** stored in the standby module).
- Reactor temperature: 40 °C.
- Back pressure: 5 bar.
- Gas flow rate set: MFC1 = MFC2 = 9 mL/min.
- Actual liquid flow rate: from each sample loop: 1.8 mL/min. Total liquid flow rate = 3.6 mL/min.
- Injection time: 0 s.
- Cycle time: 408 s (6 min 48 s).
- Residence time in the heated reactor: 5 min 30s.

Table 3.12. Destination at all valves for step **L1**

	Divergent Valve (**E**) [a]	Convergent Valve (**F**) [a]	Forwarding Valve (**G**)	Standby Loop (**H**)	Injection Valve (**I**)	Time (s)
Initial position	14	14	DRAIN	LOAD	15	
Injection time	14	14	2	INJECT	14	0
Cycle time	14	14	2	LOAD	15	408
Final position	14	14	DRAIN	LOAD	15	

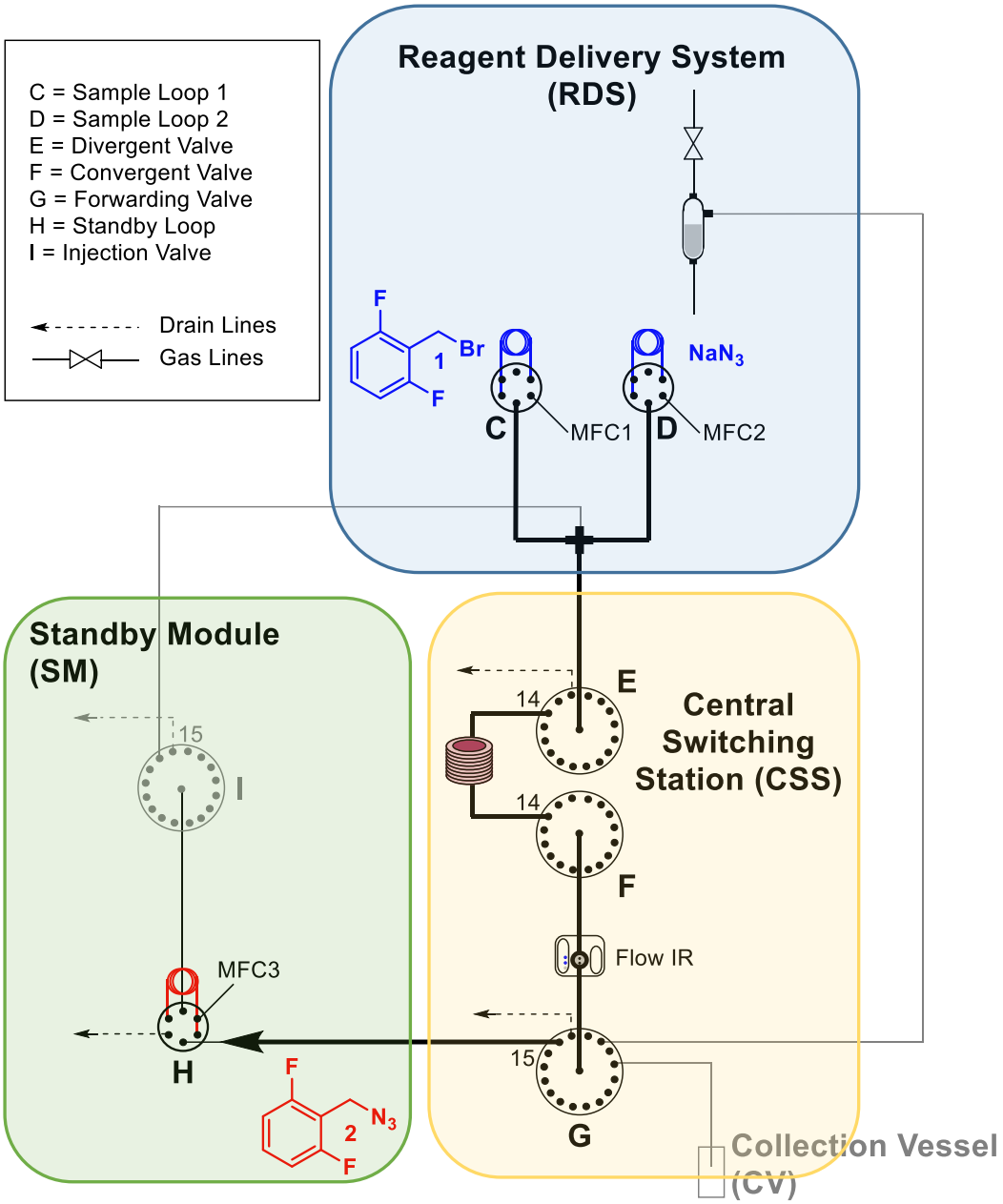

Figure 3.9. First step (**L1**) of the radial linear synthesis of rufinamide (**R-S**). Starting materials are reported in blue and products in red.

L2 (Figure 3.10):

- Reagents withdrawn from vessel 7 (**3**) and vessel 10 (CuI).
- **S-S** pathway: reagents coming from both RDS and standby module, product sent through port 15 of forwarding valve towards the standby loop (intermediate **6** stored in the standby module).
- Reactor temperature: 60 °C.
- Back pressure: 5 bar.
- Gas flow rate set: MFC1, MFC2, MFC3 = 2 mL/min.
- Actual liquid flow rate: from each sample loop and standby loop: 0.4 mL/min. Total liquid flow rate = 1.2 mL/min during the injection time; 0.8 mL/min during the rest of the cycle.
- Injection time: 180 s.
- Cycle time: 1440 s (24 min).
- Residence time in the heated reactor = 1200 s (20 min).

Table 3.13. Destination at all valves for step **L2**

	Divergent Valve (**E**) [a]	Convergent Valve (**F**) [a]	Forwarding Valve (**G**)	Standby Loop (**H**)	Injection Valve (**I**)	Time (s)
Initial position	14	14	DRAIN	LOAD	15	
Injection time	14	14	15	INJECT	14	180
Cycle time	14	14	15	LOAD	15	1440
Final position	14	14	DRAIN	LOAD	15	

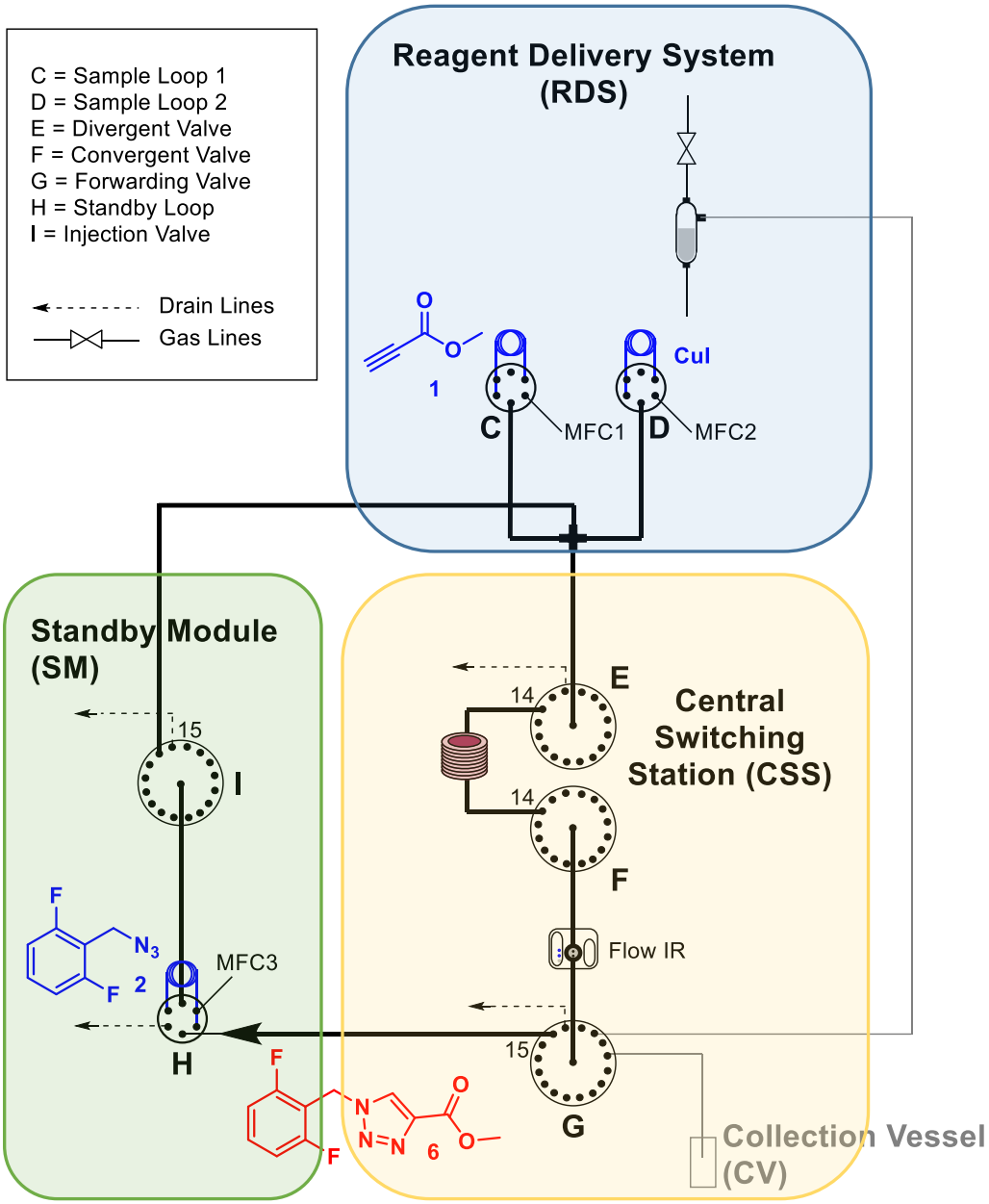

Figure 3.10. The second step (**L2**) of the radial linear synthesis of rufinamide (**S-S**). Starting materials are reported in blue and products in red.

L3 (Figure 3.11):

- Reagents withdrawn from vessel 9 (NH_3) and vessel 14 (H_2O).
- **S-C** pathway: reagents coming from both RDS and standby module, product sent through port 14 of forwarding valve towards a pressurized collecting vial.
- Reactor temperature: 60°C.
- Back pressure: 5 bar.
- Gas flow rate set: MFC1 = MFC2m = MFC3 = 2 mL/min.
- Actual liquid flow rate: from each sample loop and standby loop = 0.4 mL/min. Total liquid flow rate during injection time = 1.2 mL/min. Total liquid flow rate during rest of the cycle = 0.8 mL/min
- Injection time: 180 s.
- Cycle time: 1290 s (21 min 30 s).
- Residence time in the heated reactor = 1200 s (20 min).

Table 3.14. Destination at all valves for step **L3**

	Divergent Valve (**E**)[a]	Convergent Valve (**F**)[a]	Forwarding Valve (**G**)	Standby Loop (**H**)	Injection Valve (**I**)	Time (s)
Initial position	14	14	DRAIN	LOAD	15	
Injection time	14	14	DRAIN	INJECT	14	180
Cycle time	14	14	DRAIN	LOAD	15	1290
Final position	14	14	4	LOAD	15	

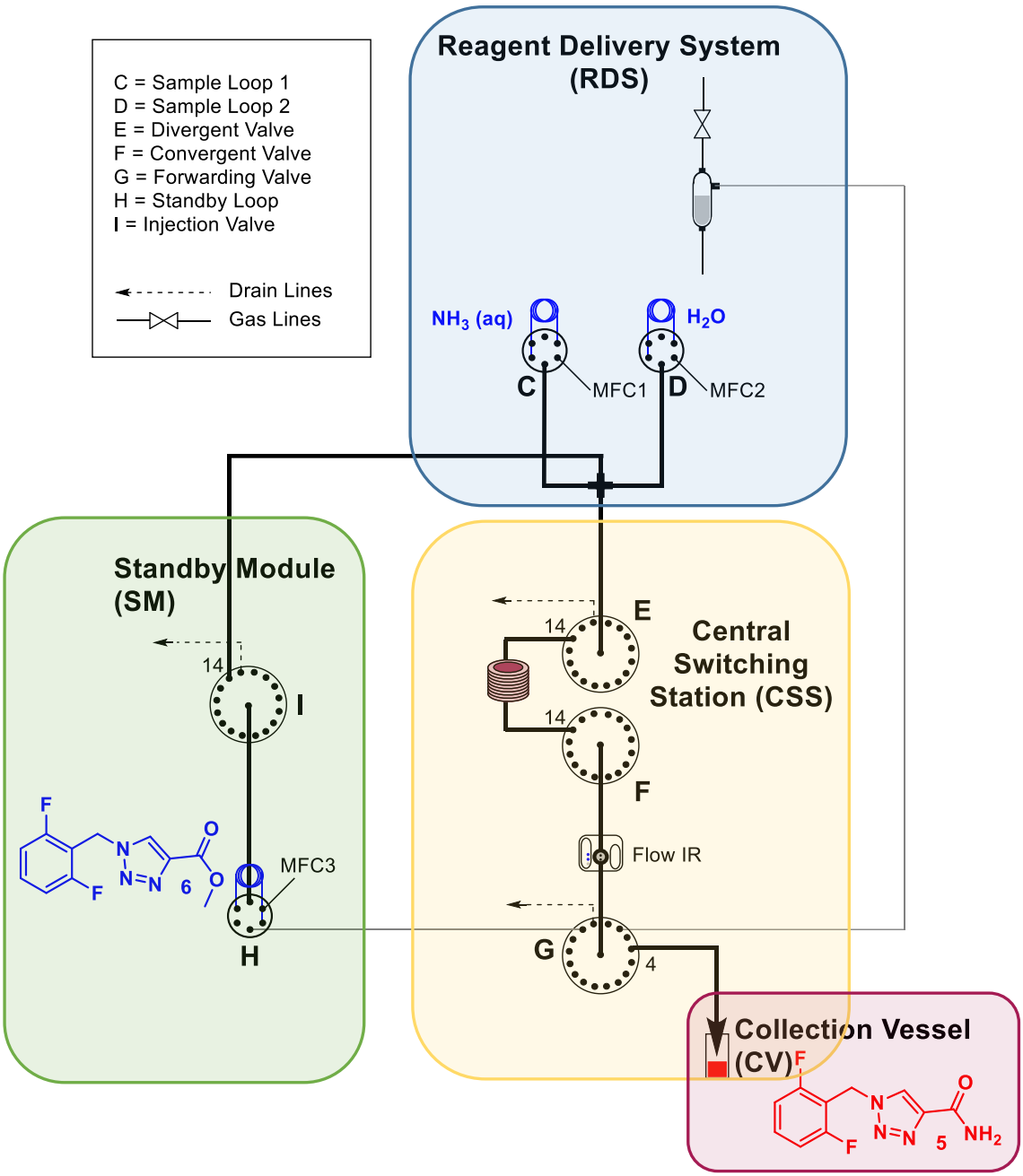

Figure 3.11. The third step (**L3**) of the radial linear synthesis of rufinamide (**S-C**). Starting materials are reported in blue and products in red.

The ^{1}H NMR yield vs 1,3,5-trimethoxybenzene was 83% over the 3 steps. Demineralized water (1 mL) was added to the crude solution to crystallize rufinamide, achieving a 45% crystallized yield.

The different synthetic pathways to a target molecule executed on the same instrument allow for the direct comparison of synthetic routes. Rufinamide is achieved through the convergent route in a shorter time (20 minutes) compared to the linear one (45 minutes). Furthermore reaction conditions required in the convergent process are milder (the first step requires 40 °C and second and third step take place at room temperature). The rufinamide syntheses compared here identified the solubility of the heterocyclic adduct as a key challenge. Formation of this species in the final step of the convergent process allows for more concentrated solutions of **1** to be used (1.5 M versus the 1.0 M of the linear pathway) as starting materials. Rufinamide purification is simpler via the convergent route because the product crashes out upon exiting the instrument, while the linear route required the addition of water. Finally, not only is the convergent route higher yielding than the linear path after room temperature crystallization (70% versus 45%) but also by ^{1}H NMR (88% versus 83%).

3.2 Library Generation

The ability to access multiple synthetic routes and different conditions on one instrument without the need of physical intervention allows for the generation of libraries of derivatives (Figure 3.12). This opens the door to the application of the radial synthesizer to fields like medicinal chemistry which are based on the systematic, synthetic alteration of known core structures.

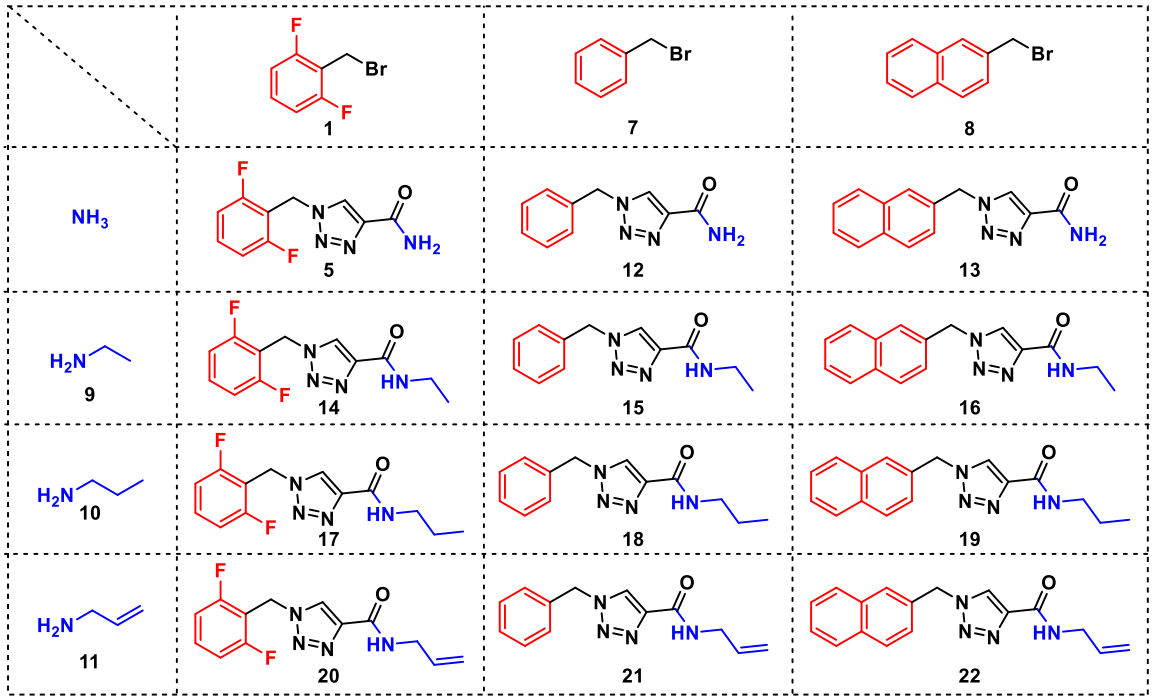

Figure 3.12. Library of rufinamide derivatives achievable via combination of different aryl cores and amine functionalities.

Both the arene core and the amide functionality of rufinamide can be replaced by playing with different combinations of substrates and reagents. The synthetic pathway to use for the synthesis of each derivative can be chosen on the basis of the least number of re-optimizations required. Due to differences in reactivity between the two new sets of reagents, several of the steps require different reaction temperature, time, or concentration. By judicious choice between either the convergent or the linear route already optimized for rufinamide, it was possible to identify the easiest synthetic process for each molecule of the library saving time and efforts. For example, the arene core of rufinamide is introduced first in both the convergent and the linear pathways. However, for the convergent route, variation of this group would result in two potential re-optimizations (the **C2** step is independent as shown in Figure 3.13 a), whereas all three steps of the linear path could be affected. Likewise, the amine is introduced in the last step of the linear pathway (only one re-optimization required), whereas two re-optimizations might be required to change the amide functionality via the convergent route (Figure 3.13 b).

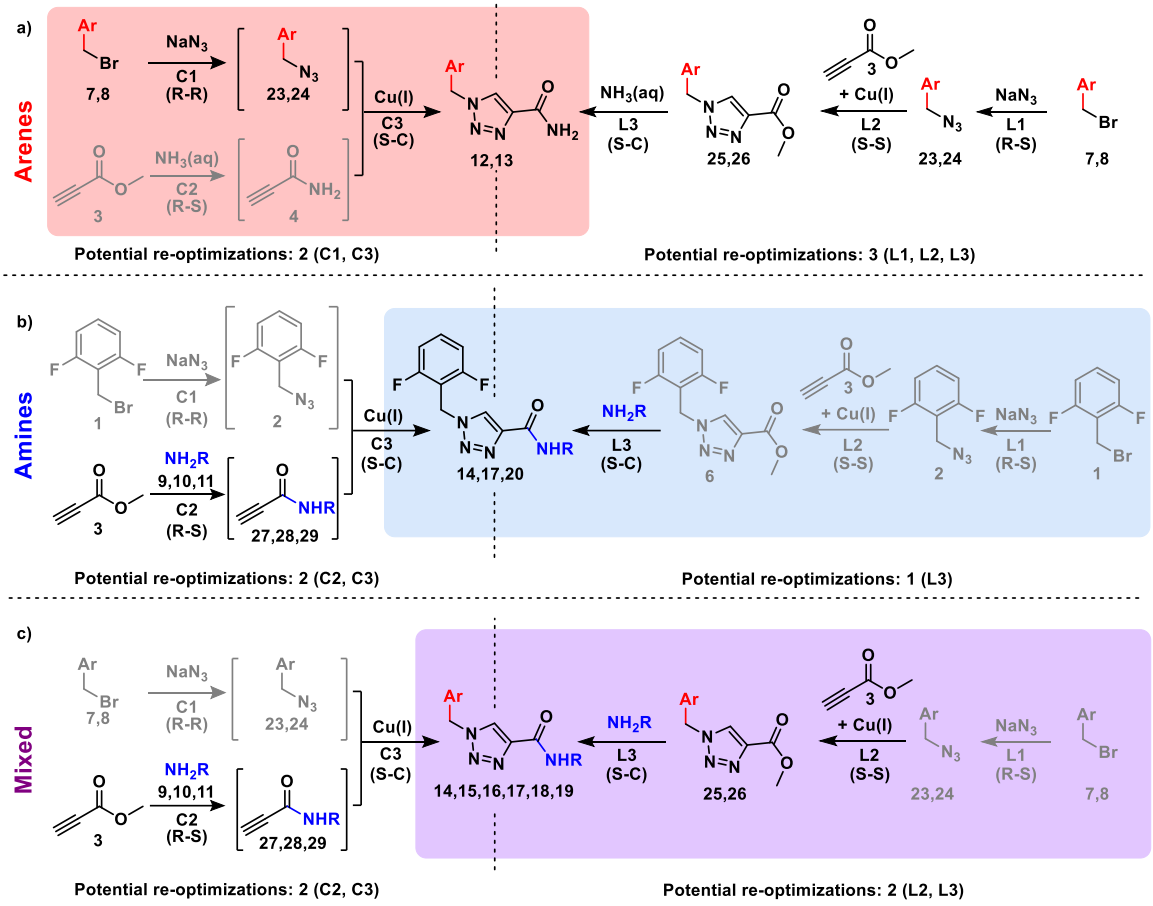

Figure 3.13. The synthetic route for each class of derivatives was selected based on the minimal number of steps potentially requiring re-optimization, which are highlighted in colored boxes. Steps that don´t require re-optimization are grayed.

3.2.1 Arenes scope

The investigation started from the synthesis of derivatives **12** and **13** (Scheme 3.9) in which the 2,6-difluorobenzyl core of rufinamide is replaced respectively by a benzyl and a naphthyl core (Figure 3.12). The more straightforward way to introduce this modification is through the convergent synthesis because using this synthetic pathway step **C2** is identical to step **C2** of rufinamide, thus only steps **C1** and **C3** need to be optimized.

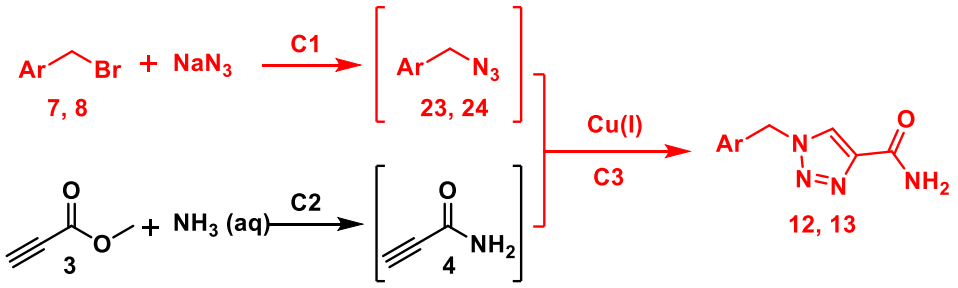

Scheme 3.9. Synthesis of derivatives **12** and **13**. The bromides scope was investigated using the convergent synthesis. Step **C2** is not affected and only steps **C1** and **C3** potentially require optimization.

3.2.1.1 Synthesis of benzyl azide 23 (C1/L1)

The formation of benzyl azide **23** was first tested starting from benzyl bromide (**7**) and sodium azide, under the same conditions used to synthesize 2,6-difluorobenzylazide **2** (Table 3.2 entry 5) using the **R-C** path.

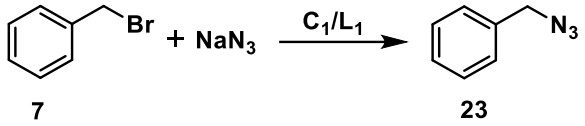

Scheme 3.10. Synthesis of benzyl azide **23** (**C1/L1**).

The reaction did not show any phase separation and good conversion was achieved when the reaction was run at 40 °C for 5 minutes. The reaction was monitored via Flow-IR, following the formation of the peak at 2090 cm^{-1}. In order to calculate the yield, one test was run in D_2O, MeOD, and CH_3CN. Upon collection, 0.2 mL of DMSO-d6 were added to the sample and the mixture was analyzed by ^1H NMR spectroscopy, providing benzyl azide **23** in 95% conversion (the presence of non-deuterated CH_3CN is the reason for the tall peak at 1.97 ppm in Figure 6.31 of the appendix). Note that this intermediate was never isolated, the spectrum in Figure 6.31 is the ^1H NMR of the crude reaction.

3.2.1.2 Optimization of the synthesis of 2-(azidomethyl)naphthalene 24 (C1/L1)

Also the formation of 2-(azidomethyl)naphthalene (**24**) started from 2-(bromomethyl)naphthalene (**8**) and sodium azide testing at first the same conditions found optimal for 2,6-difluorobenzylazide **2** (Table 3.2 entry 5). However, due to the poor solubility of bromide **8** in water, precipitation was observed as soon as the solution came into contact with the solution of sodium azide (which contains 35% of water).

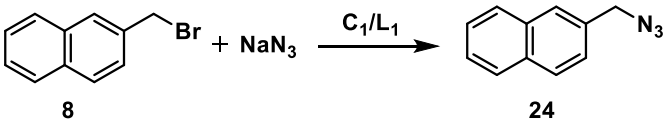

Scheme 3.11. Synthesis of 2-(azidomethyl)naphthalene **24** (**C1**/**L1**).

Different concentrations and solvents ratios were screened using the **R-C** path on the synthesizer to find the best conditions. These tests are reported in Table 3. 15. The solution exiting the synthesizer was dried on the rotavap and analyzed via ^1H NMR. Optimal conditions are given in entry 3.

Table 3. 15. Condition screening for the synthesis of 2-(azidomethyl)naphthalene **24** [a]

Entry	Conc. **8** (M)	Conc. NaN_3 (M)	Solvent (NaN_3)	t (min)	Precipitation	Conv. % [b]
1	1.5	1.6	MeOH (65) H_2O (35)	- [c]	At mixing station	-
2	1	1.05	MeOH (65) H_2O (35)	- [c]	At mixing station	-
3	0.5	0.53	MeOH (80) H_2O (20)	5	none	>95%

[a] Conditions screened using the **R-C** path on the synthesizer; **8** solubilized in CH_3CN:MeOH = 1:4; reactor temperature: 40 °C; back pressure: 5 bar; set gas flow rates: MFC1 = MFC2 = 9 mL/min. The reaction was monitored via Flow-IR, following the formation of the peak at 2090 cm^{-1}. [b] Conversion determined by the ratio of the integrated area of benzylic peak of **24** to the total area for benzylic peaks of **8** + **24** in ^1H NMR. [c] When precipitation was observed the reaction mixture was expelled as reported in the general information from the unpressurized port of the divergent valve **E**.

3.2.1.3 Optimization of the synthesis of derivative 12 (C3)

For the synthesis of 1-benzyl-1H-1,2,3-triazole-4-carboxamide (**12**) the same conditions found optimal for step **C3** of the synthesis of rufinamide were initially screened.

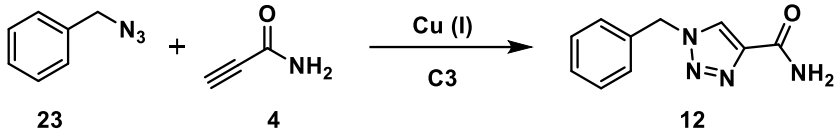

23 **4** **12**

Scheme 3.12. Synthesis of derivative **12** (**C3**).

Intermediate **4** (**C2**) was synthesized as described in Table 3.3 entry 3 using the **R-S** pathway in the synthesizer. The resulting 1 M solution of **4** was then reacted with a 0.75 M solution of **23** and a 0.0375 M solution of CuI (Table 3.5, entry 5) using the **S-C** pathway on the synthesizer. The reaction was monitored via Flow-IR, following the disappearance of peak at 2090 cm^{-1} and the formation of peaks at 1610 and 1500 cm^{-1}.

Optimization of the residence time was performed by setting the flow rate of the three MFCs to 3 mL/min (resulting residence time in the reactor: 11 minutes). The residence time was adjusted progressively in order to avoid precipitation within the flow reactor. When precipitation was observed the mixture was expelled as reported in section 2.2 using the unpressurized line at the forwarding valve **G**. Using this methodology, the residence time for **12** was determined to be four minutes.

The process proceeded smoothly, with the product precipitating in the collection vessel 5 minutes after reagent mixing. Crystals were filtered, washed with water, and analyzed by ^1H NMR spectroscopy. The ^1H NMR NMR yield of the crude material vs 1,3,5-trimethoxybenzene was 78%. The yield of the crystallized material (**12**) was 59%.

3.2.1.4 Optimization of the synthesis of derivative 13 (C3)

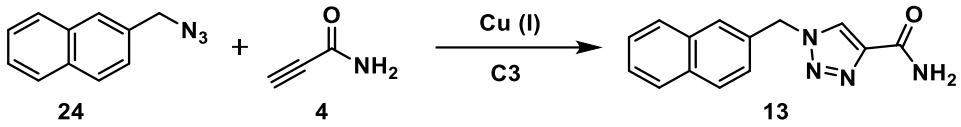

Scheme 3.13. Synthesis of derivative **13** (**C3**).

Compound **24** was synthesized as reported in Table 3. 15, entry 3 (final concentration of **24** was 0.25 M) and stored in the RDS (**R-R** path on the synthesizer). Propiolamide **4** was prepared as reported in Table 3.3, entry 4 (final concentration of **4** was 0.5 M) and stored in the SM using the **R-S** path on the synthesizer. A solution of CuI (0.0125 M in CH_3CN) is accessed from the RDS and **C3** is performed using the **S-C** path. The reaction was monitored via Flow-IR, following the disappearance of peak at 2090 cm^{-1} and the formation of peaks at 1651, 1640, and 1029 cm^{-1}.

After a residence time of 8 minutes, precipitation was observed. The reaction mixture was then expelled from the synthesizer as reported in section 2.2 using the unpressurized line at the forwarding valve **G**. After stirring for 15 minutes the crystals of derivative **13** are filtered, washed with demineralized water, and analyzed via ^1H NMR. NMR yield (77%) was calculated via ^1H NMR vs 1,3,5-trimethoxybenzene as standard. The yield of the crystallized material (**13**) was 52%.

3.2.2 Amines scope

In order to vary the amide group of rufinamide, the more straightforward way is through the linear synthesis. The syntheses of rufinamide derivatives which share the 2,6-difluorobenzyl core indeed, do not need any optimization until the very last step (**L3**) when following the linear route (Scheme 3.14).

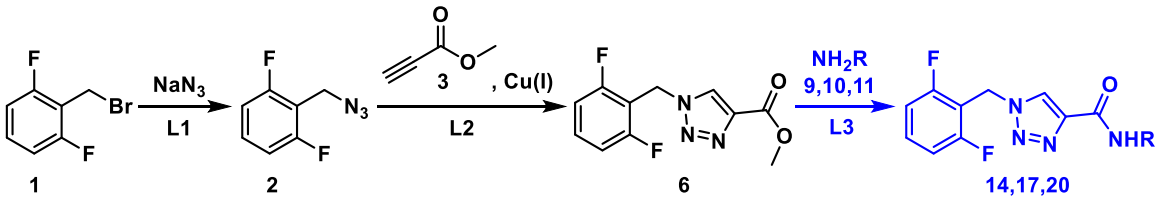

Scheme 3.14. Synthesis of derivatives **14**, **17** and **20**. The amines scope was investigated using the linear synthesis. Steps **L1** and **L2** are not affected and only step **L3** potentially requires optimization.

3.2.2.1 Optimization of the synthesis of derivative 17 (L3)

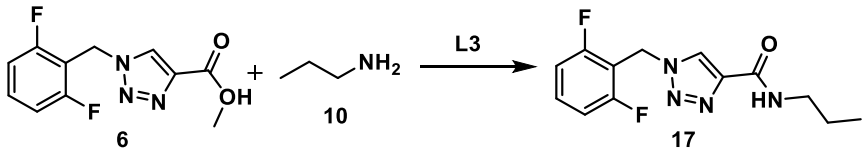

Scheme 3.15. Synthesis of derivative **17** (**L3**).

Intermediate **6** was synthesized following the same protocol already developed for the linear synthesis of rufinamide: **L1** (**R-S**, Table 3.9, entry 2), **L2** (**S-S**, Table 3.10, entry 6). A series of tests varying concentration, temperature, and residence time were performed in order to optimize **L3** for alkyl amines.

Neat propylamine was loaded in one of the vessels of the reagent selector **A** and diluted with acetonitrile coming from the solvent selector **S** to screen different concentrations. Stoichiometry, temperature, and residence time were screened using the **S-C** pathway and results are given in Table 3.16.

Table 3.16. Condition scouting synthesis of derivative **17**.[a]

Entry	Conc. **10**	T (°C)	t (min)	Conv. %[b]
1	6 M	60	10[c]	50
2	6 M	100	10[c]	50
3	Neat (12 M)	100	10[c]	87
4	Neat (12 M)	100	20[d]	>95%

[a] Conditions screened using the **S-C** pathway on the synthesizer; conc. of **6** 0.5 M; back pressure 5 bar. The reaction was monitored via Flow-IR following the disappearance of peak at 1722 cm^{-1} and the formation of peaks at 2880, 1615, 1605 and 1315 cm^{-1}. [b] Conversion determined by the ratio of the integrated area of the triazole peak of **17** to the total area for the triazole peaks of **6** + **17** in ^1H NMR. [c] Set gas flow rates: MFC1 = MFC2 = MFC3 = 3.5 mL/min. [d] Set gas flow rates: MFC1 = MFC2 = MFC3 = 2 mL/min. No precipitation was observed.

Water (1 mL) was added to the collected crude mixture to crystallize derivative **17**. The NMR yield (86%) was determined for this derivative via ^1H NMR vs 1,3,5-trimethoxybenzene. After stirring for 4 hours at room temperature, 9.4 mg of compound **17** was obtained (40% yield).

3.2.2.2 Optimization of the synthesis of derivative 14 (L3)

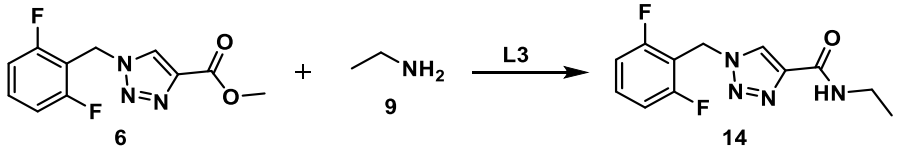

Scheme 3.16. Synthesis of derivative **14** (**L3**).

Intermediate **6** was synthesized following the same protocol developed for the linear synthesis of rufinamide: **L1** (**R-S**, Table 3.9, entry 2), **L2** (**S-S**, Table 3.10, entry 6). The same conditions of Table 3.16, entry 4 were tested using ethylamine (70% solution in water) for **L3** using the **S-C** pathway. The reaction was monitored via Flow-IR, following the disappearance of peak at 1722 cm^{-1} and the formation of peaks at 2880, 1605, 1500, and 1316 cm^{-1}. No precipitation was observed.

Upon collection, the solvent was evaporated, and the residue was analyzed by ^{1}H NMR (74% vs 1,3,5-trimethoxybenzene. Water (1 mL) was added to the collected crude mixture to crystallize derivative **14**. After stirring for 4 hours at room temperature, 10.2 mg of pure compound was obtained (46% yield).

3.2.2.3 Optimization of the synthesis of derivative 20 (L3)

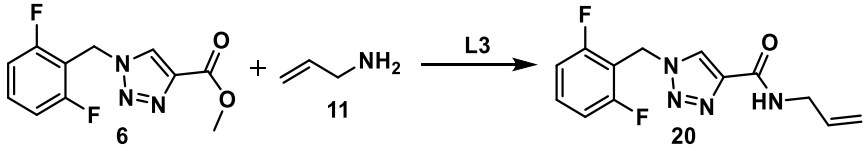

Scheme 3.17. Synthesis of derivative **16** (**L3**).

Intermediate **6** was synthesized following the same protocol developed for the linear synthesis of rufinamide: **L1** (**R-S**, Table 3.9, entry 2), **L2** (**S-S**, Table 3.10, entry 6). Based on the assumption that allylamine is a worse nucleophile than propylamine, I excluded the possibility that a dilute solution or temperature lower than 100 °C could result in a good yield. As such, a series of tests were chosen for step **L3** starting with neat allylamine and screening different residence times using the **S-C** pathway on the synthesizer. The results are shown in Table 3.17. Stop-flow conditions were utilized to achieve residence times longer than 20 minutes.

Table 3.17. Condition scouting synthesis of derivative **20**.[a]

Entry	Conc. **11**	T (°C)	t (min)	Conv. %[b]
1	Neat	100	20[c]	50%
2	Neat	100	40[d]	72%
3	Neat	100	60[d]	86%

[a] Conditions screened using the **S-C** path on the synthesizer; conc. of **6** 0.5 M; pressure = 5 bar. The reaction was monitored via Flow-IR following the disappearance of peak at 1722 cm^{-1} and the formation of peaks at 1670, 1596, 1315 and 1202 cm^{-1}. [b] Conversion determined by the ratio of the integrated area of the triazole peak of **20** to the total area for the triazole peaks of **6** + **20** in ^{1}H NMR. No precipitation was observed. [c] Set gas flow rates: MFC1 = MFC2 = 2 mL/min. [d] Set gas flow rates: MFC1 = MFC2 = 4.5 mL/min, stop-flow for the time necessary to achieve the specified residence time.

NMR yield (58%) was determined for this derivative via ^{1}H NMR vs 1,3,5-trimethoxybenzene. Water (1 mL) was added to the collected crude mixture to crystallize derivative **20**. After stirring for 4 hours at room temperature, 4.5 mg of pure compound was obtained (29% yield).

3.2.3 Mixed derivatives

Finally, a series of derivatives were prepared by combining two arene cores (benzyl bromide **7** and 2-(bromomethyl)Naphthalene **8**) with three alkyl amines **9**, **10** and **11**. These mixed derivatives can be grouped in two sets: derivatives sharing the benzyl core (**15**,**18** and **21** in Figure 3.12) and derivatives sharing the naphthyl core (**16**, **19** and **22 in** Figure 3.12). Once the two sets were identified the potential optimizations required by both the linear and the convergent route were investigated.

I envisioned that the linear route would give the fastest access to the mixed derivatives as it requires two individual optimizations for step **L2**, leading to intermediates **25** and **26** and three optimizations of step **L3** for each intermediate (2 + 6 = 8 step optimizations), while the convergent process would require new conditions for each amide formation (intermediates **27**, **28** and **29**) resulting in three re-optimizations for step **C2** and following combination of each of them with the two azides (intermediates **23** and **24**) resulting in six re-optimizations for step **C3** (for a total of 3 + 6 = 9 step optimizations) (Figure 3.14).

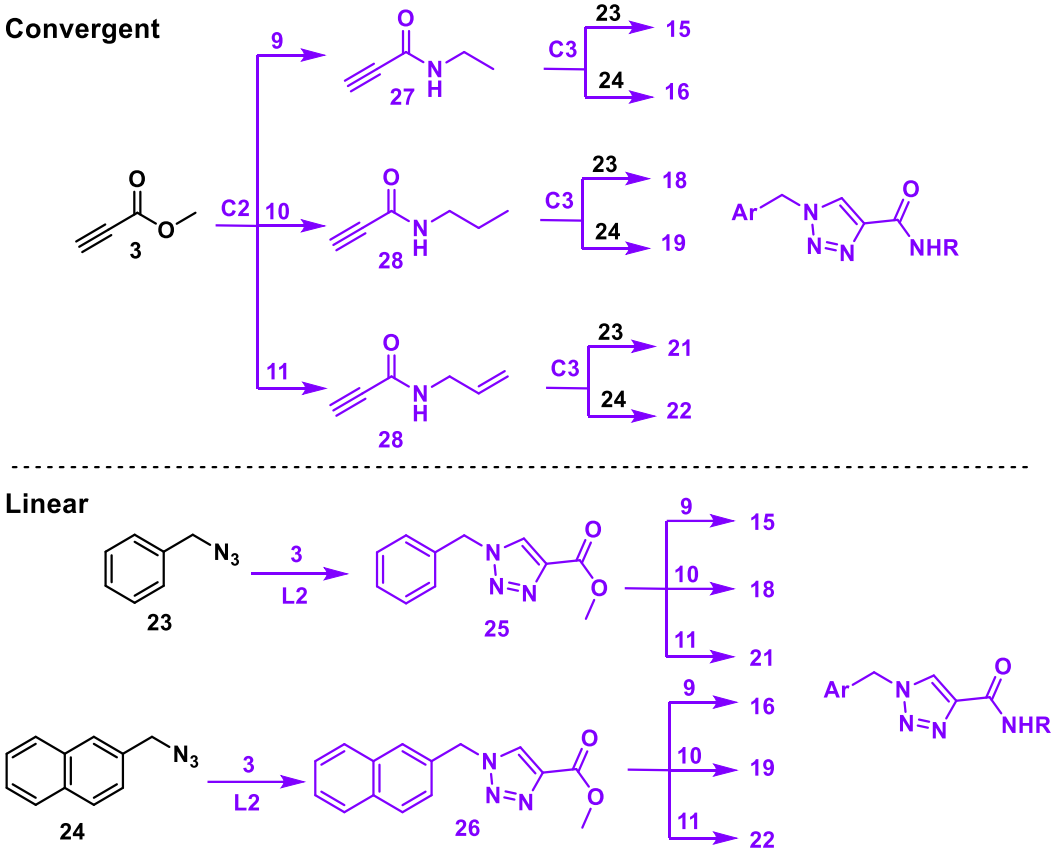

Figure 3.14. Convergent vs linear route for the syntheses of mixed derivatives (**15**, **16**, **18**, **19**, **21** and **22**). The linear route resulted being the most convenient pathway as it requires 8 vs 9 potential step re-optimizations.

3.2.3.1 Optimization of the synthesis of intermediate 25

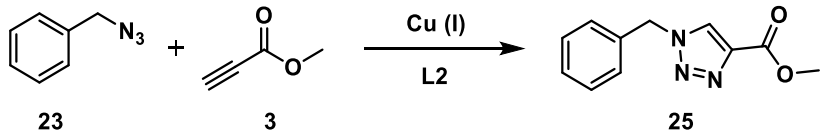

Scheme 3.18. Synthesis of intermediate **25** (**L2**).

Intermediate **23** was synthesized following the optimal protocol found for 2,6-difluorobenzylazide **2** (Table 3.9, entry 5) using the **R-S** pathway on the synthesizer. The resulting 0.375 M solution of **23** was then combined with methyl propiolate **3** and CuI applying the same optimal conditions found for the synthesis of intermediate **6** (Table 3.10, entry 7) using the **S-C** pathway. The reaction was monitored via Flow-IR, following the disappearance of peak at 2090 cm^{-1} and the formation of peak at 1722 cm^{-1}. No precipitation was observed.

Upon collection, the solvent was evaporated and the residue was analyzed by ^{1}H NMR, showing conversion >95% (conversion determined by the ratio of the integrated area of benzylic peaks of **25** to the total area for benzylic peaks of **23** + **25** in ^{1}H NMR).

3.2.3.2 Optimization of the synthesis of intermediate 26

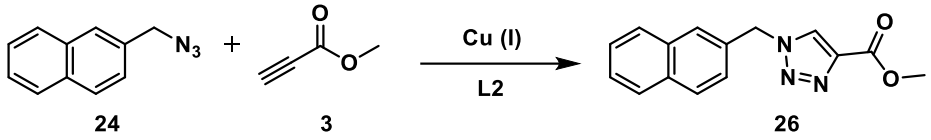

Scheme 3.19. Synthesis of intermediate **26** (**L2**).

Intermediate **24** was synthesized as described in Table 3. 15, entry 3 using the **R-S** pathway on the synthesizer. The resulting 0.25 M solution of **24** was then combined with methyl propiolate **3** and CuI, applying conditions similar to those reported in Table 3.11, entry 7, with some adjustments due to the lower initial concentrations of starting material: **24** (0.25 M), CuI (0.0125M), **3** (1 M). The reaction was performed using the **S-C** path and monitored via Flow-IR, following the disappearance of peak at 2090 cm^{-1} and the formation of peak at 1722 cm^{-1}. No precipitation was observed.

Upon collection, the solvent was evaporated and the residue was analyzed by ^{1}HNMR, showing conversion >95% (conversion determined by the ratio of the integrated area of benzylic peak of **26** to the total area for benzylic peaks of **24** + **26** in ^{1}H NMR).

3.2.3.3 Synthesis of derivative 18 (L3)

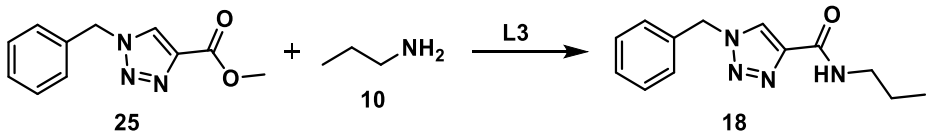

Scheme 3.20. Synthesis of derivative **18** (**L3**).

Intermediate **25** was synthesized as reported in section 3.2.3.1, using the **S-S** pathway on the synthesizer. The same optimal conditions found for the synthesis of derivative **17** were applied (Table 3.16, entry 4) to run the reaction between intermediate **25** and propylamine **10** using the **S-C** pathway. The reaction was monitored via Flow-IR, following the disappearance of peak at 1722 cm^{-1} and the formation of peaks at 2880, 1605, and 1150 cm^{-1}. No precipitation was observed.

Upon collection, the solvent was evaporated, and the residue was analyzed by ^{1}H NMR. NMR yield (83%) was determined for this derivative via ^{1}H NMR vs 1,3,5-trimethoxybenzene. Water (1 mL) was added to the collected crude mixture to crystallize derivative **18**. After stirring for 4 hours at room temperature, 7.7 mg of pure compound was obtained (38% yield).

3.2.3.4 Synthesis of derivative 19 (L3).

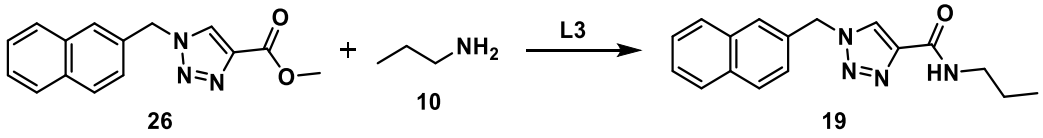

Scheme 3.21. Synthesis of derivative **19** (optimization of **L3**).

Intermediate **26** was synthesized as reported in section 3.2.3.2, using the **S-S** pathway on the synthesizer. The same optimal conditions found for the synthesis of derivative **17** were applied (Table 3.16, entry 4) to run the reaction between intermediate **26** and propylamine **10** using the **S-C** pathway. The reaction was monitored via Flow-IR, following the disappearance of peak at 1722 cm^{-1} and the formation of peaks at 2880, 1615, 1315, and 1150 cm^{-1}. No precipitation was observed.

Upon collection, the solvent was evaporated, and the residue was analyzed by ^{1}H NMR. NMR yield (79%) was determined for this derivative via ^{1}H NMR vs 1,3,5-trimethoxybenzene. Water (1 mL) was added to the collected crude mixture to crystallize derivative **19**. After stirring for 4 hours at room temperature, 2.4 mg of pure compound was obtained (20% yield).

3.2.3.5 Synthesis of derivative 21 (L3).

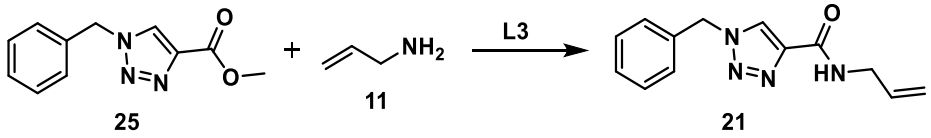

Scheme 3.22. Synthesis of derivative **21** (optimization of **L3**).

Intermediate **25** was synthesized as reported above in the related paragraph 3.2.3.1 using the **S-S** pathway on the synthesizer. The same optimal conditions found for the synthesis of derivative **20** were applied (Table 3.17, entry 3) to run the reaction between intermediate **25** and allylamine **11** using the **S-C** pathway. The reaction was monitored via Flow-IR, following the disappearance of peak at 1722 cm^{-1} and the formation of peaks at 2880, 1645, 1605, and 1150 cm^{-1}. No precipitation was observed.

Upon collection, the solvent was evaporated, and the residue was analyzed by ^{1}H NMR. NMR yield (75%) was determined for this derivative via ^{1}H NMR vs 1,3,5-trimethoxybenzene. Water (1 mL) was added to the collected crude mixture to crystallize derivative **21**. After stirring for 4 hours at room temperature, 4.4 mg of pure compound was obtained (22% yield).

3.2.3.6 Synthesis of derivative 22 (L3)

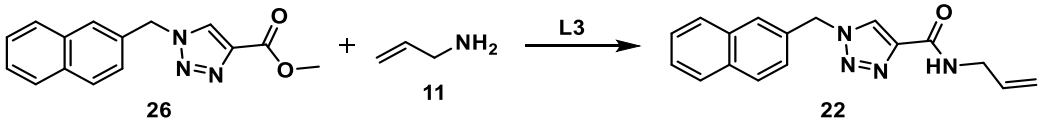

Scheme 3.23. Synthesis of derivative **22** (optimization of **L3**).

Intermediate **26** was synthesized as reported in section 3.2.3.2, using the **S-S** pathway on the synthesizer. The same optimal conditions found for the synthesis of derivative **20** were applied (Table 3.17, entry 4) to run the reaction between intermediate **26** and allylamine using the **S-C** path. The reaction was monitored via Flow-IR, following the disappearance of peak at 1722 cm^{-1} and the formation of peaks at 2880, 1675, 1615, 1500, 1312, and 1205 cm^{-1}. No precipitation was observed.

Upon collection, the solvent was evaporated, and the residue was analyzed by ^{1}H NMR. NMR yield (76%) was determined for this derivative via ^{1}H NMR vs 1,3,5-trimethoxybenzene. In order to crystallize derivative **22**, the volume of the solution exiting the synthesizer was reduced for 20 minutes on the rotavap with the bath set at room temperature. Water (1 mL) was then added. After stirring for 4 hours at 0 °C, 2.1 mg of pure compound was obtained (17% yield).

3.2.3.7 Synthesis of derivative 15 (L3).

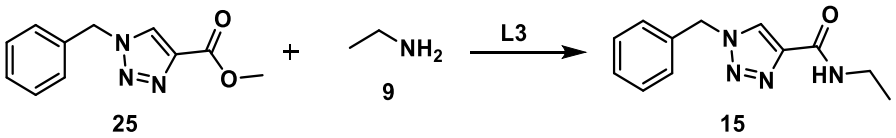

Scheme 3.24. Synthesis of derivative **15** (optimization of **L3**).

Intermediate **25** was synthesized as reported in the related paragraph 3.2.3.1, using the **S-S** pathway. The same conditions of Table 3.16, entry 4 were tested using ethylamine (70% solution in water) for **L3** using the **S-C** pathway. The reaction was monitored via Flow-IR, following the disappearance of peak at 1722 cm^{-1} and the formation of peaks at 2880, 1605, 1500, and 1150 cm^{-1}. No precipitation was observed.

Upon collection, the solvent was evaporated, and the residue was analyzed as it was by ^{1}H NMR. NMR yield (80%) was determined for this derivative via ^{1}H NMR vs 1,3,5-trimethoxy benzene. Water (1 mL) was added to the collected crude mixture to crystallize derivative **15**. After stirring for 4 hours at room temperature, 6.7 mg of pure compound was obtained (35% yield).

3.2.3.8 Synthesis of derivative 16 (L3).

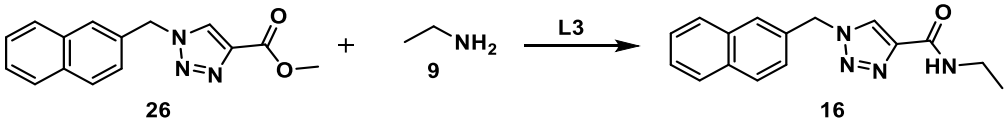

Scheme 3.25. Synthesis of derivative **16** (optimization of **L3**).

Intermediate **26** was synthesized as reported in section 3.2.3.2 using the **S-S** pathway. The same conditions of Table 3.16 entry 4 were tested using ethylamine (70% solution in water) for **L3** using the **S-C** pathway. The reaction was monitored via Flow-IR following the disappearance of peak at 1722 cm^{-1} and the formation of peaks at 2880, 1615, 1395, and 1150 cm^{-1}. No precipitation was observed.

Upon collection, the solvent was evaporated, and the residue was analyzed without any further purification by ^{1}H NMR. NMR yield (75%) was determined for this derivative via ^{1}H NMR vs 1,3,5-trimethoxybenzene. In order to crystallize derivative **16**, the volume of the solution exiting the synthesizer was reduced for 20 minutes at the rotavap with the bath set at room temperature. Water (1 mL) was then added. After stirring for 4 hours at 0 °C, 2.2 mg of pure compound was obtained (19% yield).

3.3 Modular expansion

The next feature of the radial synthesizer that we wanted to validate was the ability to easily connect new modules to the central station. With this goal in mind, we integrated a simple setup for flow-photoreactions composed of a 10 mL FEP tube (internal diameter 0.8 mm) and a LED lamp 420 nm, 72 W (Figure 3.15).

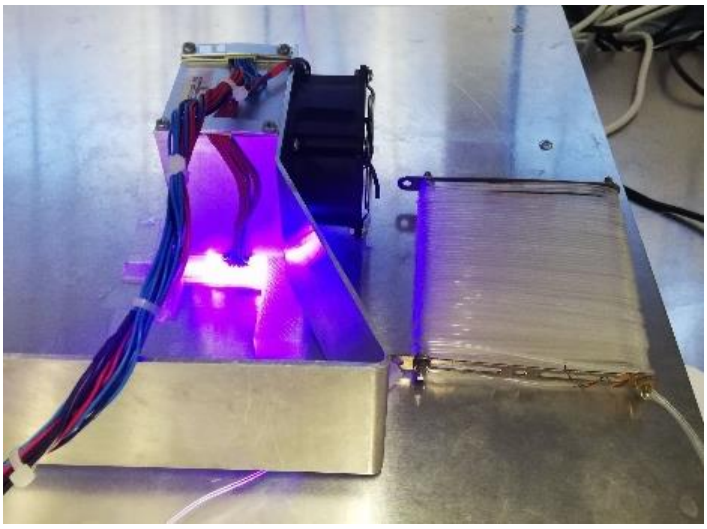

Figure 3.15. Flow-photoreactor

The integration of this new module was achieved by connecting the inlet and outlet of the coil reactor to port number 12 of both the divergent and convergent valves (**E** and **F**) of the CSS (using standard flow connectors) and introducing an on/off switch for the light source in the software interface.

Through the addition of this photochemical module, a wider and more diverse range of chemical processes could be performed on the same system. Dual nickel/photoredox-catalyzed cross-couplings were chosen to showcase the new capabilities of the radial synthesizer because they constitute a powerful synthetic methodology[33] for the formation of carbon-carbon[34] and carbon-heteroatom bonds, *e.g.* the C-N bonds of aniline derivatives[35].

Building on previous studies[35], the optimization of the coupling of pyrrolidine and 1-bromo-4-(trifluoromethyl)benzene (**30**) was performed as a two-step process (**R-R**, **R-C**) using the 420 nm LED photoreactor and flow-NMR modules. With conditions in hand, a series of couplings were sequentially performed using solutions of $Ir(dF(CF_3)ppy]_2(dtbpy))PF_6$), $NiBr_2$ and DABCO (1,4-diazabicyclo[2.2.2]octane) with either **30** or 1,4-dibromobenzene (**31**) and a series of secondary amines (pyrrolidine **32**, pyrrolidin-3-ol **33**, and piperidin-4-ol **34**) to provide aniline derivatives (**35**, **36**, **37** and **38**) in moderate isolated yields (Figure 3.16).

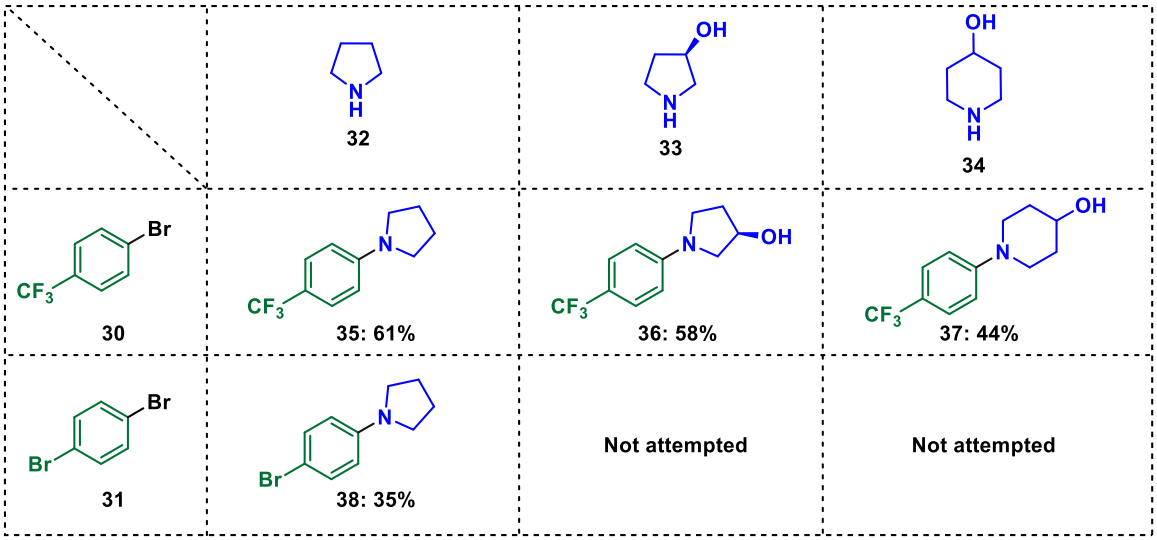

Figure 3.16. Library of new compounds achievable through photochemical processes

3.3.1 General procedure for flow metallophotoredox process

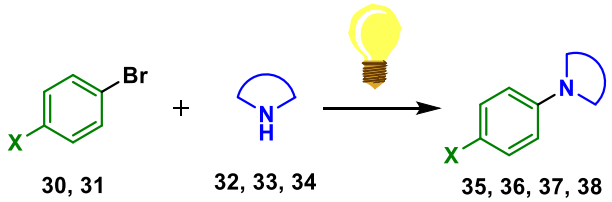

Scheme 3.26. Synthesis of aryl amines via dual nickel-photoredox catalysis processes

Following a flow protocol already established by MacMillan *et al.*[35], solutions of different aryl bromides (**30**, **31**), cyclic amines (**32**, **33** and **34**), $NiBr_2 \cdot 3H_2O$, $(Ir[dF(CF_3)ppy]_2(dtbpy))PF_6$ (**Ir cat**) and 1,4-diazabicyclo[2.2.2]octane (DABCO) in dimethyl acetamide (DMA) were loaded in the reagents pool of the radial synthesizer.

The order of mixing of the reactants turned out to be irrelevant. All the reaction mixture components can be mixed together with nothing happening until they are exposed to the blue light ((control experiments performed without irradiation for every reaction showed no conversion after 16 hours). To avoid the quenching of the Iridium photocatalyst excited state by dissolved oxygen, all solutions were degassed by bubbling Argon through them for 10 minutes before loading them in the reagent delivery system.

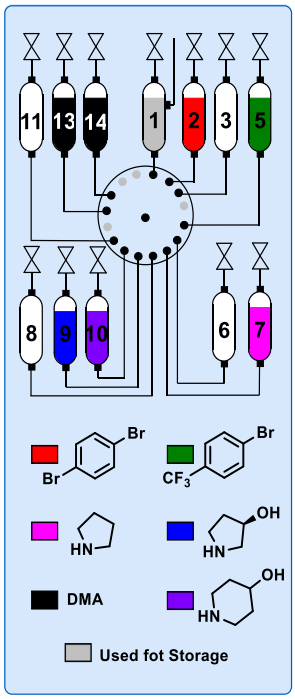

Vessel 1: empty (used for storage of products **35**, **36** and **37** to allow a second cycle through flow-NMR for in-line analysis)

Vessel 2: 1-bromo-4-(trifluoromethyl)benzene (**30**) + $NiBr_2 \cdot 3H_2O$, Ir cat + DABCO

Vessel 3: empty

Vessel 5: 1,4-dibromobenzene (**31**) + $NiBr_2 \cdot 3H_2O$, Ir cat + DABCO

Vessel 6: empty

Vessel 7: pyrrolidine (**32**)

Vessel 8: empty

Vessel 9: pyrrolidin-3-ol (**33**)

Vessel 10: piperidin-4-ol (**34**)

Vessel 11: empty

Vessel 13: DMA

Vessel 14: DMA

Figure 3.17. Five reagents were loaded in the RDS and combined to generate the library of Figure 3.16. White vessels were left empty and grey dots represent ports that are dedicated to other purposes than connecting the reagent selector to the reagent vessels (see section 2.1.2.1).

Different combinations of reactants, as well as different ratios of $NiBr_2$, Ir catalyst and DABCO, were screened under different residence time and light voltage.

A first cycle (**P1**) was programmed to send the reaction mixture to port 12, connected to the 10 mL photoreactor and then store the product in the reagent delivery system using the **R-R** pathway. A second cycle (**P2**) then mixed the product with deuterated DMSO and sent the mixture towards port 15 connected to the flow-NMR. The ^{19}F NMR of the sample was measured while the stop-flow mode was selected for 10 minutes. Using the **R-C** pathway, the final mixture was collected in the collection vessel.

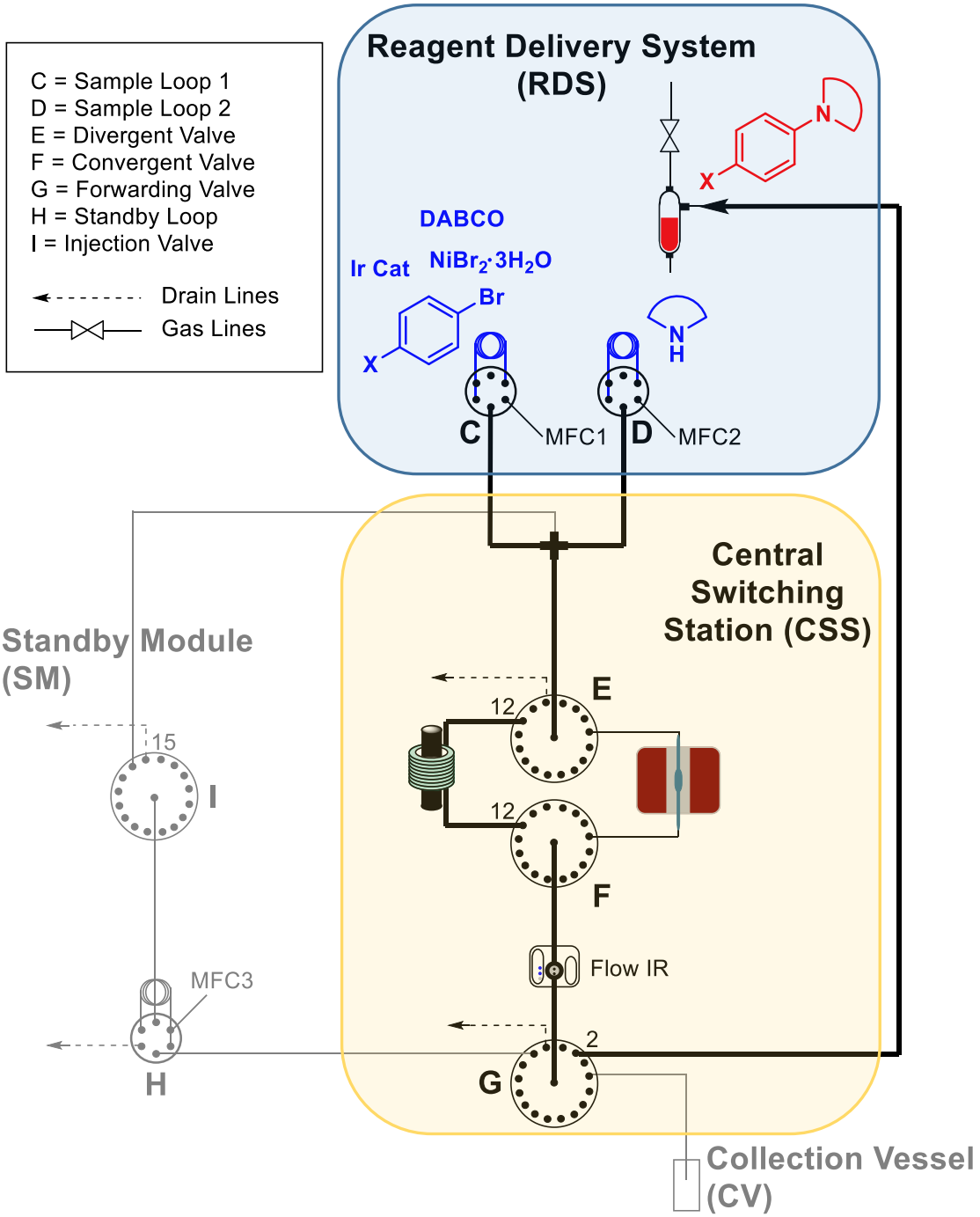

Figure 3.18. Step **P1** for the synthesis of aryl amines (**R-R** pathway). Starting materials are reported in blue and products in red.

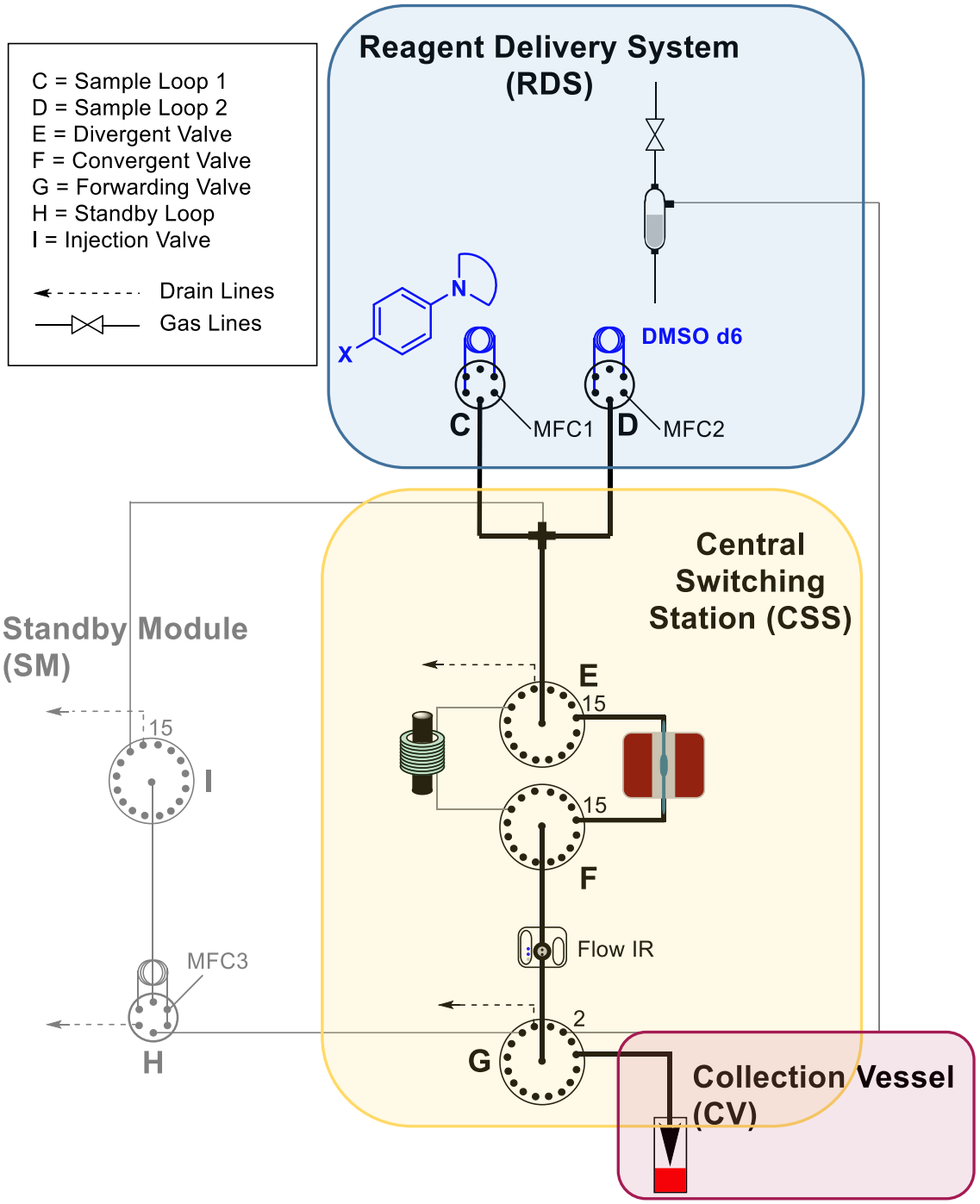

Figure 3.19. Step **P2** for the synthesis of aryl amines (**R-C** pathway). On-line analysis through flow-NMR.

3.3.1.1 Synthesis of 1-(4-(trifluoromethyl)phenyl)pyrrolidine (35) (P1, P2).

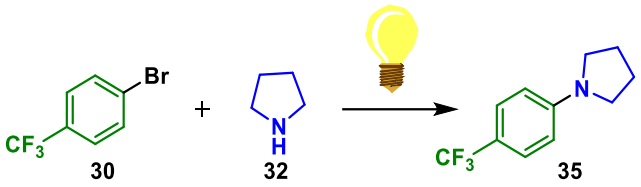

Scheme 3.27: Synthesis 1-(4-(trifluoromethyl)phenyl)pyrrolidine (**35**).

A solution of 4-bromobenzotrifluoride (**30**) 0.27 M, $NiBr_2 \cdot 3H_2O$ 5%, Ir cat. 0.2% and DABCO 1.8 equiv. in DMA and a solution of pyrrolidine **32** 1.5 equiv. in DMA were mixed and sent through the photoreactor using the **R-R** pathway (sending the outcoming solution back to the RDS). The system was pressurized at 5 bar and 0.5 mL/min flow rate for the three MFCs was set resulting in a 1-hour residence time (**P1**). A second cycle (**P2**) was performed mixing the solution coming from step P1 with deuterated DMSO and opening port 15 (connected to the flow-NMR in the CSS) using the **R-C** pathway. A 5-bar pressure was applied also for this step and flow rate was set at 2.5 mL/min for the three MFC. The time necessary for injection was 99 seconds and after that a 10 minutes stop-flow mode was applied, switching to port 2 for 10 minutes and finally reopening port 12 once the NMR experiment was over, (see section 2.1.3.2).

The inline ^{19}F NMR analysis showed a conversion >95%.

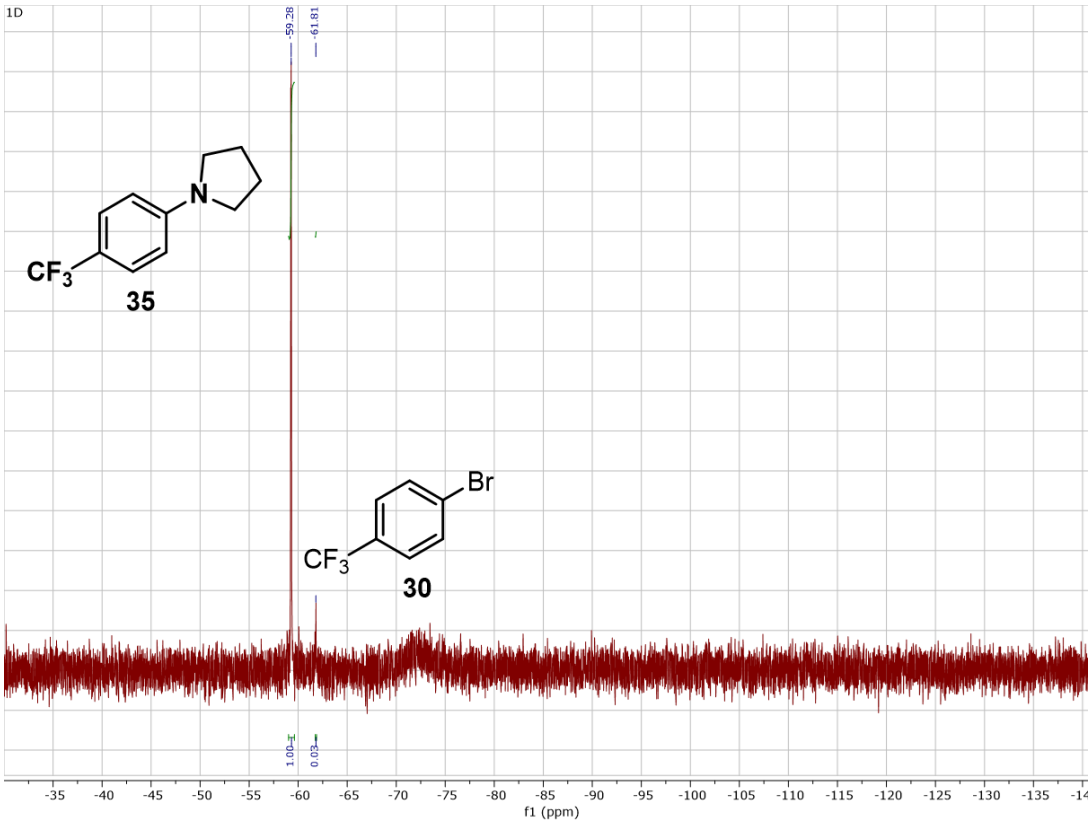

Figure 3.20. ^{19}F NMR spectrum collected through flow-NMR.

In order to corroborate the results of the flow-NMR the same solution was transferred in an NMR tube and analyzed on a Varian 400 MHz Varian adding 1 equiv. of 4-fluorotoluene as internal standard to measure the NMR yield. The conversion was found to be 87%.

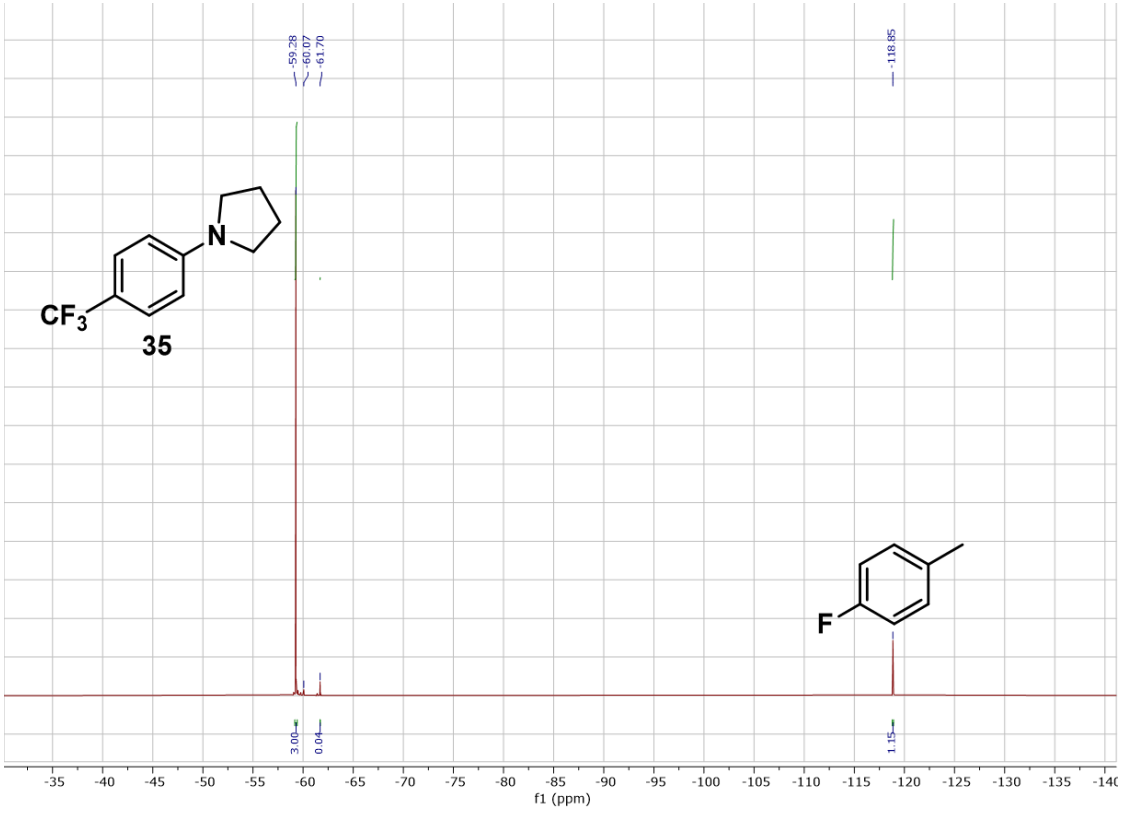

Figure 3.21. ^{19}F NMR spectrum collected through Varian 376 MHz NMR.

The remaining solution (≈ 0.5 mL left in the RDS) was concentrated and the residue purified by column chromatography (eluent Hexane:Et_2O 8:2) giving 61% isolated yield.

3.3.1.2 Synthesis of 1-(4-bromophenyl)pyrrolidine (38) (P1).

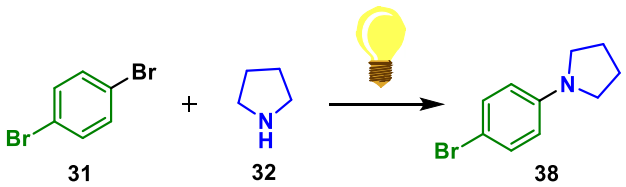

Scheme 3.28. Synthesis 1-(4-bromophenyl)pyrrolidine (**38**).

Due to the absence of a fluorinated moiety in the molecule was not possible to exploit the flow-NMR spectrometer and measure the conversion of this reaction on-line, therefore this process was composed of only step **P1** and yield was measured offline.

A solution of 1,4-dibromobenzene (**31**) 0.27 M, $NiBr_2 \cdot 3H_2O$ 5%, Ir cat 0.2% and DABCO 1.8 equiv. in DMA and a solution of pyrrolidine **32** 1.5 equiv. in DMA were mixed and sent through the photoreactor using the **R-R** pathway (sending the outcoming solution back to the RDS). A pressure of 5 bar was applied and 0.5 mL/min flow rate for the 3 MFCs was set resulting in a 1-hour residence time. The resulting solution was concentrated and the residue purified by column chromatography (eluent Hexane:Et_2O 8:2) giving 35% isolated yield.

3.3.1.3 Synthesis of 1-(4-(trifluoromethyl)phenyl)pyrrolidin-3-ol (36) (P1 + P2).

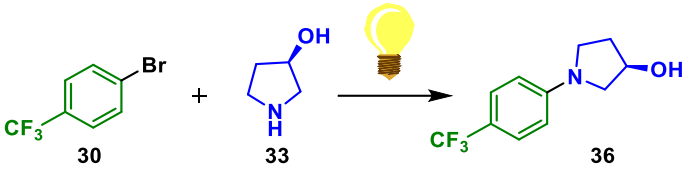

Scheme 3.29. Synthesis 1-(4-(trifluoromethyl)phenyl)pyrrolidin-3-ol (**36**).

A solution of 4-bromobenzotrifluoride (**30**) 0.27 M, $NiBr_2 \cdot 3H_2O$ 5%, Ir cat. 0.2% and DABCO 1.8 equiv. in DMA and a solution of pyrrolidin-3-ol (**33**) 1.5 equiv. in DMA were mixed and sent through the photoreactor using the **R-R** pathway (sending the outcoming solution back to the RDS). A pressure of 5 bar was applied and 0.5 mL/min flow rate for the 3 MFCs was set resulting in a 1-hour residence time (**P1**).

A second cycle (**P2**) was performed mixing the solution coming from step P1 with deuterated DMSO and opening port 15 (connected to the flow-NMR in the CSS) using the **R-C** pathway. A 5-bar pressure was applied also for this step and flow rate was set at 2.5 mL/min for the 3 MFC. 99 seconds were necessary for injection time and after that a 10 minutes stop-flow mode (see section 2.1.3.2). The inline ^{19}F NMR analysis showed a conversion of 52%.

Different ratios of pyrrolidin-3-ol **33**, $NiBr_2 \cdot 3H_2O$, Ir cat and DABCO as well as different light voltage and residence time were then screened to improve the conversion of this reaction. The results for these tests are reported in Table 3.18.

Table 3.18. Condition scouting synthesis of derivative **36**.[a]

Entry	$NiBr_2$ (%)	Ir cat (%)	**33** (equiv.)	DABCO (equiv.)	t (h)	light (V)	Conv.%[d]
1	5	0.2	1.5	1.8	1 h	36	52
2	5	0.4	1.5	1.8	1 h	36	58
3	5	0.02	1.5	1.8	1 h	36	24
4	5	0.2	5	1.8	1 h	36	17
5	5	0.2	1.5	1.8	1 h	30	51
6	5	0.2	1.5	1.8	2 h[b]	30	76
7	5	0.2	1.5	3.6[c]	1 h	36	95
8	10	0.2	1.5	1.8	1 h	36	>95

[a] **24** 0.27 M; back pressure: 5 bar; set gas flow rates: MFC1 = MFC2 = 0.5 mL/min. [b] to achieve the longer residence time stop-flow mode was used: gas stream diverted to port 2 for 1 h. [c] using double the amount of DABCO caused the formation of a sticky solid which was a risk for clogging the system. When this was observed the reaction mixture was expelled as reported in the general information from the unpressurized port of the divergent valve **E**. [d] conversion measured by determining the ratio of the integrated areas of the peak at −61.6 ppm belonging to **30** and the area of the new peak at −59.1 ppm in the ^{19}F NMR spectrum.

The resulting solution was concentrated, and the residue was solubilized in Et_2O and washed with brine. Organic layers were concentrated giving 58% isolated yield.

3.3.1.4 Synthesis of 1-(4-(trifluoromethyl)phenyl)piperidin-4-ol (37) (P1 + P2).

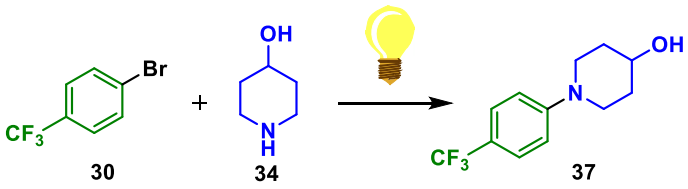

Scheme 3.30. Synthesis 1-(4-(trifluoromethyl)phenyl)piperidin-4-ol (**37**).

Considering the presence of the hydroxyl group I decided to start from the optimal conditions found for compound **36** (Table 3.18, entry 8). A solution of 4-bromobenzotrifluoride (**30**) 0.27 M, $NiBr_2 \cdot 3H_2O$ 10%, Ir cat. 0.2% and DABCO 1.8 equiv. in DMA and a solution of piperidin-4-ol **34** 1.5 equiv. in DMA were mixed and sent through the photoreactor using the **R-R** pathway (sending the outcoming solution back to the RDS). A pressure of 5 bar was applied and 0.5 mL/min flow rate for the 3 MFCs was set, resulting in a 1-hour residence time (**P1**). A second cycle (**P2**) was performed mixing the solution coming from step **P1** with deuterated DMSO and opening port 15 (connected to the flow-NMR in the CSS) using the **R-C** pathway. A 5-bar pressure was applied also for this step

and flow rate was set at 2.5 mL/min for the 3 MFC. 99 seconds were necessary for injection time and after that a 10 minutes stop-flow mode (see section 2.1.3.2).

Inline ^{19}F NMR analysis was not possible due to overlap with the debrominated side product. Offline ^{19}F NMR analysis showed a conversion of 76%.

The resulting solution was concentrated and the residue solubilized in Et_2O and washed with brine. Organic layers were concentrated giving 44% isolated yield.

3.4 Comparison of radial and continuous flow

The validations reported in the previous sections show that the radial synthesizer is optimal for the discovery stage of a synthetic process. It uses only a few milliliters of reagent solutions and it is capable of adjusting reaction conditions and reaction stream pathways in an automated manner, thus allowing for the rapid screening of multiple synthetic options while wasting a minimum amount of material.

Reproducibility is another important advantage of automated systems and so far, we observed high reproducibility when transferring a synthesis from the published continuous flow conditions to radial flow. Next, we wanted to showcase that reactions optimized using our radial synthesizer can be translated (in terms of temperature, pressure, concentration and residence time) in a continuous flow system such as a commercially available Vapourtec R4, for scale-up.

The only difference between the two approaches is the way reagents are delivered and passed through the system because the actual modules where reactions take place are the same. Therefore, we expected to see similar, if not the same, results when applying the same conditions. With this last demonstration of the capabilities of our instrument, we wanted to demonstrate that the step from the discovery stage using the radial paradigm to the scale-up in a continuous flow system is as easy and straightforward as for synthetic processes fully developed in continuous flow. In this way, identification of the optimal synthetic process could be achieved with the automated radial synthesizer, wasting a minimum amount of materials, and then repeated on a larger scale using a commercial continuous flow system.

To showcase the importance of rapid access to new convenient routes to pharmaceuticals combined with an effortless scale-up we chose to carry out a study on the synthesis of two drugs which were listed among medications in short supply in Germany during the COVID-19 pandemic[36]: paracetamol[37] and nifedipine[38,39]. Additionally, we investigated also the synthesis of lidocaine[25] (Figure 3.22).

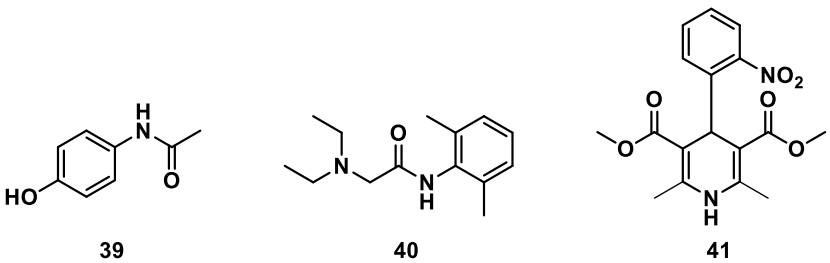

39 paracetamol **40** lidocaine **41** nifedipine

Figure 3.22. Three examples from the WHO list of essential APIs that served as examples for comparing radial and continuous flow synthesis. A painkiller **1**, a local anesthetic **2** and a hypertension drug **3**[40].

3.4.1 Synthesis of paracetamol (39)

Paracetamol is one of the most commonly used and inexpensive painkillers, yet it was in short supply in Germany during the COVID-19 pandemic in early 2020. Aiming at developing a scalable process to produce paracetamol from starting materials available in Europe, I evaluated the possible starting points for the synthesis. Phenol[41], 4-nitrophenol[42] and 4-aminophenol[37] can serve as starting materials and I identified 4-aminophenol as the most cost-efficient starting material (Figure 3.23 a). An alternative route starts from hydroquinone and uses ammonium acetate for both formation of para-aminophenol and its acetylation[43] (Figure 3.23 b), but it is again more expensive than the simple acetylation of para-aminophenol.

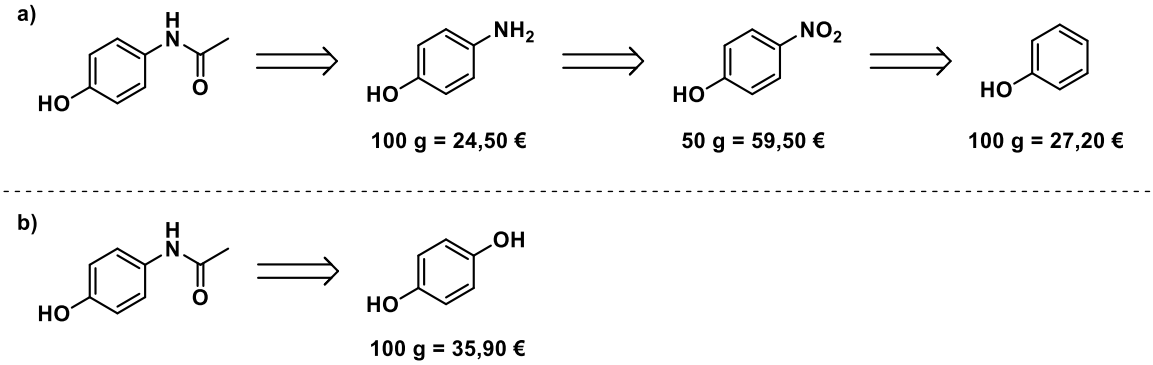

Figure 3.23. Starting materials candidates for the synthesis of paracetamol. Prices on Merck´s web catalog up to date 08/07/2020.

The greenest process for the acetylation of para-aminophenol uses water as a solvent[41]. However, 4-Aminophenol (**42**) has poor solubility in water, making it difficult to obtain a homogeneous solution that is required for the flow process. On the contrary, **42** is readily soluble when acetic anhydride (**43**) is added to the mixture. After screening different solvents, I found that acetic acid is also a good solvent for **42**. Attempting to keep water as the main solvent, I investigated the solubility of **42** in a mixture of water/acetic acid and I found that one millimole of **42** is soluble in 0.5 mL of a 4:1 mixture of water and acetic acid. Acetic anhydride (**43**), on the other hand, is not miscible with water, therefore I decided to use it as a neat reagent.

3.4.1.1 Optimization of the synthesis of paracetamol (39) in the radial synthesizer

A 2 M solution of 4-aminophenol (**42**) in a mixture of water/acetic acid (4:1) and neat acetic anhydride (**43**) were loaded in the reagent delivery system of the radial synthesizer. Screening of solvents, temperature, stoichiometries and residence times for the acetylation of 4-aminophenol (**42**) was performed selecting the **R-C** pathway, using 0.5 mL of each reagent solution (Figure 3.24).

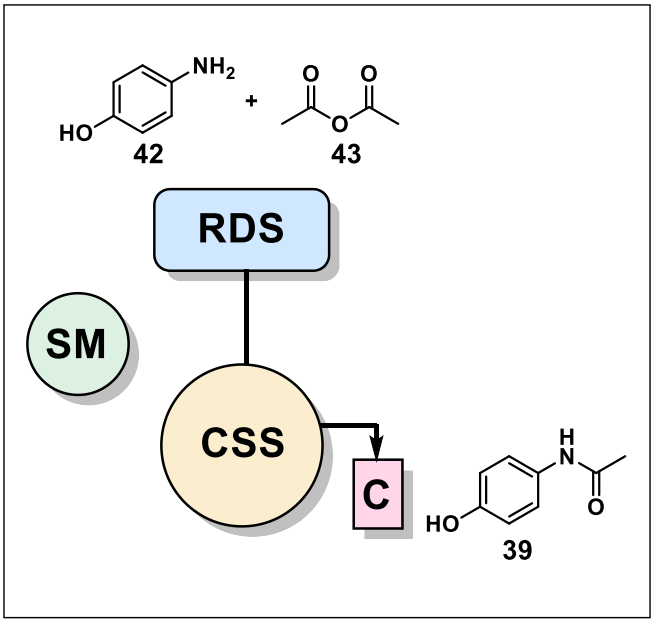

Figure 3.24. Process optimization for the synthesis of paracetamol carried out in the radial synthesizer using the **R-C** pathway

The results, summarized in Table 3.19 revealed that full conversion of **42** to **39** is achieved after only five minutes at room temperature with no precipitation observed when using neat acetic anhydride (**43**) (Table 3.19, entry 9). Reducing the amount of **43**, which is a good solvent for paracetamol (**39**), resulted in direct crystallization of the product. Crystallization started after ten minutes from addition when working with three equivalents of **43** (Table 3.19, entry 4). I isolated by crystallization 143.5 mg of paracetamol (yield: 95%).

Table 3.19. Conditions screening for acetylation of 4-aminophenol (**42**)

Entry	Conc. **42** (M)	Solvent of **42**	Equiv. **43**	Solvent of **43**	T (° C)	t (min)	Yield %
1	2	H_2O	3	-	60	5	93[a]
2	2	H_2O	3	-	R.T.	5	94[a]
3	2	H_2O	3	H_2O	-	-	- [a]
4	2	H_2O/AcOH 4:1	3	-	R.T.	5	95[b]
5	2	H_2O/AcOH 4:1	3	DMF	60	5	(50)[c]
6	2	H_2O/AcOH 4:1	3	*i*-PrOH	60	30	(>99)[c]
7	2	H_2O/AcOH 4:1	3	*i*-PrOH	R.T.	30	(62)[c]
8	2	H_2O/AcOH 4:1	5 (neat)	-	60	5	(>99)[c]
9	2	H_2O/AcOH 4:1	5 (neat)	-	R.T.	5	(>99)[c]

[a] Results for batch test, due to poor solubility of **42** in H_2O and/or lack of miscibility of **43** with H_2O, this test could not be carried out in the radial synthesizer. Product **39** precipitates after less than 10 minutes after reaction completion. The reported yield is the crystallized yield after 1 h stirring at room temperature. [b] Test in radial synthesizer. The product **39** precipitates after less than 10 minutes from collection. The reported yield is the crystallized yield after 1 h stirring at room temperature upon collection in an unpressurized vessel. [c] Test in radial synthesizer. Product **39** does not precipitate. The result reported in parenthesis is the conversion of the starting material calculated from the ^{1}H NMR of the crude, by the ratio of the integrated area of the aromatic peaks of **42** to the total area of aromatic peaks of **42** + **39**.

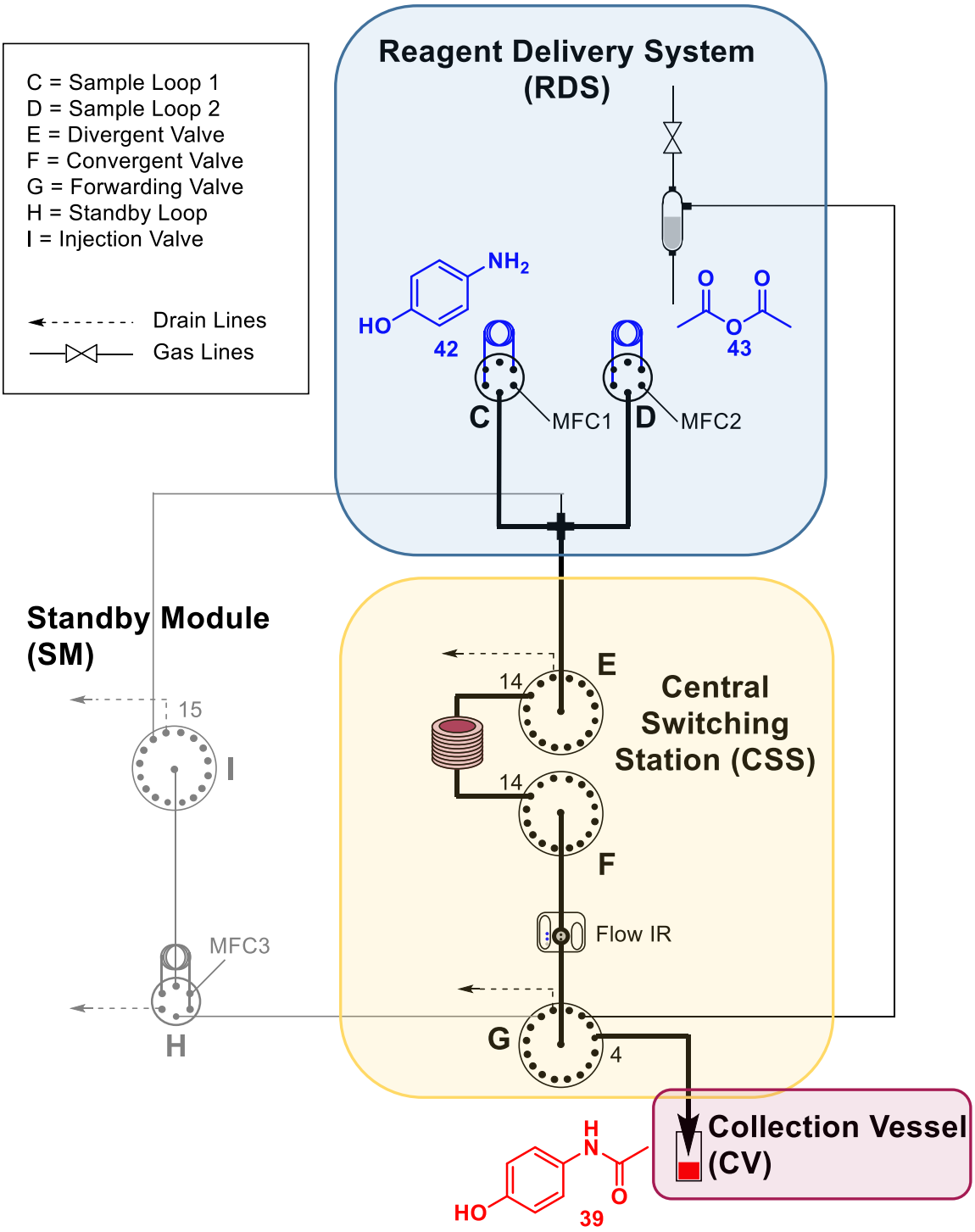

Figure 3.25. The synthesis of paracetamol was optimized using the **R-C** pathway in the radial synthesizer. Reagents are delivered by the RDS, pass through a heated or room temperature coil and the product is collected in a non-pressurized collection vessel (C). Starting materials are reported in blue and products in red.

3.4.1.2 Scale-up of the synthesis of paracetamol (39) in continuous flow

This process was scaled up using a Vapourtec R2 pump module, feeding a 2 M solution of **42** in water/acetic acid 4:1 from pump A and neat acetic anhydride (**43**) from pump B. When a 10 mL coil reactor was used, the two feeds were set respectively at 1.5 and 0.45 mL/min and the resulting solution was collected upon reaction in a flask and

stirred at room temperature for 1 h. After running the system for 15 minutes I achieved 6.36 g of crystallized **39** (94% crystallization yield) (Figure 3.26).

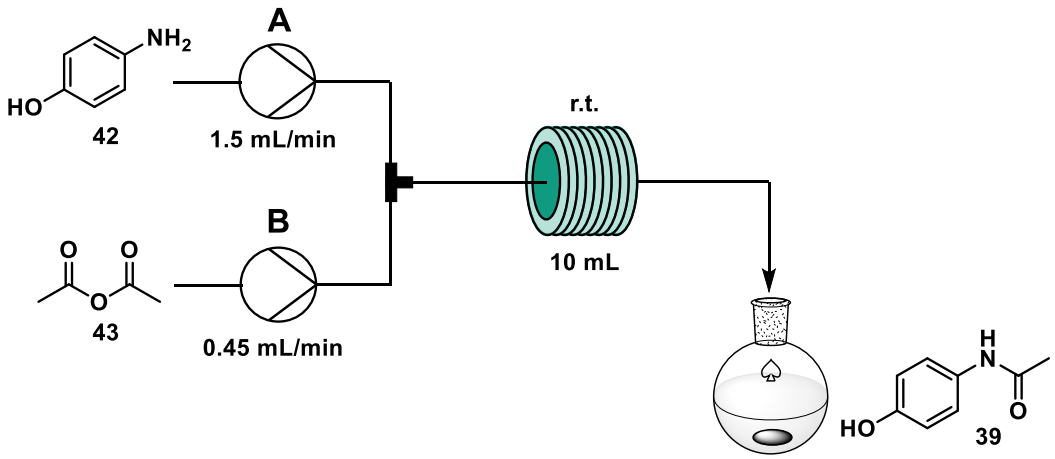

Figure 3.26. Continuous flow synthesis of paracetamol carried out using a Vapourtec R2 pump module and a room temperature reactor coil (10 mL) in PFA (i.d. 0.8 mm). Direct crystallization of the product was achieved by stirring the solution exiting the flow setup for 1 h.

Since crystallization happens spontaneously after reaction completion, without the need for any antisolvent addition and/or heating/cooling operations, I envisioned the possibility of telescoping an in-line flow-crystallization module. This module was based on the SMBR (serial micro-batch reactors) technique[44] that generates a segmented flow, spaced by nitrogen, which can carry slurries minimizing clogging phenomena that generally affect solid-liquid systems in flow.

The flow crystallization module was built by wrapping a 20 mL PFA coil (i.d. 1.6 mm) around a 1 L glass bottle which can be used to control the temperature by filling it with an appropriate liquid/mixture and heating it up or cooling it down. Connecting one end of the crystallization coil with the outlet of the reactor and a nitrogen gas feed through a Tee junction generated the segmented flow (Figure 3.27).

In order to allow longer residence times in the crystallization module the 10 mL coil reactor originally used for the continuous flow scale-up of the synthesis of **39** was replaced with a 1.5 mL one and flow rates were dropped at 0.25 mL/min and 0.075 mL/min respectively for pump A and pump B. N_2 flow rate was set at 0.5 mL/min. Crystallization occurs in droplets and the slurry exiting the telescoped process is directly filtered to give pure crystals of paracetamol. Collecting for 15 minutes on the filter I achieved 634.7 mg of paracetamol (56%) after a 30 minutes residence time in the crystallization module at 25 °C. This value, to some extent, reflected the results achieved with the batch crystallization. Stirring for one hour at room temperature in batch gave a 95% yield (Table 3.19, entry 4), while 30 minutes of flow crystallization gave 56%.

Attempts to increase the residence time in the flow-crystallization module to 1 hour (comparable to batch crystallization process) were made, however, using a lower flow rate was not possible due to the limits of the Vapourtec pumps (minimum flow rate achievable is 0.05 mL/min). Resizing the crystallization module from 20 to 40 mL raised the crystallization yield to 93%, although after 3 minutes of collection a destabilization of the segmented flow, due to clogging phenomena, was observed. Lowering the temperature from 25 to 5 °C by filling the glass bottle with water and ice did not lead to a significant increase in the yield.

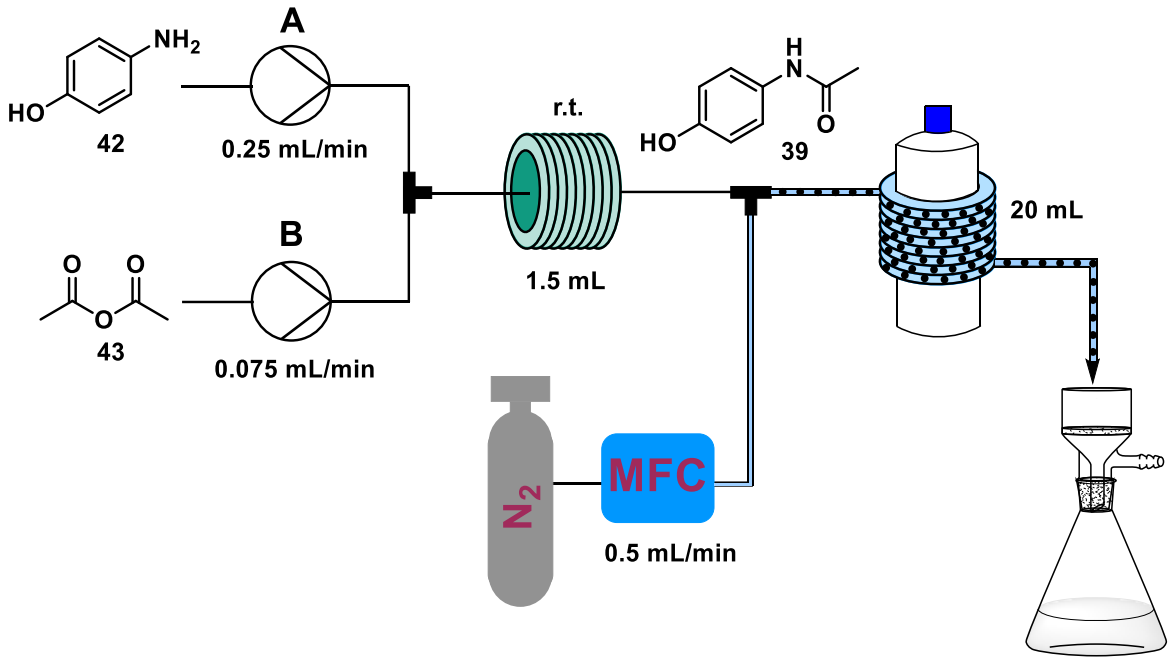

Figure 3.27. Continuous flow synthesis of paracetamol followed by flow crystallization and filtration.

Considering that the productivity of a process is dependent on the flow rate applied, the flow synthesis followed by batch crystallization (Figure 3.26) was more efficient, as it allows for the preparation of 25.6 g/h of paracetamol. This translates to about 1229 doses/day if we consider that one dose is one tablet (500 mg of active ingredient). At its best (not considering clogging issues), the flow crystallization could yield 4 g/h of paracetamol, due to the lower flow rate necessary to reach the 1 hour residence time in the crystallization module. For the scale-up of the synthesis of paracetamol, I therefore opted for the setup described in Figure 3.26.

3.4.2 Synthesis of lidocaine (40)

Lidocaine is a widely employed local anesthetic[45] produced via a two-step process. In the first step 2,6-dimethyl aniline (**44**) reacts with chloroacetyl chloride (**45**) to give the corresponding 2-chloro-N-(2,6-dimethylphenyl)acetamide (**46**), and in the second step,

diethylamine (**47**) substitutes the other chlorine atom giving the final product (Scheme 3.31).

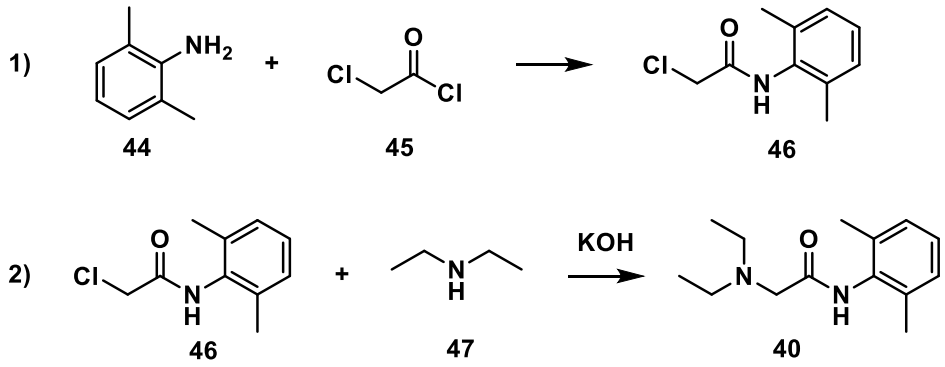

Scheme 3.31. Two-step synthesis of lidocaine **40**

Flow syntheses of lidocaine were already reported in several works[24,25,46], some involving automated synthesizers[24,25] therefore we started developing the process testing the published conditions.

3.4.2.1 Optimization of the synthesis of 40 in the radial synthesizer

The reagent delivery system was loaded with a solution of 2,6-dimethyl aniline (**44**) in N-methyl-2-pyrrolidone (NMP) and a solution of chloroacetyl chloride (**45**) in NMP to screen the conditions for the first step using the **R-C** path.

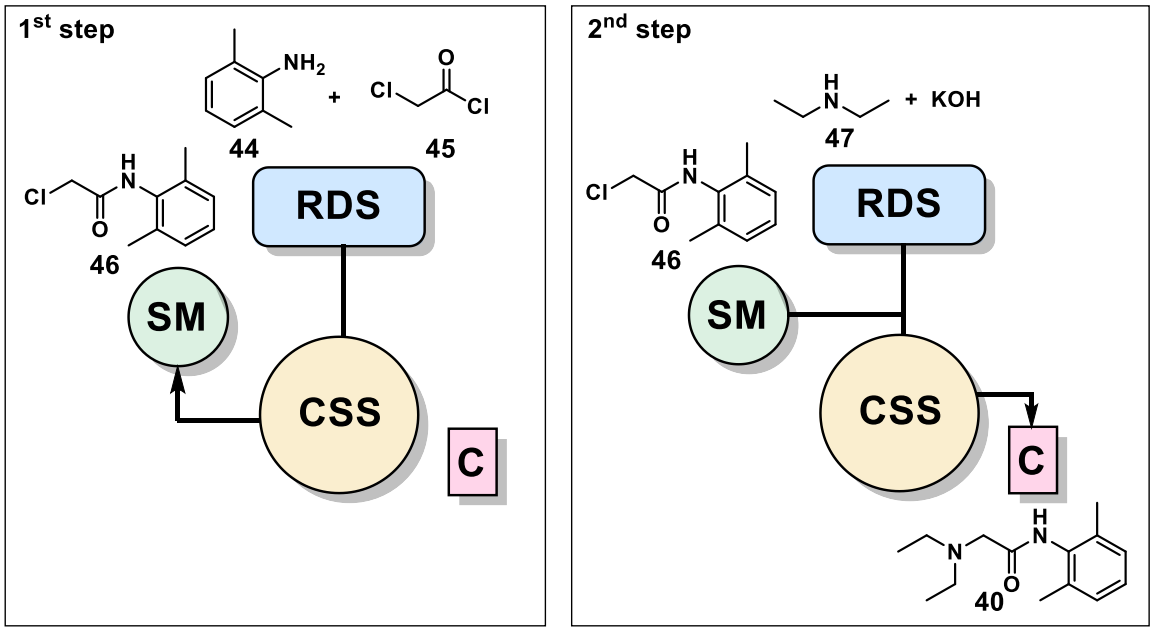

Figure 3.28. Process optimization for the synthesis of lidocaine carried out in the radial synthesizer using the **R-S** path for the first step and the **S-C** path for the second step

The reaction is completed in ten minutes at room temperature (Table 3.20, entry 3) compared to the 120 °C reported in literature[24,25].

Table 3.20. Screening of conditions for the synthesis of intermediate **46** (Li-1).

Entry	Conc. **44** (M)	Solvent of **44**	Equiv. **45**	Solvent of **45**	T (° C)	t (min)	Yield %[a]
1[b]	1	NMP	1.15	NMP	120	20	-[c]
2	1	NMP	1.15	NMP	R.T	20	95
3	1	NMP	1.15	NMP	R.T.	10	95

[a] Yield determined by weighing the solid intermediate **46**, crystallized upon addition of H_2O to the crude mixture (1 mL of H_2O in 1 mL sample of reaction mixture). [b] Conditions reproduced from literature[24,25]. [c] No crystallization occurred.

A second step was coupled using the combination **R-S** + **S-C** paths. Two new solutions were loaded in the RDS: a 0.6 M solution of potassium hydroxide in Methanol/Water 1:1 and a 1.5 M solution of diethylamine (**47**) in the same solvent mixture. Intermediate **46** was generated as reported in Table 3.20, entry 3 and stored in the stand-by module. The three liquid segments were mixed and conditions for the second step (Li-2) were screened using the **S-C** path (Figure 3.30).

The crude reaction mixture exiting the synthesizer was extracted with hexane and NH_4Cl/NaCl (1:1) and the residue, after evaporation of the solvent, was dissolved in $CDCl_3$ and analyzed via ^1H NMR. The highest isolated yield was achieved applying 130 °C for 20 minutes (Table 3.21, entry 6). This result was in accordance with reported literature data[24,25].

Crystallization via formation of lidocaine HCl salt: After extraction with NH_4Cl/NaCl (1:1), the organic layers were concentrated to ≈ 5 mL and 0.2 mL of HCl solution in Et_2O 2 N (2 equiv.) were slowly added. The slurry generated was stirred for 1 h and then filtered and washed with n-hexane, achieving 41.971 mg of lidocaine HCl (yield: 62%). Crystals of lidocaine HCl were dissolved in $CDCl_3$ and analyzed via ^1H NMR.

Table 3.21. Screening of conditions for the synthesis of lidocaine **40** (Li-2).

Entry	Conc. **46** (M)[a]	Equiv. **47**[b]	T (°C)	t	Conv. (%)[c]	Yield (%)
1[e]	0.5	3	60	20 h	97	81[d]
2	0.5	3	60	3.5 h	85	71[d]
3	0.5	3	60	20 min	-	
4	0.5	Neat (15)	60	20 min	-	
5	0.5	3	130	5 min	79	52[d]
6	0.5	3	130	20 min	93	62[f]

[a] The concentration of **46** is given assuming a 100% yield in step Li-1 since the second step Li-2 is performed directly from the crude mixture of Li-1. [b] KOH and **47** were both dissolved in H_2O/MeOH

1:1, then added simultaneously to the crude mixture of Li-1 using the **S-C** path. [c] Conversion was estimated via ^{1}H NMR by the ratio of the integrated area of the CH_2 peak of **40** (3.29 ppm) and the total area of CH_2 peaks of **40** + **46** (4.25 ppm) [d] Isolated yield after extraction with hexane and evaporation. Yield is calculated from the weight of the residue and the conversion. [e] Test performed in batch. [f] Final yield after crystallization.

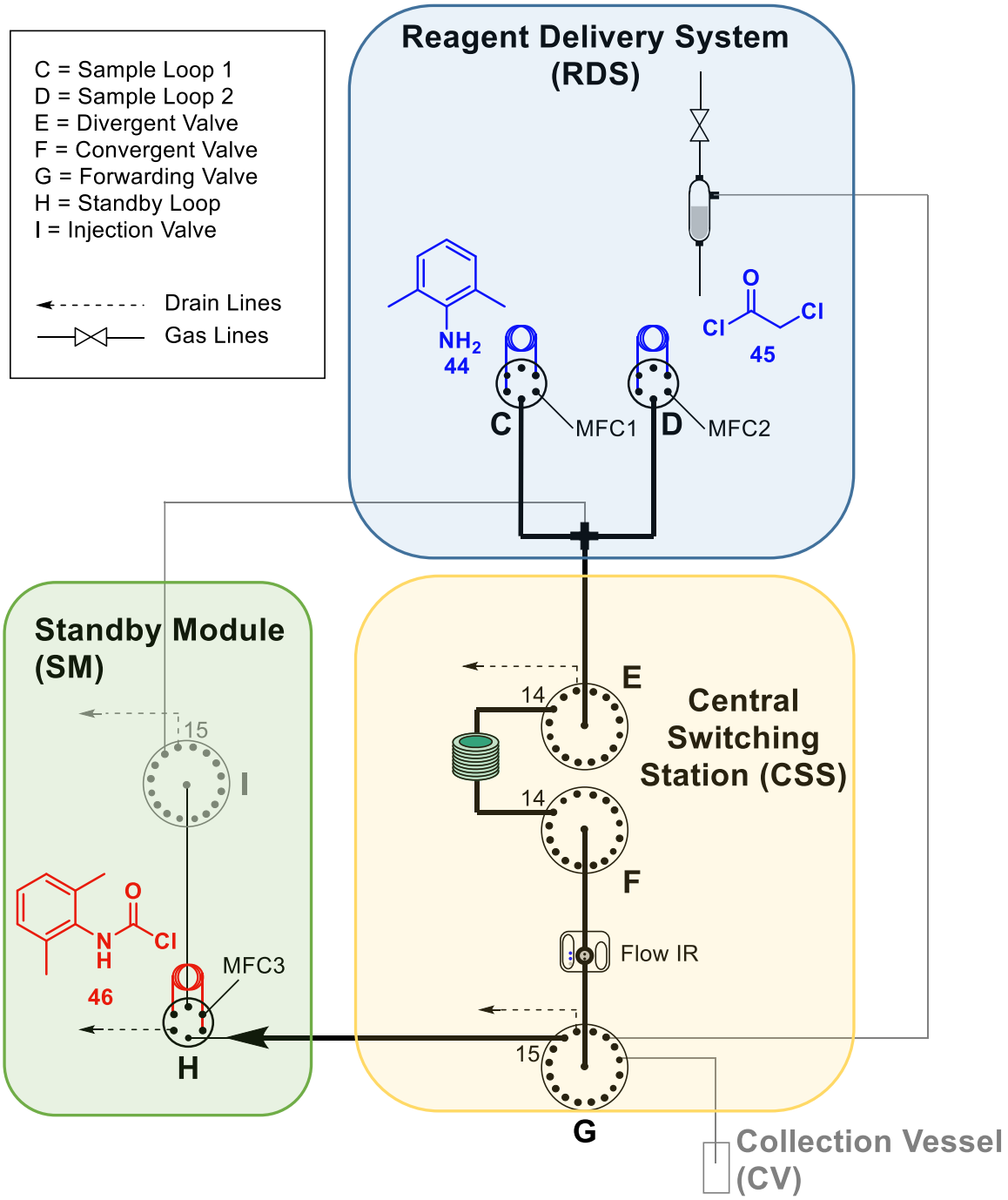

Figure 3.29. First step of the radial synthesis of lidocaine (Li-1) performed using the **R-S** pathway. Starting materials are reported in blue and products in red.

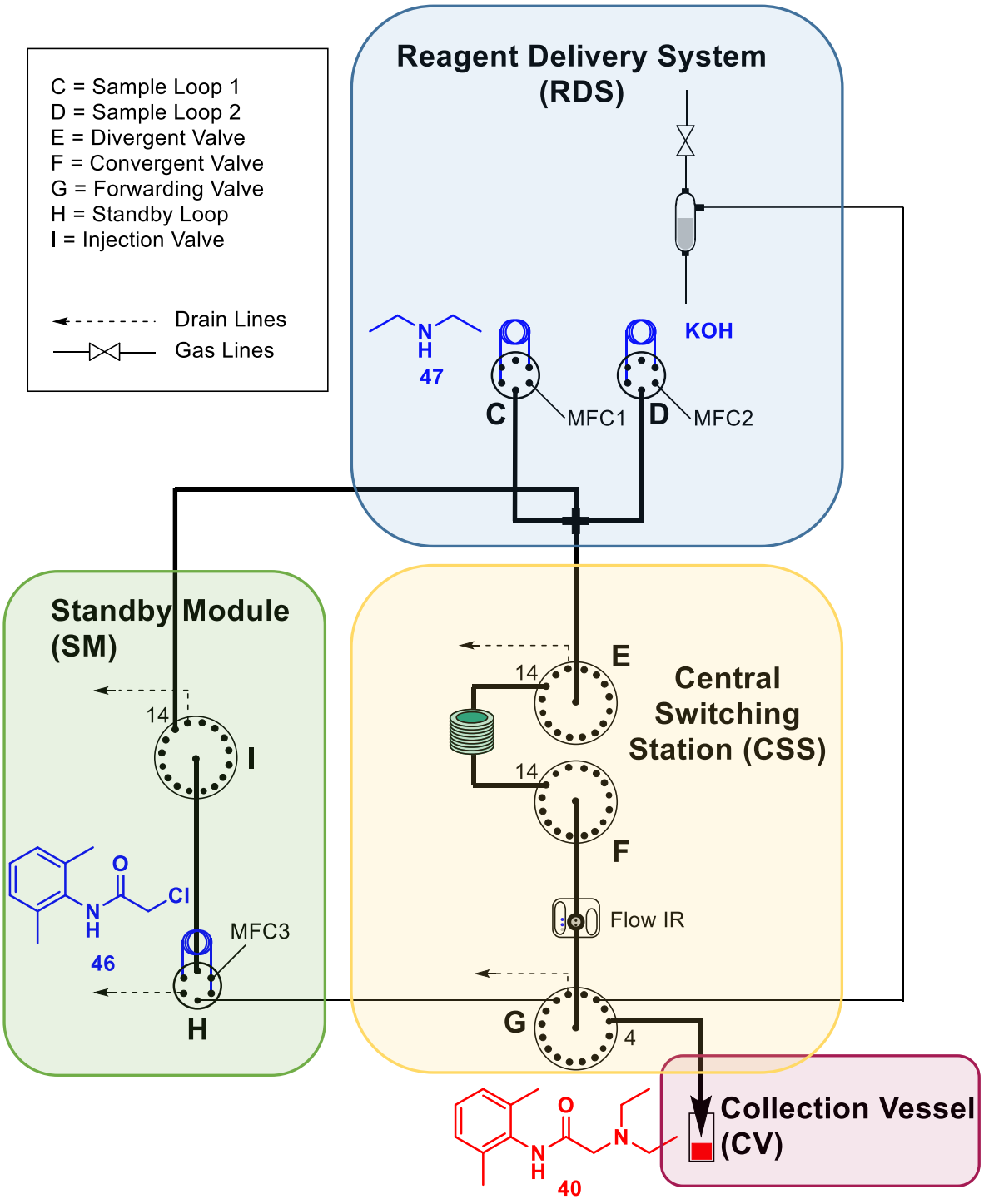

Figure 3.30. Second step of the radial synthesis of lidocaine (Li-2) performed using the **S-C** pathway. Starting materials are reported in blue and products in red.

3.4.2.2 Scale-up of the synthesis of lidocaine (40) in continuous flow[i]

The flow synthesis of lidocaine was scaled up using a Vapourtec R2 pump module and a 1.6 mL room temperature coil for the first step. Solutions of **44** (1 M in NMP) and **45** (1.15 M in NMP) were pumped at 0.08 mL/min each to achieve a 10-minute residence

[i] The continuous flow process for the synthesis of lidocaine was developed and performed in collaboration with Lucia Anghileri.

time. The second step was telescoped pumping a solution of diethylamine **47** (0.75 M) and KOH (0.3 M) in methanol/water 1:1 at 0.34 mL/min (total flow rate 0.5 mL/min) through a 10 mL coil heated at 130 °C by a Vapourtec R4 module (20 min residence time) (Figure 3.31). The crude reaction mixture exiting the system was collected for 90 minutes (45 mL) and was extracted with hexane and NH_4Cl/NaCl (1:1). The organic layers were evaporated and the residue re-dissolved in 10 mL of hexane. 7.2 mL of HCl solution in Et_2O 2 N (2 equiv.) were slowly added. The slurry generated was stirred for 1 h and then filtered and washed with n-hexane, achieving 1.15 g of lidocaine HCl (yield: 59%). Crystals of lidocaine HCl were dissolved in $CDCl_3$ and analyzed via ^1H NMR.

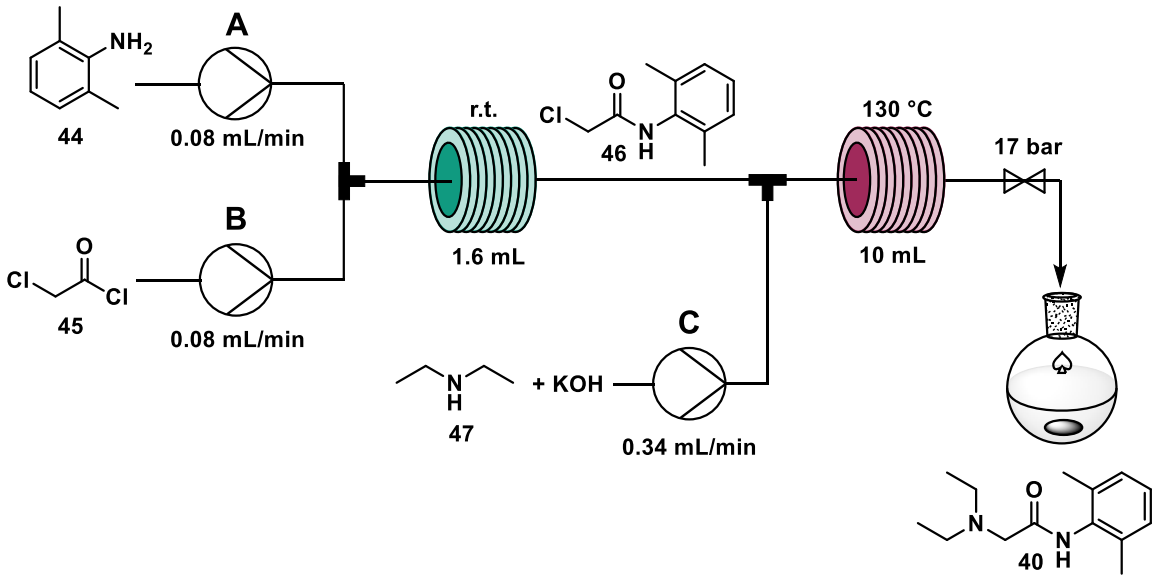

Figure 3.31. Continuous flow synthesis of lidocaine **40**. First step: two feeds A and B, pumped by a Vapourtec R2 pump module pass through a room temperature coil (PFA, i.d. 0.8 mm). Second step: the solution exiting the first reactor is combined with a third feed (C) and passes through a stainless steel reactor (i.d. 1 mm) heated at 130 °C by a Vapourtec R4.

3.4.3 Synthesis of nifedipine (41)

Nifedipine is a medication used to treat angina and high blood pressure among other ailments[47] and it appeared on the list of drugs in shortage in Germany during the COVID-19 pandemic[36]. Traditionally, nifedipine is synthesized in batch through a one-step multicomponent reaction by mixing 2-nitrobenzaldehyde (**48**), methyl acetoacetate (**49**), and methyl 3-aminocrotonate (**50**) at high temperatures in alcohol solvents[38,39] (Scheme 3.32). This reaction requires several hours and is usually carried out overnight. Performing this reaction in flow permitted the safe application of temperatures well above the boiling point of the solvent and accelerate the synthesis that is completed in just 1 hour. This is the first reported flow synthesis of nifedipine.

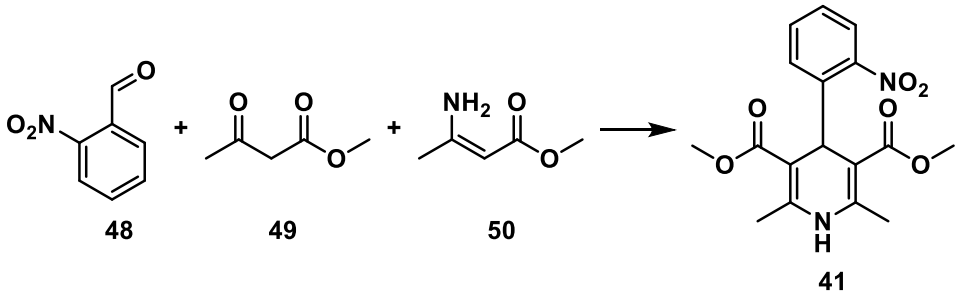

Scheme 3.32. Synthesis of nifedipine **41**

3.4.3.1 Optimization of the synthesis of nifedipine (41) in the radial synthesizer

In the optimization study of this process two solvents were investigated: ethanol and methanol. Running the reaction in ethanol resulted in a significant amount of side product at high temperature due to transesterification.

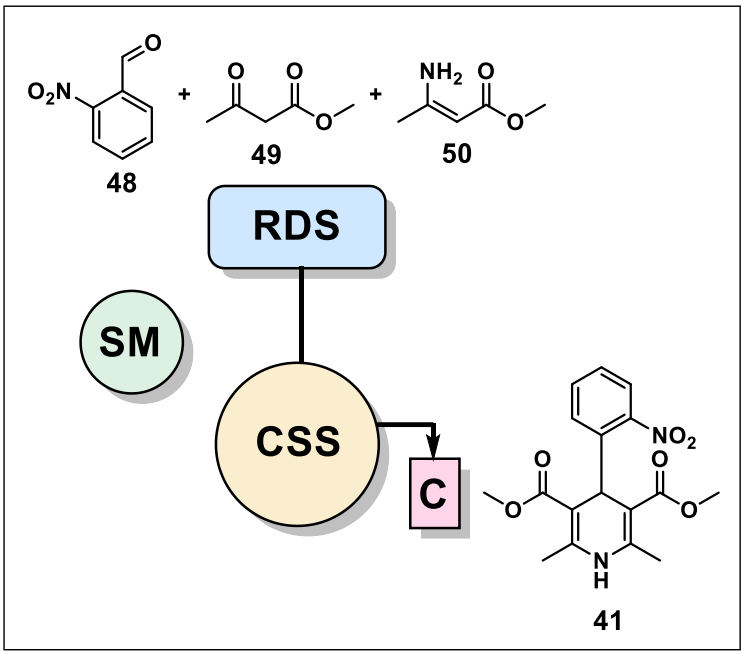

Figure 3.32. Process optimization for the synthesis of nifedipine carried out in the radial synthesizer using the **R-C** path.

Solutions of 2-nitrobenzaldehyde (**48**), methyl acetoacetate (**49**) (1.1 equiv.) and methyl (2Z)-3-amino-2-butenoate (**12**) (1 equiv.) in both ethanol and methanol were prepared and loaded into the reagent delivery system of the radial synthesizer. The effects of temperature and residence time on the conversion of **48** were screened using the **R-C** path (Figure 3.33). Aiming at accelerating the reaction, temperatures from 80 °C to 150 °C and a residence time range between 5 minutes and 3 hours were screened. Stop flow conditions were applied for longer residence times (see section 2.1.3.2).

Reaction time decreased as expected with increasing temperature and the best conversion was found employing ethanol as solvent (60 minutes residence time at 140

°C). However, a high amount of side product was generated at this temperature due to transesterification of **41** by ethanol and only a 30% yield of the desired product was obtained (Table 3.22 entry 2). This issue was solved by changing the solvent from ethanol to methanol (Table 3.22, entry 6). After collection, the solvent was evaporated, and the crude was analyzed via ^{1}H NMR. NMR yield (68%) was determined for this product via ^{1}H NMR vs 2,2,6,6-tetramethylpiperidine.

Table 3.22. Conditions screening for the synthesis of nifedipine.[a]

Entry	Conc. **48** (M)	Solvent	T (°C)	t (min)	Conversion of **48**	Yield %[b]
1	0.5	EtOH	140	5	45	<5
2	0.5	EtOH	140	60	>95	30
3	0.5	MeOH	90	60	71	20
4	0.5	MeOH	110	60	74	35
5	0.5	MeOH	130	60	95	55
6	0.5	MeOH	140	60	96	66
7	0.5	MeOH	150	60	97	68

[a] Conditions screened using the **R-C** pathway on the synthesizer; the reaction was monitored via ^{1}H NMR. [b]Yield determined by the ratio of the integrated areas using internal standard (2,2,6,6-tetramethylpiperidine) in ^{1}H NMR.

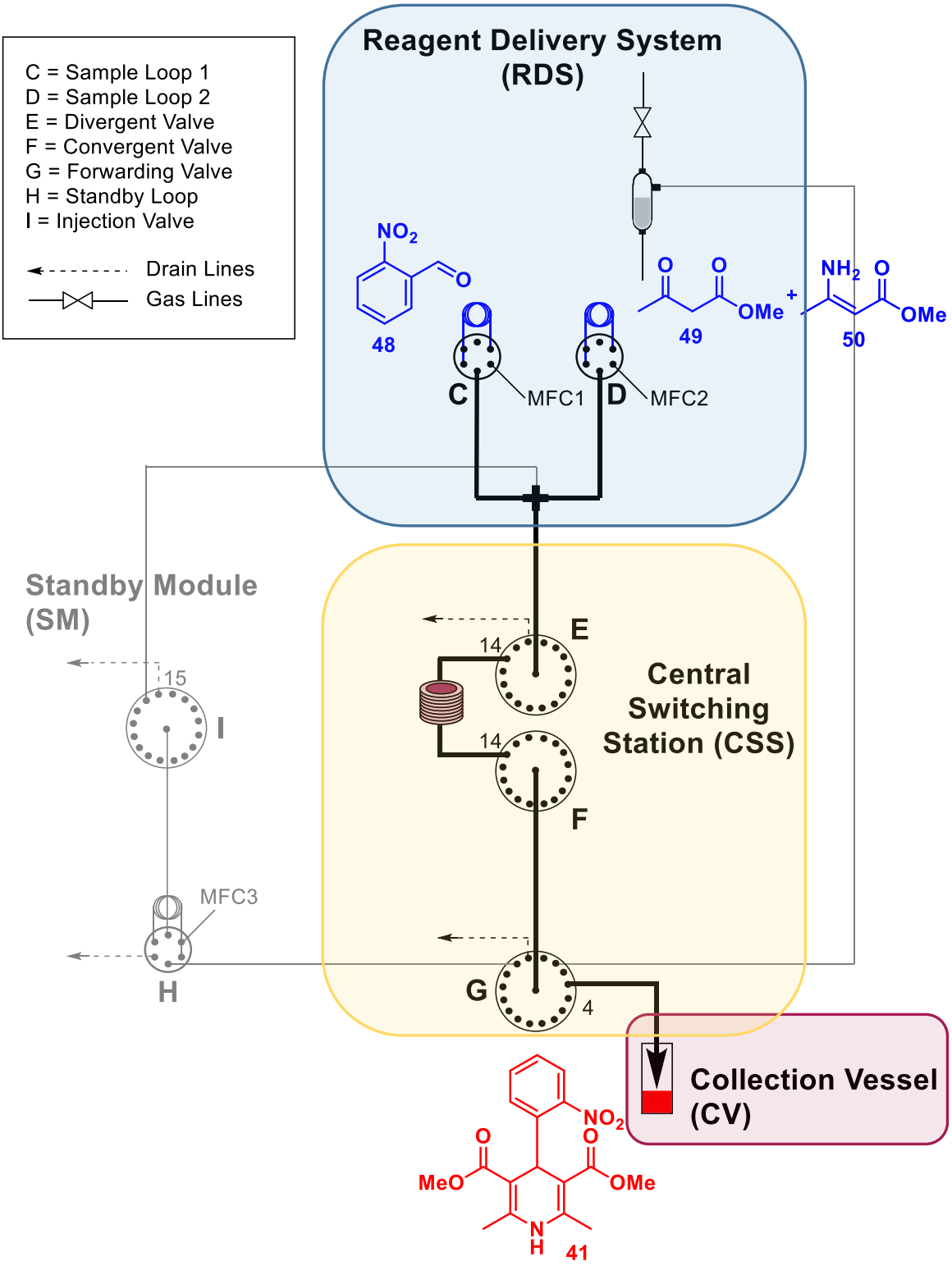

Figure 3.33. Radial synthesis of nifedipine (**R-C** pathway). Starting materials are reported in blue and products in red.

3.4.3.2 Scale-up of the synthesis of nifedipine (41) in continuous flow[ii]

For the scale-up of this process Vapourtec R2 pump module was used to feed a 0.5 M solution (25 mL, 12.5 mmol) of **48** (1 eq.), **49** (1.1 equiv.), and **50** (1 equiv.) in methanol in a 10 mL heated stainless steel coil reactor (150 °C) at 0.167 mL/min (heating module: Vapourtec R4). The starting material was fully consumed, and crude NMR showed clean formation of the desired product within 60 minutes (Figure 3.34). The system was run for 150 minutes, collecting 25 mL of crude solution. The volume of the crude solution was reduced by evaporation to 10~15 mL and crystallization of nifedipine was achieved by slowly adding 15 mL of H_2O to the crude mixture and stirring for 1 hour. We isolated 3.06 g of crystallized nifedipine (**41**) (71% yield).

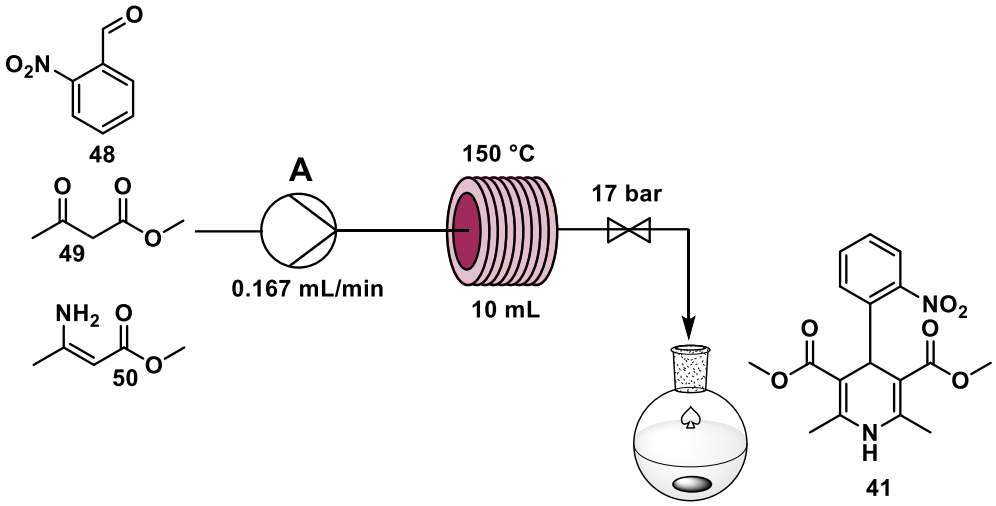

Figure 3.34. Continuous flow synthesis of nifedipine carried out using a Vapourtec R2 pump module and a PFA reactor coil (10 mL, i.d. 0.8 mm) heated by a Vapourtec R4 module.

Higher temperatures were screened for this continuous flow process, but despite full conversion of the starting material was shown, the yield of nifedipine **41** dropped when increasing temperature over 150°C (Table 3.23 and Figure 3.35).

This confirmed that optimal conditions were those of Table 3.22, entry 6 found with the radial synthesizer.

[ii] The continuous flow process for the synthesis of nifedipine was developed and performed in collaboration with Dr. Sooyeon Moon.

Table 3.23. Conditions screening for the synthesis of nifedipine in radial synthesizer and continuous flow conditions.[a]

Entry	Conc. **48** (M)	Solvent	T (°C)	t (min)	Conversion of **48**	Yield %[b]
1	0.5	EtOH	140	5	45	<5
2	0.5	EtOH	140	60	>95	30
3	0.5	MeOH	90	60	71	20
4	0.5	MeOH	110	60	74	35
5	0.5	MeOH	130	60	95	55
6	0.5	MeOH	140	60	96	68
7	0.5	MeOH	150	60	97	68
8 [c]	0.5	MeOH	170	60	98	55
9 [c]	0.5	MeOH	190	60	99	38

[a]the reaction was monitored via ^{1}H NMR. [b]Yield determined by the ratio of the integrated areas using internal standard (2,2,6,6-tetramethylpiperidine) in ^{1}H NMR. [c] tests performed only in continuous flow conditions.

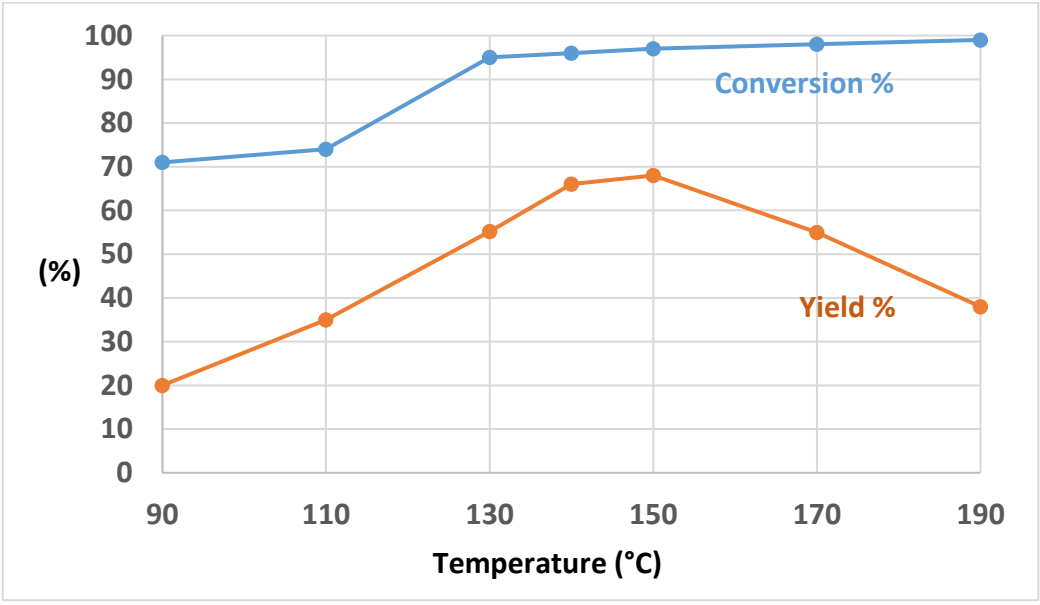

Figure 3.35. Reaction results by temperature change at 0.5 M in Methanol, nifedipine: blue = conversion, orange = 1H NMR yield.

4 Experimental section

4.1 General chemical information

Chemicals and solvents were purchased from commercial suppliers and used as received. ^{1}H NMR, ^{13}C NMR, and ^{19}F NMR spectra were recorded on a Varian 400 MHz, Bruker 400 MHz, Varian, 600 MHz or Bruker 700 MHz spectrometer. Chemical shifts were referenced using the residual solvent peak as an internal reference ($CDCl_3$: 7.26 ppm ^{1}H NMR, 77.16 ppm ^{13}C NMR; DMSO d_6: 2.50 ppm ^{1}H NMR, 39.52 ppm ^{13}C NMR; CD_3OD 3.31 ppm ^{1}H NMR, 49.00 ppm ^{13}C NMR). Multiplicity is indicated as follows: s (singlet), d (doublet), t (triplet), q (quartet), m (multiplet), dd (doublet of doublet), tt (triplet of triplet). IR spectra were recorded on a Mettler Toledo Flow-IR™ and processed with its own software (ICIR), subtracting the previously recorded solvent spectra. High-resolution mass spectra were obtained using a 6210 ESI-TOF mass spectrometer (Agilent).

All the tests were performed using 0.5 mL sample loops (on valve **C** and **D**) and 0.5 mL standby loop (on valve **H)**. The heated reactor is a 20 mL coil connected to port 14 of divergent valve **E** (reactor inlet) and port 14 of convergent valve **F** (reactor outlet) and heated by a Vapourtec R4 heating module. the photoreactor is a 10 mL FEP coil irradiated by a 420 nm LED light source, connected to port 12 of divergent valve **E** (reactor inlet) and port 12 of convergent valve **F** (reactor outlet). Final products are collected in either a pressurized or unpressurized vessel connected to the forwarding valve **G**.

4.2 Compound characterization

2,6-difluorobenzyl azide (**2**)

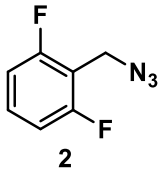

2

Compound **2** was prepared from 2,6-difluorobenzyl bromide **1** and sodium azide following the procedure described in section 3.1.1.1. Following collection, the solvent was evaporated, and the residue was fully dissolved in 0.5 mL of $CDCl_3$. ^{1}H NMR (400 MHz, Chloroform-*d*) δ 7.33 (tt, *J* = 8.5, 6.5 Hz, 1H), 7.02 – 6.90 (m, 2H), 4.44 (d, *J* = 1.4 Hz, 2H). These data are in accordance with those previously published[48].

Propiolamide (**4**)

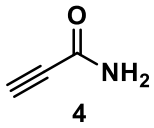

4

Compound **4** was prepared from methyl propiolate **3** and aqueous ammonia following the procedure described in section 3.1.1.2. Following collection, the solvent was evaporated, and the residue was fully dissolved in 0.5 mL deuterated methanol. ^{1}H NMR (400 MHz, Methanol-d_4) δ 3.59 (s, 1H). ^{13}C NMR (101 MHz, Methanol-d_4) δ 156.9, 77.6, 76.7. These data are in accordance with those previously published[49].

1-(2,6-difluorobenzyl)-1H-1,2,3-triazole-4-carboxamide (rufinamide **5**)

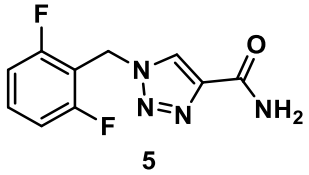

5

Compound **5** was prepared from 2,6-difluorobenzyl azide **2**, propiolamide **4**, and catalytic amount of copper iodide following the procedure described on section 3.1.1.3. The product crystallizes spontaneously upon collection. Crystals were dissolved in 0.5 mL deuterated DMSO. ^{1}H NMR (400 MHz, DMSO-d_6) δ 8.56 (s, 1H), 7.88 (s, 1H), 7.59 – 7.44 (m, 2H), 7.26 – 7.13 (m, 2H), 5.72 (s, 2H). ^{13}C NMR (101 MHz, DMSO-d_6) δ 162.1 (d, *J* = 7.4 Hz), 161.3, 159.6 (d, *J* = 7.4 Hz), 142.9, 131.9 (t, *J* = 10.4 Hz), 126.9, 112.1 (d, *J* = 5.7 Hz), 111.9 (d, *J* = 5.6 Hz), 111.1 (t, *J* = 19.1 Hz), 41.2 (t, *J* = 3.8 Hz). These data are in accordance with those previously published[50].

Methyl 1-(2,6-difluorobenzyl)-1H-1,2,3-triazole-4-carboxylate (**6**)

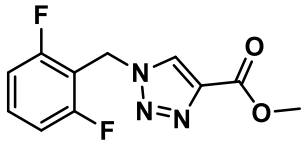

6

Compound **6** was prepared from 2,6-difluorobenzyl azide **2**, methyl propiolate **3**, and catalytic amount of copper iodide following the procedure described in section 3.1.2.2. Following collection, the product was crystallized by water. Crystals were dissolved in 0.5 mL deuterated DMSO. ^{1}H NMR (400 MHz, DMSO-d_6) δ 8.90 (s, 1H), 7.51 (tt, J = 8.5, 6.7 Hz, 1H), 7.25 – 7.09 (m, 2H), 5.75 (s, 2H), 3.80 (s, 3H). ^{13}C NMR (101 MHz, DMSO-d_6) δ 162.1 (d, J = 7.3 Hz), 160.6, 159.6 (d, J = 7.3 Hz), 138.5, 132.0 (t, J = 10.5 Hz), 129.6, 112.1 (d, J = 5.6 Hz), 111.9 (d, J = 5.5 Hz), 110.9 (t, J = 19.0 Hz), 51.9, 41.4 (t, J = 3.7 Hz). These data are in accordance with those previously published[51].

1-benzyl-1H-1,2,3-triazole-4-carboxamide (**12**)

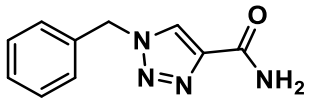

12

Compound **12** was prepared from benzyl azide **23**, propiolamide **4**, and catalytic amount of copper iodide following the procedure described in section 3.2.1.3. Following collection, the product was crystallized by water. Crystals were dissolved in 0.5 mL deuterated DMSO. ^{1}H NMR (400 MHz, DMSO-d_6) δ 8.61 (s, 1H), 7.89 (s, 1H), 7.49 (s, 1H), 7.43 – 7.28 (m, 5H), 5.64 (s, 2H). ^{13}C NMR (101 MHz, DMSO-d_6) δ 161.5, 143.2, 135.8, 128.9, 128.3, 128.0, 126.7, 53.1. m/z (HRMS+) for $C_{10}H_{10}N_4ONa^+$ [M+Na]$^+$ calcd. 225.0747, found 225.0751.

1-(naphthalen-2-ylmethyl)-1H-1,2,3-triazole-4-carboxamide (**13**)

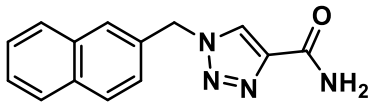

13

Compound **13** was prepared from 2-(azidomethyl)naphthalene **24**, propiolamide **4**, and catalytic amount of copper iodide following the procedure described in section 3.2.1.4. Following collection, the product was crystallized by water. Crystals were dissolved in 0.5 mL of deuterated DMSO. ^{1}H NMR (400 MHz, DMSO-d_6) δ 8.67 (s, 1H), 7.99 – 7.85 (m, 5H), 7.58 – 7.44 (m, 4H), 5.82 (s, 2H). ^{13}C NMR (101 MHz, DMSO-d_6) δ 161.5, 143.2,

133.3, 132.8, 132.6, 128.6, 127.9, 127.7, 127.0, 126.9, 126.7, 126.6, 125.8, 53.2. m/z (HRMS+) for $C_{14}H_{12}N_4ONa^+$ [M+Na]$^+$ calcd. 275.0903, found 275.0911.

1-(2,6-difluorobenzyl)-N-ethyl-1H-1,2,3-triazole-4-carboxamide (**14**)

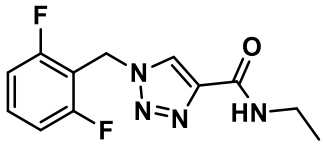

14

Compound **14** was prepared from intermediate **6** and ethylamine (70% solution in water), following the procedure described in section 3.2.2.2. Following collection, the product was crystallized by water. Crystals were dissolved in 0.5 mL deuterated DMSO. ^{1}H NMR (400 MHz, DMSO-d_6) δ 8.54 (d, J = 11.8 Hz, 2H), 7.52 (tt, J = 8.5, 6.7 Hz, 1H), 7.27 – 7.12 (m, 2H), 5.72 (s, 2H), 3.24 (qd, J = 7.1, 5.7 Hz, 2H), 1.07 (t, J = 7.2 Hz, 3H). ^{13}C NMR (101 MHz, DMSO-d_6) δ 162.1 (d, J = 7.3 Hz), 159.6 (d, J = 7.3 Hz), 159.2, 142.9, 131.8 (d, J = 10.6 Hz), 126.6, 112.2, 111.9, 111.2 (d, J = 19.1 Hz), 41.2, 33.3, 14.9. $C_{12}H_{12}F_2N_4ONa^+$ [M+Na]$^+$ calcd. 289.0871, found 289.0877.

1-benzyl-N-ethyl-1H-1,2,3-triazole-4-carboxamide (**15**)

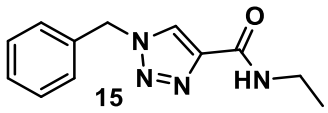

15

Compound **15** was prepared from intermediate **25** and ethylamine (70% solution in water), following the procedure described in section 3.2.3.7. Following collection, the product was crystallized by water. Crystals were dissolved in 0.5 mL deuterated DMSO. ^{1}H NMR (400 MHz, DMSO-d_6) δ 8.62 (s, 1H), 8.55 (t, J = 5.9 Hz, 1H), 7.44 – 7.25 (m, 5H), 5.64 (s, 2H), 3.25 (qd, J = 7.2, 5.7 Hz, 2H), 1.08 (t, J = 7.2 Hz, 3H). ^{13}C NMR (101 MHz, DMSO-d_6) δ 159.4, 143.3, 135.8, 128.9, 128.3, 128.0, 126.5, 53.1, 33.3, 14.9. m/z (HRMS+) for $C_{12}H_{14}N_4ONa^+$ [M+Na]$^+$ calcd. 253.1060, found 253.1063.

N-ethyl-1-(naphthalen-2-ylmethyl)-1H-1,2,3-triazole-4-carboxamide (**16**)

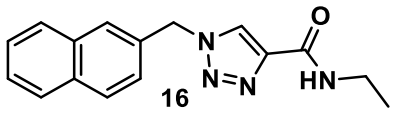

16

Compound **16** was prepared from intermediate **26** and ethylamine (70% w/w solution in water), following the procedure described in section 3.2.3.8. Following collection, the product was crystallized by water. Crystals were dissolved in 0.5 mL deuterated DMSO. ^{1}H NMR (400 MHz, DMSO-d_6) δ 8.68 (s, 1H), 8.55 (t, J = 5.9 Hz, 1H),

8.00 – 7.85 (m, 4H), 7.61 – 7.40 (m, 3H), 5.81 (s, 2H), 3.32 – 3.16 (m, 2H), 1.08 (t, *J* = 7.1 Hz, 3H). ^{13}C NMR (101 MHz, DMSO-d_6) δ 159.3, 143.3, 133.3, 132.8, 132.6, 128.6, 127.9, 127.7, 127.0, 126.7, 126.6, 126.5, 125.7, 53.3, 33.3, 14.9. m/z (HRMS+) for $C_{17}H_{16}N_4ONa^+$ $[M+Na]^+$ calcd. 303.1216, found 303.1220.

1-(2,6-difluorobenzyl)-N-propyl-1H-1,2,3-triazole-4-carboxamide (**17**)

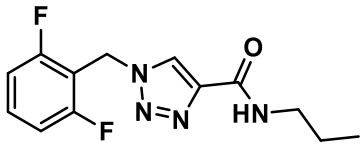

17

Compound **17** was prepared from intermediate **6**, following the procedure described in section 3.2.2.1. Following collection, the product was crystallized by water. Crystals were dissolved in 0.5 mL deuterated DMSO. ^{1}H NMR (400 MHz, DMSO-d_6) δ 8.54 (d, *J* = 19.3 Hz, 2H), 7.52 (tt, *J* = 8.4, 6.7 Hz, 1H), 7.19 (t, *J* = 8.1 Hz, 2H), 5.72 (s, 2H), 3.17 (dt, *J* = 7.6, 6.2 Hz, 2H), 1.49 (h, *J* = 7.4 Hz, 2H), 0.84 (t, *J* = 7.4 Hz, 3H). ^{13}C NMR (101 MHz, DMSO-d_6) δ 162.1 (d, *J* = 7.3 Hz), 159.6 (d, *J* = 7.3 Hz), 159.4, 142.9, 131.9 (t, *J* = 10.4 Hz), 126.6, 112.1 (d, *J* = 5.7 Hz), 111.9 (d, *J* = 5.6 Hz), 111.1 (t, *J* = 19.1 Hz), 41.2 (t, *J* = 3.9 Hz), 40.2, 22.5, 11.4. m/z (HRMS+) for $C_{13}H_{14}F_2N_4ONa^+$ $[M+Na]^+$ calcd. 303.1028, found 303.1036.

1-benzyl-N-propyl-1H-1,2,3-triazole-4-carboxamide (**18**)

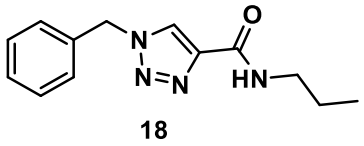

18

Compound **18** was prepared from intermediate **25** and propylamine, following the procedure described in section 3.2.3.3. Following collection, the product was crystallized by water. Crystals were dissolved in 0.5 mL deuterated DMSO. ^{1}H NMR (400 MHz, DMSO-d_6) δ 8.62 (s, 1H), 8.53 (t, *J* = 6.0 Hz, 1H), 7.44 – 7.28 (m, 5H), 5.64 (s, 2H), 3.18 (dt, *J* = 7.6, 6.2 Hz, 2H), 1.50 (h, *J* = 7.4 Hz, 2H), 0.84 (t, *J* = 7.4 Hz, 3H).^{13}C NMR (101 MHz, DMSO-d_6) δ 159.5, 143.2, 135.8, 128.9, 128.3, 128.0, 126.5, 53.1, 40.2, 22.5, 11.4. m/z (HRMS+) for $C_{13}H_{16}N_4ONa^+$ $[M+Na]^+$ calcd. 267.1216, found 267.1225.

1-(naphthalen-2-ylmethyl)-N-propyl-1H-1,2,3-triazole-4-carboxamide (**19**)

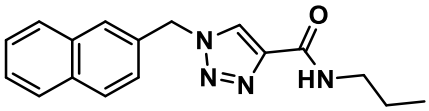

19

Compound **19** was prepared from intermediate **26** and propylamine, following the procedure described in section 3.2.3.4. Following collection, the product was crystallized by water. Crystals were dissolved in 0.5 mL deuterated DMSO. ^{1}H NMR (400 MHz, DMSO-d_6) δ 8.68 (s, 1H), 8.54 (t, *J* = 6.0 Hz, 1H), 8.00 – 7.84 (m, 4H), 7.61 – 7.41 (m, 3H), 5.81 (s, 2H), 3.18 (dt, *J* = 7.7, 6.2 Hz, 2H), 1.50 (h, *J* = 7.4 Hz, 2H), 0.84 (t, *J* = 7.4 Hz, 4H). ^{13}C NMR (101 MHz, DMSO-d_6) δ 159.6, 143.3, 133.3, 132.8, 132.6, 128.6, 127.9, 127.7, 127.1, 126.7, 126.6, 126.6, 125.8, 53.3, 40.2, 22.5, 11.4. m/z (HRMS+) for $C_{17}H_{18}N_4ONa^+$ $[M+Na]^+$ calcd. 317.1373, found 317.1383.

N-allyl-1-(2,6-difluorobenzyl)-1H-1,2,3-triazole-4-carboxamide (**20**)

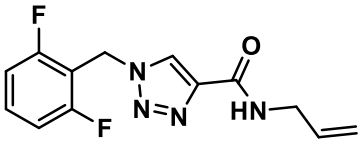

20

Compound **20** was prepared from intermediate **6**, allylamine, following the procedure described in section 3.2.2.3. Following collection, the product was crystallized by water. Crystals were dissolved in 0.5 mL deuterated DMSO ^{1}H NMR (400 MHz, DMSO-d_6) δ 8.68 (t, *J* = 6.0 Hz, 1H), 8.60 (s, 1H), 7.52 (tt, *J* = 8.5, 6.7 Hz, 1H), 7.19 (t, *J* = 8.1 Hz, 2H), 5.85 (ddt, *J* = 17.2, 10.3, 5.2 Hz, 1H), 5.73 (s, 2H), 5.20 – 4.97 (m, 2H), 3.85 (tt, *J* = 5.6, 1.7 Hz, 2H). ^{13}C NMR (101 MHz, DMSO-d_6) δ 162.1 (d, *J* = 7.2 Hz), 159.6 (d, *J* = 7.3 Hz), 159.3, 142.7, 135.3, 131.9 (t, *J* = 10.4 Hz), 126.7, 115.1, 112.1 (d, *J* = 5.7 Hz), 111.9 (d, *J* = 5.6 Hz), 111.1 (t, *J* = 19.1 Hz), 41.3 (t, *J* = 3.8 Hz), 40.8. m/z (HRMS+) for $C_{13}H_{12}F_2N_4ONa^+$ $[M+Na]^+$ calcd. 301.0871, found 301.0880.

N-allyl-1-benzyl-1H-1,2,3-triazole-4-carboxamide (**21**)

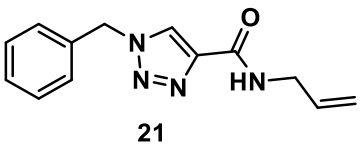

21

Compound **21** was prepared from intermediate **25** and allylamine, following the procedure described in section 3.2.3.6. Following collection, the product was crystallized by water. Crystals were dissolved in 0.5 mL deuterated DMSO ^{1}H NMR (400 MHz, DMSO-d_6) δ 8.68 (d, *J* = 19.9 Hz, 1H), 7.48 – 7.26 (m, 3H), 5.85 (ddt, *J* = 17.2, 10.3, 5.2 Hz, 1H),

5.65 (s, 1H), 5.20 – 4.96 (m, 1H), 3.85 (td, *J* = 5.6, 2.8 Hz, 1H). ^{13}C NMR (101 MHz, DMSO-d_6) δ 159.5, 143.0, 135.7, 135.3, 128.9, 128.3, 128.1, 126.6, 115.1, 53.1, 40.8. m/z (HRMS+) for $C_{13}H_{14}N_4ONa^+$ [M+Na]$^+$ calcd. 265.1060, found 265.1063.

N-allyl-1-(naphthalen-2-ylmethyl)-1H-1,2,3-triazole-4-carboxamide (**22**)

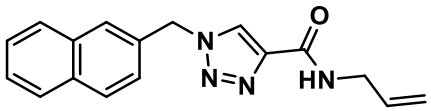

22

Compound **22** was prepared from intermediate **26** and allylamine, following the procedure described in section 3.2.3.6. Following collection, the product was crystallized by water. Crystals were dissolved in 0.5 mL deuterated DMSO ^{1}H NMR (400 MHz, DMSO-d_6) δ 8.70 (d, *J* = 2.9 Hz, 2H), 7.97 – 7.86 (m, 4H), 7.57 – 7.45 (m, 3H), 5.90 – 5.75 (m, 3H), 5.17 – 4.98 (m, 2H), 3.85 (tt, *J* = 5.6, 1.7 Hz, 2H). ^{13}C NMR (101 MHz, DMSO-d_6) δ 159.5, 143.0, 135.3, 133.2, 132.8, 132.6, 128.6, 127.9, 127.7, 127.1, 126.7, 126.7, 126.6, 125.8, 115.1, 53.3, 40.8. m/z (HRMS+) for $C_{17}H_{16}N_4ONa^+$ [M+Na]$^+$ calcd. 315.1216, found 315.1233.

Benzyl azide (**23**)

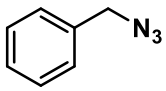

23

Compound **23** was prepared from benzyl bromide **7** and sodium azide following the procedure described in section 3.2.1.1 using deuterated water, deuterated methanol, and non-deuterated acetonitrile as solvents. Intermediate **23** was not isolated, a sample of 0.25 mL of solution was analyzed after addition of 0.25 mL of deuterated DMSO. ^{1}H NMR (400 MHz, DMSO-d_6) δ 7.39 – 7.21 (m, 5H), 4.32 (s, 2H). These data are in accordance with those previously published[52].

2-(azidomethyl)naphthalene (**24**)

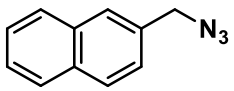

24

Compound **24** was prepared from 2-(bromomethyl)naphthalene **8** and sodium azide following the procedure described in section 3.2.1.2. Following collection, the solvent was evaporated, and the residue was fully dissolved in 0.5 mL of deuterated DMSO. ^{1}H

NMR (400 MHz, DMSO-d_6) δ 8.01 – 7.83 (m, 4H), 7.58 – 7.44 (m, 3H), 4.60 (s, 2H). These data are in accordance with those previously published[53].

Methyl 1-benzyl-1H-1,2,3-triazole-4-carboxylate (**25**)

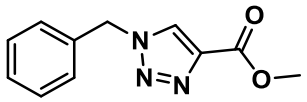

25

Compound **25** was prepared from benzyl azide **23**, methyl propiolate **3**, and catalytic amount of copper iodide following the procedure described in section 3.2.3.1. Following collection, the product was crystallized by water. Crystals were dissolved in 0.5 mL deuterated DMSO. ^{1}H NMR (400 MHz, DMSO-d_6) δ 8.92 (s, 1H), 7.43 – 7.28 (m, 5H), 5.67 (s, 2H), 3.82 (s, 3H). These data are in accordance with those previously published[54].

Methyl 1-(naphthalen-2-ylmethyl)-1H-1,2,3-triazole-4-carboxylate (**26**)

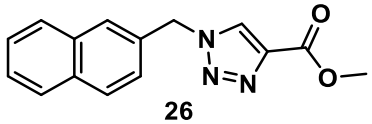

26

Compound **26** was prepared from 2-(azidomethyl)naphthalene **24**, methyl propiolate **3**, and catalytic amount of copper iodide following the procedure described in section 3.2.3.2. Following collection, the product was crystallized by water. Crystals were dissolved in 0.5 mL deuterated DMSO. ^{1}H NMR (400 MHz, DMSO-d_6) δ 8.97 (s, 1H), 7.98 – 7.84 (m, 4H), 7.59 – 7.43 (m, 3H), 5.83 (s, 2H), 3.82 (s, 3H). ^{13}C NMR (101 MHz, DMSO-d_6) δ 160.7, 138.9, 133.0, 132.8, 132.6, 129.5, 128.6, 127.9, 127.7, 127.1, 126.7, 126.6, 125.7, 53.3, 51.9. m/z (HRMS+) for $C_{11}H_{11}N_3O_2Na^+$ $[M+Na]^+$ calcd. 240.0743, found 240.0755.

1-(4-(trifluoromethyl)phenyl)pyrrolidine (**35**)

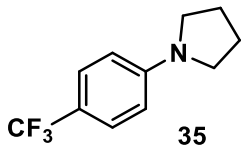

35

Compound **35** was prepared from 4-bromobenzotrifluoride (**30**) and pyrrolidine, with catalytic amount of $NiBr_2 \cdot 3H_2O$ 5% and Ir cat 0.2% as described in section 3.3.1.1. The product purified by column chromatography was dissolved in 0.5 mL $CDCl_3$. ^{1}H NMR (400 MHz, Chloroform-*d*) δ 7.43 (d, *J* = 8.5 Hz, 2H), 6.55 (d, *J* = 8.5 Hz, 2H), 3.37 – 3.26 (m, 4H), 2.03 (q, *J* = 3.3 Hz, 4H). These data are in accordance with those previously published[35].

1-(4-(trifluoromethyl)phenyl)pyrrolidin-3-ol (**36**)

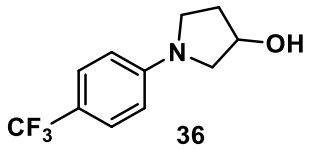

36

Compound **36** was prepared from 4-bromobenzotrifluoride (**30**) and pyrrolidin-3-ol, with catalytic amount of $NiBr_2 \cdot 3H_2O$ 5% and Ir cat 0.2% as described in section 3.3.1.3. The product purified by column chromatography was dissolved in 0.5 mL $CDCl_3$, ^{1}H NMR (400 MHz, Chloroform-*d*) δ 7.44 (d, *J* = 8.4 Hz, 2H), 6.55 (d, *J* = 8.4 Hz, 2H), 4.63 (s, 1H), 3.60 – 3.20 (m, 4H), 2.25 – 2.00 (m, 2H), 1.85 (s, 1H). ^{13}C NMR (101 MHz, Chloroform-*d*) δ 149.7, 128.6, 126.6 (q, *J* = 3.8 Hz), 124.0, 117.4 (q, *J* = 32.5 Hz), 115.5, 111.1, 71.2, 56.2, 45.6, 34.2. m/z (HRMS+) for $C_{11}H_{12}F_3NOH^+$ $[M+H]^+$ calcd. 232.0943, found 232.0947.

1-(4-(trifluoromethyl)phenyl)piperidin-4-ol (**37**)

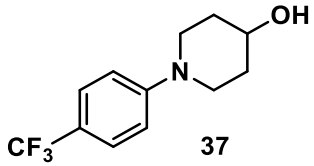

37

Compound **37** was prepared from 4-bromobenzotrifluoride (**30**) and piperidin-4-ol, with catalytic amount of $NiBr_2 \cdot 3H_2O$ 5% and Ir cat 0.2% as described in section 3.3.1.4. The product purified by column chromatography was dissolved in 0.5 mL $CDCl_3$, ^{1}H NMR (400 MHz, Chloroform-*d*) δ 7.65 – 7.38 (m, 2H), 6.91 (ddd, *J* = 15.5, 8.9, 2.6 Hz, 2H), 3.90 (s, 1H), 3.75 – 3.54 (m, 2H), 3.03 (ddt, *J* = 13.0, 10.1, 3.0 Hz, 2H), 1.99 (td, *J* = 8.4, 7.2, 3.9 Hz, 2H), 1.67 (dddt, *J* = 12.8, 9.6, 6.3, 3.2 Hz, 2H). ^{13}C NMR (101 MHz, Chloroform-*d*) δ 153.1, 127.2 (d, *J* = 3.7 Hz), 126.6 (q, *J* = 3.8 Hz), 123.6, 120.0, 115.6, 114.9, 67.8, 46.1, 33.8. m/z (HRMS+) for $C_{11}H_{14}F_3NOH^+$ $[M+H]^+$ calcd. 246.1110, found 246.1112.

1-(4-bromophenyl)pyrrolidine (**38**)

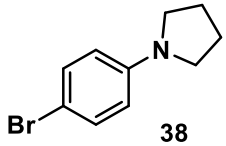

38

Compound **38** was prepared from 1,4-dibromobenzene (**31**) and pyrrolidine, with catalytic amount of $NiBr_2 \cdot 3H_2O$ 5% and Ir cat 0.2% as described in section 3.3.1.2. The product purified by column chromatography was dissolved in 0.5 mL $CDCl_3$, ^{1}H NMR (400 MHz, Chloroform-*d*) δ 7.43 – 7.14 (m, 2H), 6.58 – 6.30 (m, 2H), 3.36 – 3.14 (m, 4H), 2.12 – 1.84 (m, 4H). These data are in accordance with those previously published[55].

N-acetyl-para-aminophenol (paracetamol **39**)

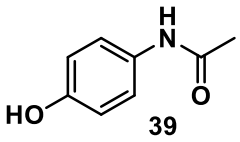

39

Compound **39** was prepared from 4-aminophenol (**42**) and acetic anhydride (**43**) as described in section 3.4.2.2. The product purified by crystallization was dissolved in 0.5 mL of deuterated DMSO: ^{1}H NMR (400 MHz, DMSO) δ 9.66 (s, 1H), 9.16 (s, 1H), 7.33 (d, *J* = 8.8 Hz, 2H), 6.67 (d, *J* = 8.8 Hz, 2H), 1.97 (s, 3H). These data are in accordance with those previously published[56].

N-(2,6-dimethylphenyl)-N^2,N^2-diethylglycinamide (lidocaine **40**)

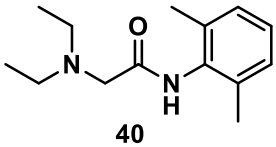

40

Compound **40** was prepared from intermediate **46** and diethylamine **47** as described in section 3.4.2.2. After extraction the residue was dissolved in $CDCl_3$: ^{1}H NMR (400 MHz, $CDCl_3$) δ 8.94 (s, 1H), 7.10 – 7.08 (m, 3H), 3.23 (s, 2H), 2.70 (q, *J* = 7.1 Hz, 4H), 2.23 (s, 6H), 1.14 (t, *J* = 7.1 Hz, 6H). These data are in accordance with those previously published[24]. Compound **40** was purified by crystallization as HCl salt and was then dissolved in $CDCl_3$: ^{1}H NMR (400 MHz, $CDCl_3$) δ 7.07 – 7.00 (m, 3H), 4.32 (s, 2H), 3.62 – 3.34 (m, 4H), 2.27 (s, 6H), 1.54 (t, *J* = 7.3 Hz, 6H). These data are in accordance with those previously published[24,25].

Dimethyl-2,6-dimethyl-4-(2-nitrophenyl)-1,4-dihydropyridine-3,5-dicarboxylate (nifedipine **41**)

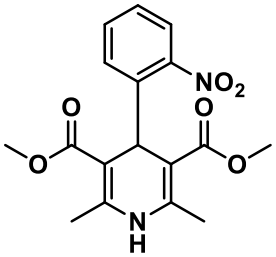

41

Compound **41** was prepared from 2-nitrobenzaldehyde (**48**), methyl acetoacetate (**49**), and methyl 3-aminocrotonate (**50**) as described in section 3.4.3.2. The product purified by crystallization was dissolved in 0.5 mL of $CDCl_3$: ^{1}H NMR (400 MHz, $CDCl_3$) δ 7.61 (dd, *J* = 8.0, 1.4 Hz, 1H), 7.44 (dd, *J* = 8.0, 1.6 Hz, 1H), 7.38 (td, *J* = 7.6, 1.4 Hz, 1H),

7.21 – 7.15 (m, 1H), 5.85 (s, 1H), 5.65 (s, 1H), 3.52 (s, 6H), 2.26 (s, 6H). These data are in accordance with those previously published[57].

2-chloro-N-(2,6-dimethylphenyl)acetamide (**46**)

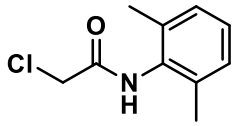

46

Compound **46** was synthesized from 2,6-dimethyl aniline (**44**) and chloroacetyl chloride (**45**) as described in section 3.4.2.2. The product purified by crystallization with water and upon filtration was dissolved in 0.5 mL of $CDCl_3$: ^1H NMR (400 MHz, $CDCl_3$) δ 7.87 (s, 1H), 7.20 – 7.04 (m, 3H), 4.25 (s, 2H), 2.24 (s, 6H). These data are in accordance with those previously published[31].

5 Conclusions and perspective

A fully automated, remotely accessible instrument capable of synthesizing small organic molecules based on a radial arrangement of continuous flow modules has been developed. The sequential, non-simultaneous nature of multistep radial synthesis is more versatile than linear or iterative synthetic approaches since each step of a multistep process is functionally independent from the others. Thereby, reactors can be reused at different temperatures and flow rates while intermediates can be stored for convergent syntheses and multistep optimizations.

This is the first automated platform capable of exploring both linear and convergent synthetic routes, performing concentration and solvent screening inline, and allowing for equipment reutilization, also at variable conditions, within the same process, all without physical reconfiguration.

The radial synthesizer showed high flexibility over different reaction conditions for single or multistep syntheses, good reproducibility of results and ability to synthesize libraries of compounds through combination of a set of starting materials and reagents in different orders and under different conditions.

Its synthetic and analytical capabilities could be easily expanded by integration of new modules that proved to be operationally simple. Finally, the equivalence between radial and continuous flow was demonstrated, thus establishing the radial synthesizer as a powerful tool for process discovery. Reaction conditions optimized using the radial synthesizer could be translated without any modification in a commercially available continuous flow system (Vapourtec R2 and R4), for scale-up and continuous operation.

These capabilities were demonstrated through the comparison of two alternative synthetic routes for the API rufinamide (convergent and linear, section 3.1), the generation of a library of twelve derivatives (section 3.2), the integration of a photochemical module for metallaphotoredox C-N cross-couplings and of a flow-NMR spectrometer for determination of inline NMR yield[29] (section 3.3). Finally, the optimization and scale-up of the synthesis of three drugs (paracetamol, lidocaine and nifedipine) demonstrated the equivalence between radial and continuous flow (section 3.4).

The radial synthesizer utilizes commercially available equipment and hardware and can be operated in manual or fully automated mode through a software interface. Given the remarkable and constantly growing number of flow modules already existing, from home-made devices to commercially available systems, the capabilities of the radial synthesizer can potentially be expanded even further. New synthetic modules can be integrated in the central station of the instrument granting access to new chemistries.

As the equivalence between flow modules linked in radial and linear telescoped arrangement was already successfully proved, the next easiest exhibition of the potential of radial synthesis could be the demonstration of the same equivalence with iterative synthesis (section 1.3.2). This could be done by integrating a continuous stirred tank reactor (CSTR) containing resin beads for the solid-phase synthesis of biopolymers[6,7,8] or cartridges and packed bed modules for the iterative cross-coupling and purification of MIDA boronates[27]. If that would prove possible, we would have in a single instrument the capability to explore all the different approaches to organic synthesis and performing high throughput, automated condition screening of extremely diverse processes, and potentially the ability to perform building block synthesis and coupling within the same automated platform.

Another future goal to expand the applicability of the radial synthesizer would be the introduction of purification modules. The radial synthesizer is suited for the development of a hybrid platform that bridges flow and batch technologies by taking the best elements from both. Extraction, crystallization, and solvent-switch modules can be designed to be integrated in the central station to purify and isolate final products or synthetic intermediates.

Besides the evolution of the hardware, an effort must be taken for the implementation of algorithms for data processing and machine learning. Such a versatile automated platform can be used for the generation of large data sets of highly reproducible and data-rich synthetic procedures, including positive and negative results.

Compared to conventional continuous flow chemistry, that employs a large amount of material for each test, the radial synthesizer works with small volumes of solutions that can be miniaturized even further, allowing for the production of sufficient data in an automated manner, within a reasonable time frame and with minimum waste of material.

Automated systems, in general, ensure reproducibility because they reduce the error introduced by manual operations. A given input instruction, in principle, should be operated in the same way on an equivalent system, nevertheless each existing system nowadays relies on different protocols, resulting in a lack of standardization that limits the potential of automation applied to chemistry. Scientists have already identified and tried to address this problem, proposing a general programming language for chemical operations[2]. The implementation of software based on a universal language could bridge the gap between the many already existing automated synthesizers based on batch[2], flow[24,25,27,29] or solid-phase synthesis[6,7,8], thus framing the radial synthesizer within the context of a big network of automated platforms using the same modules and generating transferable universal protocols for chemical synthesis.

As a whole, these platforms for automated synthesis could reshape how research is conducted. Since such systems can be operated remotely, it is possible to envision the creation of “chemistry server farms”, intended as facilities containing hundreds of automated platforms, which scientists could control from anywhere in the world. This would truly standardize and democratize research, overcoming economic and geographic barriers by granting access to state-of-the-art technology.

6 References

1) Milo, A. *Science* **2019**, 363, 6423, 122–123.
2) Steiner, S.; Wolf, J.; Glatzel, S.; Andreou, A.; Granda, J. M.; Keenan, G.; Hinkley, T.; et al. *Science* **2019**, 363, 6423. DOI: 10.1126/science.aav2211.
3) Burger, B.; Maffettone, P. M.; Gusev, V. V.; Aitchison, C. M.; Bai, Y.; Wang, X.; Li, X.; et al. *Nature* **2020**, 583, 237–241.
4) Plutschack, M. B.; Pieber, B.; Gilmore, K.; Seeberger, P. H. *Chem. Rev*. **2017**, 117, 11796–11893.
5) Trojanowicz, M. *Molecules* **2020**, 25, 1434; DOI: 10.3390/molecules25061434
6) Merrifield, R. B. *Science* **1965**,150, 178–185.
7) Alvarado-Urbina, G.; Sathe, G. M.; Liu, W. C.; Gillen, M. F.; Duck, P. D.; Bender, R.; Ogilvie, K. K. *Science* **1981**, 214, 270–274.
8) Plante, O. J.; Palmacci, E. R.; Seeberger, P. H. *Science* **2001**, 291, 1523–1527.
9) Guidi, M.; Seeberger, P. H.; Gilmore, K. *Chem. Soc. Rev.* **2020**, DOI: 10.1039/c9cs00832b
10) Sambiagio, C.; Noël, T. *Trends Chem.* **2020**, 2, 92–106.
11) Dallinger, D.; Gutmann, B.; Kappe, C. O. *Acc. Chem. Res.* **2020**, 53, 7, 1330–1341.
12) Yoshida, J.; Nagaki, A.; Yamada, T. *Chem. Eur. J.* **2008**, 14, 7450–7459.
13) Yoshida, J.; Takahashia, Y.; Nagakia, A. *Chem. Commun*. **2013**, 49, 9896 – 9904.
14) Su, Y.; Kuijpers, K.; Hessel, V.; Noël, T. *React. Chem. Eng*. **2016**, 1, 73−81.
15) Ahn, G.-N.; Yu, T.; Lee, H.-J. Gyak, K.-W.; Kang, J.-H.; You, D.; Kim. D.-P. *Lab Chip* **2019**, 19, 20, 3535–3542.
16) Hughes, D. L. *Org. Process Res. Dev.* **2020**, DOI: 10.1021/acs.oprd.0c00156.
17) Baumann, M.; Moody, T. S.; Smyth, M.; Wharry, S. *Org. Process Res. Dev.* **2020**, DOI: 10.1021/acs.oprd.9b00524.
18) Ghislieri, D.; Gilmore, K.; Seeberger, P. H. *Angew. Chem. Int. Ed*. **2015**, 54, 678–682.
19) Jensen, K. F. *Nature* **2020**, 579, 346–348.
20) Deadman, B. J.; Battilocchio, C.; Sliwinski, E.; Ley, S. V. *Green Chem*. **2013**, 15, 2050–2055.
21) Smith, C. D.; Baxendale, I. R.; Lanners, S.; Hayward, J. J.; Smith; S. C.; Ley, S. V. *Org. Biomol. Chem.* **2007**, 5, 1559–1561.
22) Muller, P. *Pure Appl. Chem*. **1994**, 66, 5, 1007–1184
23) Trobe, M.; Burke, M. D. *Angew.Chem. Int. Ed.* **2018**, 57, 4192–4214
24) Adamo, A.; Beingessner, R. L. ; Behnam, M.; Chen, J.; Jamison, T. F.; Jensen, K.

F.; Monbaliu, J-C. M.; et al. *Science* **2016**, 352, 6281, 61–67

25) Coley, C. W.; A.; Thomas III, D. A.; Lummiss, J. A. M.; Jaworski, J. N.; Breen, C. P.; Schultz, V.; et al. *Science* **2019** 365, 6453, DOI: 10.1126/science.aax1566.

26) Vitaku, E.; Smith, D. T.; Njardarson, J. T. *J. Med. Chem.* **2014**, 57, 24, 10257–10274.

27) Li, J.; Ballmer, S. G.; Gillis, E. P.; Fujii, S.; Schmidt, M. J.; Palazzolo, A. M. E.; Lehmann, J. W.; et al. *Science* **2015**, 6227, 1221–1226.

28) Baxendale I. R.; Ley S. V.; Smith, C. D.; Tranmer G. K. *Chem. Commun*. **2006**, 4835–4837.

29) Chatterjee, S.; Guidi, M.; Seeberger, P. H.; Gilmore, K. *Nature* **2020**, 579, 379–384.

30) Hwang, Y. J.; Coley, C. W.; Abolhasani, M.; Marzinzik, A. L.; Koch, G.; Spanka, C.; Lehmann, H.; Jensen, K. F. *Chem. Commun*. **2017**, 53, 6649–6652.

31) Fitzpatrick, D. E.; Maujean, T.; Evans, A. C.; Ley, S. V. *Angew. Chem. Int. Ed.* **2018**, 57, 15128–15132.

32) Padmaja, R. D.; Chanda, K. A. *Org. Process Res. Dev*. **2018**, 22, 457–466.

33) Twilton, J.; Le, C.; Zhang, P.; Shaw, M. H.; Evans, R. W.; MacMillan, D. W. C. *Nat. Rev. Chem.* **2017**, 1, 0052. DOI: 10.1038/s41570-017-0052.

34) Milligan, J. A.; Phelan, J. P.; Badir, S. O.; Molander, G. A. *Angew. Chem. Int. Ed.* **2019**, 58, 6152–6163.

35) Corcoran E. B. et al. *Science* **2016**, 353, 279–283.

36) List of medications that went under shortage in Germany during the COVID-19 pandemic: https://www.gelbe-liste.de/lieferengpaesse/lieferengpaesse-medikamente

37) Sato, M.; Matsushima, K.; Kawanami, H.; Chatterjee, M.; Yokoyama, T.; Ikuhsima, Y.; Suzuki, T. M. *Lab Chip* **2009**, 9, 2877–2880.

38) Filipan-Litvić, M.; Litvić, M.; Cepanec, I.; Vinković, V. *Molecules* **2007**, 12, 2546–2558.

39) Berwe, M.; Diehl, H.; Rittner, K.; Wahl, K.; Wirges, H. (Bayer Aktiengesellschaft), US6294673B1, **2001**.

40) Paracetamol, Lidocaine and Nifedipine are in the WHO list of essential drugs: https://apps.who.int/iris/bitstream/handle/10665/325771/WHO-MVP-EMP-IAU-2019.06-eng.pdf?sequence=1&isAllowed=y

41) Ralph, J.; Karlen, S.; Mobley, J. (Wisconsin Alumni Research Foundation), US10286504B2, **2018**.

42) Huber, J. Jr. (Penick Corporation), US4264525A, **1979**.

43) Lemaire, M. L.; Joncour, R.; Duguet, N. F. D.; Metay, E. C. D.; Ferreira, A. (Minakem), EP 2 860 172 A1, **2015**.

44) Pieber, B.; Shalom, M.; Antonietti, M.; Seeberger, P. H.; Gilmore, K. *Angew. Chem. Int. Ed*. **2018**, 57, 9976–9979

45) Hermann, H.; Hollmann, M. W.; Stevens, M. F.; Lirk, P.; Brandenburger, T.; Piegeler, T.; Werdehausen, R. *Br. J. Anaesth*. **2019**, 123, 3, 335–349.

46) Britton, J.; Chalker, J. M.; Raston, C. L. *Chem. Eur. J*. **2015**, 21, 10660–10665

47) Nifedipine is a dihydropyridine derivative and is a calcium-channel blocking agent. It is used to treat different diseases: https://www.drugs.com/monograph/nifedipine.html

48) Taylor, N. J.; Emer, E.; Preshlock, S.; Schedler, M.; Tredwell, M.; Verhoog, S.; Mercier, J.; Genicot, C.; Gouverneur, V. *J. Am. Chem. Soc.* **2017**,139, 8267–8276.

49) Barr, L.; Lincoln, S. F.; Easton, C. J.. *Supramol. Chem.* **2005**, 17, 547–555.

50) Zhang, P.; Russell, M. G.; Jamison, T. F. *Org. Process Res. Dev.* **2014**, 18, 1567–1570.

51) Borukhova, S.; Noel, T.; Metten, B.; de Vos, E.; Hessel, V. *ChemSusChem*, **2013**, 6, 2220–2225.

52) Pietruszka, J.; Solduga, G. *Eur. J. Org. Chem*, **2009**, 34, 5998–6008

53) Maddani, M.; Prabhu, K. R.; *Tetrahedron Lett.* **2008**, 49, 5436–5436.

54) Jlalia, I.; Meganem, F.; Herscovici, J.; Girard, C. *Molecules*, **2009**, 14, 528–539.

55) Jiang, D. S.; Fu, H.; Jiang, Y. Y.; Zhao, Y. F. *J. Org. Chem.* **2007**, 72, 672–674.

56) Drillaud, N.; Banaszak-Léonard, E.; Pezron, I.; Len, C. *J. Org. Chem*. **2012**, 77, 21, 9553–9561.

57) Bridgwood, K. L.; Veitch, G. E.; Ley, S. V. *Org. Lett*. **2008**, 10, 16, 3627–3629.

7 Appendix: NMR spectra

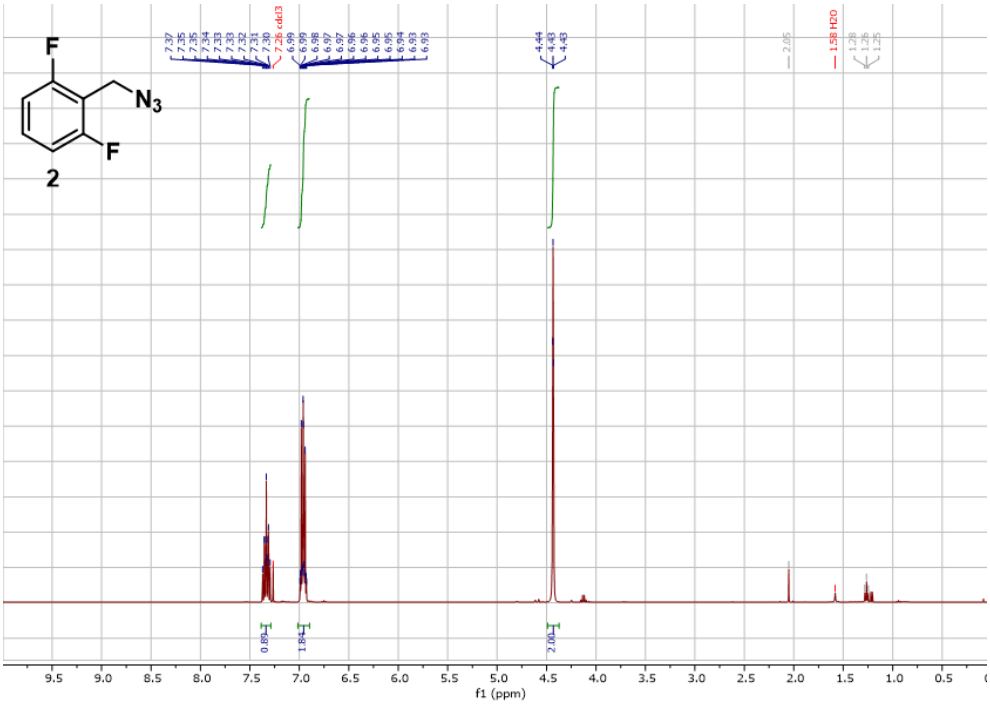

Figure 6.1. ^{1}H NMR **2**

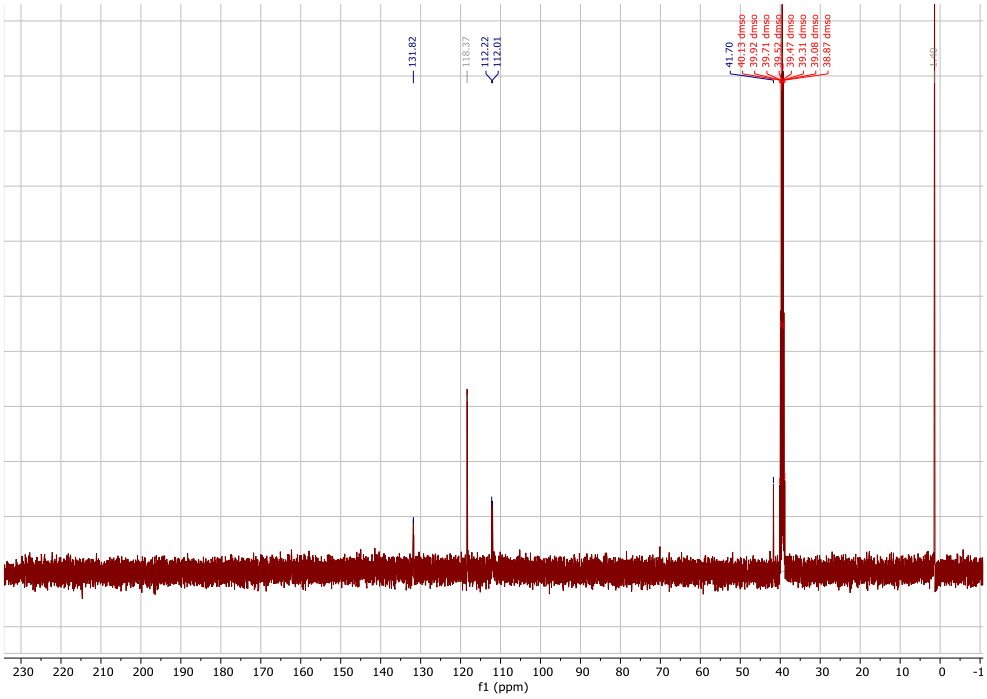

Figure 6.2. ^{13}C NMR **2**

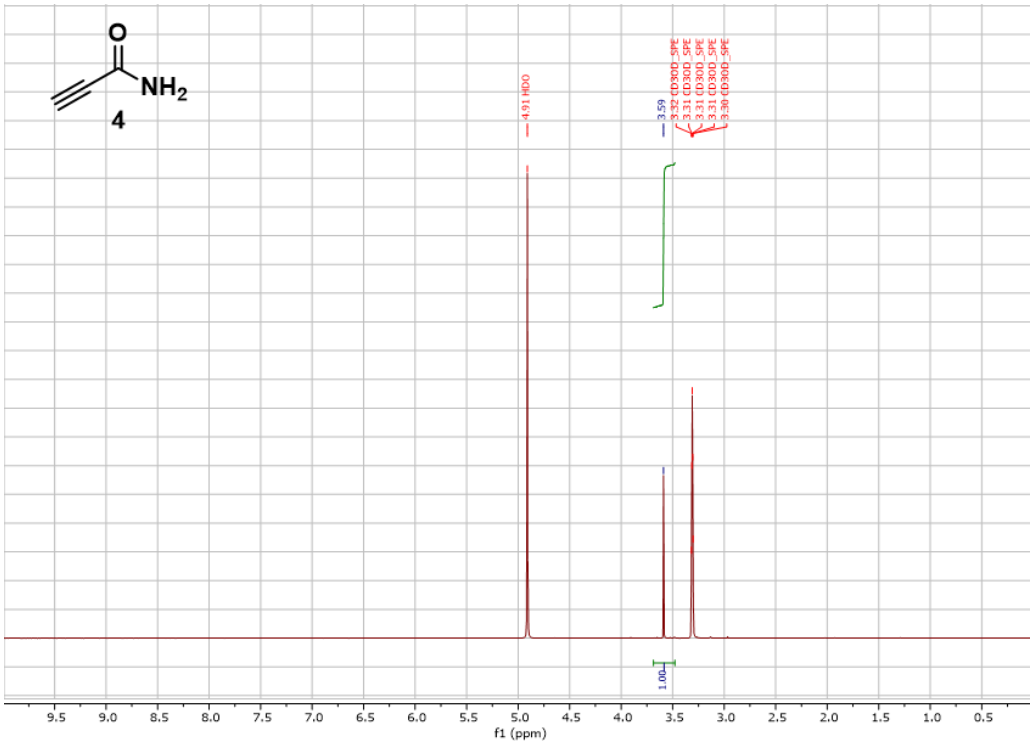

Figure 6.3. ^{1}H NMR **4**

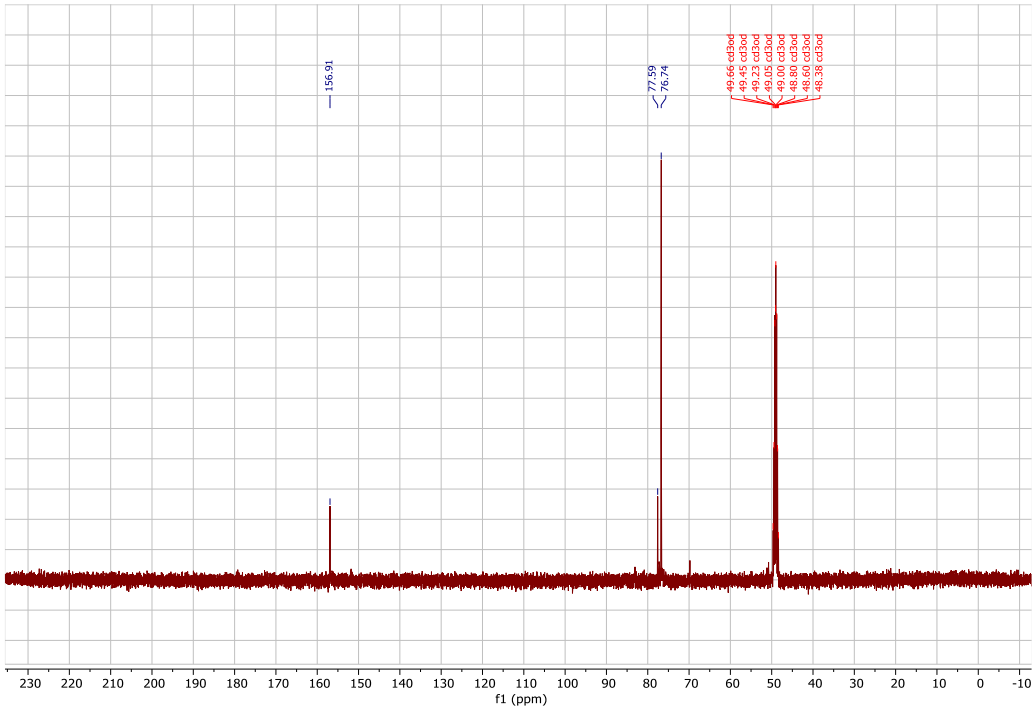

Figure 6.4. ^{13}C NMR **4**

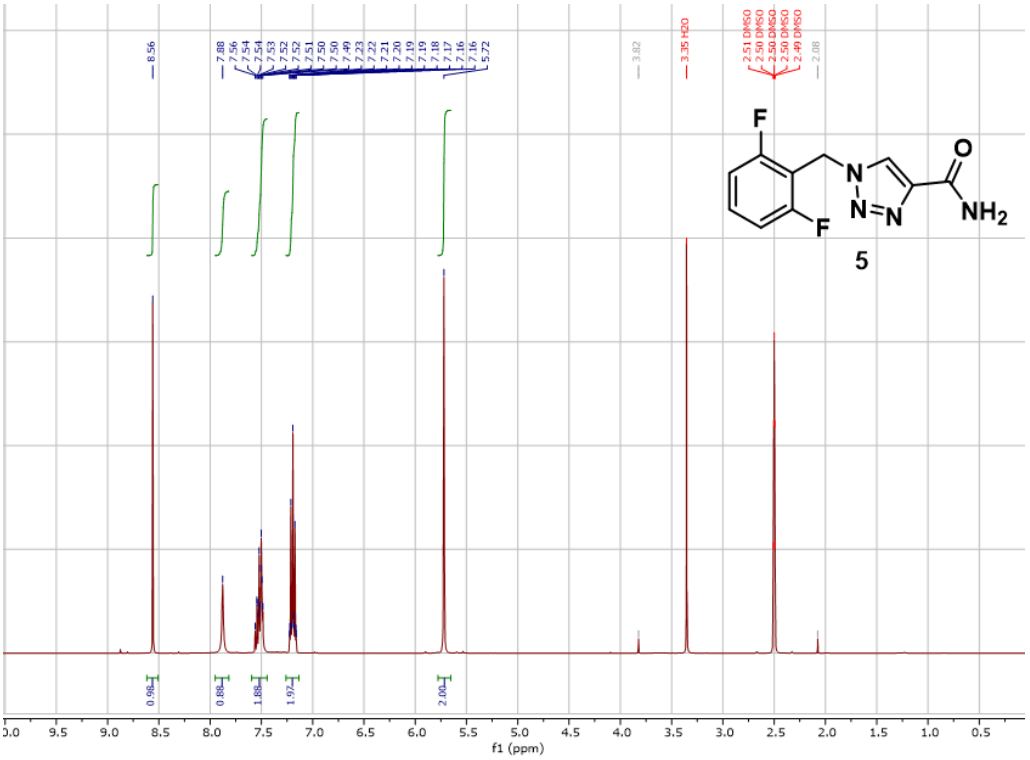

Figure 6.5. ^{1}H NMR **5**

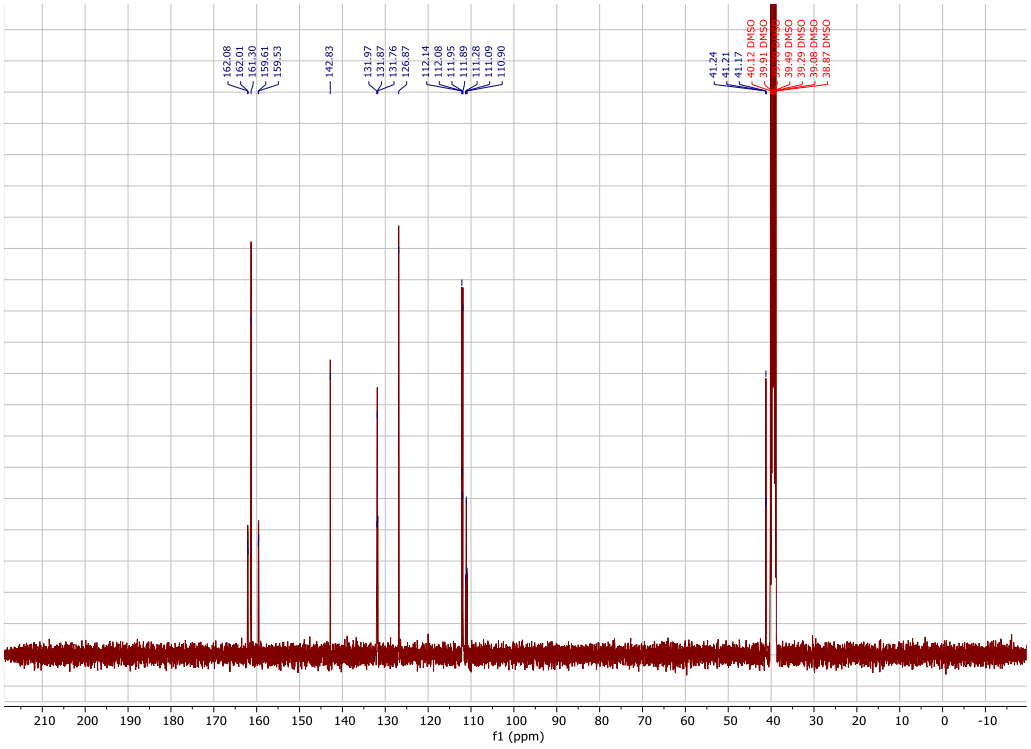

Figure 6.6. ^{13}C NMR **5**

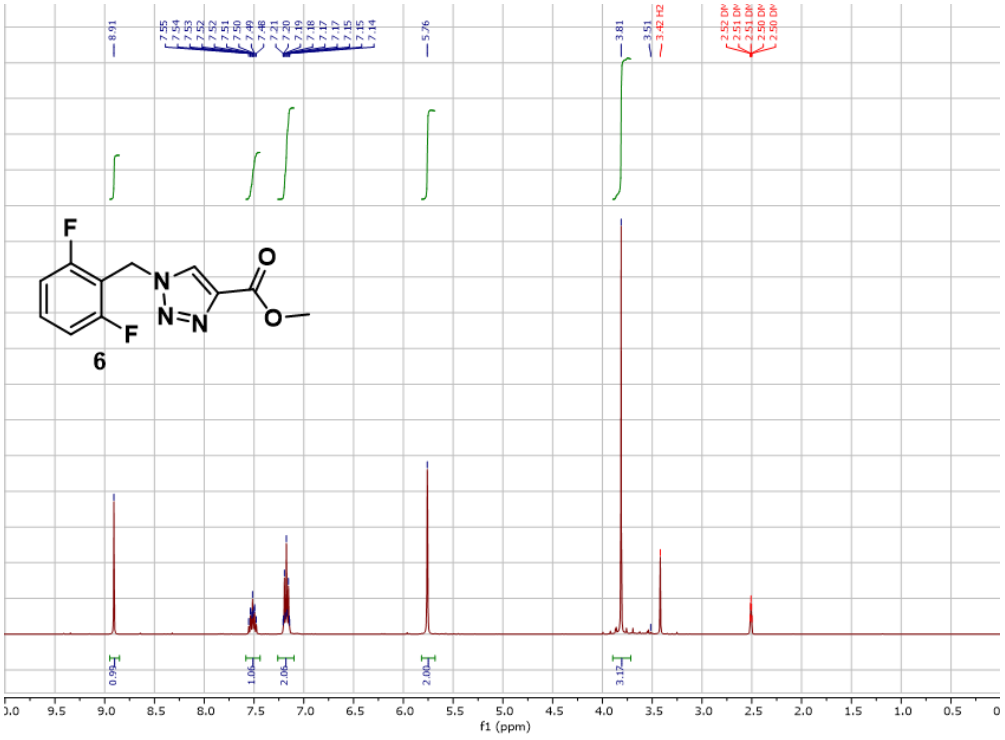

Figure 6.7. ^{1}H NMR **6**

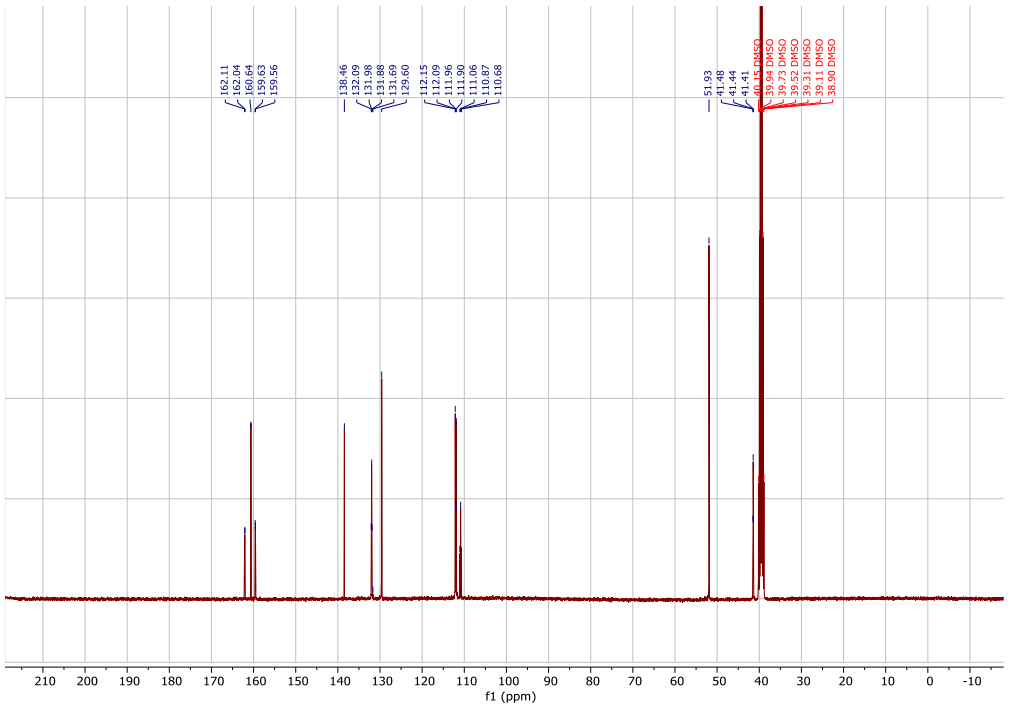

Figure 6.8. ^{13}C NMR **6**

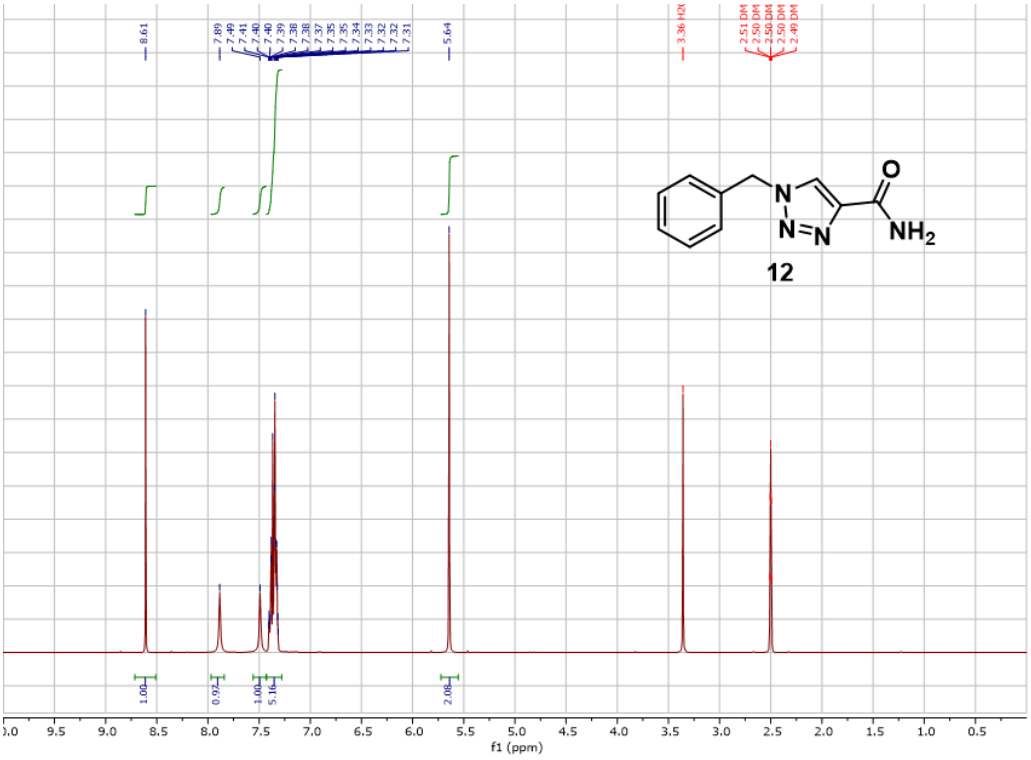

Figure 6.9. ^{1}H NMR **12**

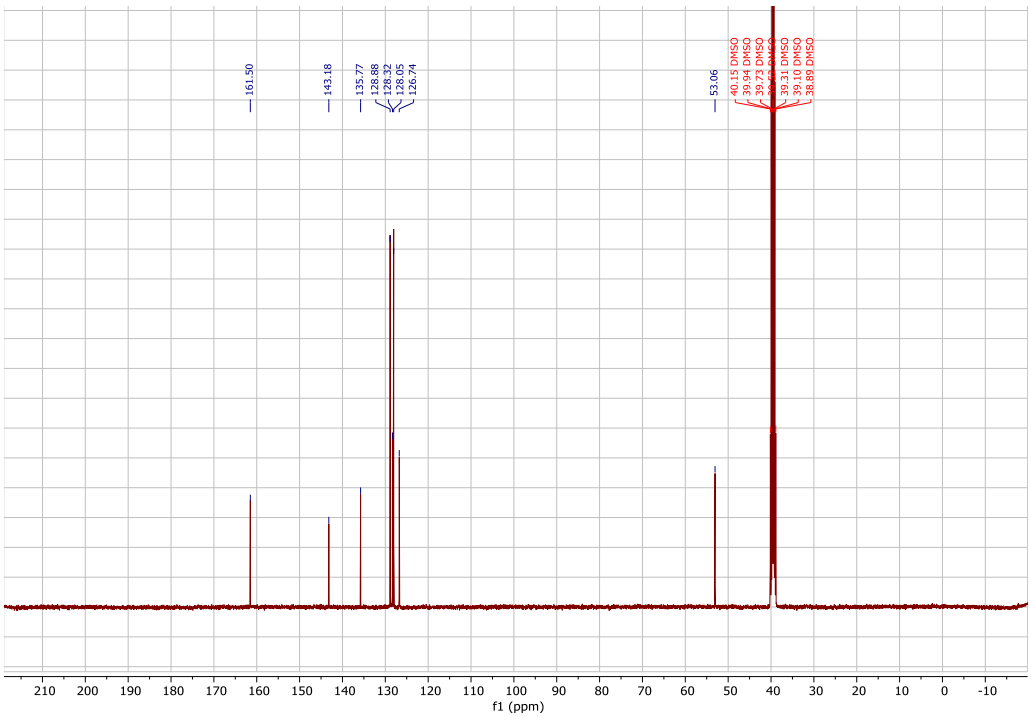

Figure 6.10. ^{13}C NMR **12**

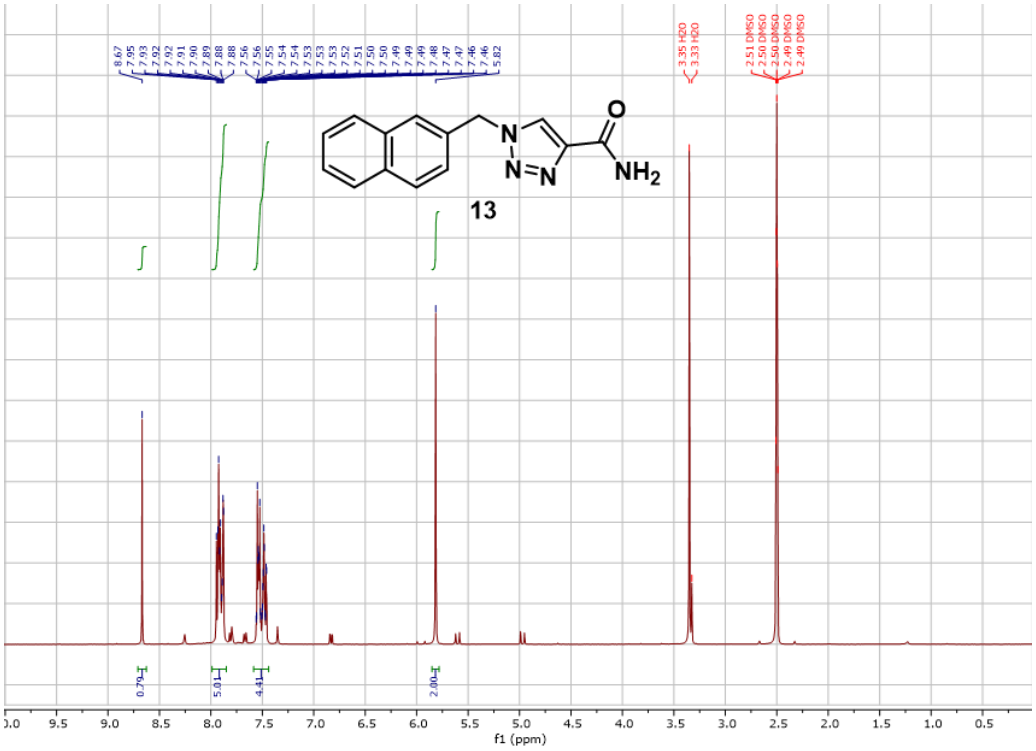

Figure 6.11. ^{1}H NMR **13**

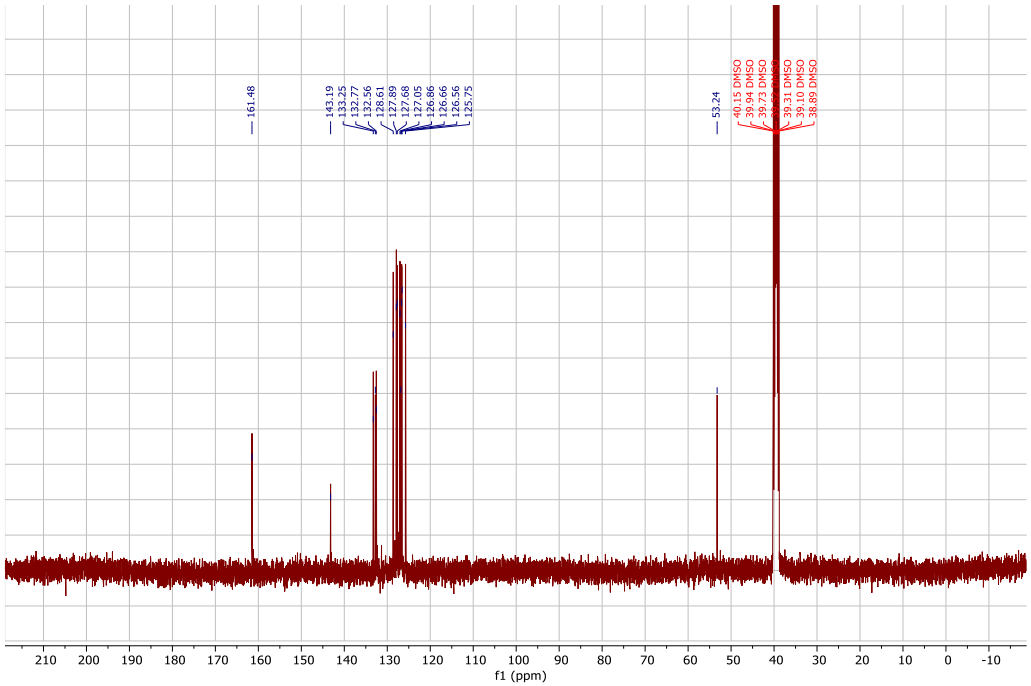

Figure 6.12. ^{13}C NMR **13**

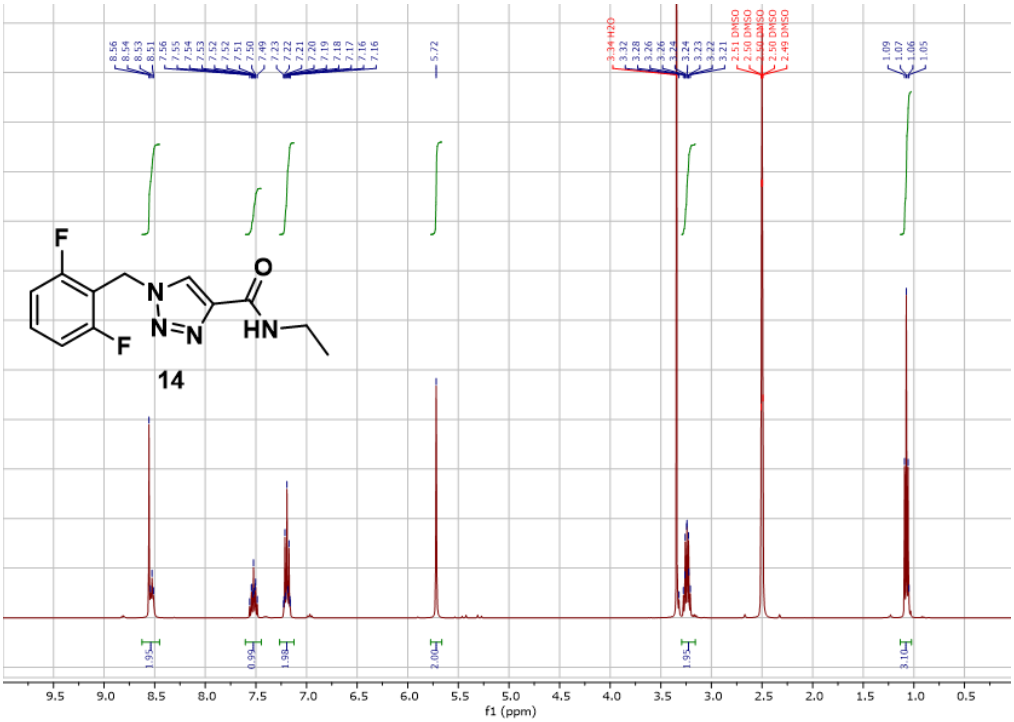

Figure 6.13. ^{1}H NMR **14**

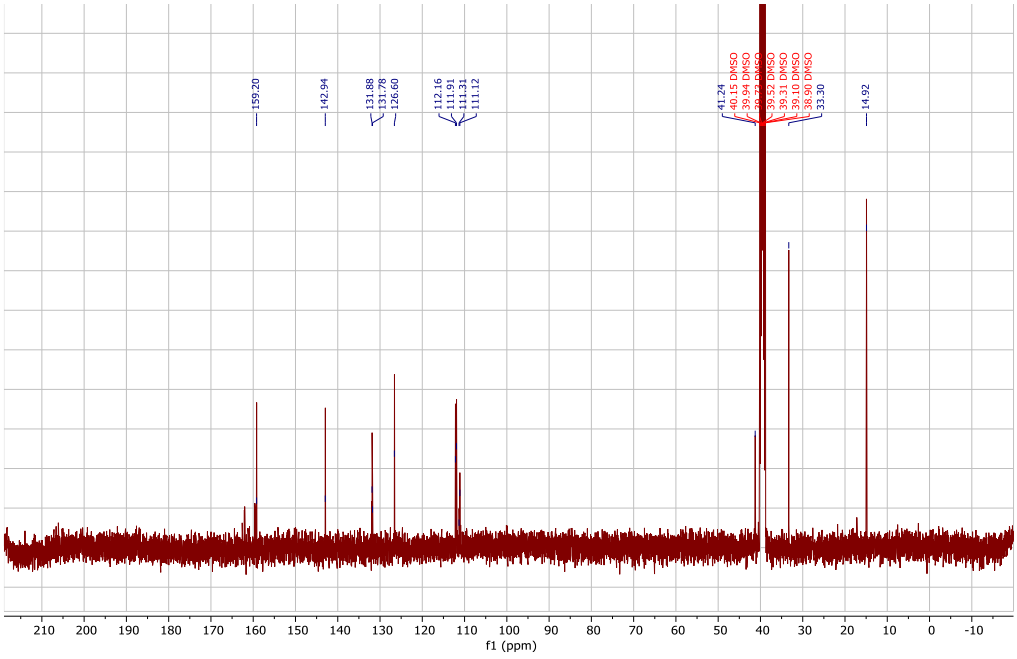

Figure 6.14. ^{13}C NMR **14**

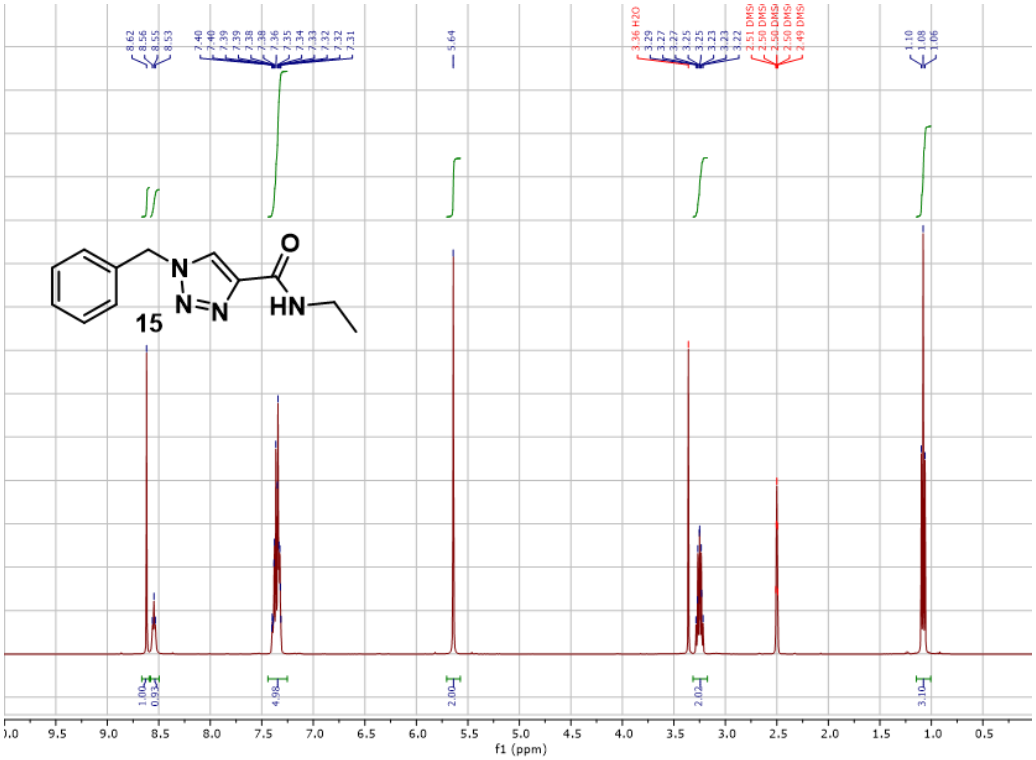

Figure 6.15. ^{1}H NMR **15**

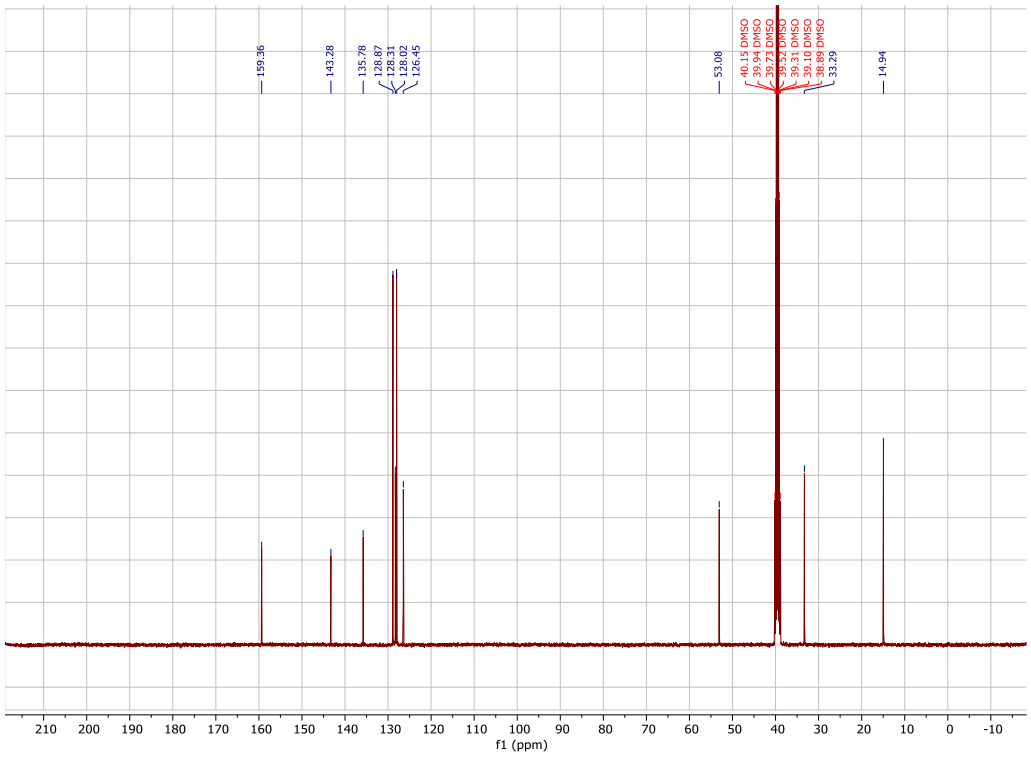

Figure 6.16. ^{13}C NMR **15**

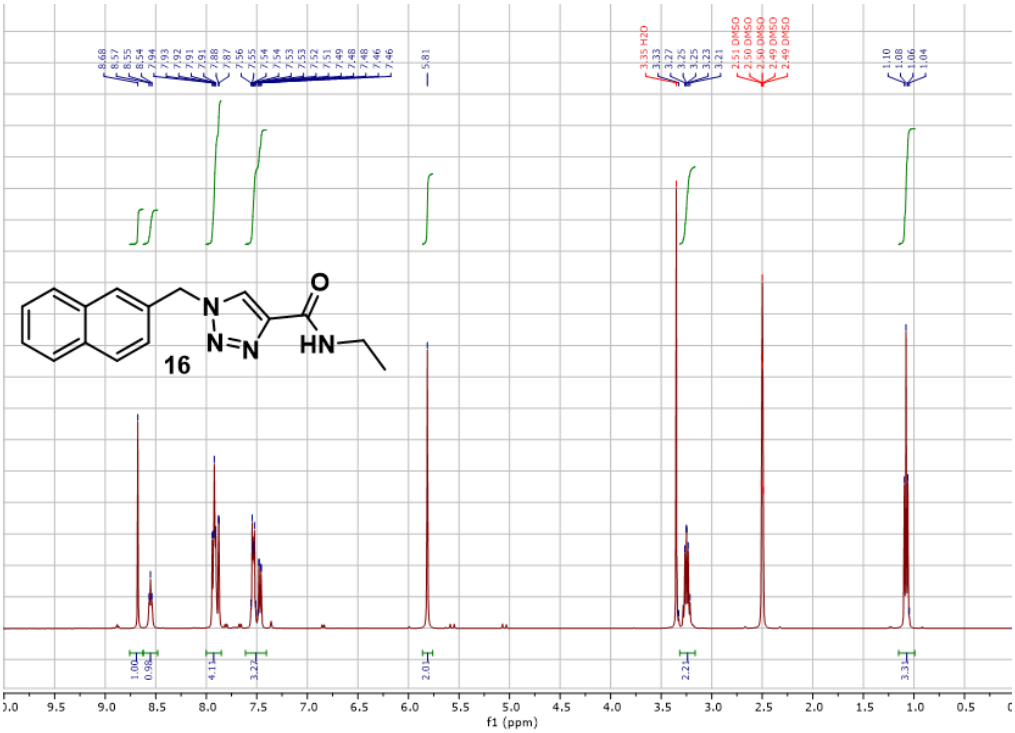

Figure 6.17. ^{1}H NMR **16**

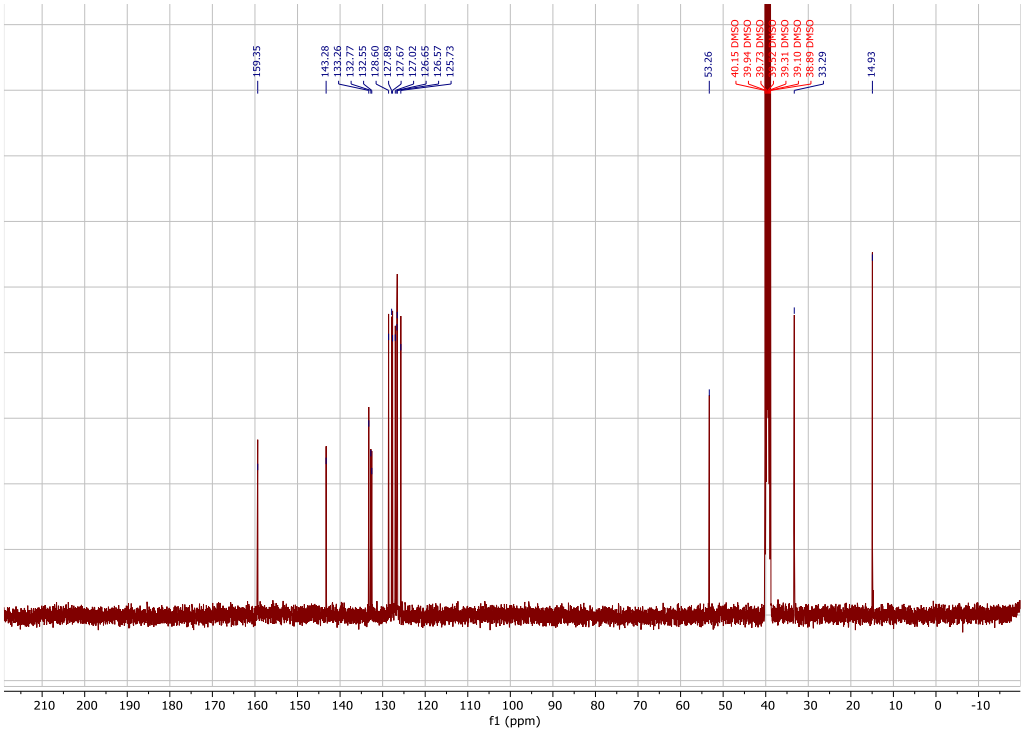

Figure 6.18. ^{13}C NMR **16**

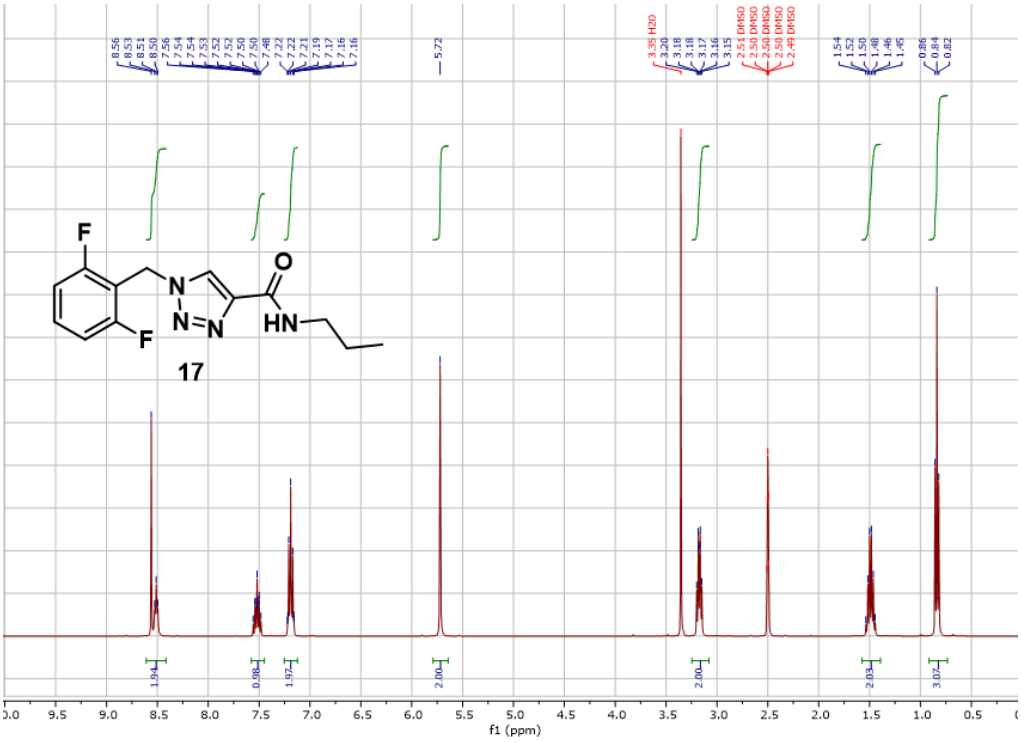

Figure 6.19. ^{1}H NMR **17**

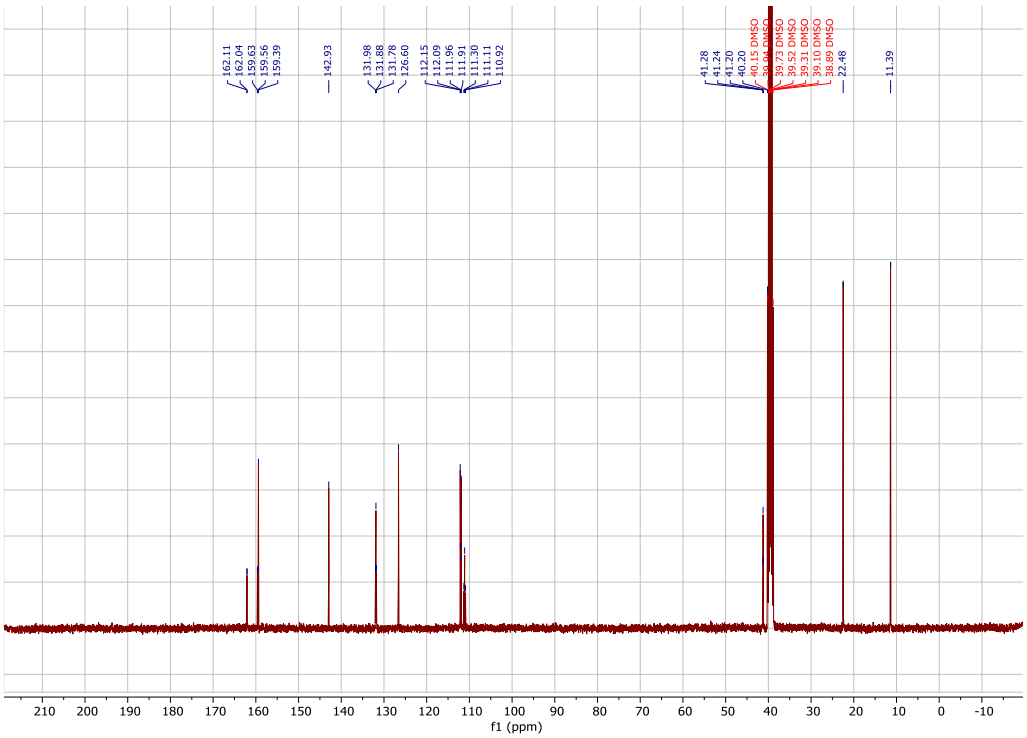

Figure 6.20. ^{13}C NMR **17**

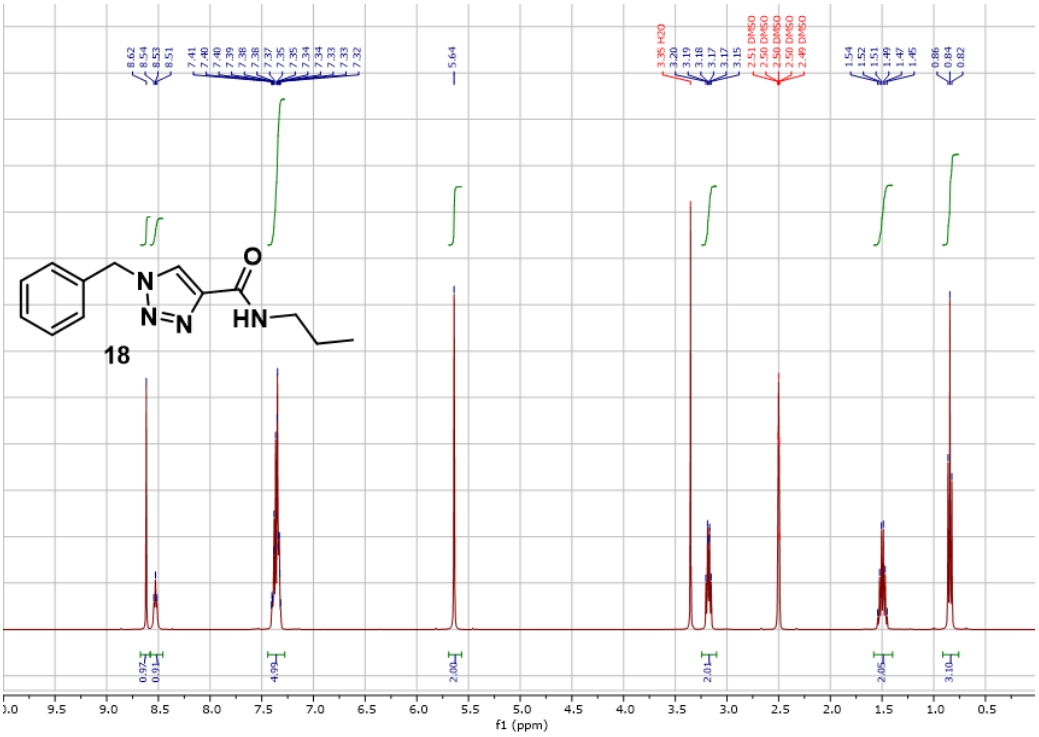

Figure 6.21. ^{1}H NMR **18**

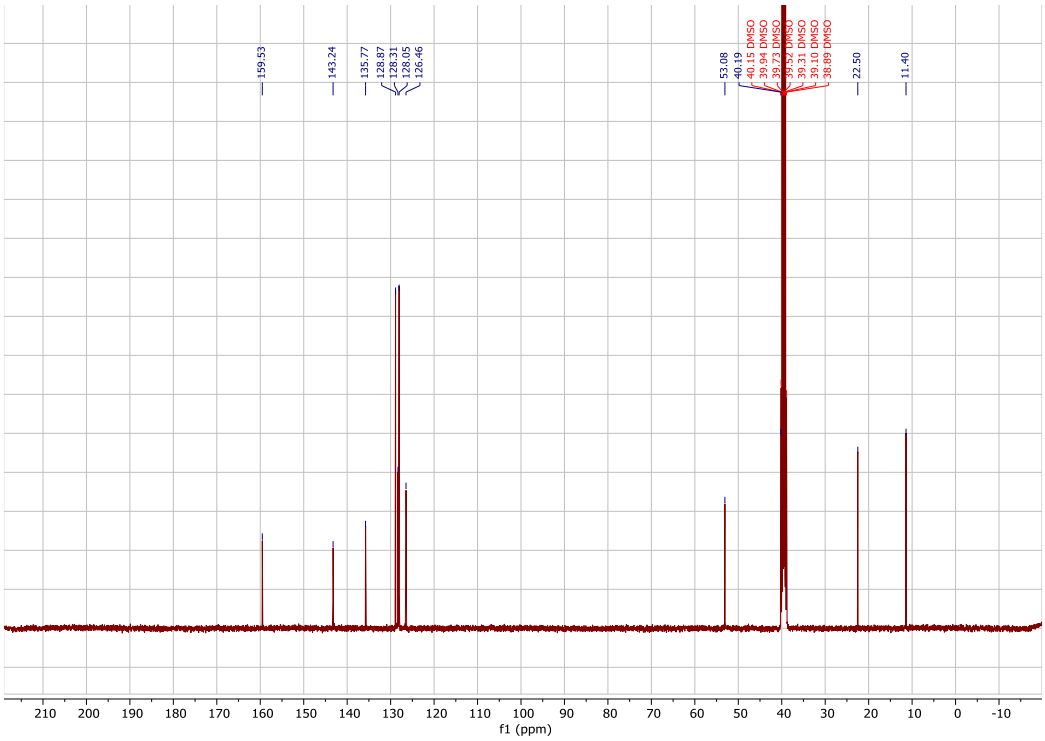

Figure 6.22. ^{13}C NMR **18**

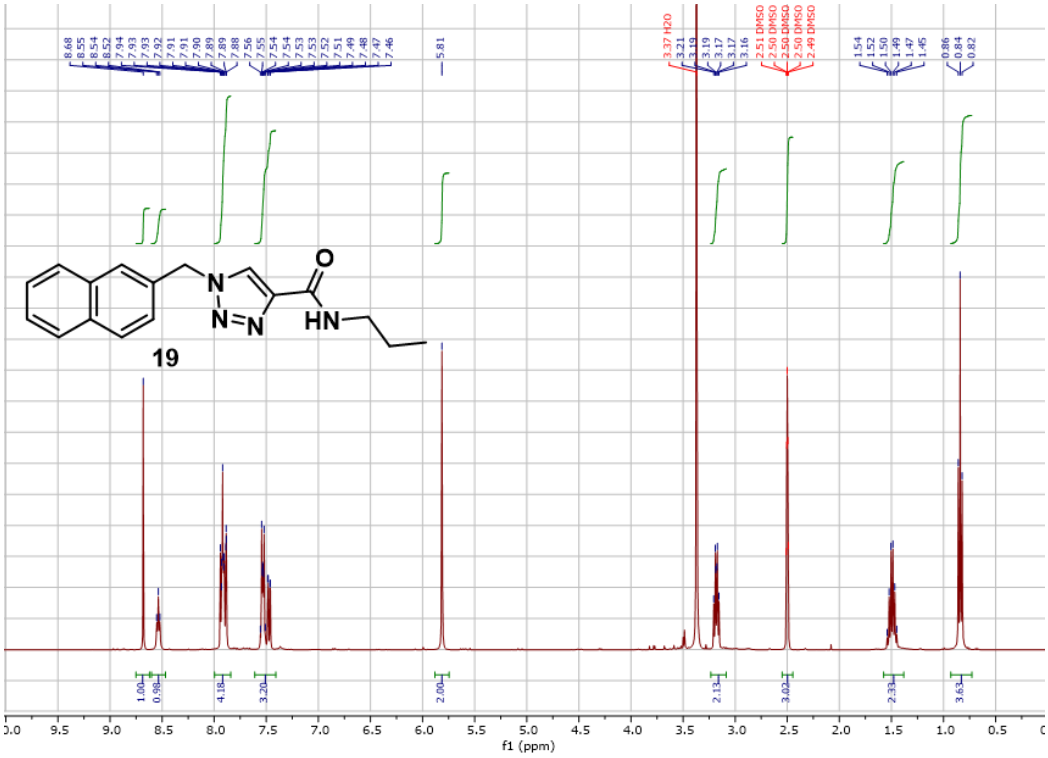

Figure 6.23. ^{1}H NMR **19**

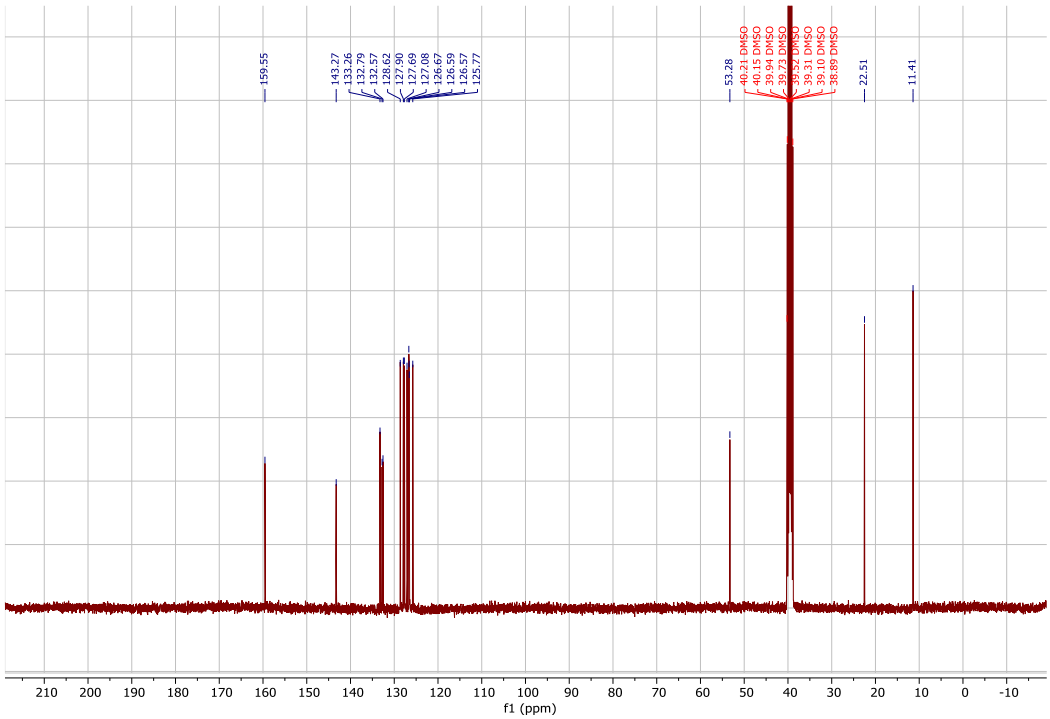

Figure 6.24. ^{13}C NMR **19**

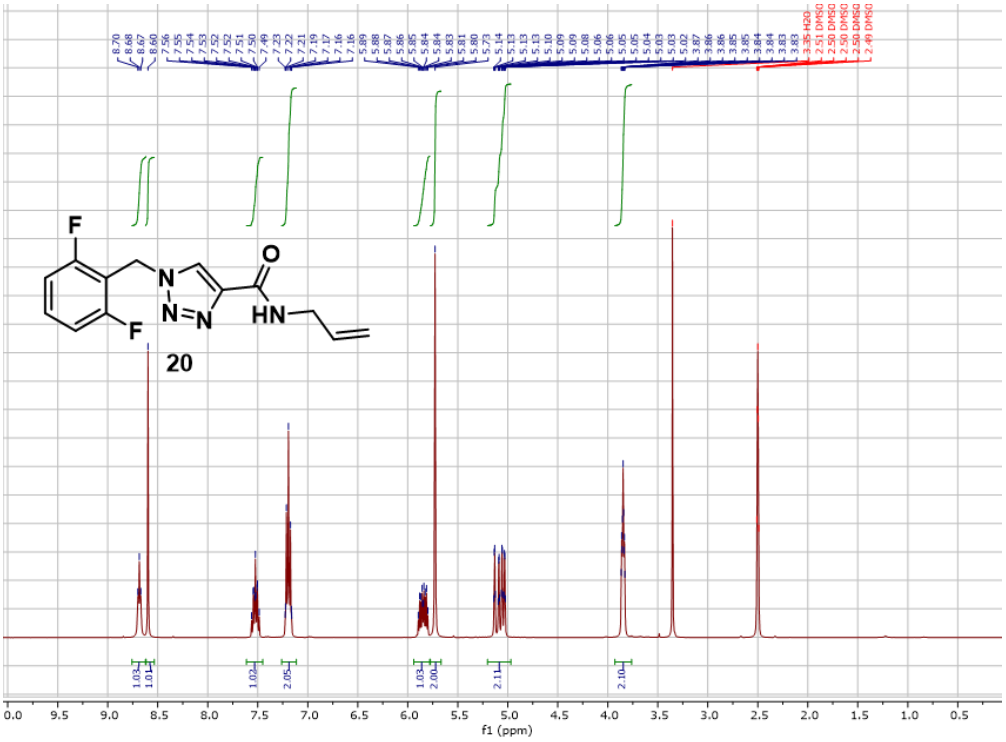

Figure 6.25. ^{1}H NMR **20**

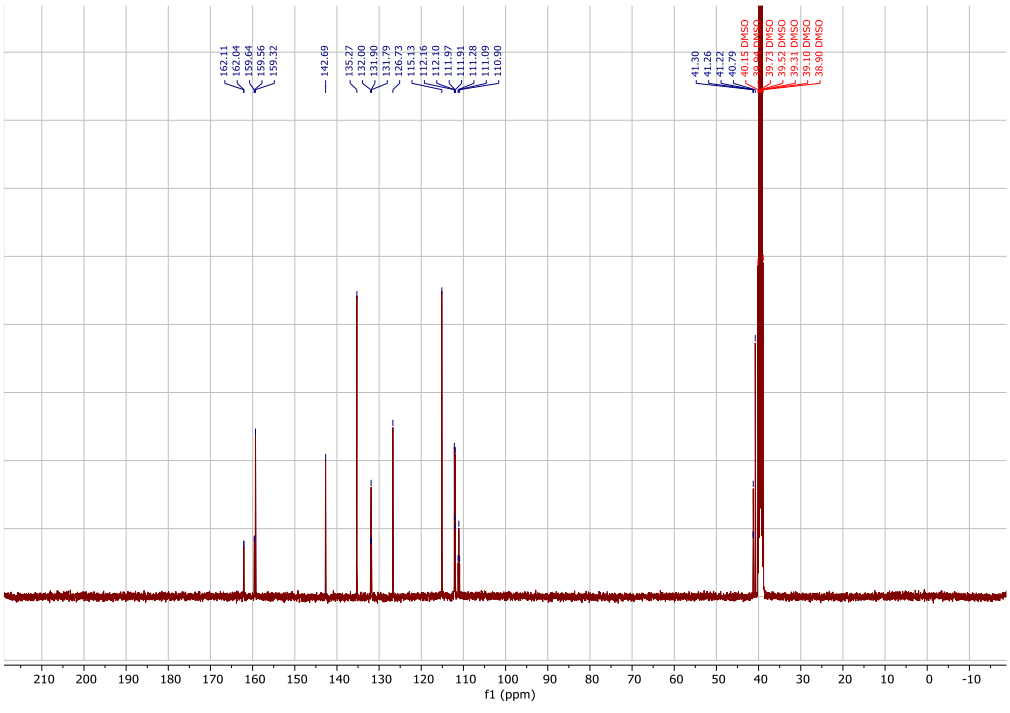

Figure 6.26. ^{13}C NMR **20**

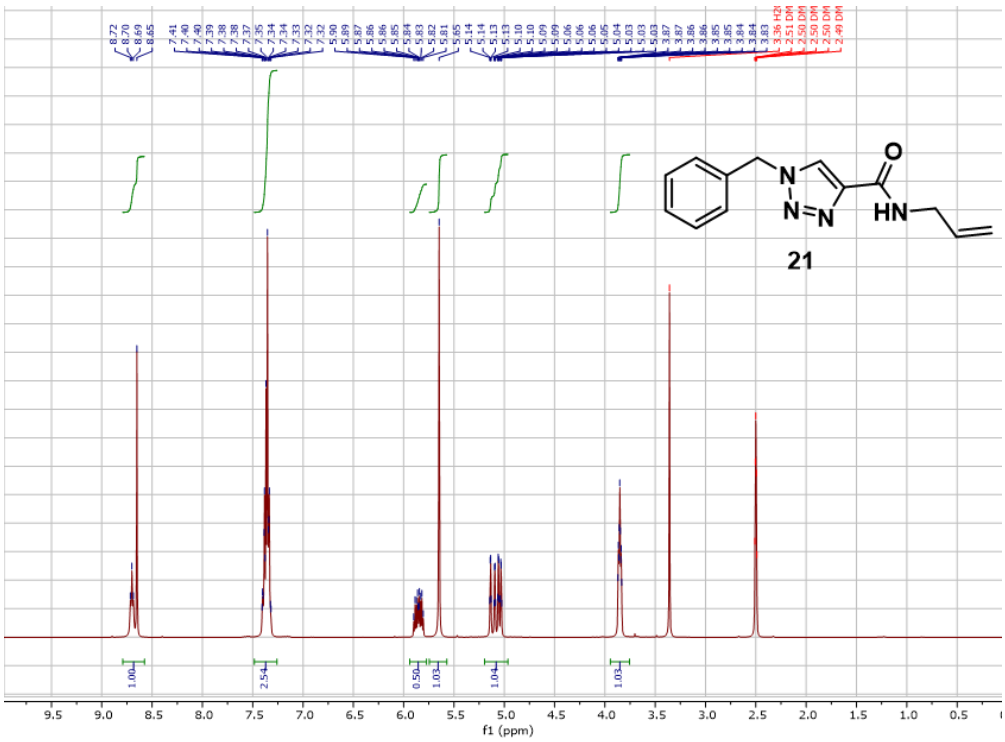

Figure 6.27. ^{1}H NMR **21**

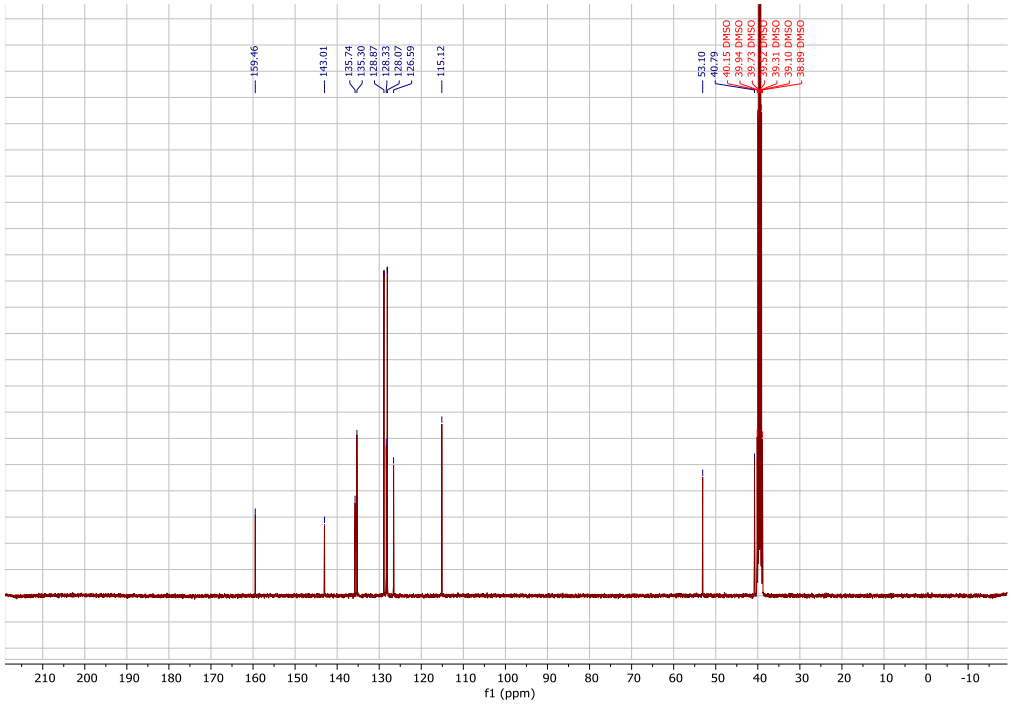

Figure 6.28. ^{13}C NMR **21**

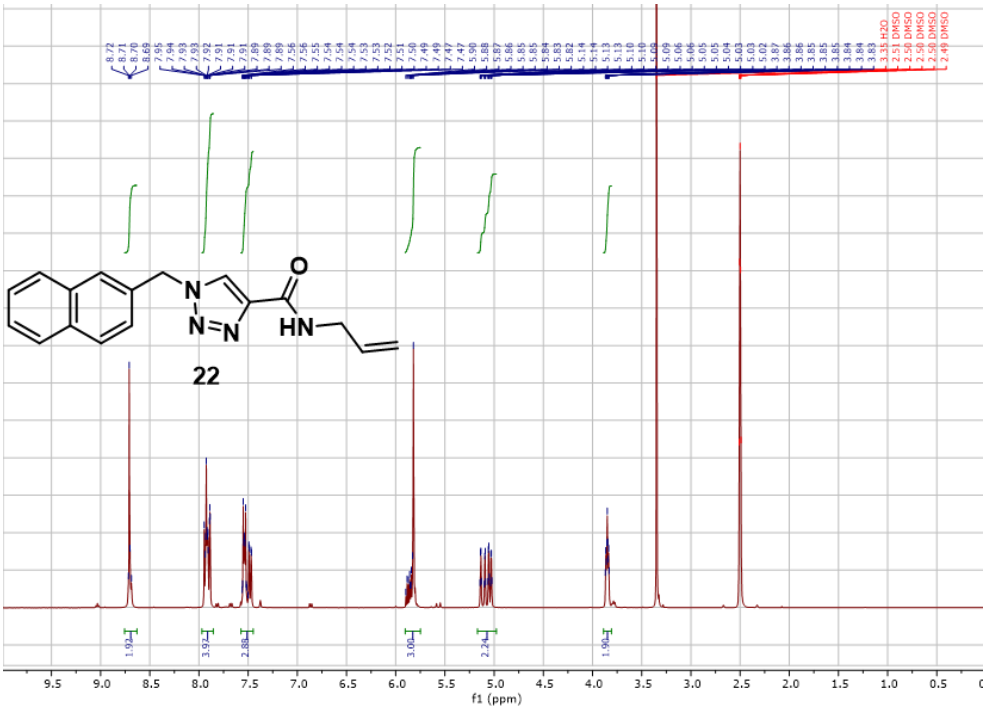

Figure 6.29. ^{1}H NMR **22**

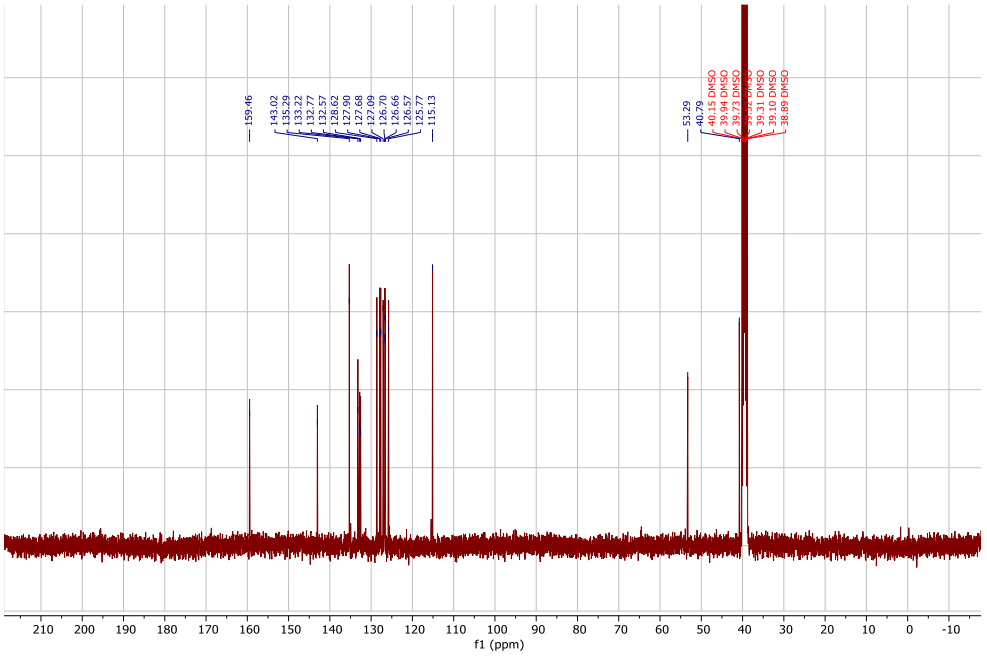

Figure 6.30. ^{13}C NMR **22**

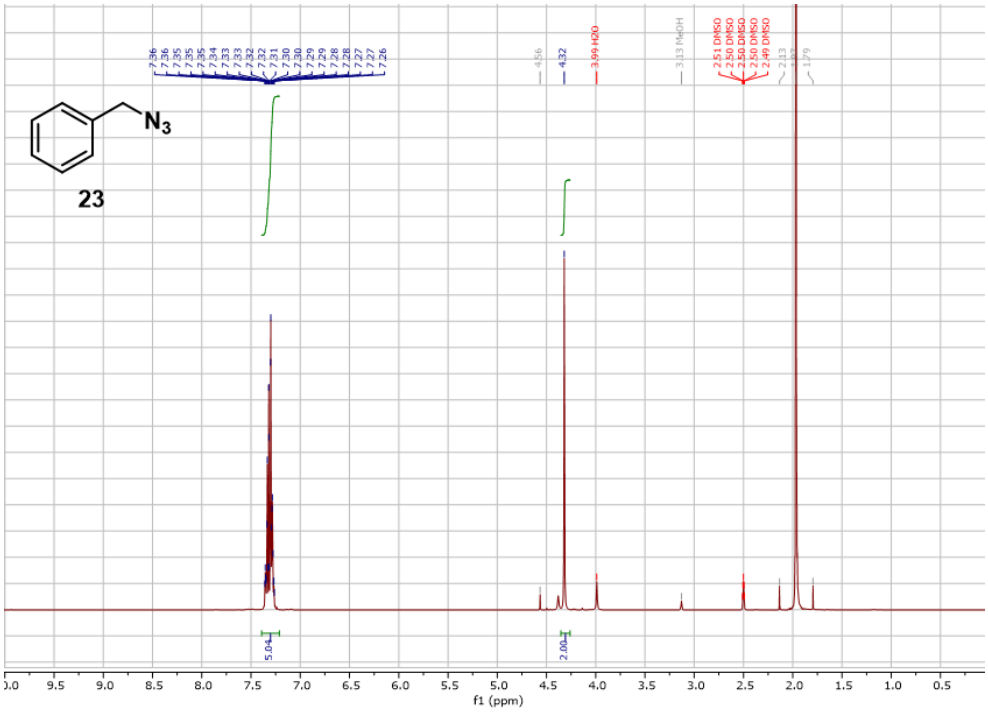

Figure 6.31. ^{1}H NMR **23**

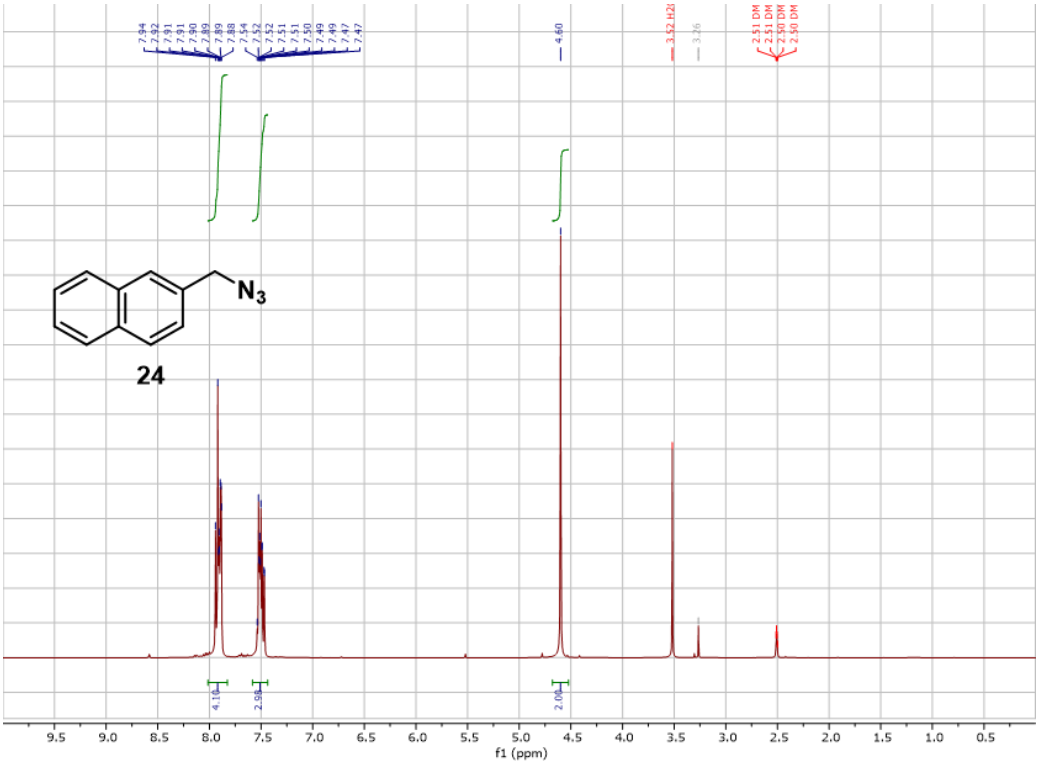

Figure 6.32. ^{1}H NMR **24**

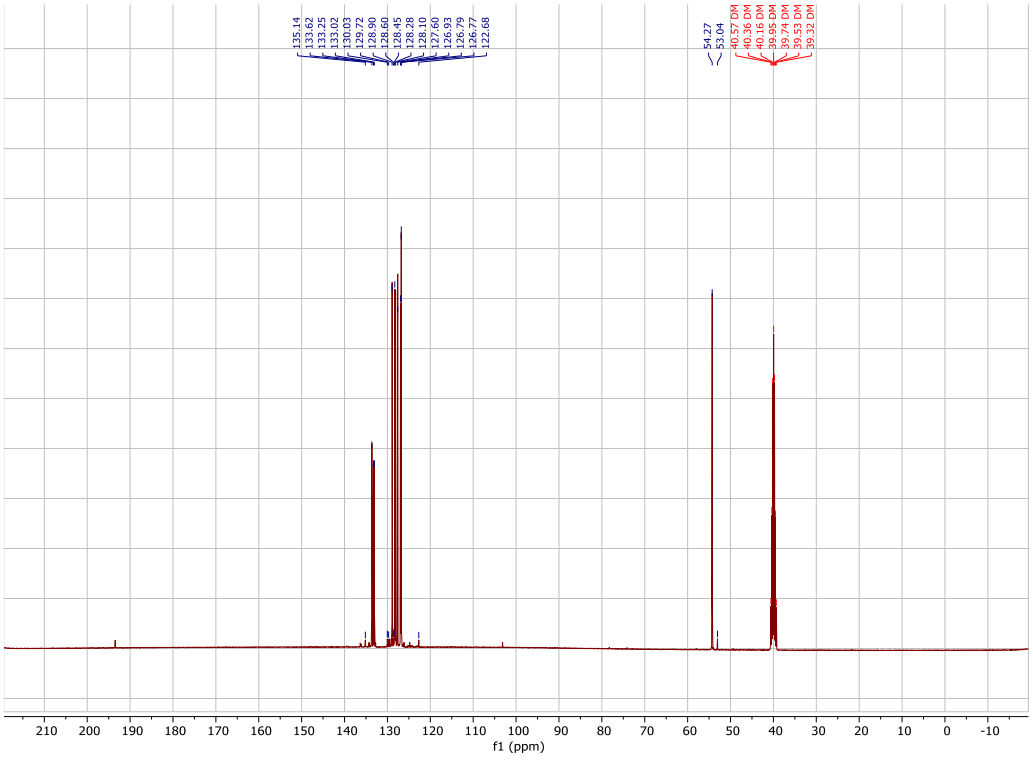

Figure 6.33. ^{13}C NMR **24**

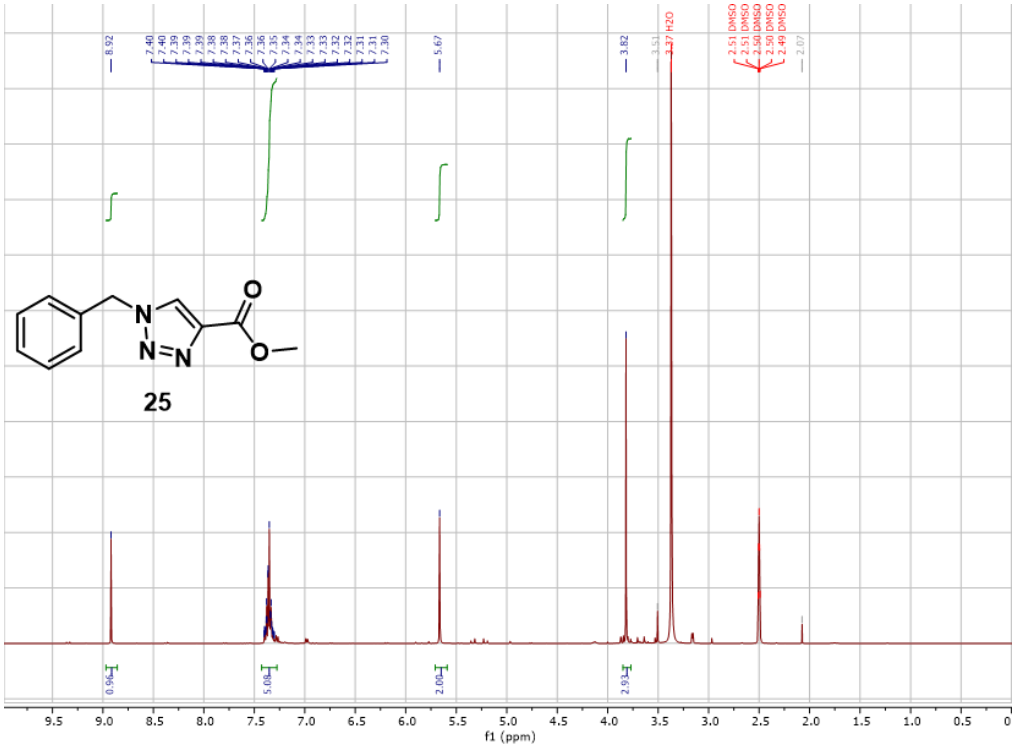

Figure 6.34. ^{1}H NMR **25**

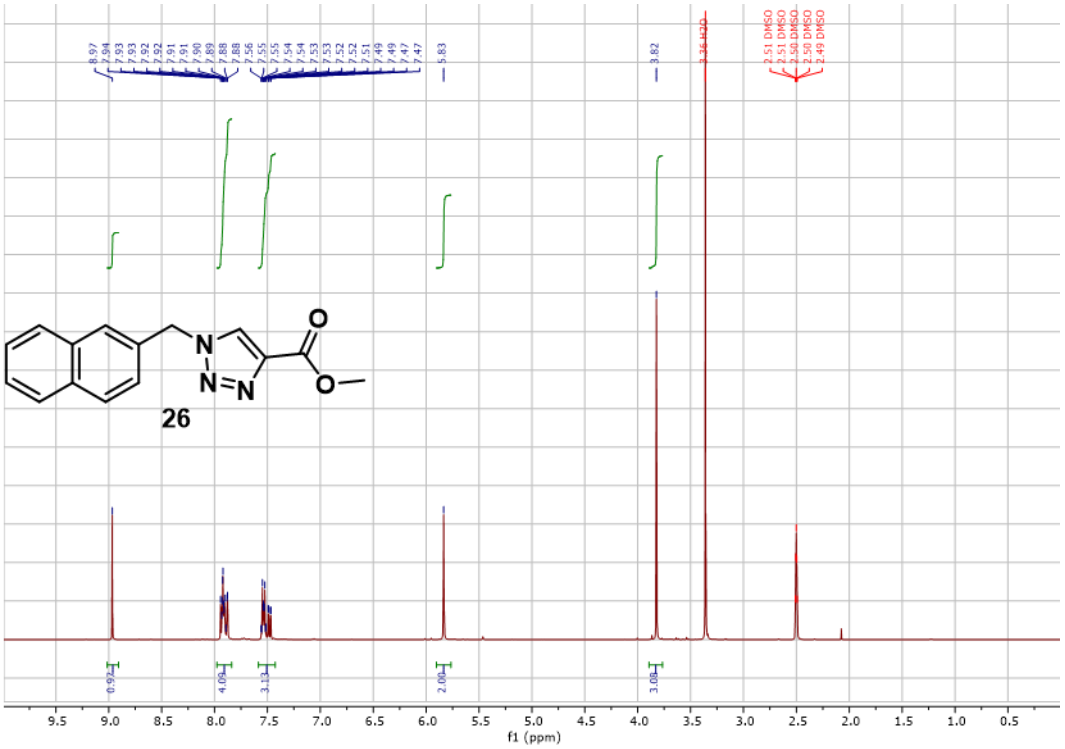

Figure 6.35. ^{1}H NMR **26**

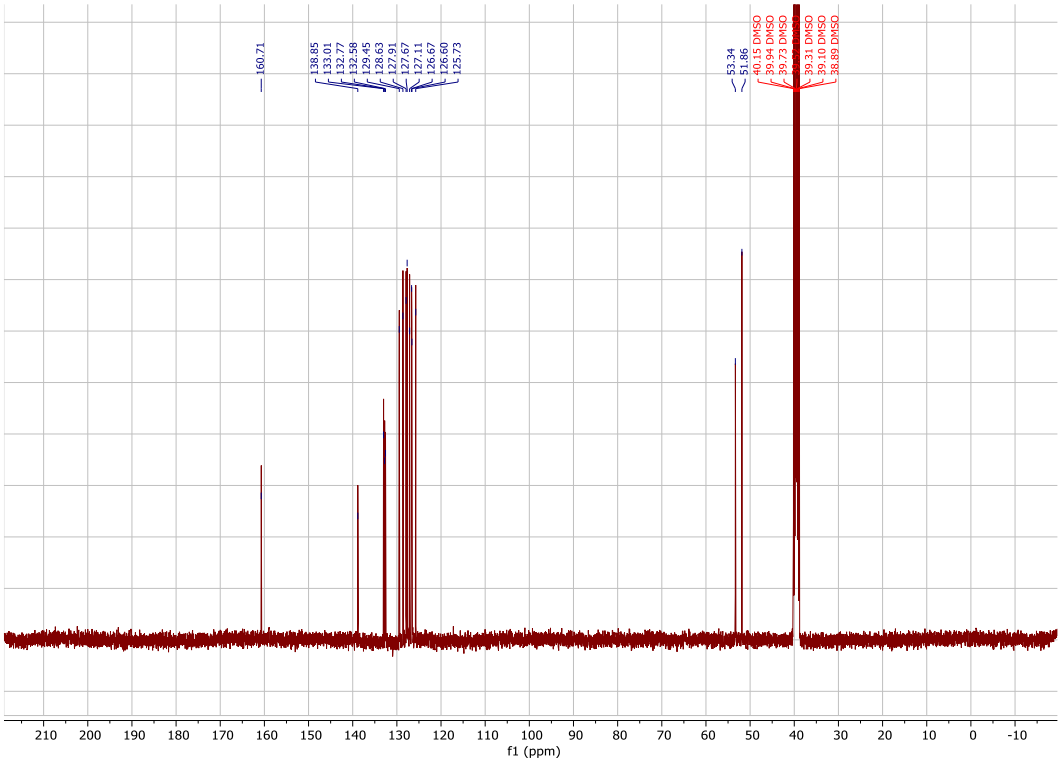

Figure 6.36. ^{13}C NMR **26**

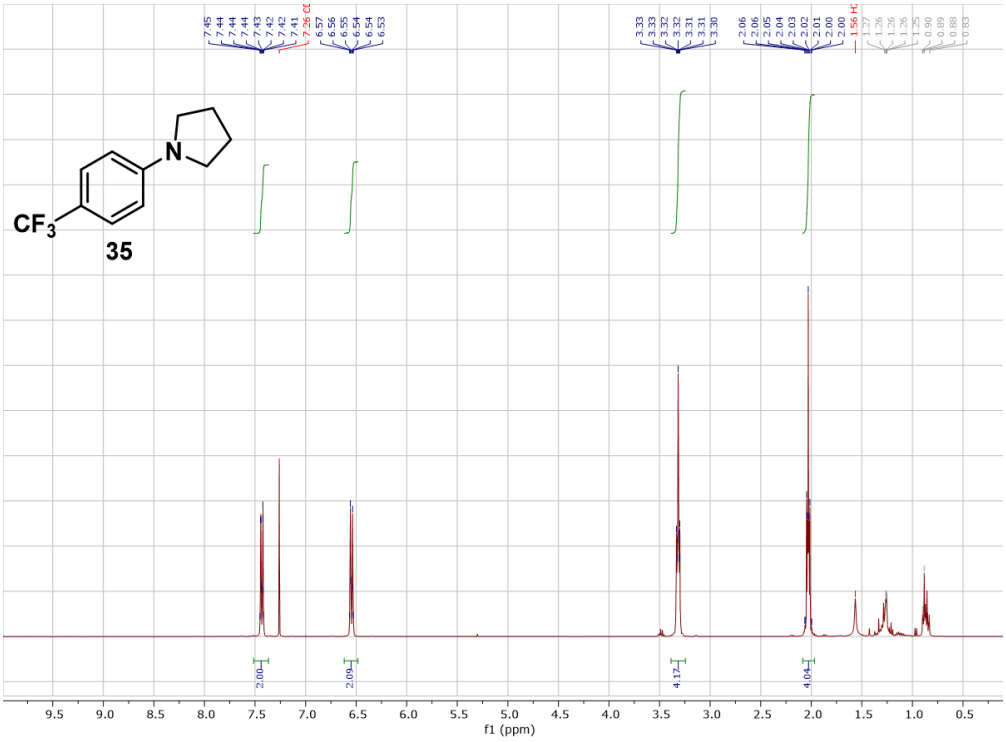

Figure 6.37. ^{1}H NMR **35**

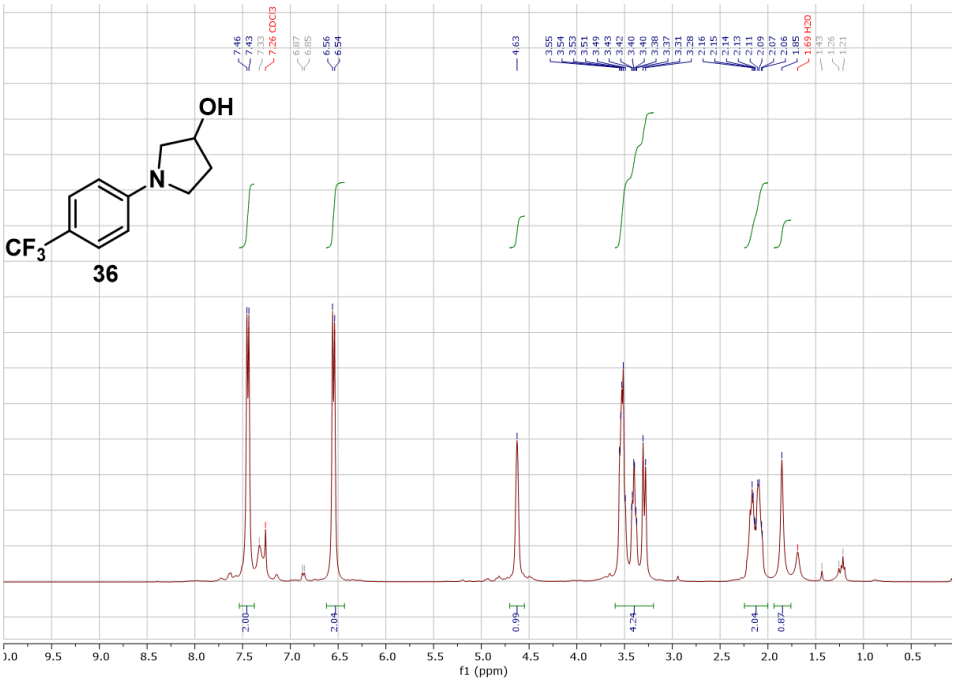

Figure 6.38. ^{1}H NMR **36**

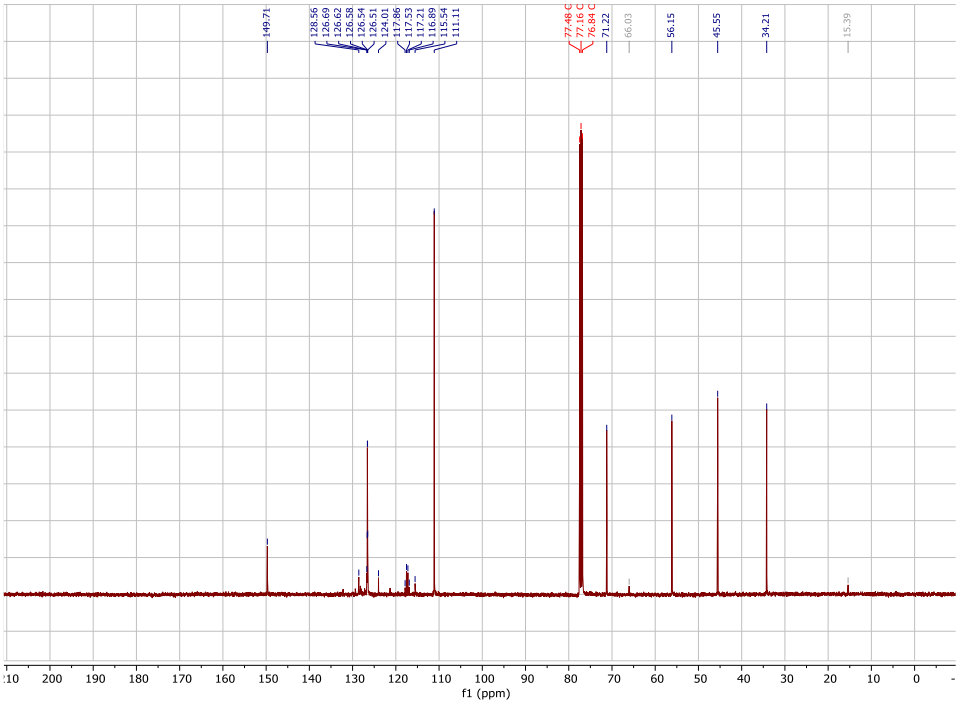

Figure 6.39. ^{13}C NMR **36**

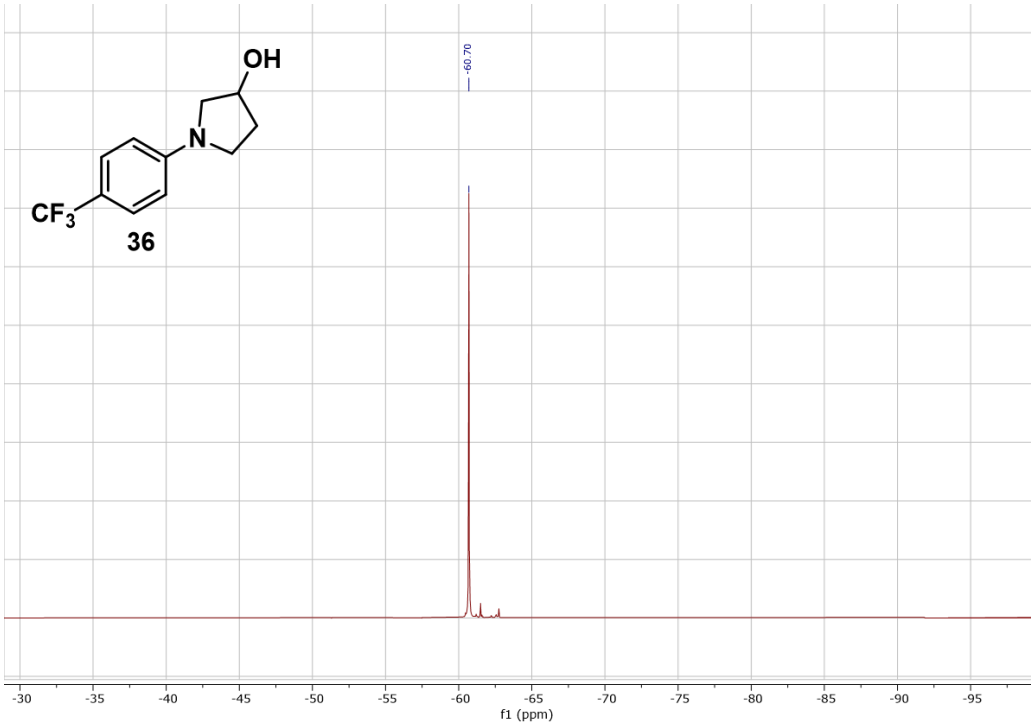

Figure 6.40. ^{19}F NMR **36**

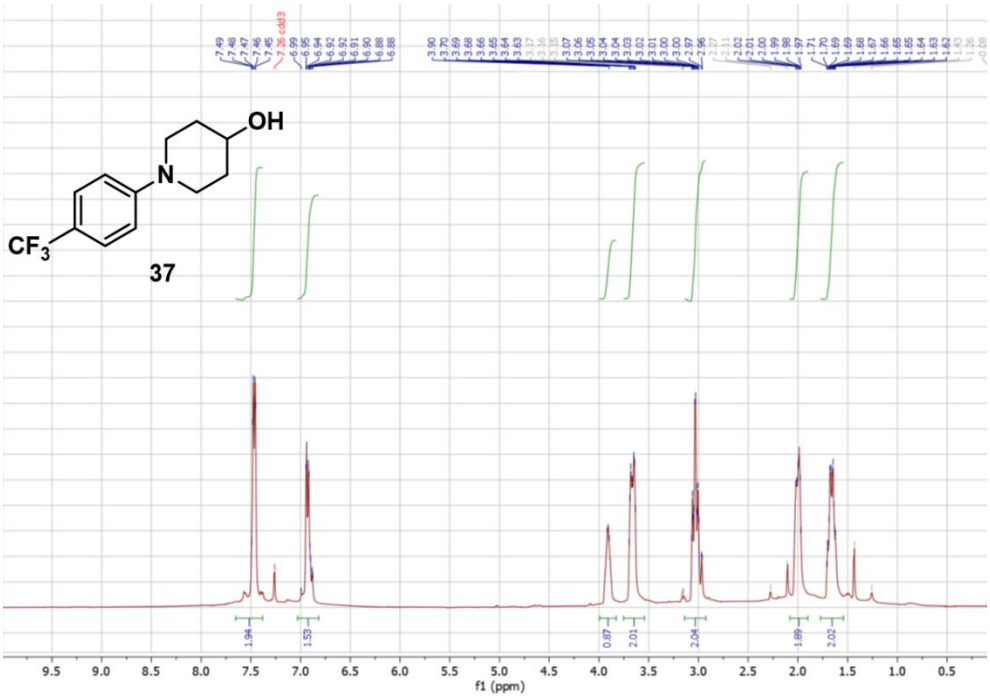

Figure 6.41. ^{1}H NMR **37**

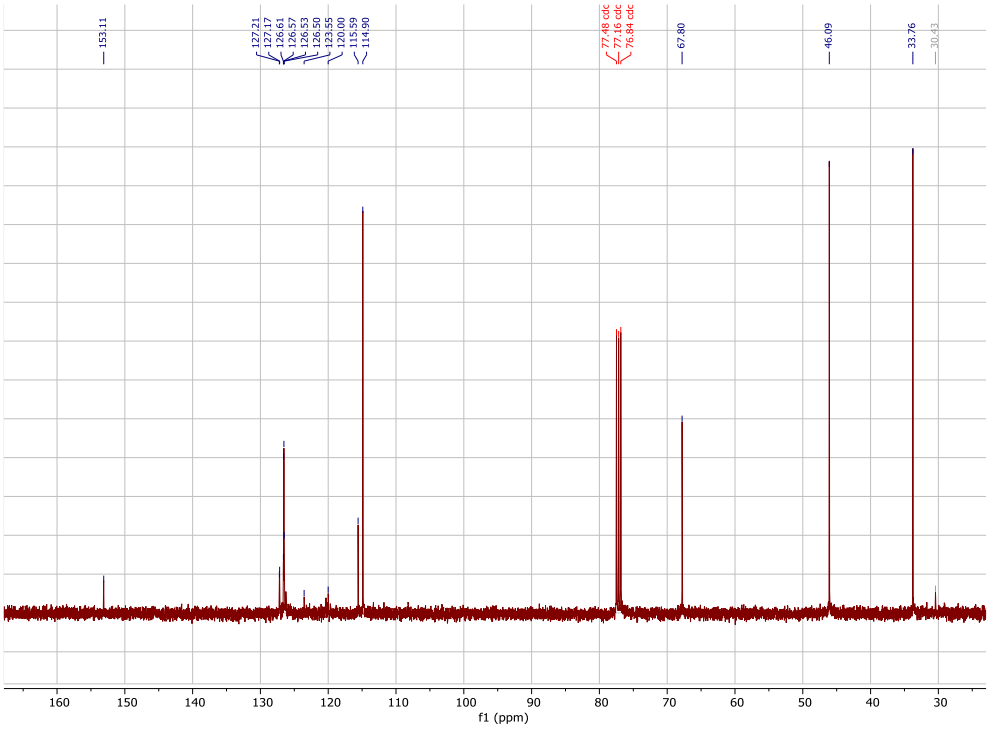

Figure 6.42. ^{13}C NMR **37**

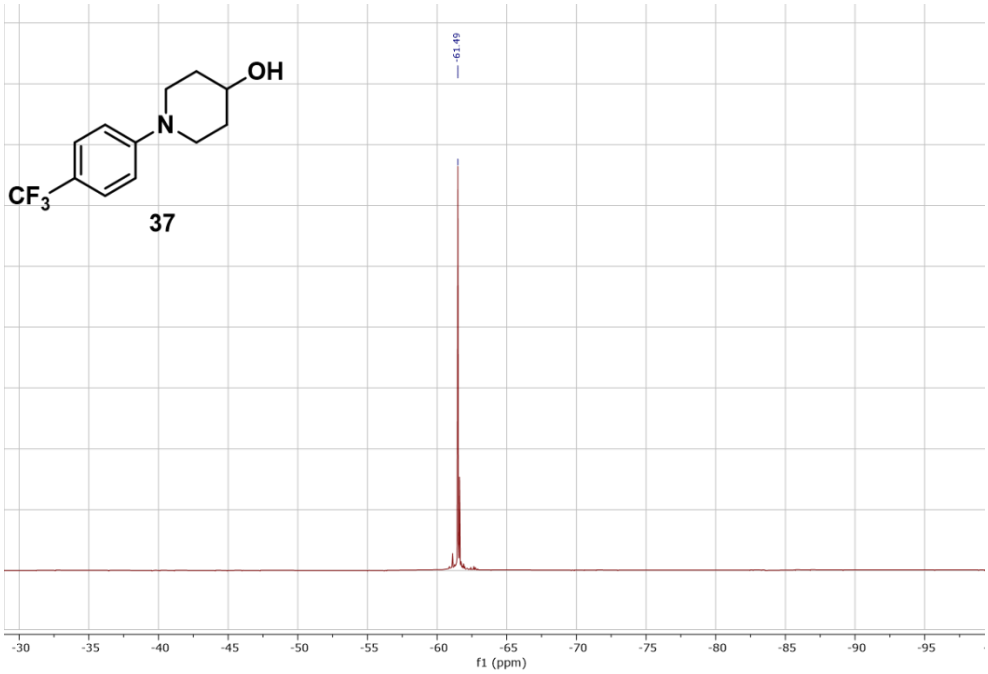

Figure 6.43. ^{19}F NMR **37**

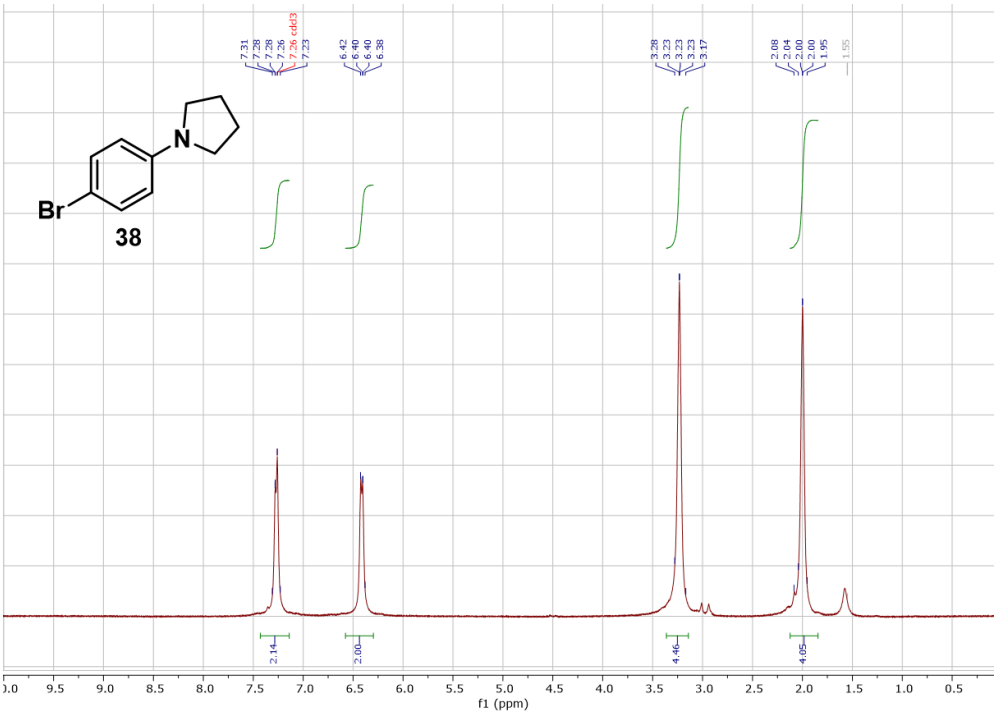

Figure 6.44. ^{1}H NMR **38**

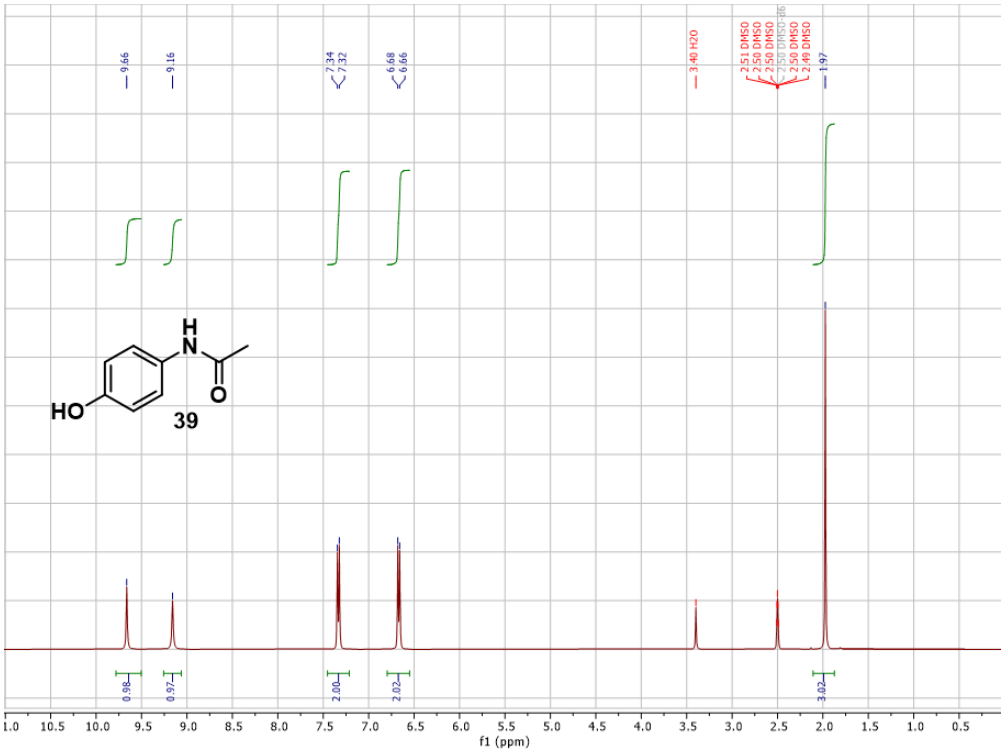

Figure 6.45. ^{1}H NMR **39**

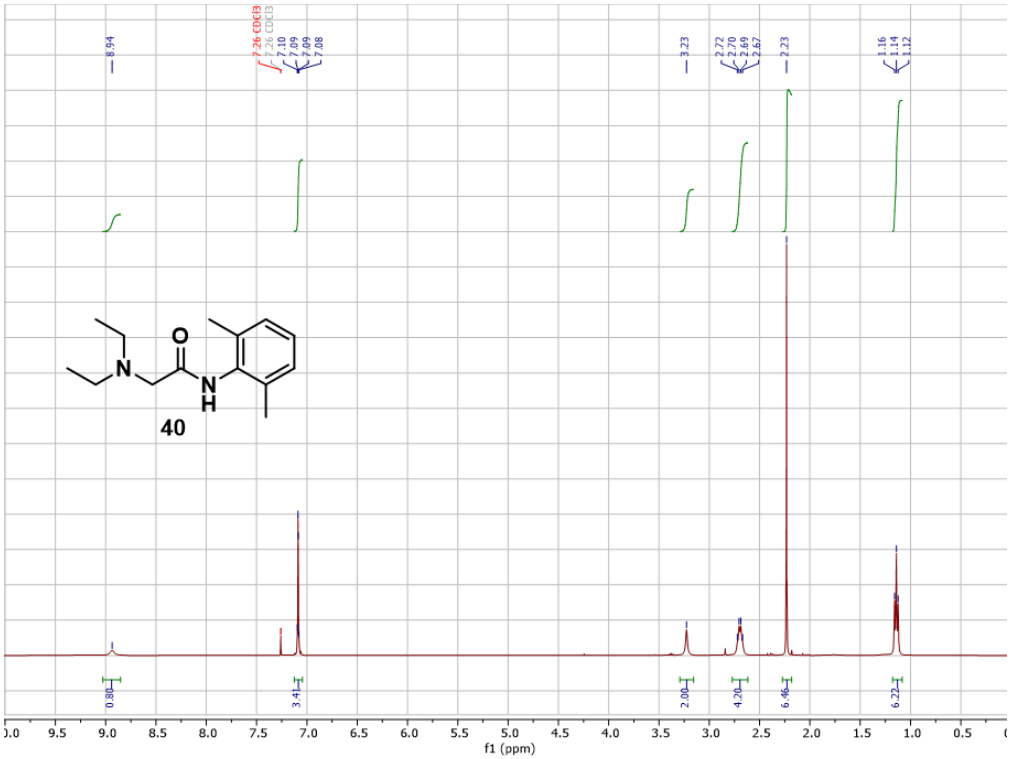

Figure 6.46. ^{1}H NMR **40**

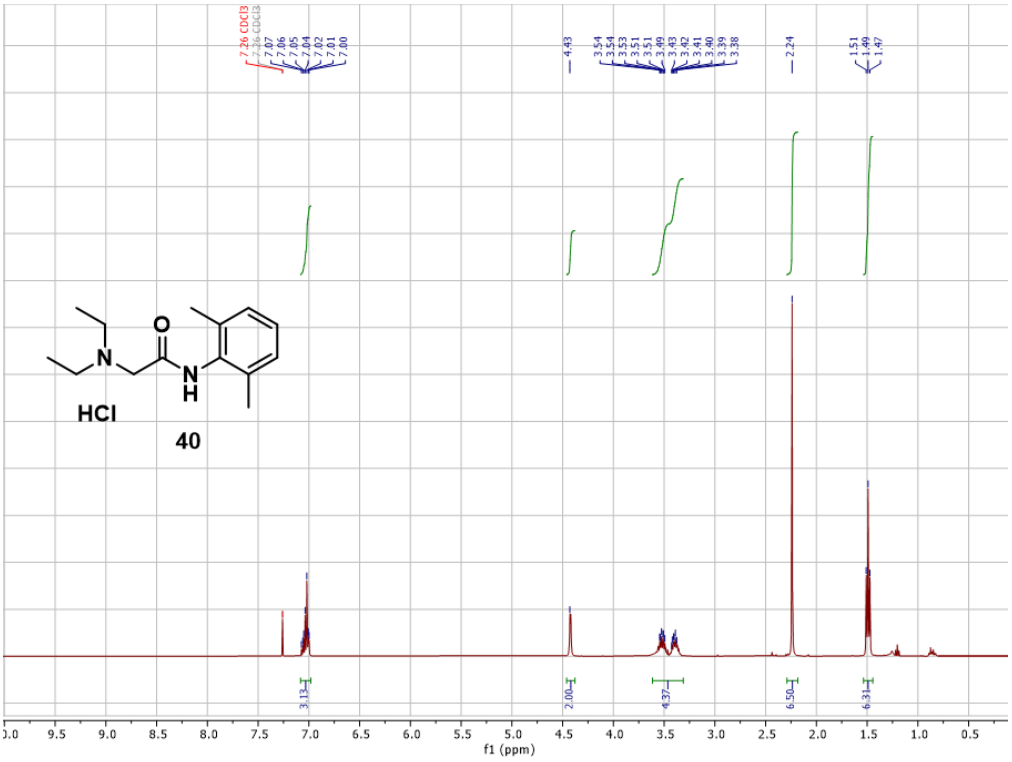

Figure 6.47. ^{1}H NMR **40** HCl

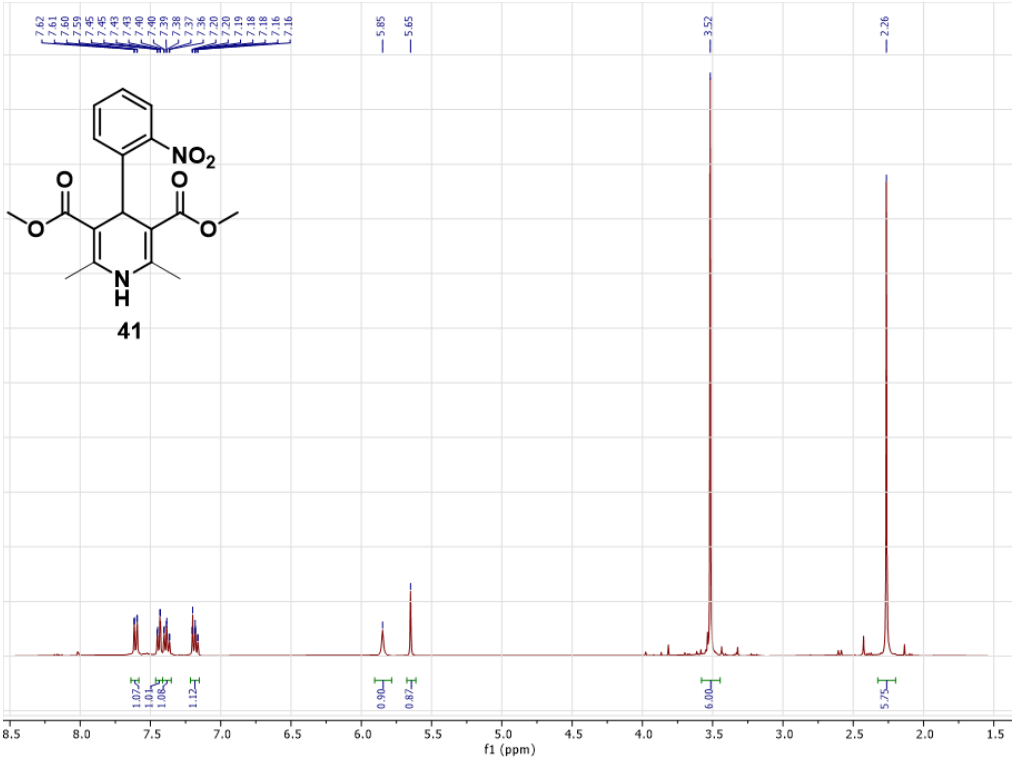

Figure 6.48. ^{1}H NMR **41**

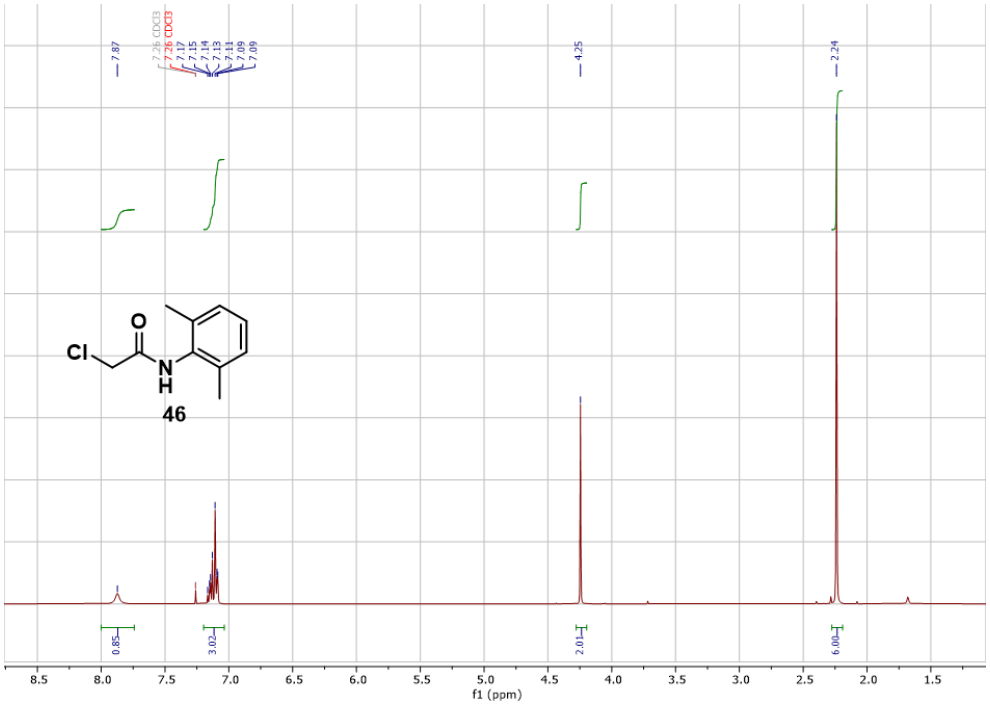

Figure 6.49. ^{1}H NMR **46**